STUDIES ON NARROW BANDWIDTH HIGH REPETITION RATE DYE LASER

By

NAGESHWAR SINGH

PHYS03201004004

Raja Ramanna Centre for Advanced Technology, Indore

A thesis submitted to the

Board of Studies in Physical Sciences

In partial fulfillment of requirements

For the Degree of

DOCTOR OF PHILOSOPHY

of

HOMI BHABHA NATIONAL INSTITUTE

December, 2013

Homi Bhabha National Institute

Recommendations of the Viva Voce Committee

As members of the Viva Voce Board, we certify that we have read the dissertation prepared by **Nageshwar Singh** entitled "**Studies on narrow bandwidth high repetition rate dye laser**" and recommend that it may be accepted as fulfilling the thesis requirement for the award of Degree of Doctor of Philosophy.

Chairman: Dr. S. M. Oak — Date: 11/6/2014

Guide/Convener: Dr. S. K. Dixit — Date: 11/6/2014

Member 1: Dr. G. S. Lodha — Date: 11/6/2014

Member 2: Dr. S. M. Gupta — Date: 11/6/14

Member 3: Dr. K. Dasgupta — Date:

Member 4: Dr. H. S. Rawat — Date: 11/6/14

Sandip Kumar Deb.
Member 5: Dr. S. K. Deb — Date:

Examiner: Professor N. V. Unnikrishnan — Date: 11/6/14

Final approval and acceptance of this thesis is contingent upon the candidate's submission of the final copies of the thesis to HBNI.

I hereby certify that I have read this thesis prepared under my direction and recommend that it may be accepted as fulfilling the thesis requirement.

Date: 11th June 2014

Place: RRACT, Indore

Guide:

(Dr. S. K. Dixit)

STATEMENT BY AUTHOR

This dissertation has been submitted in partial fulfillment of requirements for an advanced degree at Homi Bhabha National Institute (HBNI) and is deposited in the Library to be made available to borrowers under rules of the HBNI.

Brief quotations from this dissertation are allowable without special permission, provided that accurate acknowledgement of source is made. Requests for permission for extended quotation from or reproduction of this manuscript in whole or in part may be granted by the Competent Authority of HBNI when in his or her judgment the proposed use of the material is in the interests of scholarship. In all other instances, however, permission must be obtained from the author.

Nageshwar Singh

DECLARATION

I, hereby declare that the investigation presented in the thesis has been carried out by me. The work is original and has not been submitted earlier as a whole or in part for a degree / diploma at this or any other Institution / University.

Nageshwar Singh

List of Publications arising from the thesis

Journal

1. "A study of flow characteristics of a high repetition rate dye laser gain medium", **Nageshwar Singh,** Abhay Kumar and H. S. Vora, *Laser Physics*, **2014**, Vol.24, 025004-6
2. Studies on gain medium inhomogeneity and spectral fluctuations coupled with high repetition rate dye laser", **Nageshwar Singh**, Abhay Kumar and H. S. Vora, *Laser Physics*, **2013**, Vol.23**,** 125003-6
3. "Spectral fluctuations of a high repetition rate dye laser through a flowing gain medium", **Nageshwar Singh a**nd H. S. Vora, *Laser Physics,2013, V*ol.23**,** 085008-**7**
4. "Spectral intensity variation by the correlation function of refractive index fluctuations of the liquid medium", **Nageshwar Singh**, *International Journal of Optics*, **2013**, Vol.2013, 525142-7
5. "High repetition rate dye laser spectral fluctuations through dye cells", **Nageshwar Singh** and H. S. Vora, *Optik: International Journal for Light and Electron Optics,* **2013**, Vol.124, 7027-7031
6. "Studies on thermo-optic characteristics of a high repetition rate dye laser", **Nageshwar Singh,** R. Jain, S. K. Dixit and H. S. Vora, *Optics & Laser Technology*, **2013**, Vol.48, 309-314
7. "Fluorescence fluctuation of Rhodamine 6G dye for high repetition rate laser excitation", **Nageshwar Singh,** H. K. Patel, S. K. Dixit and H. S. Vora, *Journal of Luminescence*, **2013**, Vol.134, 607-613
8. "Study of a new dye cell for a high repetition rate dye laser", **Nageshwar Singh,** H. K. Patel and H. S. Vora, *Optics & Laser Technology,* **2013**, Vol.45, 256-261

9. “On the coherence measurement of a narrow bandwidth dye laser”, **Nageshwar Singh** and H. S. Vora, *Applied Physics **B*** , **2013**, Vol.110, 5283-3
10. “Design, modelling and performance evaluation of a novel dye cell for a high repetition rate dye laser”, **Nageshwar Singh,** H. K. Patel, S. K. Dixit and H. S. Vora, *Review of Scientific Instruments*, **2012**, Vol.83**,** 105114-8
11. “On the microstructure of thermal and fluid flow field in a lasing medium of a high repetition rate dye laser”, **Nageshwar Singh,** *Optik: International Journal for Light and Electron Optics*, **2010**, Vol.121, 1642-1648
12. “Analysis of the spectral variation of a dye laser by gain medium inhomogeneity”, **Nageshwar Singh,** *Optics & Laser Technology* **201**0, Vol.42, 225-229
13. “Study of the influence of the input electric power on the spectral width of the 510.6 nm line of an atomic copper vapor laser”, **Nageshwar Singh** and H. S. Vora, *Optics & Laser Technology*, **2010**, Vol.42, 866-872
14. “Composite (stacked) picture generation technique for spectral profile representation of dye laser”, H. S. Vora and **Nageshwar Singh,** *Optics Communication*, **2009**, Vol.282, 4259-4264
15. “Influence of buffer gas pressure on the spectral width of 510.6 nm line of an atomic copper vapor laser”, **Nageshwar Singh** and H. S. Vora, *Optical Engineering*, **2009**, Vol.48, 094201-094207
16. “On the hyperfine spectral lines of an atomic copper vapor laser”, **Nageshwar Singh** and H. S. Vora, *Optics Communication ,* **2009**, Vol.182, 1393-1398

Other publications relevant to the work

1. “Effect of liquid flow on spectral properties of a dye laser pumped a copper vapor laser”, **Nageshwar Singh**, *Optics Journal*, **2008**, Vol.2**,** 2-6

2. “The spectral measurement of a high repetition rate tunable dye laser output using Fabry-Perot fringe”, **Nageshwar Singh** and H. S. Vora, *Optics & Laser Technology,* **2007**, Vol.39, 733-737
3. “Influence of the medium on the fluorescence of copper vapor laser pumped rhodamine 6G dye: introduction, experimental details and stationary case”, N. Sharma, **Nageshwar Singh**, H. S. Vora and S. Goyal, *Optics Journal* , **2007**, Vol.1, 13-17
4. “Influence of the medium on the fluorescence of copper vapor laser pumped rhodamine 6G dye: dynamic case”, N. Sharma, **Nageshwar Singh**, H. S. Vora and S. Goyal, *Optics Journal* , **2007**, Vol.1, 18-22
5. “Comparison of the performance of a near 360^0 curved and a straight channel dye cell for high repetition rate copper vapor laser pumped dye laser”, **Nageshwar Singh,** *Journal of Physics D: Applied Physics,* **2006**, Vol.39, 2084-2089
6. “Influence of optical in-homogeneity in the gain medium on the bandwidth of a high repetition rate dye laser pumped by copper vapor laser”, **Nageshwar Singh,** *Optical Engineering,* **2006**, Vol.45, 104204-104208
7. “Single mode operation of a narrow bandwidth dye laser in single prism grazing incidence grating cavity”, **Nageshwar Singh,** *Optics & Laser Technology,* **2006**, Vol.39, 1140-1143
8. “On the stability of the output characteristics of a grazing incidence grating dye laser transversely pumped by a copper vapor laser”, **Nageshwar Singh** and H. S. Vora, *Applied Physics* **B, 2006,** Vol.82, 71-74
9. “Design of a transversely pumped, high repetition rate, narrow bandwidth dye laser with high wavelength stability”, R. Bhatnagar, **Nageshwar Singh**, R. Chaube and H. S. Vora, *Review of Scientific Instruments,* **2004**, Vol.75, 5126-5130

(Nageshwar Singh)

DEDICATIONS

Dedicate to my parents,

Late *Shri Ram Ishwar Singh*

And

Late *Smt. Chandra Baso Devi*

ACKNOWLEDGEMENTS

It is a matter of great pleasure for me to express thanks and gratitude to all those who have contributed to this thesis work, directly or indirectly.

First of all, I wish to express my profound gratitude to *Shri H. S. Vora* for his encouragement and motivation throughout my Ph.D. work. I am thankful to him for his wholehearted help in planning and carrying out various experiments, analysing the results, amending his software as per my investigational needs, and finally in documenting the results in this thesis. His indefatigable enthusiasm has always been a source of inspiration for me.

I am extremely thankful to *Dr. P. D. Gupta*, Director, RRCAT, for allowing me to conclude my Ph.D. work in the dye laser field, despite my transfer to Materials and Advanced Accelerator Sciences Division.

I am very much indebted to *Dr. S. B. Roy*, for his helping nature. It would have been impossible to complete the thesis work without his kind-heartedness.

I am highly grateful to *Dr. P. A. Naik* for his encouragement, and valuable help in manuscript formulations during initial stage of my career. He went through my manuscripts thoroughly, critically, and gave several valuable suggestions which helped a lot in improving my skill in presenting the scientific results in journals.

I wish to acknowledge *Dr. S. K. Dixit*, for valuable suggestions and guidance in completing this thesis.

I also wish to thank *Shri Bijendra Singh*, for the fruitful scientific discussions. I would like to give special thanks to *Dr. Rajeev Khare* for some of his critical comments, which have led to some of the publications. I wish to admit help on gain medium flow through dye cells by *Shri Hemant K. Patel.* The wholehearted help out by *Shri Abhay Kumar* on thermal and flow analysis of dye laser gain medium at the vital time is fully acknowledged.

I thank *Dr. H. S. Rawat*, for the critical review of some of the manuscripts pertaining to this thesis, and also *Dr. Rama Chari*, *Dr. S. R. Mishra*, *Dr. Anand Moorti*, *Dr. M. P. Singh*, and *Dr. T. Ganguli* for their valuable suggestions from time to time on the manuscripts. I am highly thankful to *Dr. M. K. Chattopadhyay* for his wholehearted help during the compilation of this thesis.

Thanks are due to *Dr. L. Abhinandan* for fabrication of the mechanical components of dye laser, and some critical adapters during the experiments; to *Shri S.S. Mahras* for fabricating the pinched dye cell, which was a challenging task; to *Dr. S. Chatterjee* and his team for fabricating and polishing the dye cells and other optical windows; to *Shri B. Q. Khattak* for dye solution spectroscopic measurements and analysis; and to *Dr. C. Mukherjee* for mirrors coating and reflectivity measurements.

My special thanks to *Shri Rajiv Jain* for his prompt conceptualization and device installation for the PC based dye solution temperature data acquisition system and related software, as per experimental needs. I would like to thank *Shri P. Saxena* and his electronics team members *Shri V. K. Dubey, Shri I. Singh, and Shri D. Shukla* for their quick electronic supports involved in power supplies and all other measuring devices, *Shri R. P. Kushwaha* and *Shri R. K. Mishra* for maintaining the CVL power supply during initial stage of the work. I wish to extend my thanks to *Shri S. R. Daultabad* for his initial help in dye laser alignments. I am also grateful to *Mr. Devendra Sinnarkar* in formatting and improving the aesthetics of my thesis presentations.

Thanks are due to *Dr. R. Bhatnagar*, ex-head, erstwhile LSED, for introducing me to the field of dye laser technology and to *Dr. K. Dasgupta*, BARC for providing help in high resolution spectral measurements during my early stage of career. I wish to acknowledge *Shri A. Chakraborty* for help in CVL operation and maintenance, and in dye laser experiments during the final stages of the thesis work.

I am thankful to all the staff of erstwhile Laser Systems Engineering Division for providing help in maintaining CVL system and other experimental setups used during this work; and members of the LSED Mechanical Work Shop for their help in fabrication of different components as and when required during the experiments. Particularly, I thank *Shri A. K. Sarkar and his team* for their help in design, fabrication, and assembly of dye circulation system and some of the optical work stations.

I take this opportunity to thank all the members of my Ph.D. advisory committee (*Dr. S. M. Oak, Dr. K. Dasgupta, Dr. S. K. Deb, Dr. G. S. Lodha* and *Dr. S. M. Gupta)* for their valuable suggestions during the yearly review presentations.

I wish to acknowledge a friendly environment created by my present colleagues *Smt. Parul Arora, Dr. M. A. Manekar*, *Dr. Vishnu Sharma*.

My thanks are due to all my close friends who encouraged and supported me during this work. I specially acknowledge *Mr. Mukesh Kumar* for his help in many numerical calculations and 2D/3D visualization of some of the figures. I also wish to express appreciation to *Mr. Amalendu Sharma* for help in solving some of the numerical problems involved in dye laser, through C language programming.

I am indebted to my parents for their blessings from heaven, elder brother and his family for their support, in difficult times in my life, and my nephew *Deepak* for the love he showered on me. I wholeheartedly thank my wife *Dr. Pratibha Singh* for her support, understanding, and willingness to allow me to sacrifice the precious family time during compilation of the thesis work. I thank my one and a half year old daughter *Kuchu* for providing cheerful atmosphere at home and relaxation from all stresses during writing of the thesis.

Last but not the least, I wish to express my profound reverence to *Shri K. C. Kaushik*, then Principal, Hindu College, Sonipat, Haryana for nurturing and supporting me during the most difficult period of my life. To fulfill his very strong wish to see me climbing great heights, it will be my endeavor to strive to prove worthy of his expectations.

Nageshwar Singh

CONTENTS

Page No.

SYNOPSIS vii

LIST OF FIGURES xv

LIST OF TABLES xxiv

THESIS CHAPTERS

CHAPTER 1: Review on high repetition rate dye laser: Gain medium 1

1.1 Scope of the work 1

1.2 Physical properties of dye laser gain medium 6

1.2.1 Coumarin dyes 7

1.2.2 Pyrromethene–BF_2 (PM–BF_2) dyes 8

1.2.3 Rhodamine dyes 9

1.3 Spectroscopic properties of laser dyes 10

1.4 Photo physical properties of Rhodamine 6G dye 13

1.4.1 Solvent effects 14

1.4.2 Concentration effects 17

1.4.3 Temperature effects 20

1.5 Summary 22

References 23

CHAPTER 2: Diagnostic techniques for high repetition rate dye laser 26

2.1 Introduction 26

2.2 Review of dye laser data presentations 26

2.3 Description of hardware and software 28

2.4 Methodology adopted for spectral investigation 29

2.4.1 Theoretical formulation of the spectral measurement 30

2.4.2 Experimental technique for the data acquisition and analysis of spectral structure 32

2.4.3 Identification of peaks and rings diameter 33

2.4.4 Technique for spectral data representation: Composite image generation 35

2.4.5 Spectral measurement from the composite image 37

2.5 Instruments detail used for the investigation of dye laser 40

2.5.1 Tuning range 40

2.5.2 Pulse shape 40

2.5.3 Optical average power 41

2.5.4 Beam size and divergence 42

2.6 Coherence measurements of pulsed dye laser 42

2.6.1 Spatial coherence 43

2.6.2 Temporal coherence 46

2.7 Summary 51

References 53

CHAPTER 3: Review and studies on Copper Vapour Laser 56

3.1 Pulsed Excitation Sources 56

3.2 Copper Vapour Laser 56

3.2.1 Energy levels and laser transitions 56

3.2.2 Kinetics of CVL 59

3.2.3 Design, assembly and excitation source of CVL 60

3.2.4 Operating characteristics of CVL 63

3.3 Spectral Characteristics of CVL 63

	3.3.1	Review of spectral characteristics of CVL	63
	3.3.2	Relevant theory and analysis of hyperfine spectral lines of CVL	64
3.4	Results and discussion		67
	3.4.1	Hyperfine lines of CVL	67
	3.4.2	Effect of electrical input power on spectral width of CVL	71
	3.4.3	Buffer gas pressure	74
3.5	Summary		78
	References		80
CHAPTER 4:	**Studies on pulsed dye laser resonator**		83
4.1	Introduction		83
4.2	Theory of pulsed dye laser resonator		84
	4.2.1	Theoretical analysis	84
	4.2.2	Numerical analysis	89
	4.2.3	Optimization of dye laser output power	93
4.3	Spectral width of a dye laser		97
4.4	Single mode dye laser		100
4.5	Summary		105
	References		106
CHAPTER 5:	**Studies on high repetition rate dye laser subsystem**		108
5.1	Studies on dye laser flow subsystem		108
	5.1.1	Design detail of the dye circulation system	109
	5.1.2	Studies on mechanical vibrations	110
5.2	Development and studies on dye cells		112

	5.2.1	Planar duct dye cell	113
	5.2.2	Concave-convex duct dye cell	114
	5.2.3	Pinched dye cell	115
	5.2.4	Convex-plano duct dye cell	118
	5.3	Microstructure of the flowing gain medium	120
	5.4	Summary	125
		References	127
CHAPTER 6:	**Studies on spectral stability of a high repetition rate dye laser**		129
	6.1	Experimental details	130
	6.2	Results and discussion	131
	6.2.1	Planar dye cell	131
	6.2.2	Concave-convex dye cell	133
	6.2.3	Pinched dye cell	134
	6.2.4	Convex-plano dye cell	135
	6.3	Spectral fluctuations with Reynolds number of the gain medium flow	137
	6.4	Summary	149
		References	152
CHAPTER 7:	**Studies on fluorescence of Rhodamine 6G dye under high repetition rate excitation**		155
	7.1	Review of Rhodamine 6G fluorescence characteristics	155
	7.2	Studies on fluorescence characteristics under high repetition rate excitation	157
	7.2.1	Fluorescence characteristics in the stationary	

medium 157
7.2.2 Fluorescence characteristic in the flowing medium 160
7.2.3 Fluorescence characteristics in alternatively stationary and flowing medium 162
7.3 Summary 167
References 169

CHAPTER 8: Studies on thermo-optics characteristics of high repetition rate dye laser 171
8.1 Introduction 171
8.2 Theoretical analysis of thermo-optics of a high repetition rate dye laser 171
8.2.1 Theoretical analysis 171
8.2.2 Numerical analysis 174
8.3 Dye laser characteristics during gain medium bulk temperature variation 176
8.3.1 Introduction 176
8.3.2 Experimental details 177
8.3.3 Results and discussion 178
8.3.4 Summary 186
8.4 Dye laser characteristics during gain medium bulk temperature stabilization 187
8.5 Theoretical studies for dye laser spectral intensity fluctuations 191
References 199

CHAPTER 9: Summary, conclusion and scope for the future work 201

9.1 Summary and conclusion 201

9.2 Scope for further research work 210

SYNOPSIS

There are many applications where broadly tunable pulsed coherent radiation, having narrow bandwidth and high average optical powers are needed. Solid-state dye lasers are emerging as compact tunable light sources, however, so far best performance is limited to low pulse-repetition-frequency operation while high repetition rate operation still eludes operational stability. These days, optical parametric oscillators (OPOs) are emerging as compact, state-of-the-art all-solid-state, tunable light sources, alternative to the conventional organic dye laser. However, the delicate requirement of phase matching, system complexity and thermal issues at high pulse repetition rate operation limit their application potential. Thus, in present scenario, dye laser based on organic dye molecules in liquid solvent as gain medium, is the most comprehensively utilized pulsed tunable laser. Continuous wavelength tunability, efficient narrow bandwidth operation, wide spectral coverage, and simplicity have made a dye laser an indispensible tool in many areas of laser research, scientific, industrial and medical applications. Narrow bandwidth high repetition rate (~ kHz) dye lasers, tunable in the visible region of spectrum, are exclusively used in application like atomic vapor laser isotope separation (AVLIS) scheme. Dye laser pumped by copper vapour laser (CVL), operating typically in the range of 5-10 kHz in the visible region, capable of delivering high average power, is extremely appropriate for this purpose. This thesis work is a study on CVL pumped dye laser system.

In a dye laser, since absorption of the pump beam radiation follow the exponential law, the maximum absorption predominantly lies close to the pump beam entrance window of the dye cell. A fraction of the pump radiation is converted into heat, within a confined area (i.e. in the pumped region) through non-radiative processes. The thermal energy deposited causes change in density, as a result, the dye laser gain medium suffers from refractive index nonuniformities which leads to refraction/deflection of the dye laser beam passing through it. These thermal effects degrade the optical quality of the medium, reduce the output energy, and change the spectral characteristics. Inhomogeneity in the gain medium created by thermal field is severe, particularly for excitation at high pulse repetition frequency, if the dye medium is static. The simplest technique to minimize these thermal effects in the gain medium and to improve the optical quality of the medium is to rapidly exchange the irradiated dye molecules exposed to the pump laser, before the arrival of the next pulse. Replacement of the dye molecules is easily implemented by flowing of the dye gain medium. The mass flow rate is chosen so as to replace the optically pumped dye molecules after each excitation pulse. Thus, a high repetition rate dye laser requires large flow velocity across the optical pump region. A large liquid flow velocity can be accomplished by linearly constricting the dye cell cross-sectional area, near the dye laser axis. The flow related issues such as dye cell geometry, stagnant boundary layers, flow velocity profiles, cavitations, eddies etc. degrade the optical quality of the lasing medium. Thus, the issues related to the dye cell geometry and the dye gain medium flows are of the main concern for a high repetition rate dye laser. These aspects have not been paid sufficient attention in the past. Thus, a need was felt to design dye cell and studies spectral stability of high repetition rate dye laser. The research work presented in this thesis is primarily directed to extend the understanding of narrow bandwidth high repetition rate dye laser and thereby developing technology to improve its spectral stability. The thesis is organized in nine chapters. In almost all the chapters, after brief review of the topic under investigation, experimental data generated during the course of investigation is presented at length, followed by discussion of results and summary.

Chapter 1: Review on high repetition rate dye laser: Gain medium

Chapter 1 begins with an overview of dye lasers, significance of high repetition rate dye lasers, and issues related to high repetition rate dye lasers. The characteristics of a dye laser gain medium are described**.** The physics of dye laser gain medium which deals with the physical properties of the laser dyes, and important classes (families) of laser dyes that are widely used for laser application, are presented. Spectroscopic properties related to the energy levels, and the possible absorption and emission processes that occur in the typical laser dyes and which are of importance in dye laser action, are discussed. Photo-physical properties of Rhodamine 6G (Rh6G) dye, which is used as the gain medium for the high repetition rate dye laser, are briefly described. A review of the environmental factors such as solvent, concentration and temperature effects on the absorption characteristics of Rh6G dye is presented. These studies help in understanding of the photo-physics of the Rh6G dye laser.

The subsequent chapters describe the studies on the investigated aspects of a high repetition rate dye laser such as experimental methods and diagnostic tools for analysis of the output of the dye laser, characteristics of high repetition rate excitation source, pulsed dye laser resonator, dye circulation system, dye cell, gain medium flow, and finally results of the experiments performed, after putting together these components.

Chapter 2: Diagnostic techniques for high repetition rate dye laser

Chapter 2 covers the diagnostic tools for data visualization/representation and formulation of the experimental technique for dye laser spectral characteristics investigation. A novel method for dye laser output data presentation was proposed and realized. The composite image generation technique, for representing the spectral characteristics of dye laser, was used for the real-time analysis of the dye laser performances. Methodical formulation of the measurement technique for spectral parameters such as wavelength, bandwidth and mode structure etc., were put into practice for dye laser spectral investigations. A diagnostic technique was established for the analysis of the spectral distribution of a high repetition rate dye laser by deriving explicit relationship of the parameters with ring diameter of the Fabry-Perot interference pattern and reference He-Ne laser. An expression for the number of axial modes present and their separation, by knowing the diameter of Fabry-Perot pattern, was realized. The experimental technique for spectral description of the dye laser beam is also discussed in this chapter. The spectral contents and the performance of the dye laser were investigated using high resolution spectroscopy based on Fabry-Perot interferometric technique and composite image generation software. All major instruments involved for the dye laser diagnostics are briefly described.

Chapter 3: Review and studies on Copper Vapour Laser

Chapter 3 gives an overview of CVL, the high repetition rate excitation source for the dye laser. CVL is used as efficient excitation source for tunable dye lasers. Therefore, knowledge of fundamentals of this laser is an essential before its practical application for exciting the dye laser. The characteristics of CVL are reviewed. It covers spectroscopy of a copper atom, energy levels and transition mechanisms, kinetics of CVL, design, assembly details and operating characteristics of CVL. This chapter also covers the theoretical and experimental work done during the present course of investigations on spectral structure of CVL and the effect of electrical input power and buffer gas pressures on the spectral width. Other relevant CVL data such as laser power, pulse shape, etc. are also presented.

Chapter 4: Studies on pulsed dye laser resonator

Chapter 4 of the thesis focuses on the spectral narrowing in a pulsed dye laser resonator. A narrowband dye laser resonator is theoretically and numerically investigated. The dye laser resonator, typically, consists of a partially transmitting output coupler and dispersive optical elements. For a short pulse dye laser, the spectral width of the emission depends mainly on the passive bandwidth of the resonator. Narrow spectral emission through a pulsed dye laser is usually achieved by incorporating a diffraction grating and a beam expander. A prism is used as a compact one-dimensional intra-cavity beam expander. The design parameters of the prism beam expander, and the dispersion of the grating in grazing incidence configuration, are numerically investigated. The dye laser dispersive resonator was simplified to a two-mirror cavity and the transmission coefficient of the partially transmitting output coupler for optimum output dye laser power was numerically and experimentally investigated. A novel technique has been proposed for single mode operation of the dye laser and is experimentally demonstrated.

Chapter 5: Studies on high repetition rate dye laser subsystem

Chapter 5 describes the studies on high repetition rate dye laser subsystems. High repetition rate dye laser subsystems, typically consist of a dye circulation and cooling system for minimization of thermal effects, dye cell for containing gain medium, and a system for characterizing the mass flow through the dye cell. The dye circulation and cooling system was especially designed, fabricated, and employed for the temperature stabilization of the dye gain medium. The mechanical pump, which is one of the key components in any dye solution circulation system, inherently produces vibrations which are transmitted in the flow loop system and hence around dye laser axis. The frequency of the vibrations produced by the dye circulating mechanical pump was studied. This subsystem plays an important part towards stability of the dye laser. The dye cell used to contain the gain medium is one of the crucial components of the dye laser. The dye cell aspect in the dye laser system is explored in this chapter. A dye cell of rectangular straight channel in the pump region has been conventionally used for high repetition rate dye laser to replace the dye solution between successive pump laser pulses. Therefore, one needs a suitable dye cell with smooth liquid flow in the optical pump region. Several dye cells were designed, some of them were modeled and flow characteristics are numerically investigated.

Chapter 6: Studies on spectral stability of a high repetition rate dye laser

Spectral stability of a tunable dye laser is of vital concern in spectroscopic applications. In **Chapter 6**, the spectral stability of CVL pumped dye laser using different dye cells and as a function of Reynolds number of the flow, has been experimentally investigated. Influence of the dye cell geometries and mass flow rates on the stability of a high repetition rate dye laser have not paid much attention so far. During the course of our studies, it was evident that dye solution flow channel and mass flow rates significantly affect the dye laser performance. The spectral stability (wavelength, bandwidth) of dye laser using conventional straight channel, curved (convex-concave), pinched, and spatially profiled convex-plano dye cell in narrow bandwidth resonator were investigated. The methodology adopted for the investigation is spectral stability of the dye laser outputs. It is demonstrated that the geometries of the dye cell as well as mass flow rates significantly affect the spectral stability of a high repetition rate dye laser. Computational analysis of the dye laser gain medium flow has been carried out to explain the observed trends on spectral fluctuations as a function of Reynolds number.

Chapter 7: Studies on fluorescence of Rhodamine 6G dye under high repetition rate excitation

Investigation of the spectral properties of dyes under high repetition rate excitation is of fundamental importance in the utilization of dye as a stable and good optical quality amplifying medium. In **Chapter 7**, the fluorescence characteristic of Rhodamine 6G dye, under high repetition rate excitation, was experimentally investigated in stationary and flowing dye gain medium. A commercially available spectrometer, along with specially developed diagnostics software described in Chapter 2, was used for the investigation of fluorescence emission fluctuations. An estimation of the peak wavelength, spectral width, and area under the widths of an individual spectrum were carried out from the composite image of the recorded spectra. It was observed that the spectral width broadened and large fluctuations are visible in stationary solution as compared to dye flowing medium.

Chapter 8: Studies on thermo-optics characteristics of high repetition rate dye laser

In **Chapter 8**, theoretical and numerical investigations of the dye gain medium inhomogeneity induced by high repetition rate excitation, and its influence on the spectral emission are described. The thermo-optical properties of a narrow spectral width CVL pumped dye laser were experimentally investigated by changing the dye gain medium temperature from 23-35 ^{o}C. The dye laser output parameters such as average optical power, spectral width, wavelength, and beam divergence were experimentally investigated during the dye solution temperature rise from 23 to 35 ^{o}C. The dye laser optical characteristics through gain medium bulk temperature stabilization were also experimentally investigated.

Finally, in **Chapter 9,** a summary of the work carried out during the course of investigations is given. This chapter also provides a brief discussion about the scope of further work in this field.

In summary, the present thesis comprehensively investigates the issues coupled with high repetition rate dye laser, which incorporates studies on inclusive dye laser system i.e. gain medium, resonator, excitation source, diagnostics tools, dye cells, gain medium flow analysis and thermo-optic properties.

LIST OF FIGURES

Figure No.	Title	Page No.
Figure 1.1:	(a) General chemical structure, (b) Absorption, fluorescence and triplet-triplet absorption spectrum of the Coumarin 120	8
Figure 1.2:	(a) General structure of PM dye, (b) Typical absorption, fluorescence and triplet-triplet absorption spectrum of the PM dyes	9
Figure 1.3:	(a) General structure of Rhodamine dye, (b) Absorption, fluorescence and triplet-triplet absorption spectrum of the Rhodamine dyes	10
Figure 1.4:	Simplified typical (a) energy (Jablonski) diagram, (b) energy band diagram	12
Figure 1.5:	(a) Chemical structure, (b) Typical molecular 3D arrangement of Rh6G dye	13
Figure 1.6:	Typical (a) absorption, (b) absorption, fluorescence and triplet-triplet absorption cross-sections of the Rh6G dye	14
Figure 1.7:	(a) Variation of maximum absorbance of Rh6G in methanol, ethanol, ethylene glycol and glycerol with wavelength, (b) absorbance at 510.6 nm in the solvents	17
Figure 1.8:	Typical variation of absorbance of Rh6G with (a) wavelength at 0.1, 0.6 and 2.0 mM, (b) concentration at 510.6 nm and 530 nm	20
Figure 1.9:	Typical variation of absorbance of Rh6G with temperature at (a) 530, and (b) 510.6 nm	22

Figure 2.1:	Optical arrangements for obtaining FP fringe of the dye laser and of the He-Ne laser	33
Figure 2.2:	Typical dye laser (a) fringe, (b) intensity modulation along a line scan across diameter of the fringe	33
Figure 2.3:	Typical identification of peaks position and widths of line intensity profile (a) the first inner most ring, (b) second inner most ring, (c) third inner most ring	34
Figure 2.4:	Typically generated composite image from fringe of (a) dye laser, (b) He-Ne laser, and (c) dye laser	37
Figure 2.5:	Typical (a) window of intensity profiles (multi curves) of the composite image data of Fig.2.4 (a), (b) window menu for setting parameters	38
Figure 2.6:	Dialog window (a) to mark tentative peaks position, (b) for setting parameters of the etalon and widths at peaks percentage height	39
Figure 2.7:	Typical variation of visibility of dye laser (576.00 nm) with slit separation	44
Figure 2.8:	Typical record of Young's double slit (a) fringe, (b) intensity modulation, for copper vapor laser, at 100 microns slit separation	45
Figure 2.9:	The typical record of Young's (a) fringe, (b) intensity modulation, for dye laser, at 100 microns slit separation	46
Figure 2.10:	Typical Fabry-Perot fringe of (a) multimode dye laser, (b) single mode dye laser, (c) He-Ne laser	50
Figure 3.1:	Typical energy level diagram of CVL	58

Figure 3.2: CVL discharge tube schematic 62

Figure 3.3: Typical power supply high voltage circuit 62

Figure 3.4: Typical energy levels splitting of copper atom and its transitions (a) 510.6, (b) 578.2 nm 65

Figure 3.5: Transition probabilities of the hyperfine components of (a) 510.6 nm, (b) 578.2 nm 66

Figure 3.6: Transition probabilities versus frequency shift of hyperfine transitions of (a) 510.6 nm, (b) 578.2 nm, lines for both the isotopes 67

Figure 3.7: Typical (a) Fabry-Perot fringe, (b) intensity modulation along a line of the fringe, for 510.6 nm just above threshold 68

Figure 3.8: Typical (a) Fabry-Perot fringe far above the threshold, (b) composite image of a line scan across the diameter of the fringe, of 510.6 nm lines 69

Figure 3.9: Typical Fabry-Perot (a) fringe, (b) composite image of a line scans across the diameter of the fringe, of 578.2 nm lines near the threshold 70

Figure 3.10: Typical Fabry-Perot (a) fringe, (b) intensity modulation along a line scan across the diameter of the fringe, of 578.2 nm, far above the lasing threshold 70

Figure 3.11: Typical Fabry-Perot (a) fringe, (b) intensity modulation along a line scan across diameter of fringe at 4.2 kW power 73

Figure 3.12: Typical Fabry-Perot (a) fringe, (b) intensity modulation of a line scan across diameter of fringe, of 510.6 nm at 180 mbar pressure 76

Figure 3.13: Typical Fabry-Perot (a) fringe, (b) intensity modulation of a line scan across the diameter of the fringe, of 510.6 nm lines at 470 mbar 76

Figure 3.14: Typical variation of (a) linewidth of peaks **AB** and **B**, (b) relative intensity of peak **B,** with buffer gas pressure 76

Figure 4.1: Typical dye laser setup in (a) Littrow, (b) GIG configuration. 85

Figure 4.2: Systematic of (a) angles involved in beam transmission through prism, and (b) beam expanding view through the right angle prism 88

Figure 4.3: Variation of magnification with (a) angle of incidence, and (b) refractive index, of the prism 90

Figure 4.4: Variation of beam transmission and reflection coefficient with the angle of incidence on the prism 90

Figure 4.5: Variation of bandwidth with angle of incidence on the (a) prism, and (b) grating 92

Figure 4.6: Variation of (a) bandwidth with beam waist size, (b) ratio of bandwidth and wavelength with beam waist size. 92

Figure 4.7: Schematic representation of the (a) dye laser setup, (b) simplified symbolic representation of the dye laser resonator 94

Figure 4.8: Typical variation of normalized output intensity with transmission coefficient of the grating-mirror 96

Figure 4.9: Variation of normalized output (a) intensity (b) optical power with transmission coefficient (0.1- 0.9) of the coupler mirror 97

Figure 4.10: Schematic diagram of dye laser 102

Figure 4.11: Dye laser fringe of (a) three axial modes, (b) double modes,

	and (c) single mode	103
Figure 4.12:	Schematic of rotated positions and direction of tuning mirror	104
Figure 5.1:	Dye circulation and cooling unit schematic	109
Figure 5.2:	Simplified schematics of dye cell and flow loop	110
Figure 5.3:	Variation of vibrational frequency (a) on pipe from dye cell, (b) with Reynolds number of the flow	111
Figure 5.4:	Schematic of the planar duct dye cell	114
Figure 5.5:	Schematic of flow channel of concave-convex duct dye cell	115
Figure 5.6:	Photograph of dye cell fitted in SS assembly and flowing dye solution with (a) optical pumping region, (b) dye laser emission region, faces	116
Figure 5.7:	Velocity profile of the liquid flow through the dye cell as analyzed by CFD along (a) width, (b) length	117
Figure 5.8:	Liquid flow (a) velocity contour, (b) velocity vector, through the dye cell	117
Figure 5.9:	(a) Photograph of glass piece, (b) 3D model, of the dye cell flow channel	118
Figure 5.10:	Typical (a) velocity vector of the liquid flow through the dye cell, (b) photograph of dye cell assembly along with dye solution	119
Figure 5.11:	Velocity profile of the liquid flow through the dye cell as analyzed by CFD along (a) length, (b) width	119
Figure 6.1:	Schematic layout of the dye laser setup	130
Figure 6.2:	Typical Fabry-Perot (a) fringe, (b) composite image generated from a line scan across the diameter of the fringes,	

using the planar dye cell 132

Figure 6.3: Variation of bandwidth and wavelength with time, using planar dye cell 132

Figure 6.4: Typical Fabry-Perot (a) fringe, (b) composite image generated from a line scan across the diameter of the fringes, using concave-convex duct dye cell. 133

Figure 6.5: Variation of bandwidth and wavelength with time, using concave-convex duct dye cell. 133

Figure 6.6: Typical Fabry-Perot (a) fringe, (b) composite image generated from a line scan across the diameter of the fringes, using pinched dye cell 134

Figure 6.7: Variation of bandwidth and wavelength with time, using pinched dye cell 134

Figure 6.8: Typical Fabry-Perot (a) fringe, (b) composite image generated from a line scan across the diameter of the fringes, using convex-plano dye cell 135

Figure 6.9: Typical variation of bandwidth and wavelength with time, using convex-plano dye cell. 135

Figure 6.10: Fluctuations of bandwidth and wavelength with dye cells 136

Figure 6.11: Typical Fabry-Perot fringe of dye laser at 1012 Reynolds number 137

Figure 6.12: Composite images at typical Reynolds number (a) 221, (b) 681, and (c) 1012 138

Figure 6.13: Typical variation of wavelength of modes with time 139

Figure 6.14: (a) Bandwidth and wavelength fluctuations of the central

mode, (b) fluctuations in $\Delta\lambda/\lambda$ with Reynolds number 139

Figure 6.15: Typical composite image of line scans of fringe generated during continuing Reynolds number variation in the range 1012-221 140

Figure 6.16: Typical variation of bandwidth and wavelength with flow rates the continuing Reynolds number variation in the range 1012-221 140

Figure 6.17: Composite image of line scan of fringe generated at the Reynolds numbers 1129, 2258, 3387, 4516, 5645 and 6774 141

Figure 6.18: Variation of bandwidth and wavelength fluctuation as a function of Reynolds number. 142

Figure 6.19: Variation of beam size and intensity of He-Ne laser with Reynolds number 143

Figure 6.20: Temperature variation as a function of distance from the wall, at average flow velocity 0.019 m/s. 144

Figure 6.21: Typical temperature variation as a function of distance from the wall at mean flow velocity (a) 0.5, 1.0 and 1.5 m/s, and (b) 2-8 m/s 145

Figure 6.22: Typical variation of (a) turbulence kinetic energy, and (b) turbulence intensity as a function of distance from window wall 146

Figure 6.23: Variation of maximum kinetic energy and its distance from the wall as a function of Reynolds number 147

Figure 7.1: Systematic of experimental layout for dye excitation and fluorescence measurement 158

Figure 7.2: Typical fluorescence spectrum of Rh6G in the stationary dye solution 158

Figure 7.3: Variation of the fluorescence spectral width and peak wavelength with number of spectrum taken during the observation period 159

Figure 7.4: Variation of peak wavelength intensity and total counts under the lines with number of spectrum taken during the observation period 160

Figure 7.5: Typical fluorescence spectrum at different Reynolds number 161

Figure 7.6: Variation of fluorescence peak wavelength and width with Reynolds number 161

Figure 7.7: Variation of peak wavelength intensity with Reynolds Number 162

Figure 7.8: Composite image of number of successive fluorescence spectrum with time in stationary and flowing medium 163

Figure 7.9: Variation of the fluorescence (a) width, (b) peak wavelengths, with number of spectrum in stationary and flowing medium 164

Figure 7.10: Variation of fluorescence accumulated counts under the width with number of spectrum in the stationary and in the flowing medium 165

Figure 8.1: Schematic of the (a) dye laser layout, (b) photograph of setup 178

Figure 8.2: Variation of the dye solution temperature with time during (a) cooling off , and (b) cooling on 179

Figure 8.3: Variation of dye laser average power with temperature 180

Figure 8.4: Typical dye laser (a) FP fringe at 23.3 ^{0}C, (b) composite

image of the line scan across the diameter of the fringe during temperature change 181

Figure 8.5: Variation of dye laser (a) spectral width with time, and (b) wavelength with number of fringes taken, in the temperature 23-35 ^{0}C range 182

Figure 8.6: Variation of the dye laser horizontal and vertical divergence with time during the gain medium temperature change 183

Figure 8.7: Typical variation of pulse width and total counts under the pulse width with number of pulses taken during the temperature rise in 23.0-35.0 ^{0}C range 183

Figure 8.8: Variation of cavity temperature and gain medium temperature with time 189

Figure 8.9: Typical Fabry-Perot (a) fringe, (b) composite image of the successive fringe 190

Figure 8.10: Typical variation of bandwidth and wavelength with time 190

Figure 8.11: Variation of (a) spectral width with wavelength, (b) average power with time 191

LIST OF TABLES

Table No.	Title	Page No.
Table 1.1:	Typical laser parameters required for AVLIS scheme	4
Table 3.1:	Typical operating characteristics of CVL	63
Table 8.1:	Typical parameter of the materials	174

Chapter 1

Review on high repetition rate dye laser: Gain medium

1.1 Scope of the work

Lasers have become an integral part of life. While they appear in different aspects of our regular activities like shopping and listening to music, they play a vital role in the industries and hospitals improving quality of our life. The technique of making laser light involves various technological challenges, including tailoring the properties of light according to the specific needs. Many practical applications require high output power, high efficiency, good beam quality and, more importantly, wavelength tunability. Development of such tunable laser sources, catering to ever-demanding spectroscopic applications, is a very active field of research [1.1]. Ever since the invention of the laser, there has always been a great deal of interest in the development of continuously tunable coherent light sources. Such sources had a great impact not only on research and industry, but also on the society as a whole.

Tunable lasers are among the most studied and successful lasers [1.1]. These lasers are categorized into group of broadly tunable, discretely tunable and/or line-tunable [1.1]. Broadly tunable lasers are the sources of highly coherent emission in which the output wavelength can be changed continuously, without discontinuous changes in output power. The organic dye lasers, commonly known as dye lasers, are the first broadly tunable laser [1.1]. Continuous wavelength tunability, efficient narrow bandwidth operation, wide spectral coverage and simplicity had made the organic dye lasers to create profound impact on a plethora of fields [1.1-1.2]. Dye laser spectral tunability from near ultraviolet (UV) to near infrared (IR) is possible by the existence of hundreds of laser dyes as well as the availability of optical pump sources of appropriate wavelength [1.1-1.7]. The tuning range of dye laser can also be extended to

UV and IR ranges by frequency mixing in nonlinear optical materials. Tunable operations are available from broadband to narrowband single mode, by virtue of variety of optical resonators [1.4, 1.7]. Due to these varied characteristics, the dye lasers had been very efficiently applied to physics, astronomy, spectroscopy, photochemistry, isotope separation, material diagnostics, medicine, etc [1.1].

Optical parametric oscillators (OPOs) offer attractive alternative solution to obtain tunable coherent radiation in spectral regions, $300 \leq \lambda \leq 3000$ nm [1.1]. These days, OPOs are emerging as compact, state-of-the-art all-solid-state, tunable light sources, alternative to the conventional dye laser. An OPO relies on a nonlinear optical process termed as parametric down-conversion. This process can only produce significant output when a so-called phase matching condition is satisfied. Despite their remarkable capabilities, as demonstrated in years of research, the OPOs have so far not found widespread use in commercial products. Some of the reasons for this are as follows

(a) Containing at least pump laser, OPO and a temperature-stabilized crystal oven, hence parametric oscillator systems are more complex than pure laser systems,

(b) The requirement for phase matching makes the operation more delicate than laser gain media, which are usually more tolerant in terms of crystal temperature. The OPOs requiring a temperature-stabilized oven for the crystal are certainly less attractive for many applications due to the complexity, heat dissipation, etc.

(c) Some nonlinear crystal materials are hygroscopic and some are difficult to obtain with robust anti-reflection coatings

(d) Enhancement of thermal de-phasing at high repetition rate operation.

In spite of all these, for spectroscopic applications demanding considerable wavelength range, an OPO system would be a most attractive option [1.1].

The landscape of tunable sources seems to change deeply with the advent of supercontinuum sources, which offer broadband spatially coherent light covering the whole visible and IR spectrum (400–1800 nm). However, these sources still have low output powers per unit nm (typically, mW/nm) and are not very useful whenever only a specific spectral region has to be addressed, since in that case only a tiny fraction of the light is available after filtering.

Tunable organic solid-state dye laser devices have been worked so far best in the low pulse-repetition-frequency (prf) operational domain and are mostly suited for analytical applications in the laboratory [1.2]. Development opportunities, for narrow-linewidth solid-state oscillator-amplifiers system delivering Joule level pulsed energies, still remains [1.1-1.2].

Therefore, liquid organic dye laser is probably the most conceptually simple and reliable tunable laser source, operating at high pulse repetition frequency, in the visible regions. Moreover, dye laser based on liquid solution possesses unique advantages such as excellent solubility of dye, low laser threshold, wide tuning range, long service life and homogeneous optical quality medium. In liquid dye laser, dye gain medium is easily cooled by a dye solution flow system. Thus, at present there is no substitute for the liquid dye laser operating at kHz repetition rate and delivering high average power for the pilot product projects. This is the reason why the liquid dye laser had been the most commonly used coherent tunable radiation sources in various fields over the last four decades.

Dye lasers have been around nearly as long as the laser itself. As a result, there is now a wide range of commercially available technologies meeting the diversified needs of applications [1.1]. Indeed, nature of the applications dictates the use of a particular laser system. The suitability of a laser system to a given application take account of spectral region, tuning range, output power or energy, emission linewidth, pulse duration and pulse repetition frequency (in case of pulsed lasers). The dye laser continues to offer unique and exciting tunable coherent radiation directly in the visible spectrum, specifically, in the applications like atomic vapor laser isotope separation (AVLIS) schemes which require high average powers [1.8-1.12]. The necessities for such dye laser [1.11] are narrow linewidth (few GHz) to separate the absorption line between ^{235}U and ^{238}U (isotope shift), high repetition rate (few kHz) to fully illuminate high speed uranium vapor stream and high average power for efficient separation. Additionally, these schemes require that the dye laser output such as wavelength and spectral width should be stable over sufficiently long-time. The typical tunable laser parameters needed for this scheme is summarised in Table 1.1.

Table 1.1: Typical laser parameters required for AVLIS scheme [1.11]

Laser characteristics	Requirements	Remarks
Pulse duration	20-200 ns	Short in comparison with atomic state lifetime
Pulse repetition frequency	10 kHz	Adequate to illuminate the entire flowing vapor
Pulse energy	0.1-1 J	Pulse energy sufficient to saturate atomic transitions
Wavelength	Tunable	Overlap with atomic transitions
Bandwidth	$\sim$ 1-3 GHz	Should match inhomogeneously broadened atomic line
Wavelength stability	$\sim \pm$ 30 MHz	Good spectral overlap of the laser and atomic line should be maintained.

Therefore, development of stable pulsed dye laser system is essential for an application requiring high pulse repetition frequency and high pulse energy.

In the last few years [1.1], a huge progress is made on the dye laser pump sources such as frequency doubled crystalline lasers technology, both in repetition rate and average power. The most recent work by Yu-Ye et al [1.13] and references there in account for availability of an average power 165-W green laser (wavelength 532 nm, pulse width 162 ns, pulse repetition rate 25 kHz) by employing intracavity frequency doubling of a diode-side-pumped double Q-switched composite ceramic Nd:YAG. Frequency doubling of fiber lasers, whose most of the wavelength lie in the infrared, can provide laser output in the visible. For example, a neodymium doped fiber laser operating at 1064 nanometers can be frequency doubled to emit in the green at 532 nanometers. However, 2^{nd} harmonic efficiency is poor due to large bandwidth of fiber lasers. Recent reports [1.1, 1.14] demonstrated leading-edge scientific applications of fiber lasers systems.

All these sources are reliant on nonlinear conversion stages (i.e. through indirect processes) and hence add to system complexity. Therefore, despite the enormous development in solid-state laser sources, copper-vapor-laser pumped dye lasers emitting in the 565-605 nm region continue to be rather unique sources of tunable narrow-linewidth coherent radiation given their capability to reach high-average powers at repetition rates in the kHz region [1.2-1.3]. Though mature technology exists for CVL pump dye laser oscillator as well as MOPA system, it has been well recognized that thermal problem create beam instability and are of the main concern for application of such high repetition rate dye lasers. In high repetition rate dye laser, issues of spectral stability linked with dye cell flow channel geometry, gain medium inhomogeneity and flow characteristics and thermo-optics properties were not been paid sufficient attention in the past. Therefore, in the present work, in-house developed CVL pumped dye laser is being considered for further technological advancements in terms of spectral stability. Studies on the related crucial issues associated with high repetition rate dye laser have been taken up for the investigations, which constitute the present thesis.

A brief review of visible dye laser gain medium physical, spectroscopic properties and photo physics of Rhodamine 6G dye, the most commonly utilized in high repetition rate operation, is presented in the subsequent sections of this chapter.

1.2 Physical properties of dye laser gain medium

Organic dye molecules are complicated structures composed of a large number of atoms of several species, which impart color to the otherwise colorless material. However, the main characteristic of such organic compounds is to have a strong absorption band somewhere in between ultraviolet to the near infrared regions [1.16]. The absorption distinctiveness of the dye is depicted via a unit(s) called chromophore (color-bearing group). In addition to chromophores, most dyes also contain groups known as auxochromes (color helpers), examples of which are carboxylic acids, sulfonic acid, amino, and hydroxyl groups. Presence of auxochromes, which are not responsible for color, can shift the color of a colorant. Based on the molecular structure and other properties of thousands of organic dyes available, only some of the dyes meet the stringent criteria for becoming useful laser dyes, which have the following characteristics [1.16-1.24]:

- High solubility in practical solvents
- Strong absorption at excitation wavelength and minimal absorption at lasing wavelength, i.e., minimum overlap between absorption and emission spectra
- High quantum yield (0.5–1.0)
- Good photochemical and photophysical stability
- A short fluorescence lifetime (few ns)

• Low absorption in the first excited state at the pumping and lasing wavelengths

• Low probability of intersystem crossing to the triplet state

• High purity

Generally, laser dyes are complex molecules containing a number of ring structures. The laser dyes can also be categorized into different classes on the basis of their structures that are chemically similar. The structure and composition of the molecule has an important influence on spectral absorption/emission characteristics. Coumarins, boron-dipyrromethene (also known as PM dyes) and xanthenes are important classes (families) of laser dyes that were extensively used for laser applications. Succinct structural preface of these families of laser dyes is presented for completeness.

1.2.1 Coumarin dyes

It consists of a benzene ring to which a benzene heterocycle, has been fused. Coumarin derivatives with an amino group in the 7-position are very efficient laser dyes in the blue and green regions of the spectrum [1.23-1.24]. A number of derivates such as Coumarin 1, Coumarin 153, Coumarin 480, Coumarin 481, Coumarin 503, Coumarin 521 etc. are the most commonly used Coumarin dyes. Fig.1.1 depicts a typical (a) structure of Coumarin dye [1.23], (b) absorption, fluorescence and triplet-triplet absorption spectrum of the Coumarin 120 [1.26]. It's spectroscopic and, consequently, laser-action characteristics strongly depend on the nature of the auxochromes such as –OH, –OCH3, –NH2, –NHCH3, –N(CH3)2 and other electron-donating substituent's in the 7-position in the ring. Coumarin dyes have the tendency for low photostability and degrade due to UV absorption.

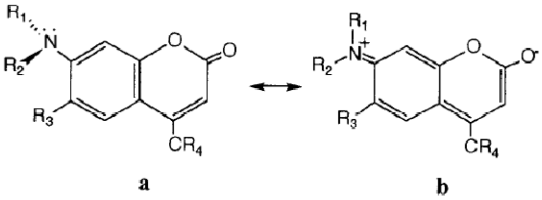

(a)

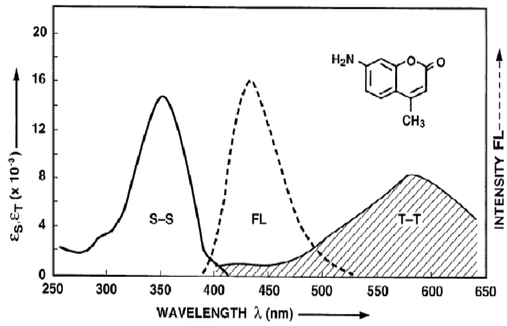

(b)

Figure 1.1: (a) General chemical structure [1.24], (b) Absorption, fluorescence and triplet-triplet absorption spectrum of the Coumarin 120 [1.26]

1.2.2 Pyrromethene–BF_2 (PM–BF_2) dyes

Pyrromethenes are composed of dipyrromethene complexed with a disubstituted boron atom, typically, a BF_2 unit. The PM BF_2 are an important class of laser dyes. They are fluorescent in the green–yellow visible region of the electromagnetic spectrum. The properties of these dyes can be modulated to some extent by incorporating the adequate substitution in the molecular structure of the parent chromophore. The general structure of PM dye is shown in Fig.1.2 (a) while their typical absorption, fluorescence and triplet-triplet absorption spectrum in Fig.1.2 (b). A PM-BF_2 is a highly efficient laser dye, which has low intersystem crossing rate, reduced triplet absorption coefficient, low excited-state-absorption coefficient, and high fluorescence quantum yield. Unfortunately, it is a relatively unstable laser dye because of the presence of aromatic amine groups in its structure that leave it vulnerable to photochemical reactions with oxygen. PM567, PM580 and PM597 are the most studied dye in this family.

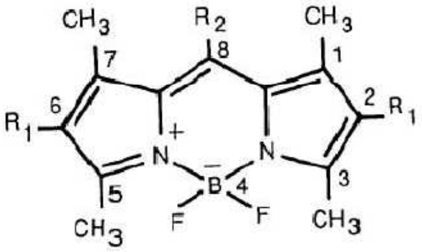

(a)

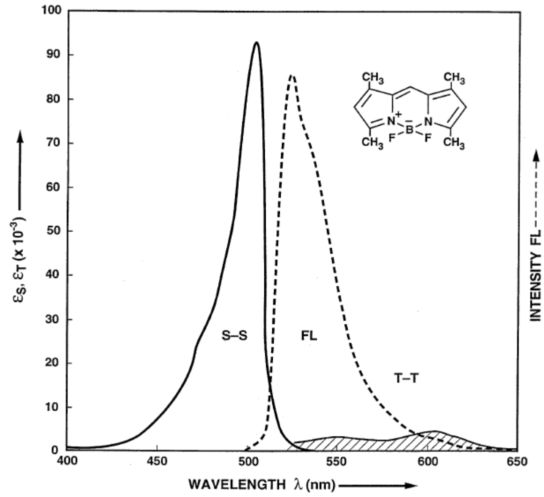

(b)

Figure 1.2: (a) General structure of PM dye, (b) Typical absorption, fluorescence and triplet-triplet absorption spectrum of the PM dyes [1.26]

1.2.3 Rhodamine dyes

The Rhodamines are often referred to as xanthene dyes, which are cationic dyes derived from the xanthylium ring with two amino groups at the 3- and 6- positions and a pendant ortho-carboxyphenyl group at the central C9 carbon, as shown in Fig.1.3 (a). Fig.1.3 (b) shows the typical absorption, fluorescence and triplet-triplet absorption spectrum of Rhodamine dyes. They cover the green to red portion of the spectrum and generally have good photo-stability [1.28]. The wavelength of the most intense fluorescence depends on the length of the chromophore, with longer chromophores giving rise to longer wavelength emission. Rhodamine 6G, Rhodamine B, Rhodamine 640 and Rhodamine 110 dyes belong to this family.

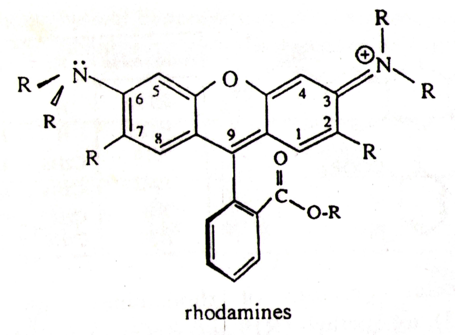

(a)

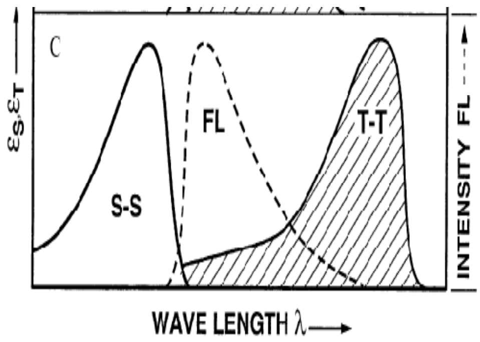

(b)

Figure 1.3: (a) General structure of Rhodamine dye, (b) Absorption, fluorescence and triplet-triplet absorption spectrum of the Rhodamine dyes [1.26]

1.3 Spectroscopic properties of laser dyes

Dyes are atoms of the conjugated chain lying in a common plane linked by σ bonds while π bond is formed by the lateral overlap of the π electron orbitals. The π electrons have a node in the plane of the molecule and form charge cloud above and below this plane along the conjugated chain [1.16]. The π-bond is responsible for a variety of properties, such as the *torsional rigidity* of a double bond but more importantly for the *electron delocalization* along the backbone of the molecule. This extended system of conjugated bonds not only has a profound effect on chemical reactivity, but also influence the spectroscopic properties. The basic mechanism responsible for light absorption by compounds containing conjugated double bonds is the same, in whatever part of the spectrum these compounds have their longest wavelength absorption band, whether near-infrared, visible or near-ultraviolet. The absorption and fluorescence spectroscopic properties of organic compounds are very well documented [1.29-1.33].

Electronic levels in organic molecules, similar to atoms, consist of discrete energy levels, E_1, E_2, . . . Dye molecules have two set of electronic states, one is singlet manifolds and other is triplet manifolds (referred as S and T). The five most important states required for a description of the dye laser are shown in Fig.1.4 (a). S_0 is the ground state, S_1 and S_2 are the first and second excited single state. T_1 and T_2 are the first and second triplet state of the dye molecule. Each electronic state has a number of vibrational levels superimposed on it. For dye molecules, the average separation between the vibrational levels is generally in the 1200-1600 cm^{-1} range [1.20]. In addition, each vibronic level has closely spaced rotational levels superimposed on it. These rotational levels are broadened by frequent collisions with solvent molecules and form a near continuum between each vibrational level. This gives rise to the characteristic broad, structureless absorption and emission bands in the electronic spectra of dye molecules in solution [1.11]. This is depicted in Fig.1.4 (b). At the room temperature ($kT \backsimeq 200\ cm^{-1}$), most of the molecules are in the lowest vibrational level of S_0, if the ground state S_0 of the molecule is in thermal equilibrium with its surroundings. In transition from S_0 to various rotational-vibrational levels of the excited singlet states S_0, S_1, S_2 ..., the electron maintains its spin orientation, in accordance with the Franck-Condon principle. These processes referred to as the singlet–singlet (S–S) absorption. Depending on the wavelength of excitation, the dye molecule may be excited to the first excited singlet state or higher excited singlet state, from which they relax rapidly through nonradiative transition within picoseconds [1.16, 1.21] to the lowest vibronic level of S_1. These times are very short in comparison to the lifetime of the S_1 state, which is of the order of nanoseconds [1.16]. The relative probabilities of these different modes of de-excitation are governed by the structure of the dye and the properties of the solvent used [1.16-1.19].

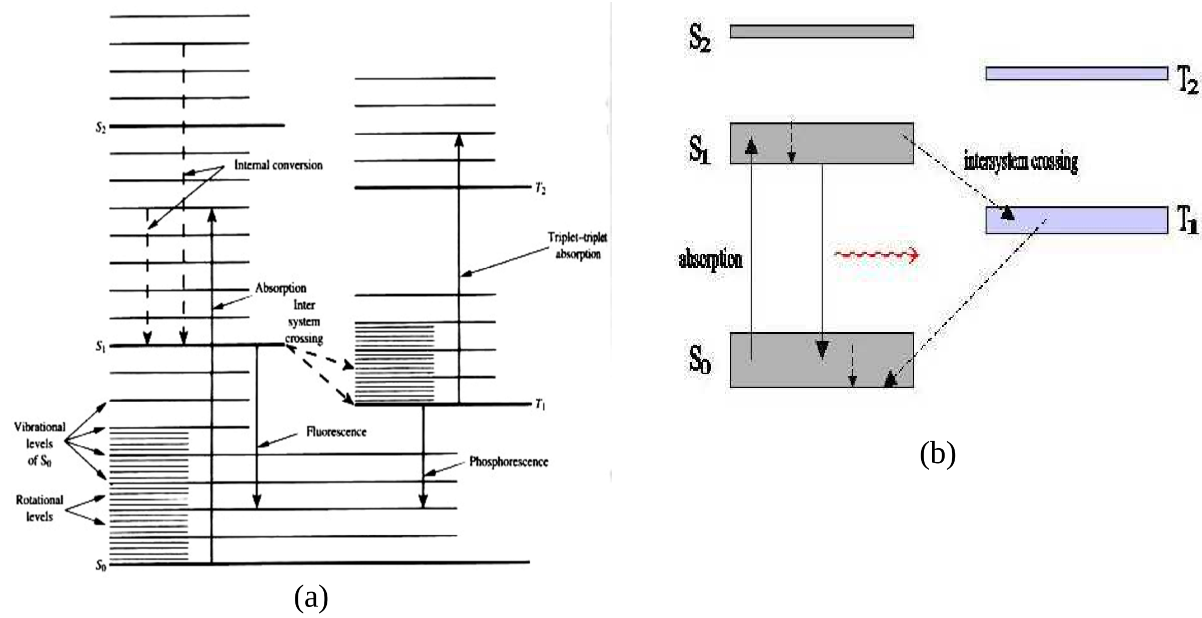

Figure 1.4: Simplified typical (a) energy (Jablonski) diagram [1.26], (b) energy band diagram

Besides the nonradiative decay of the excited singlet state S_1 directly to the ground state, a molecule may enter into a triplet state where electron also switch its spin orientation. These radiationless transition termed *intersystem crossing*, can be induced by internal perturbation (spin-orbit coupling, substituents containing nuclei with high atomic number) as well by external perturbations (paramagnetic collision partners, like O_2 molecules in the solution or solvent molecules containing nuclei of high atomic number) [1.16]. Accumulation of molecules in the triplet state T_1 by intersystem crossing leads to subsequent optically allowed $T_1 \rightarrow T_2$ transition, which partially overlaps the $S_1 \rightarrow S_o$ fluorescence spectrum. The transition from$T_1 \rightarrow S_0$ involves flipping its spin and is a relatively slow process. The triplet state life time τ_T is relatively long [1.22] (usually in the 10^{-7} to 10^{-3} s range), depending on the environment of the dye. Thus intersystem crossing (and triplet state absorption) of dye molecules can reduce or cancel the laser gain and the population of S_1.

The other bands placed in the UV region are due to the electronic transition to higher excited states, i.e., the S_2 electronic state. The fluorescence band is nearly the mirror image of the $S_0 \rightarrow S_1$ absorption band. Ground state absorption at lasing wavelengths is due to the partial overlap of fluorescence and absorption spectra of the dye. This absorption arises from the molecular population in the higher vibrational-rotational levels of S_0.

1.4 Photo physical properties of Rhodamine 6G dye

Rhodamine 6G (Rh6G), also called Rhodamine 590 chloride, is the best known of all laser dyes. It is a xanthenes derivative, ionic and highly polar dye. The Rh6G dye exhibits an absorption peak in ethanol at 530 nm and a fluorescence peak at 556 nm. It has a high fluorescence quantum yield of 95% [1.34], a low intersystem crossing rate [1.35-1.36], and low excited-state absorption [1.37]. These properties made it a highly efficient dye for laser applications. Therefore, it is the most widely studied and is regarded as the yardstick for laser dyes. Thus, in subsequent discussion, in this thesis, Rh6G is taken as the gain medium for the dye laser. Fig.1.5 depicts (a) the chemical structure, and (b) the typical molecular 3D arrangement of Rh6G dye. Fig.1.6 shows the typical (a) absorption, (b) absorption, fluorescence and triplet-triplet absorption cross-sections of the Rh6G dye.

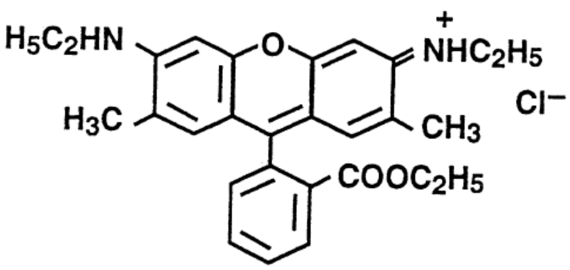

(a)

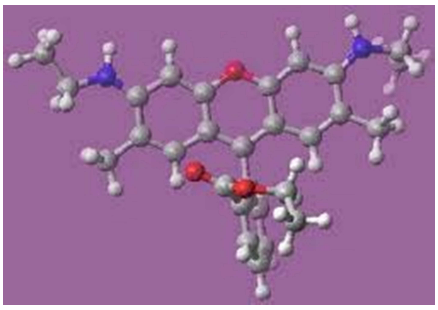

(b)

Figure 1.5: (a) Chemical structure, (b) Typical molecular 3D arrangement of Rh6G dye

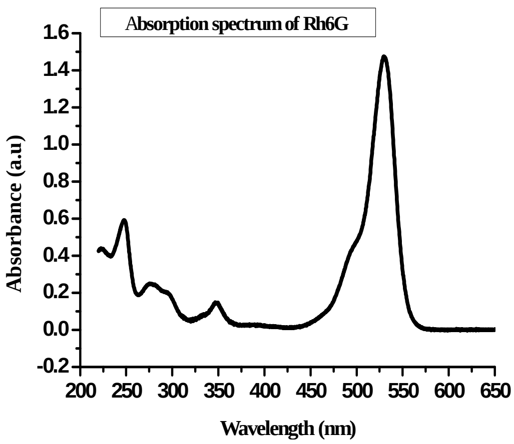

(a)

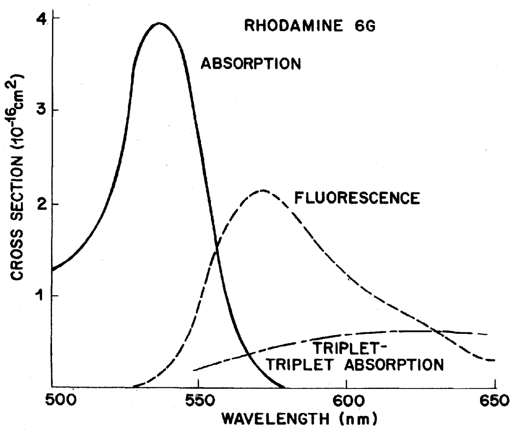

(b)

Figure 1.6: Typical (a) absorption, (b) absorption, fluorescence and triplet-triplet absorption cross-sections of the Rh6G dye [1.17]

The environmental factors such as the solvent, concentration of the dye and temperature can appreciably affect the photo-physics of laser dyes. Therefore, brief review of the solvent, concentration and the temperature effects on the photo physical properties of the dye gain medium is described here for the completeness.

1.4.1 Solvent effects

In general, the dye lasers use a lasing medium composed of a complex fluorescent organic dye whose relative amounts can vary continuously up to the limit of solubility (saturation in certain solvent). For this reason, the solvent plays a major role on the photo physics of the dyes. The solvents for dissolving organic dyes may be divided into three main categories [1.38]:

(a) Simple organic solvents e.g., methanol, ethanol, ethylene glycol, etc., or their admixtures,

(b) Water based solvent, e.g., pure water or water based solutions such as ammonyx LO (lauryl dimethylamine oxide), Triton-X100, urea etc.,

(c) Mixture of water based solvent and organic solvents, e.g., ethylene glycol/ammonyx LO etc.

The solvent used for dye laser must possess the following essential properties:

- The dye should be soluble in the solvent
- The solvent must be transparent both to the pump and to the dye laser radiation
- The solvent must be photo-chemically stable when exposed to the pump light

The effect of the solvent on the absorption and fluorescence bands of a chromophore can be divided into the general effects and the specific solute-solvent interactions. The general solvent effect is a consequence of the solvation of the dipole moment of the chromophore in both the ground and the excited states [1.39-1.40] and is associated with some macroscopic properties of the solvent, such as the solvent polarity or solvent dipolarity/polarizability. Specific solute-solvent interactions depend on the nature of both partners that includes solute-solvent H-bond interactions and any other kind of solute-solvent complex formation (charge-transfer complexses, exciples, etc.). The specific Rhodamine-protic solvent interactions [1.41-1.42] are

(a) H bonding between the hydroxyl group of the protic solvent and the electron lone pair of the amino group. This interaction prevents the participation of the amino electron lone pair in the π-system of the xanthylium, which causes a spectral shift to higher energies.

(b) Electrostatic interaction between the positive charges of the iminium group of Rhodamine with the electron lone pair of the hydroxyl group of the solvent. This interaction stabilizes the resonance structures, leading to a bathochromic spectral shift.

(c) Solvation of the carboxylate group. This interaction prevents the intramolecular electrostatic interaction between the xanthylium positive charge and the COOR group, which causes a spectral shift to lower energies.

(d) H bonding between the H atoms of non- or monoethylamino Rhodamines and the electron lone pair of the hydroxyl group of the solvent. This interaction increases the electron density of the amino group, favoring the delocalization of the amino electron lone pair throughout the xanthenes ring, which leads to a bathochromic shift.

The lasing efficiency of Rh6G based on aqueous solution is low, in spite of very favorable thermo-optical properties of water. The main reason for the reduction in the efficiency of lasing in aqueous solutions of dye is the aggregation of the dye molecules [1.43-1.44] producing nonluminescing complexes in the form of nonradiative dimers. Measurements have shown that the quantum efficiency of an aqueous solution of Rh6G falls to 0.4 in the range of working concentrations, whereas in an ethanol solution, where the association of Rh6G molecules is slight, it amounts to 0.98 [1.16]. However, water-based dye solutions with de-aggregating agents, such as surfactants [1.45] and other additives were used for dye laser [1.46]. Heavy water based solutions of Rh6G has been shown superior to both ethanol and normal water solvent on account of the lower thermo-optic effects and higher photostability of laser dye when dissolved in heavy water [1.47].

In this thesis work, the normally utilized organic solvent ethanol was used for most of the studies unless otherwise stated. For the sake of completeness, absorption characteristics of Rh6G dye in other organic solvents, from low to high viscous medium, like methanol, ethylene glycol and glycerol are also investigated. Commercially available UV-visible spectrophotometer was used for absorbance measurement of Rh6G dye in methanol, ethanol, ethylene glycol and glycerol. Absorbance in the range of radiation 400-600 nm in these solvent is presented, as excitation source (CVL) for dye is in the visible region. It is obvious that Rh6G in ethanol shows largest absorption among others. Furthermore, peak wavelength absorption and absorption at excitation wavelength of

CVL (510.6 nm) was analyzed. Fig.1.7 (a) shows the variation of maximum absorbance of Rh6G in methanol, ethanol, ethylene glycol and glycerol with wavelength, while Fig.1.7 (b) shows the absorbance at 510.6 nm in these solvents. These experimental results showed that ethanol has the highest absorptivity amongst organic solvents.

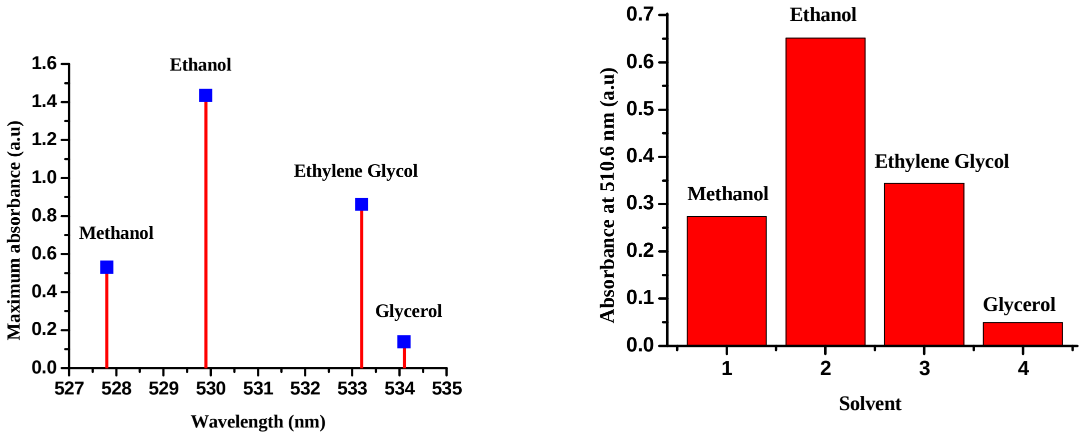

(a) (b)

Figure 1.7: (a) Variation of maximum absorbance of Rh6G in methanol, ethanol, ethylene glycol and glycerol with wavelength, (b) Absorbance at 510.6 nm in the solvents

1.4.2 Concentration effects

The shape of the absorption spectrum of Rhodamines changes with the concentration of the dye [1.48]. For dye such as Rh6G, an increase in the concentration implies an aggregation of the dye that causes changes in the absorption spectra (methachromasy effect) and on the fluorescence quenching [1.49-1.50].

Organic dyes have a natural tendency to form aggregates [1.18-1.19] in the solution, because of their typically flat geometries. The color, physical properties such as the solubility and photo physical behavior of dyes are affected due to aggregate formation [1.51]. Aggregation can cause to loss in main absorption band and the observation of a new band relative to the monomeric dye absorption. Aggregation is promoted by increasing the dye concentration in a solution or lowering the temperature [1.16]. Increase of dye concentration; produce the formation of dimers, trimers or higher aggregates [1.51-1.53]. The equilibrium between monomers and dimers shift to the latter with increasing dye concentration and with decreasing temperature. The dimers usually have a strong absorption band at shorter wavelengths than the monomers and often an additional weaker absorption band at the longer-wavelength side of the monomer band [1.16]. The dimers are generally only weakly fluorescent or not at all. They constitute absorptive loss of the pump power and also increase the cavity losses owing to their long-wavelength absorption band, which is in the same region as the fluorescence of the monomers [1.16]. Apart from the concentration, the change of solvent from polar to less polar or vice versa will also affect dye aggregation or de-aggregation. The aggregation of dyes in aqueous solution can be suppressed by the addition of organic compound, which form a cage around the hydrophobic dye molecules and thus shield them from each other and from the water [1.18].

The dye concentration also affects the fluorescence characteristics (wavelength, quantum yield, and lifetime) of laser dyes, not only due to a possible dye aggregation but also because of reabsorption and reemission phenomena. Reabsorption/reemission in any concentrated system, where absorption and emission band overlaps, affects fluorescence (and hence lasing properties). The increase in the dye concentration causes a shift in the fluorescence band to lower energies. Consecutive reabsorption/reemission processes lengthens the mean time in which the molecules are in the fluorescent excited state, thus increasing the life time.

Several types of excited state solute-solute interactions are common at high solute concentrations. The aggregation of excited solute molecules with unexcited molecules of the same type may result in new excited molecules called excimer, which may either not luminesce, or may luminesce at lower frequency than the monomeric excited molecules. As excimer formation takes place in the excited state, a shifting of fluorescence spectrum is observed. However, after fluorescence, the deactivated polymer (which is unstable in the ground state) rapidly decomposes, and hence the absorption spectrum does not reflect the presence of the excited complexes. A fluorescence quenching takes place due to the deactivation of the lowest excited singlet state by interaction with other species in the solution.

The active media of dye lasers normally use concentrated dye solution. Indeed, diluted solutions of laser dyes do not give laser signals because the losses in the resonator are higher than gains. However, at higher concentration, the pump beam is absorbed in a very thin region close to the dye cell wall. This leads to a larger divergence in the horizontal direction (transverse to the direction of propagation of the dye laser beam), resulting in a low feedback efficiency from the output coupler [1.54]. Thus, at higher concentration, the laser efficiency decreases due to aggregation as well as diffraction losses. However, at optimum concentration, which depends on the nature of the active medium and on the experimental conditions, the system can give rise to maximum laser output power. Measurement of absorption characteristics of Rh6G in ethanol at 0.1, 0.6 and 2.0 mM has been carried out. Fig.1.8 shows the typical variation of absorbance of Rh6G with (a) wavelength, at 0.1, 0.6 and 2.0 mM, (b) concentration, at 510.6 and 530 nm.

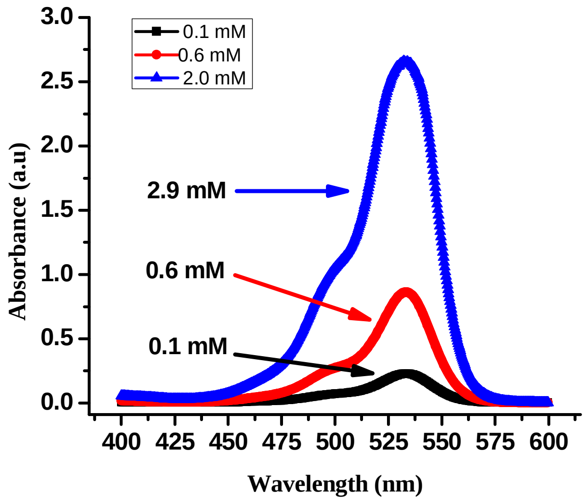

Figure 1.8 (a): Typical variation of absorbance of Rh6G in ethanol with wavelength, at 0.1, 0.6 and 2.0 mM

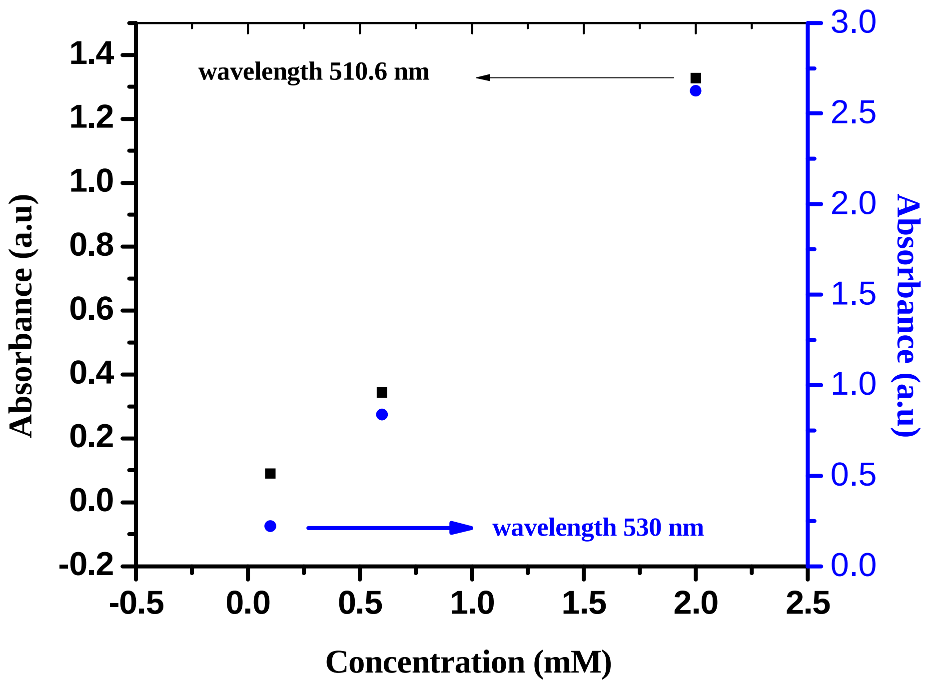

Figure 1.8 (b): Typical variation of absorbance of Rh6G with concentration, at 510.6 nm and 530 nm

1.4.3 Temperature effects

In a dye laser, using dye solution as gain medium, the performance is significantly affected by physical properties of the dye solution. The physical property of the dye solution is mainly governed by solvent properties. Temperature of dye solution influences photo physical properties of dye as well as solvent in many ways, with practically no thumb rules. Temperature plays an important role in the performance of dye laser. Apart from the dye solution physical properties (e.g., spectral range, viscosity), refractive index of dye solution is also affected by temperature [1.55]. Variations of the refractive index with temperature influence the spectral properties of the dye laser. The refractive index of thermal origin in organic dye solutions, arises from non-radiative energy transfer from the dye molecules to the solvent molecules, therefore, strongly governed by the thermo-optic properties of the solvent. El-Kashef [1.56-1.57] had theoretically and experimentally investigated the dye solution refractive index and its thermo-optic constants extensively. Wide-ranging results on macroscopic and microscopic parameter of the dye solvents were realized for thermal analysis of dye laser solutions media [1.56]. Apart from these macroscopic refractive index modulations, temperature has many more effects on microscopic molecular levels too. The temperature also perturbs the solvation energy, excited state reactions, solute-solvent caging and the rate of non-radiative processes, which in turn influences the dye emission characteristics. In this way, refractive index and thermal coefficient of refractive index are considered as decisive factors for the gain medium properties of dye lasers [1.58].

The absorption characteristics of Rh6G dye in ethanol solvent was investigated at different temperature. Fig.1.9 shows the typical variation of Rh6G absorbance with temperature, at (a) 530 and (b) 510.6 nm.

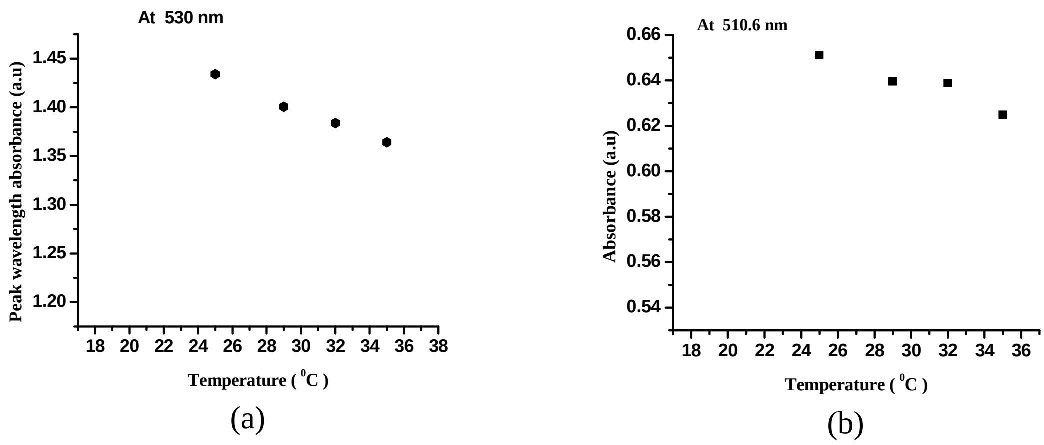

Figure 1.9: Typical variation of absorbance of Rh6G with temperature at (a) 530, and (b) 510.6 nm

1.5 Summary

The need for high repetition rate and importance of liquid dye laser are described. The recent technological advancements in this field are reviewed briefly. Properties of dye gain medium and criteria for becoming laser grade dye are explained. Succinct introduction to structural and spectral characteristic of widely used dyes such as Coumarin, Pyrromethene and Rhodamine families are presented for completeness. Spectroscopic characteristics and pathways for excitation and radiative/nonradiative deactivation of singlet and triplet states of organic molecules are understood through simplified energy (Jablonski) diagram. Photo physical properties of Rh6G are investigated. Influences of solvent, dye concentration and temperature on absorption/emission properties of Rh6G dye are reviewed and measurement of absorbance in various organic solvents such as methanol, ethanol, ethylene glycol, and glycerol are carried out. Effects of concentration and temperature on absorption characteristics of Rh6G dye in ethanol are investigated. These studies on gain medium will help in understanding the results on high repetition rate dye laser, considered in the later chapters of this thesis work.

References

[1.1] F. J. Duarte (ed.), 2nd edition, *Tunable Lasers Applications,* CRC Press, Taylor & Francis Group, New York 2009

[1.2] F. J. Duarte, Progress in Quantum Electronics **36**, 29 (2012)

[1.3] F. J. Duarte, Progress in Quantum Electronics, 2013 http://dx.doi.org/10.1016/j.pquantelec

[1.4] F. J. Duarte (ed.), *Tunable Lasers Handbook,* Academic, New York 1995

[1.5] F. J. Duarte and L. W. Hillman, *Dye Laser Principle,* Academic Press, New York, 1990

[1.6] F. J. Duarte, *High Power Dye Lasers,* Springer-Verlag, Berlin 1991

[1.7] F J Duarte, *Tunable Laser Optics,* Elsevier Academic, New York 2003

[1.8] Jensen *et al*, Laser Focus **12**, 5 (1976)

[1.9] J. A. Paisner, Appl. Phys. **B46**, 253 (1988)

[1.10] P. T. Greenland, Contemporary Phys. **31**, 405 (1990)

[1.11] Bass *et al*., Appl. Opt. **31**, 6993 (1992)

[1.12] P. Ramakoteswara Rao, Current Science **85**, 615 (2003)

[1.13] Yu-Ye *et al*, Chin. Phys. **B 21**, 094212-6 (2012)

[1.14] J. Ding, B. Samson and P. Ahmadi, Laser Focus World, page 39, February, 2011

[1.15] Costela *et al*., Appl. Phys. **B 60,** 383 (1995)

[1.16] F. P. Shäfer, *Dye Laser*, Springer-Verlag, Berlin, 1990

[1.17] C. V. Shank, Rev. Mod. Phys. **47**, 649 (1975)

[1.18] F. L. Arbeloa, T. L. Arbeloa, and I. Lopez Arbeloa, *Handbook of Advanced Electronic and Photonic Materials and Devices,* ed. H.S. Nalwa, Vol. **7**, 2001

[1.19] A. Dienes, and D.R. Yankeleich, *Tunable dye lasers*, Encyclopedia of Applied Physics, Vol. 22 (G.L. Trigg, ed.), Wiley-VCH, New York, pp. 299-334

[1.20] A. Penzkofer *et al*, Chem. Phys. Lett. **44**, 82 (1 976)

[1.21] J.B. Birks, *Photophysics of Aromatic Molecules*, Wiley Interscience, London, 1970

[1.22] F. P. Shäfer *et al*, Opt. Commun.**28**, 792 (1973)

[1.23] G. S. Shankarling and K. J. Jarag, Resonance, September 804 (2010)

[1.24] F. L. Arbeloa, T. L. Arbeloa, and I. L. Arbeloa, J. Luminescence **68,** 149 (1996)

[1.25] M. Maeda, Laser Dyes, Academic Press, New York 1984

[1.26] Theodore G. Pavlopoulos, Progress in Quantum Electronics **26,** 193 (2002)

[1.27] Paviopoulos *et al*, Appl. Opt. **31**, 7089 (1992)

[1.28] T. G. Pavlopoulos, D.J. Golich, J. Appl. Phys. **64,** 521(1988)

[1.29] S.R. Becker, *Theory and Interpretation of Fluorescence and Phosphorescence*, Wiley-Interscience, New York, 1969

[1.30] B. Berlman, *Handbook of Fluorescence Spectra of Aromatic Molecules*, Academic Press, New York 1971

[1.31] D.M. Hercules (Ed.), *Fluorescence and Phosphorescence Analysis*, Interscience, New York, 1966

[1.32] C. A. Parker, *Photoluminescence in Solutions*, Elsevier, Amsterdam, 1968

[1.33] E. L. Wehry, in: G.G. Guilbault (Ed.), *Practical Fluorescence, Theory, Methods, and Techniques*, Marcel Dekker, New York 1973, p. 79

[1.34] Arbeloa *et al*, Appl. Phys. **B 64**, 651 (1997)

[1.35] Webb *et al*, J. Chem. Phys. **53**, 4227 (1970)

[1.36] A. Dunne and M. F. Quinn, J. Chem. Soc. Faraday. Trans. I **72**, 2289 (1976)

[1.37] V. E. Korobov, V. V. Shubin, and A. K. Chibisov, Chem.Phys. Lett. **45**, 498 (1997)

[1.38] M. E. Lusty and M.H. Dunn, Appl. Phys. **B44**, 193 (1997)

[1.39] P. Suppan, J. Photochem. Photobiol., **A50**, 293 (1990)

[1.40] C. Reichardt, Chem. Rev. **94**, 2319 (1994)

[1.41] I. Lȯpez Arbeloa, K. K. Rohatgi-Mukherjee, Chem. Phys. Lett. **128** , 474 (1986)

[1.42] F. L. Arbeloa, T. L. Arbeloa, I. L. Arbeloa, Trends Photochem. Photobiol. **3**, 145 (1994)

[1.43] A. A. Viktorova, A. P. Savikin and V. B. Tsaregradskii, Sov. J. Quanrum Electron. **13**, 1140 (1983)

[1.44] W. C. Holmes, Ind. Eng. Chem. **16**, 35 (1924)

[1.45] O. G. Peterson, S. A. Tuccio and B. B. Snavely, Appl. Phys. Lett. **17**, 245 (1970)

[1.46] Ray *et al*, Appl. Opt**. 41**, 1704 (2002)

[1.47] Sinha *et al*, Appl. Phys. B 75, 85 (2002)

[1.48] G. Obermuller and C. Bojarski, Acta Phys. Pol. **A 52**, 431 (1977)

[1.49] A. Penzkofer and Y. Lu, Chem. Phys. **103**, 399 (1986)

[1.50] A. Penzkofer and W. Leupacher, J. Lumin.**37**, 61 (1987)

[1.51] C. T. Lin, A. M. Mahloudji, Li Li, M. W. Hsiao, Chem. Phys. Lett. **193**, 8 (1992)

[1.52] F. Lȯpez Arbeloa, P. Ruiz Ojeda, I. Lȯpez Arbeloa, Chem. Phys. Lett. **148**, 253 ((1988)

[1.53] D. Toptygen, B. Z. Packard, and I. Brand, Chem. Phys. Lett. **277**, 430 (1997)

[1.54] Singh *et al*, Opt. Eng. **33**, 1894(1994)

[1.55] S. Yaltkaya, R. Aydin**,** Turk J. Phys. **26**, 41 (2002)

[1.56] El-Kashef Hassan, Opt. Laser Technol. **30,** 367 (1998)

[1.57] El-Kashef Hassan, Rev. Sci. Instrum. **69,** 1243 (1998)

[1.58] B. Wellegehausen, L. Laepple, and H. Wellig, Appl. Phys. **6**, 335 (1975)

Chapter 2

Diagnostic techniques for high repetition rate dye laser

2.1 Introduction

Knowledge of dye laser output characteristics in short/long period of time is extremely important because of its practical relevance. There are many applications of dye lasers in which optical stability is of prime importance. Therefore, the acquisition, presentation and quantification of dye laser parameters such as optical average power, temporal and spectral characteristics, etc. are essential issues. The spectral structure of a dye laser is characterized by its wavelength and spectral width, also known as bandwidth or linewidth. Diagnostics of spectral characteristic, over the period of time, needs user friendly programmable software for acquisition of large number of sequential data and software for its presentation and analysis. There are no techniques available, either commercially or in the literature, to present dye laser output data over the specified period of time. Also, literatures lacks in diagnostic methods for computing the number of sequential data. In this thesis, a novel indigenous technique for data acquisition, storage and diagnostic of the dye laser output has been proposed and very effectively utilized for precise measurements of the output characteristics over a long period of time.

2.2 Review of dye laser data presentations

Pulsed dye lasers usually have mode structures [2.1-2.2], which show inherent pulse to pulse fluctuation/instability in the spectral structures. Kajava *et al.* [2.3], in a study on dye laser, have observed that the spectral structure and intensity fluctuate from pulse to pulse. They presented dye laser spectra of 8, 32 and 100 pulses, in which subsequent laser pulses were superimposed on each other. However, its visual inspection does not provide any additional information from the representation of time averaged pulses. Pease and Pearson [2.4] have observed the mode structure fluctuations and pulse to pulse dye laser spectral instability, in high repetition rate dye laser. They presented random individual pulse to pulse fluctuations as a set of spots in a graph.

To investigate the dye laser with excellent statistics, acquisition of large number of profiles are needed for better understanding of the output characteristics. Using computer graphics facilities, information can be inferred by drawing superimposed line plots of the signal acquired through 1-D array of photodiodes or CCD camera. For the ideal signal, all line plots should lie on the top of one another within the noise (random) band. This technique is adequate for small variations in parameters, but provides visually confused information for line plots having large variations in it. Situations aggravated when signal contains multiple peaks. Furthermore, in these superimposed line plots, time information is completely missing or lost. However, the time information can be represented by drawing a plot in a specific color or shades but it is difficult to remember color for each line plots. The problem of handling large numbers of line plots (spectrums or traces) having large variation requires a new representation. There are no such techniques available in the literatures to present large number of spectral profile of the tunable dye lasers. Therefore, a novel indigenous technique for spectral data representation has been proposed and implemented to investigate the spectral stability over short/long period of time [2.5]. In fact, this technique is universal and can be used to acquire and analyze many laser parameters; however, in the present thesis, this unique technique is extensively used only for spectral investigations of the dye laser.

2.3 Description of hardware and software

Modern scientific image acquisition system typically consists of tailored optical and electronic components. In the present work, to acquire an image a high resolution temperature compensated 12 bit digital CCD camera (PixelFly, PCO) [2.6] interfaced with the personal computer is used for the dye laser data acquisition. The CCD has spatial resolution of 6.4 μm x 6.4 μm without binning. This camera has also facility of programmable binning, which can be used to enhance S/N ratio of the image. The short exposure time of the camera enables to capture profile of a very fast phenomenon with minimum dark current noise.

PROMISE (***PRO***file Measurement of ***I***mage ***S***ize & ***E***nhancement), a graphical user interface (GUI) based software, devised by Vora [2.7], has been comprehensively used for the dye laser investigations. This software handles image up to 16 bits of resolution. To achieve high precision measurements, numbers of special modules has been incorporated in the *PROMISE*. This software has many unique features like generation of master dark frame and subtraction of self-generated dark current from the signal. This improves the S/N ratio of the CCD and hence the measurement accuracy. Each pixel’s dark current was captured by taking an exposure (with the same chip temperature and integration time) without the incoming light (camera shutter closed). The dark current was subtracted from the actual image, pixel by pixel, to yield the true signal.

Noise (random, hot pixels etc.) is an integral part of the digital imaging system and provides ambiguity in the measurements. Popular programmable spatial image filters [2.8-2.9] were also incorporated for noise removal and smoothing the image. A special type of low pass Median filter was incorporated in the software, which removes isolated noise effectively but does not blur the image and at the same time retains maximum information. This also diminishes the peculiar electromagnetic interference (EMI) pickup during recording of image caused by associated high voltage power supply system used in the experimental laboratory. The fast switching (~100 ns rise time) of pulse forming network associated with electrical power supply, for high repetition rate excitation source (copper vapour laser), generates the peculiar noise which were picked up by the signal cable linked with diagnostics instruments. These kinds of noises have been effectively and routinely removed using single pass median filter available in the software.

2.4 Methodology adopted for spectral investigation

While investigating tunable laser characteristics, it is essential to know precisely the spectral profile (wavelength and bandwidth). A number of methods for spectral measurement have been reported in the literature [2.10-2.16]. For absolute accuracy and high precision measurements, interferometer based techniques are normally used. The spectrum can be measured accurately by various devices such as a very high-resolution spectrometer [2.17], Michelson & Michelson-type interferometers [2.16, 2.18-2.21], Fourier-transform spectrometer [2.22] based on the Michelson interferometer, polarization-sensitive interferometer [2.10], Fizeau interferometer [2.11] and Fabry-Perot (FP) interferometer [2.12]. The Fabry-Perot interferometer (FPI), designed by C. Fabry and A. Perot, represents a tool essentially to study spectral profile, and can be used with detector to resolve fine spectral details [2.23]. The fringe governing equation represents the equation of a circle, hence fringes appear circular to the observer /detector. Therefore, diameter of fringe takes account of spectral information and has been used for spectral characterizations such as wavelengths and bandwidth [2.24]. It determines wavelength to any adjusted accuracy by choosing the single or combination of several FP etalon with different free spectral ranges (FSR). Byer *et al* [2.12] have presented the successive method of wavelength determination through a set of etalons, such that an approximate wavelength value available from the lower resolution etalon was used to determine the order number integer for the next high-resolution etalon with which the closer value of wavelength can be obtained. These methods require the thermal stabilization and precise calibration of etalon constants. To avoid this cumbersome process, an alternative method has been used in which a frequency stabilized He-Ne laser was employed as a reference, along with single FP etalon for the precise measurements [2.14, 2.23].

2.4.1 Theoretical formulation of the spectral measurement

Through FP etalon of spacing d, diameter D_p of the p[th] interference ring, when imaged onto the CCD camera using a lens of focal length f , is given by [2.24],

$$D_p^2 = \frac{4f^2\lambda(p-1+\varepsilon)}{\mu d},\ p = 1,\ 2\ldots \tag{2.1}$$

where μ is refractive index of medium at wavelength λ and ε (0 ≤ ε ≤ 1) is the fractional order number at the centre of the fringe.

Again using interference condition for etalon [2.24], we have

$$2\mu_r\, d = \lambda_r\,(m_r + \varepsilon_r), \qquad 2\mu d = \lambda(m+\varepsilon) \tag{2.2}$$

where μ_r is the refractive index of air at the wavelength λ_r, ε_r $(0 \le \varepsilon_r \le 1)$ is the fractional order number at the centre of the fringe for the reference laser, m_r *and* m are the order numbers of the first (inner most) fully formed FP fringe of the reference laser and the dye laser, respectively.

If D_{1d} is the diameter of the first FP fringe of the dye laser, D_{1r} and D_{2r} be first and second diameter of reference laser at wavelength λ_r, then from equations (2.1) and (2.2), explicit expression for the dye laser wavelength λ, in terms of rings diameters, can be written as [2.25]

$$\lambda = \left(m_r - \frac{D_{1d}^2 - D_{1r}^2}{D_{2r}^2 - D_{1r}^2} \right) \left(\frac{\mu}{\mu_r} \right) \frac{\lambda_r}{m} \tag{2.3}$$

The equation (2.3) indicates that the wavelength of dye laser increases as the diameter of the FP fringes decreases and vice versa. The initial wavelength was measured using monochromator, which was used for the calculation of order m at the centre of the fringe. The fractional order at the centre of the fringe can be obtained from the plot of square of the rings diameters against the corresponding ring numbers. The intercept on the ring number axis is $(1-\varepsilon)$. The fraction ε and hence the values m_r *and* m, using equation (2.2) for known value of FP spacing, can be easily calculated. Therefore, wavelength λ of dye laser can be easily computed by directly measuring the rings diameters of the FP fringe, using equation (2.3).

The bandwidth can be calculated from the intensity profile, expressed in terms of the diameters of different orders of the fringes, using the following relation [2.26]

$$\Delta\nu = FSR \ * \left[\frac{(D_{1b}^2 - D_{1a}^2)}{(D_{2a}^2 - D_{1a}^2)} \right] \tag{2.4}$$

where FSR is the free spectral range of the FP etalon, D is the ring diameter; 1, 2 – two adjacent orders; a, b - the two points between which $\Delta\nu$ was measured. Thus, the bandwidth of the dye laser can be measured by directly recording the FP fringe and measuring the diameters of different orders of the fringe. The bandwidth of axial modes can be measured easily using equation (2.4)

The FP etalon fringe have different ring diameter for different modes and orders. If D_P, D_{P+1} be the diameter of the p^{th} and $(p+1)^{th}$ order ring of one mode, d_{P+1} be the diameter of $(p+1)^{th}$ order ring of next mode, and if there is no overlap occurs between the order of modes then from equation (2.1), the wave number separation between modes, by knowing the ring diameters, can be expressed as follow

$$d\nu = FSR * \left[\frac{D_{P+1}^2 - d_{P+1}^2}{D_{P+1}^2 - D_P^2} \right] \tag{2.5}$$

Thus, by measuring the diameter of the rings, it is possible to evaluate the wave number difference between the modes.

2.4.2 Experimental technique for the data acquisition and analysis of spectral structure

The dye laser spectral structure was analyzed through high resolution FP etalon. Optical arrangement for obtaining the FP fringe of the dye laser and of a frequency stabilized He-Ne laser is shown in Fig.2.1. The He-Ne laser (λ = 632.816 nm, 5 mW power, 1 mm beam size), which is used as a reference wavelength, is passed through the same optical path as the dye laser beam. An aperture was used to enhance the contrast ratios of the fringe. An imaging lens of suitable focal length was used to image the fringe pattern onto a CCD camera connected to a personal computer (PC). To improve measurement accuracy, the setup was adjusted in such a way that only few number of FPI rings were covered in the entire CCD sensor area. Fig.2.2 shows the typical dye laser (a) fringe, (b) intensity modulation along a line scan across the diameter of the fringe.

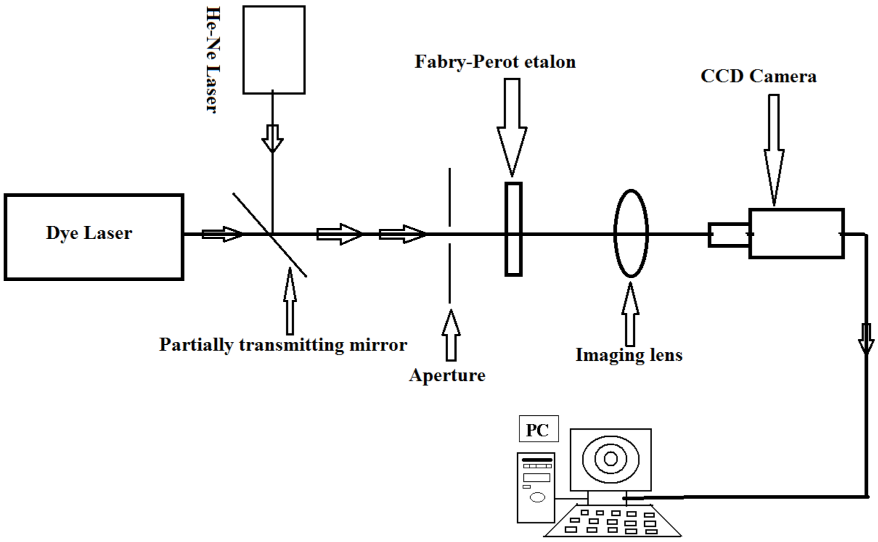

Figure 2.1: *Optical arrangements for obtaining FP fringe of the dye laser and of the He-Ne laser*

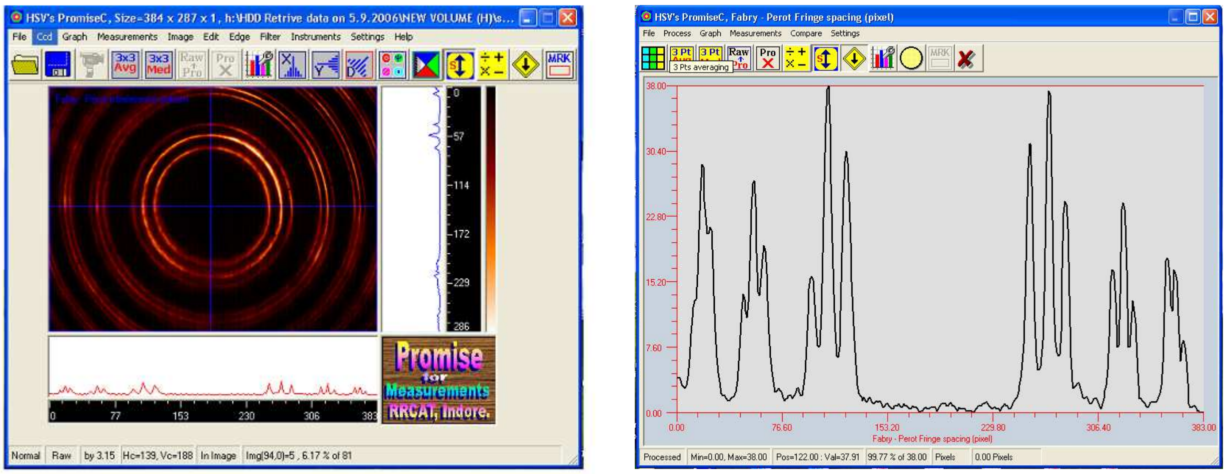

(a) (b)

Figure 2.2: *Typical dye laser (a) fringe, (b) intensity modulation along a line scan across diameter of the fringe*

2.4.3 Identification of peaks and rings diameter

Algorithm has been added in the PROMISE software to identify the number of peaks needed for the spectral structure investigation. To find the ring diameters, derivative of line data was obtained by taking the difference between successive pixels. The peaks were located by finding the slope of the fringe. The line plot of data and its slope were overlaid and the searched peak positions were highlighted while analyzing the data.

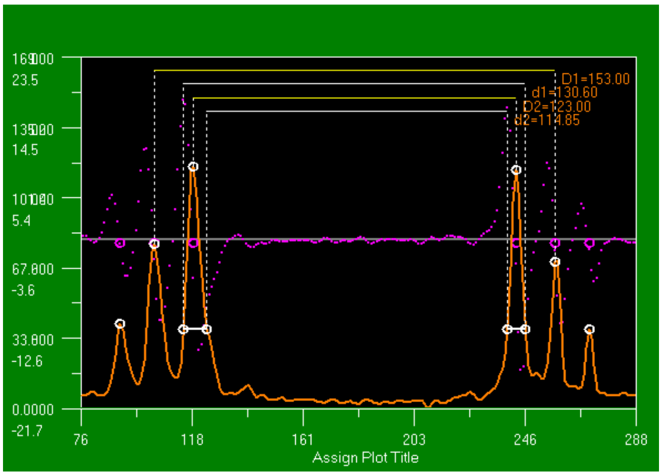

(a)

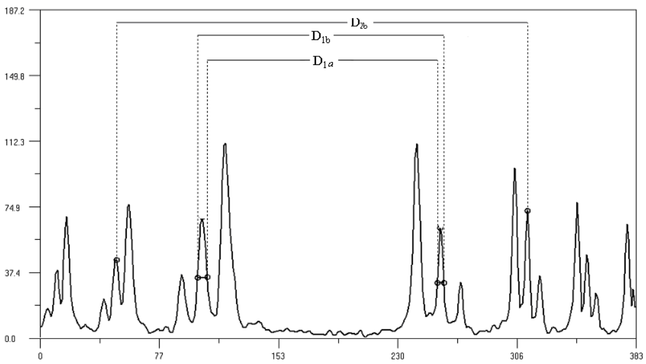

(b)

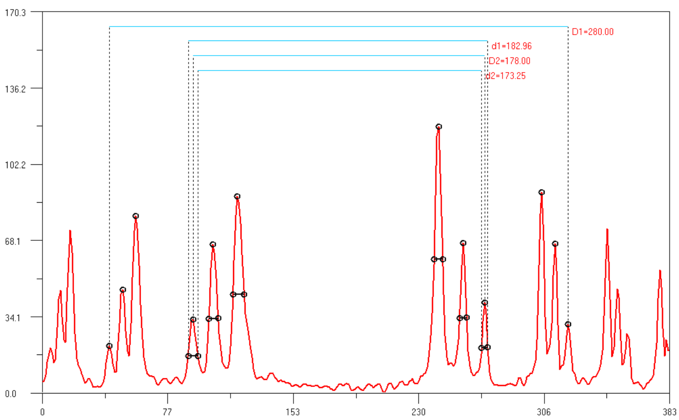

(c)

Figure 2.3*: Typical identification of peaks position and width of line intensity profile (a) first inner most ring, (b) second inner most ring, (c) third inner most ring*

Fig.2.3 shows typical identification of peaks position and widths of line intensity profile (a) the first inner most, (b) second ring, (c) third ring. From the measured ring diameters and peak separations, estimation of λ, and $\Delta\lambda$ can easily be obtained in the desired units of cm^{-1}, MHz or GHz. For stability or drift measurements, the horizontal axis can be programmed either in pixel or in the time domain i.e. time delay in acquiring the successive number of fringes.

The error in the estimation arises from error in determination of the peak position, fringe diameter and its width. The error on the fringe may arise due to random noise of the CCD or due to speckle associated with laser beam which give false peak position or height, thus introducing error in determination of the diameter and the width. The noise present in the fringe can be reduced by FFT filtering which eliminates the selected high frequency components, median filtering for removing typical EMI, averaging and binning of the lines.

2.4.4 Technique for spectral data representation: composite image generation

In order to present large number of vital scientific data simultaneously in the graphical format, a novel technique was conceptualized [2.5]. The fringe generated through FP etalon can be captured through high resolution scientific grade CCD camera and PROMISE software. After capturing the fringe, a cursor was placed on the image, across the diameter of the rings. This cursor provides the reference position to save subsequent line data in a dynamically allocated memory. During this process, two progressively growing images (corresponds to horizontal and vertical cursors), along with current acquired image, were also displayed in the dedicated window. At the end of acquiring preset number of fringe, the data acquisition process stops and software automatically displays the individual line profiles stored in the allocated memory as an image, which is named as **composite image**. In this composite image, line profiles were stored as an image line so each pixel location of line provides position (or any relevant value depending on the signal information) and its color represents signal amplitude. The number of lines to be stacked or size of generated composite image depends on the RAM available. The height of the composite image depends on the number of fringes acquired and number of lines saved from each fringe. The sideways deviation in the composite image provides the first sight tentative information about fluctuations in spectral structure of the dye laser output. The composite image generation method is independent of the hardware, hence can be used with CCD camera, spectrograph and oscilloscope too.

In the composite image only the part of the fringe has been saved so very less disk space is required compared to saving individually acquired full fringe image. The composite image concept is very general in nature and can be used to present data of any characteristics. To improve the S/N ratio of the composite image, instead of storing a single line from the acquired fringe image, a preset number of lines can be binned (added), normalized and then stored as a line. It further reduces the random noise by a factor equal to the square root of the number of lines used for binning.

Fig.2.4 (a) shows typical window of composite image data of dye laser from the present thesis (chapter). It consists of 1000 lines of FP fringe scanned across the diameter, having three longitudinal modes. To visualize it more, composite image of the line scan across the diameter of fringe of He-Ne laser was generated. Fig.2.4 (b) shows composite image of line scan of FP fringe of He-Ne laser. The composite image appears as a straight line from top to bottom, which manifests the fact of high degree of spectral stability.

Another composite image was generated from dye laser in which spectral instability was created by some means. Fig.2.4 (c) shows composite image of dye laser fringe in presence of spectral fluctuations. The zigzag lines from top to bottom in the composite image manifest the fringe to fringe spectral instability present in the dye laser. In this way, composite image gives visual qualitative information about stability.

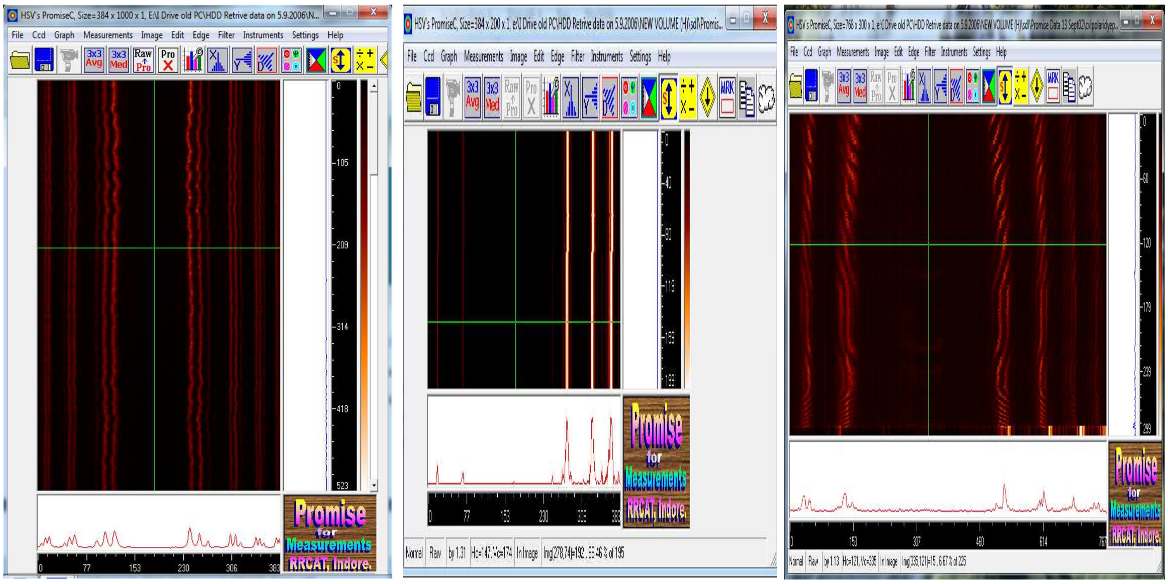

(a) (b) (c)

Figure 2.4*: Typically generated composite image from fringe of (a) dye laser, (b) He-Ne laser, and (c) dye laser*

2.4.5 Spectral measurement from the composite image

For measuring the peak positions and diameters, the software draws the intensity profiles (multi curves) of the line scans from the composite image lines in a dedicated window, as shown in Fig.2.5. From the composite image generated, measurement of wavelength and bandwidth can be performed using special algorithms inbuilt in the PROMISE software. Spectral analysis can be executed using one or two full ring, or three half ring of the FP fringes. The number of rings can be selected using an appropriate command from the Menu displayed in the window, as shown in Fig.2.5. The software plots multi peaks intensity profiles of each line of composite image, which indicate intensity variation, change in the ring diameters and base line (background) level of the fringes. The diagnostic software offers three different techniques to measure bandwidth, namely, using (a) three half rings with 3, 6 or 9 peaks, (b) one full ring with 4 or 6 peaks, and (c) two full rings with 4, 8 or 12 peaks. Depending on the number of axial modes present, number of peaks can be identified appropriately by the software. Fig.2.5 (b) shows dialog for setting parameters for measurements using 2 full rings. The peaks can be located automatically or their tentative positions can be assigned to eliminate undesired peaks. In the second case, mouse click is used to mark the tentative peaks manually, along with margins (i.e. deviation of peak position). Mouse click on multi curves over a peak location records the tentative peak coordinates in a look up table. Fig.2.6 (a) shows the dialog window to mark tentative peaks position.

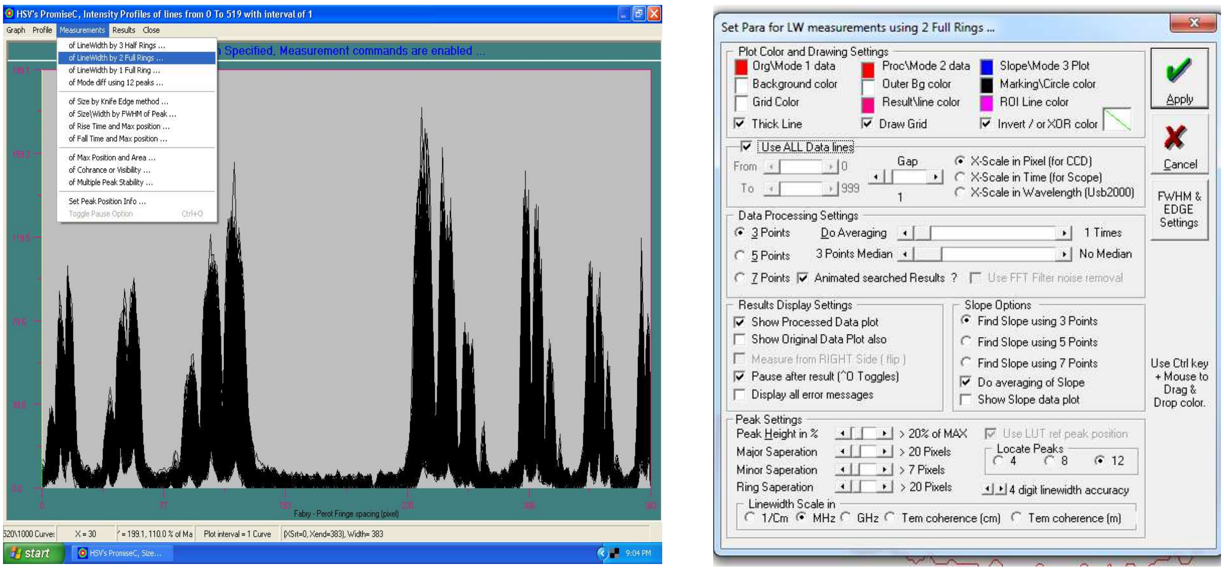

(a) (b)

Figure 2.5: *Typical (a) window of intensity profiles (multi curves) of the composite image data of Fig.2.4 (a), (b) window menu for setting parameters*

In this dialog window, the button has to be pressed according to peak positions i.e. if it is first peak then press first button or if it is 4th peak press 4th button. It saves all peak positions and peak margin information, which helps a lot in the subsequent analysis. The undesired peaks can be ignored by setting a minimum peak separation (in pixels). Any peak that lies within the set separation is ignored.

Small peaks in the base line can be bypassed by setting minimum amplitude of the peak in percentile. The FP etalon details, involved in the calculations, have to be incorporated in the software before measurement start. Fig.2.6 (b) shows dialog window menu for setting parameters for the etalon and widths position. In this way, bandwidth of one, two or any number of axial modes can be accurately measured by this technique.

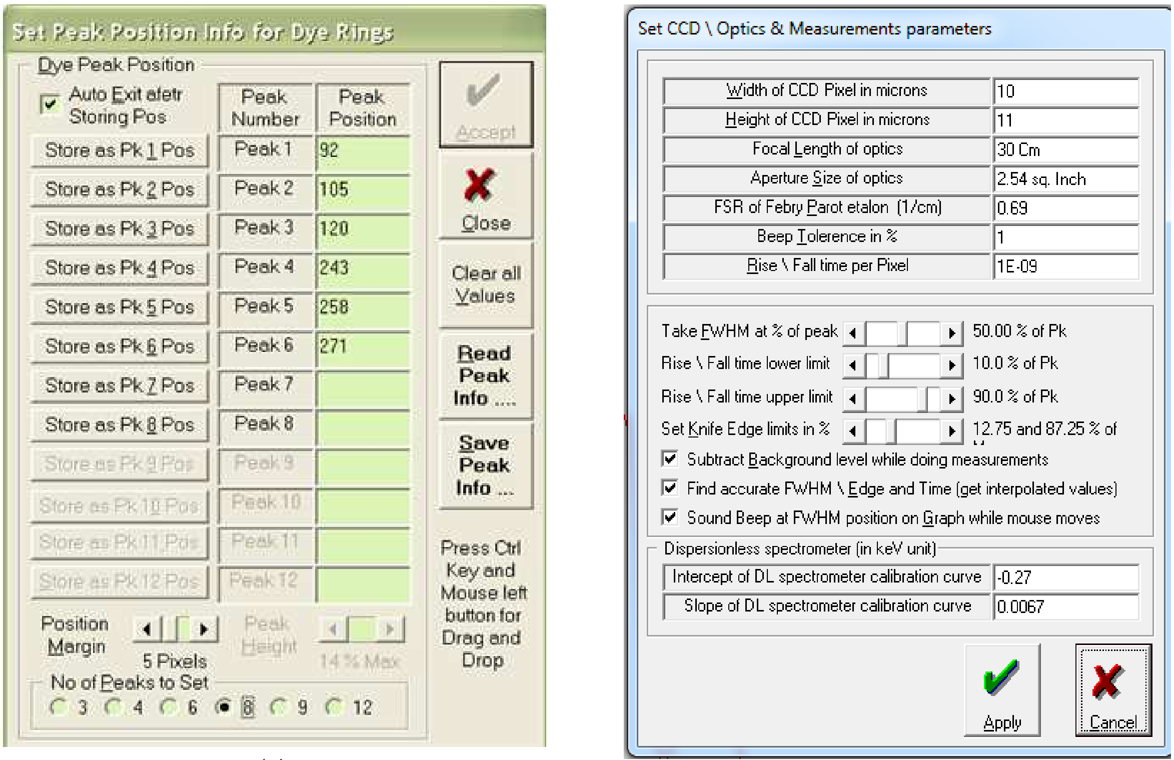

(a) (b)

Figure 2.6: *Dialog window (a) to mark tentative peaks position, (b) for setting parameters of the etalon and widths at peaks percentage height*

2.5 Instruments detail used for the investigation of dye laser

The dye laser is characterized, like other laser, in terms of output parameters such as spectral contents (wavelength and bandwidth), optical power, pulse shape, tuning range and laser beam qualities (divergence and coherence). In this section, brief description of the instruments involved in the measurements of dye laser average optical power, pulse profile, tuning range and beam qualities is presented.

2.5.1 Tuning range

For the tunable dye laser, knowledge of complete spectral coverage might be required along with spectral purity. Thus, the dye laser spectral coverage (i.e. tuning range) was measured with the help of spectrometer and software. Spectrograph (USB2000, Ocean Optics) [2.27] interfaced to the PC through USB port was used for the investigation of the dye laser tuning range. A fractional part of the dye laser beam was directed through optical fiber onto the entrance slit of the instrument to the diffraction grating of the spectrometer. The USB2000 spectrograph uses internally a line CCD to collect the photons. The complete spectrum was acquired by using GUI based another software, which was named as **Tarang**. It has a facility to generate the composite image from the acquired spectrums. To find the tuning range, composite image was generated during the wavelength tuning. By analyzing this composite image the tuning range measurement of the dye laser can be carry out.

2.5.2 Pulse shape

Knowledge of dye laser pulse profile information is very important for applications. For the detection and measurement of optical pulse of the dye laser operating in nanosecond ranges, a very fast phototube/photodiode, along with digital oscilloscope, are generally used [2.28-2.29]. Fast oscilloscopes are generally used to observe the exact wave shape of the signal generated across the detector. A commercially available biplanar phototube, capable of reproducing ultra-fast pulsed light signals with high accuracy, along with fast digital oscilloscope was used for acquisition of dye laser temporal behaviour of the pulses. Biplanar phototube model R1193U-51 (Hamamatsu, Japan) was used for the laser pulse profile measurements. The phototube system is connected through BNC to Tektronics 3052 oscilloscope, which is interfaced to PC through USB port by using GPIB to USB converter.

Dedicated software, named as **OsciloGraph,** was used for temporal investigation of the dye pulses. This GUI based software was used for the dye laser pulse data acquisition and subsequent analysis. The acquired traces are displayed on the PC, moving mouse over it displays time in the selected unit, amplitude and its percentage with respect to peak value. A composite image generation technique, similar to described earlier, has been used to acquire and measure pulse width and its fluctuations, from the acquired oscilloscope (1-D) traces. The software provides detailed measurements of amplitude, temporal width, rise & fall time and counts under the trace, etc. The height of the stacked image depends on the number of traces acquired and its width depends on the number of elements used in the digitization of the trace.

2.5.3 Optical average power

Average output power of laser beam is generally measured by a pyro-electric detector, as it covers wide spectral response. In this type of detector, the incident radiation raises the temperature of the sensor which is measured by thermocouples or temperature dependent resisters attached to it. Average output power in our experiment was measured with the help of a commercially available Ophir power meter. It consists of smart head (SH) and USB interface module, to connect the PC through the USB port for recording power. Power meter sensor heads 2A-SH and F300A-SH were used to record dye laser and copper vapour laser optical average power, respectively.

2.5.4 Beam size and divergence

The divergence of laser beam is a measure for how fast the beam expands far from the beam waist, i.e., in the so-called *far field*. There are four types of beam size measurement techniques, namely, pin hole, slit, knife-edge and camera based system. Each technique has specific advantages and disadvantages. In this work, only CCD camera and imaging system was used to measure the horizontal and vertical divergences. The intensity distribution of the dye laser beam was recorded using ***PROMISE*** software by high resolution scientific grade 12 bit PixelFly CCD camera. The measurement from the recorded data directly provides the dye laser beam size and divergence in both horizontal and vertical direction with sub pixel accuracy by using second moment's algorithm.

2.6 Coherence measurements of pulsed dye laser

Coherence is one of the fundamental characteristics of laser, which discriminate between laser radiation and other types of radiation (e.g., radiation of thermal origin). A very few studies were reported on coherence property of the tunable dye lasers [2.30]. Singh *et al* [2.30] measured the divergence of dye laser from the spatial intensity profile of the laser spot using a pinhole and photomultiplier tube (PMT). They reported that the output beam from the dye laser was elliptical in shape because of its different divergences in the horizontal and vertical directions. The divergence of the dye laser beam obtained was 10.2 mrad in the horizontal direction and 1.5 mrad in the vertical direction. This asymmetry in the beam divergence arose because of the difference in the dimensions of the gain region in the horizontal and vertical directions. However, spatial coherence is the true representation of beam quality of a laser. Further, the study of coherence properties of tunable dye laser is also very essential in order to get tunable ultra-violet laser, by frequency doubling using an intra-cavity non-linear crystal, which has many applications in laser photo-chemistry and high-resolution spectroscopy. Measurement of temporal coherence is of almost importance being linked with bandwidth of laser.

2.6.1 Spatial coherence

Since early days of laser invention the reversible shear interferometer [2.31-2.32] and Young’s double slit [2.33-2.34] have been reported in the literature to measure the spatial coherence of laser. Reversible shear interferometer requires collimated beam and also reasonable beam size for overlapping of two beams in order to get number of fringes. For the study of spatial coherence of dye laser, which has different horizontal and vertical divergence and small beam size, reversible shear interferometer is not appropriate. Young’s double slit is standard technique, used to measure the spatial coherence of light.

The visibility or contrast of the fringe due to interference of two beams of light from a source is defined in terms of the maximum intensity, I_{max}, at the center of a bright interference fringe and minimum intensities, I_{min}, at the center of the adjoining dark fringe, as

$$V = \frac{I_{max} - I_{min}}{I_{max} + I_{min}} \tag{2.6}$$

Furthermore, the intensity at any point can be written [2.35] as

$$I = I_1 + I_2 + 2\sqrt{I_1\ I_2}\,R_e\gamma_{12}(x) \tag{2.7}$$

$$I = I_1 + I_2 + 2\sqrt{I_1 I_2}\,\frac{\sin\left(\pi d s / R\lambda\right)}{\pi d s / R\lambda}\cos\left(k d x / D\right) \tag{2.8}$$

where I is the intensity at the slit location, s is source size, R is the distance of the source from the slit, D is the distance of the fringe pattern location from the slit and d is slit separation. From the above equation, the fringe visibility can be written as

$$V = \left| \frac{sin\left(\pi d s / R\lambda\right)}{\pi d s / R\lambda} \right| \tag{2.9}$$

Visibility of the fringe has been evaluated as a function of slits separation, for different source size of 0.1, 0.12 and 0.2 mm at the peak wavelength 576 nm of the dye laser [2.36]. Fig.2.7 shows the typical variation of visibility of dye laser (576.00 nm) with slit separation.

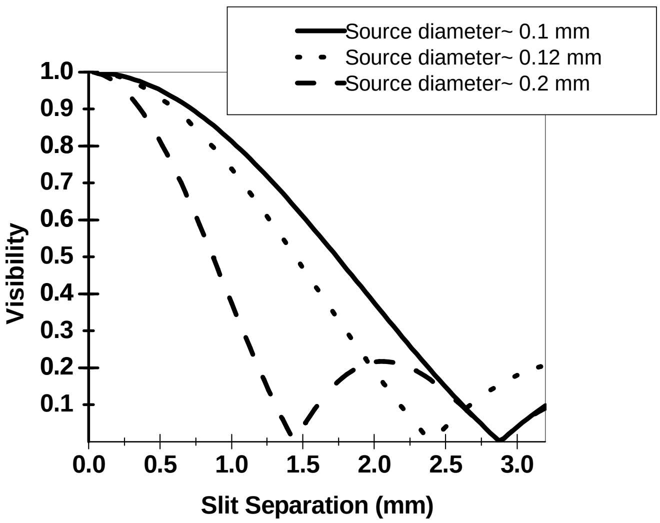

***Figure 2.7**: The typical variation of visibility of dye laser (576.00 nm) with slit separation*

The solid curve is for source size of 0.1 mm, dotted curve is for source size of 0.12 mm and dashed curve is for source size of 0.2 mm diameter. The various slit separation has been tried to maximize the visibility of the fringe of dye laser. Double slit interference fringes were recorded by the CCD camera using ***PROMISE*** software.

The interference fringe of copper vapor laser, which is used for dye laser pumping, using Young double slit set-up, was also generated [2.36]. The double slit separated at 100 microns was placed at a distance of 500 mm from the dye laser source. Fig.2.8 shows the typical (a) double slit fringe (b) intensity modulation, of copper vapor laser [2.36]. The central fringe visibility was 0.23. The same setup was used to generate fringe pattern for the dye laser. Fig.2.9 shows the typical double slit (a) fringe pattern, (b) intensity modulation, for the dye laser at 100 microns slit separation [2.36]

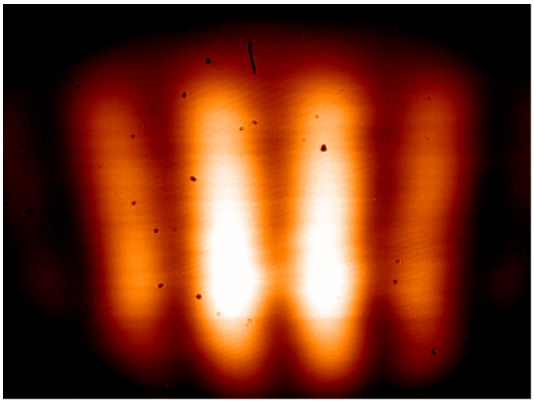

(a)

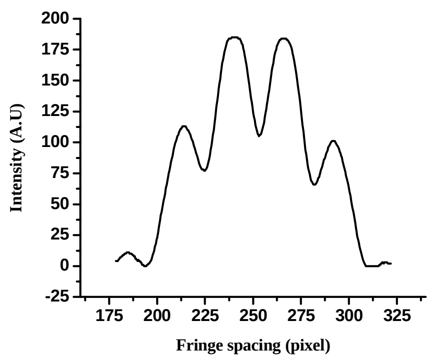

(b)

***Figure 2.8**: Typical record of Young's double slit (a) fringe, (b) intensity modulation, for CVL, at 100 microns slit separation*

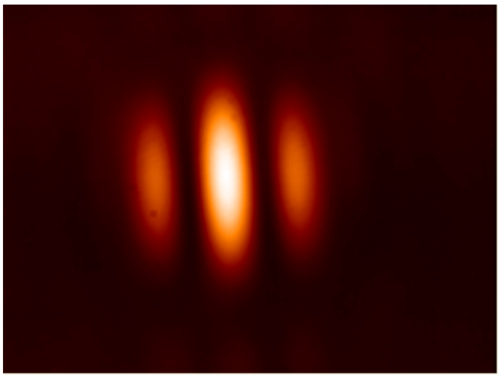

(a)

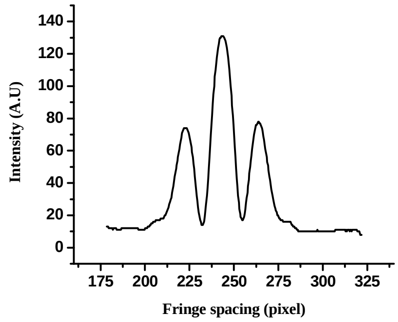

(b)

Figure 2.9*: Typical record of Young's double slit (a) fringe, (b) intensity modulation, for dye laser, at 100 microns slit separation*

The fringe visibility of 0.85 was observed for the dye laser. The dye laser is highly coherent, as compared to its pump source. It is because of the fact that the dye laser spatial coherence is primarily established by its resonator containing a point/shot type source.

2.6.2 Temporal coherence

It is known that perfectly monochromatic source is ideal one. It can be assumed that wave trains from any source contain a number of frequencies, rather than being strictly monochromatic. The intensity, therefore, involves a summation over frequency. The total intensity I_T will be then,

$$I_T = \sum_m I(\nu_m) \tag{2.10}$$

if the distribution of frequencies involved is continuous rather than discrete, then the sum is replaced by an integral. Thus, the integral becomes

$$I_T = \int_{-\infty}^{\infty} I(\nu')d\nu' \tag{2.11}$$

if ν_0 be the value at the center of the spectrum produced by the source then we write $\nu' = \nu_0 + \nu$, hence

$$I_T = \int_{-\infty}^{\infty} I(\nu)\,[1+\cos\{2\pi\Delta(\nu_0+\nu)\}]\,d\nu \qquad (2.12)$$

The cosine term of the above equation can be expanded to give

$$\cos[2\pi\Delta(\nu_0+\nu)] = \cos(2\pi\nu_0)\cos(2\pi\Delta\nu) - \sin(2\pi\Delta\nu_0)\sin(2\pi\Delta\nu) \qquad (2.13)$$

With the substitution of

$$\theta = 2\pi\Delta\nu_0 \qquad (2.14)$$

$$P = \int I(\nu)\,d\nu \qquad (2.15)$$

$$C = \int I(\nu)\cos(2\pi\Delta\nu)\,d\nu \qquad (2.16)$$

$$S = \int I(\nu)\sin(2\pi\Delta\nu)\,d\nu \qquad (2.17)$$

The intensity equation become

$$I_T = P + C\,cos\,\theta - S\,sin\,\theta \qquad (2.18)$$

Using the value of intensities, the visibility V of the fringe due to interference of two beams of light from a source can be written as

$$V = \frac{\left|\left(C^2+S^2\right)^{1/2}\right|}{P} \qquad (2.19)$$

Lasers of cavity length l operate in a number of longitudinal modes corresponding to distance $\frac{c}{2l}$, within the gain profile. For example, a laser operating in three frequencies component with relative intensity coefficients of A, B and C, then the expression for the intensity profile of the laser can be written as

$$I(\nu) = \left[A\exp\left\{-\left(\frac{\nu}{\alpha}\right)^2\right\} + B\exp\left\{-\left(\frac{\nu+\delta}{\alpha}\right)^2\right\} + C\exp\left\{-\left(\frac{\nu-\delta}{\alpha}\right)^2\right\}\right], \qquad (2.20)$$

where, δ is the peak separation between modes and α is the FWHM of the Gaussian beam. Therefore, the visibility function V for the spectral distribution of laser can be analyzed by measuring the relative intensities and spectral width of the components.

Michelson interferometer is generally used to measure the temporal coherence of the light [2.34]. In Michelson spectral interferometer the two light beams are derived from the same source, and they are brought together after traveling different path lengths. The basic properties of the Michelson interferometer are (a) the ability to make both arms equal in optical length to a fraction of a wavelength, (b) to measure changes of position as measured on a scale (the position of one of the mirror) in terms of wavelength by counting the fringes. The movable arm of Michelson's interferometer has been used to find the shape and structure of a spectral line and hence measure the temporal coherence of light sources [2.31]. This involves the measurement of fringe visibility as a function of interference order; a subsequent Fourier transformation of the visibility curve gives the profile of the line. The resolving power is equal to the order of interference reached, which is naturally limited to the order necessary to reduce the visibility practically to zero and thus resolve the line. It is suitable and convenient where the coherence length is very small. However, for narrow bandwidth source where the coherence length is of order of tens of centimeters it become very difficult to align and use the interferometer because of impractical arm length. Fabry-Perot interferometer [2.37], used for high–resolution spectrum analysis, is very compact and free from alignment problem encountered in Michelson's interferometer. In visible region it has largely superseded the Michelson interferometer (and Fourier transform spectroscopy) as a means of spectrum analysis because the spectrum can be read directly from a photographic record of the Fabry –Perot interference (FPI) pattern. FPI has been used more frequently for high-resolution spectrum analysis. The direct computation of the line profile is easier now than it was with Michelson. Additionally, the Fabry–Perot interferometer easily attains a very high resolving power, in excess of 10^6, with a fairly good instrumental profile. It also has the great advantage of simplicity.

The relation between spectral line width, and the coherence length and time of a light wave, is provided by damped simple harmonic motion. The spectral linewidth $\Delta\nu$ of a light wave made up of a series of wave trains is determined by Q of the oscillator, which also determines the exponential decay time in each wave train. The temporal coherence is the average coherence length l_c, during which the wave train exists for interference fringes [2.38] i.e.

$$l_c = \frac{c}{\Delta\nu} , \tag{2.21}$$

Where, c is the speed of light and $\Delta\nu$ is the spread in frequency (i.e. bandwidth).

Therefore, from equation (2.5) and (2.21), the temporal coherence length become

$$l_c = \frac{c}{FSR\left[\dfrac{\left(D_{1b}^2 - D_{1a}^2\right)}{D_{2a}^2 - D_{1a}^2}\right]} \tag{2.22}$$

Thus, by computing the parameters and measuring the diameter of fringe the temporal coherence length, associated with the dye laser can be measured by this technique. This technique is general in nature and can be used for any broad spectrum too.

The temporal coherence lengths of the CVL pumped dye laser were analyzed using a FPI [2.25]. The FPI setup used for temporal coherence measurement was the same as described for spectral measurement for dye lasers. Fig.2.10 (a) shows typical Fabry-Perot fringe of (a) multimode dye laser, (b) single mode dye laser, (c) He-Ne laser. The measured coherence length of this multimode dye laser was ∽10 cm. The coherence length of laser light is inversely proportional to the bandwidth of the output laser light; therefore, the coherence length can be extended by reduction of the bandwidth. The measured coherence length of single mode dye laser was ~60 cm. The temporal coherence length is related to the bandwidth of the source. The more narrow the bandwidth of the source, the longer the coherence length. The CVL pumped dye lasers have coherence length generally from a few millimeters to 7 cm [2.39].

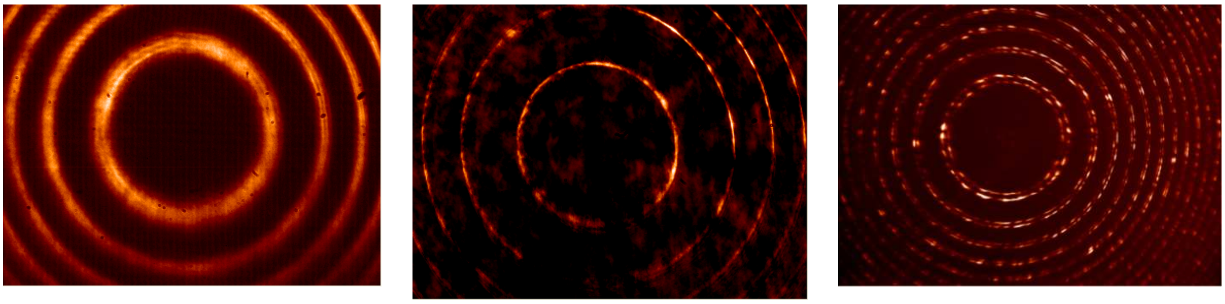

(a) (b) (c)

Figure 2.10*: Typical Fabry–Perot fringe of (a) multimode dye laser, (b) single mode dye laser, (c) He-Ne laser*

Thus, the present tunable dye laser is highly coherent. It is because of the fact that the dye laser coherence is primarily established by its resonator components.

In order to validate the alignment and performance of the FPI set-up, the temporal coherence length measurement for commercially available He-Ne (632.8 nm) laser was also carried out. Fig.2.10 (c) shows the typical Fabry-Perot fringe of He–Ne laser. The observed coherence length of He-Ne laser, used in the present experiment, was 19.2 cm. Generally, He-Ne (632.8 nm) lasers have a coherence length of around 10 to 30 cm [2.40]. The typical coherence length of the He-Ne laser is reported to be about 20 cm [2.41].

2.7 Summary

In conclusion, a novel scheme for acquiring and presenting through composite image is formulated and implemented for the investigation of the high repetition rate dye laser characteristics. The work was carried out towards the development and evaluation of a multi-parameter spectral profile data representation model for interactive visualization and investigation of very large data of the high repetition rate dye laser. This technique provides a powerful and effective basis for real-time visualization of a large number of data sets, and is used effectively to represent the statistical feature of a large amount of scientific data.

A diagnostic technique is established for the analysis of spectral structure of a high repetition rate dye laser by deriving explicit relationship of the parameters with ring diameter of the FP fringe. The output characteristics of dye laser are demonstrated by directly measuring the ring diameter of the FP ring. Techniques for precise peak identification, diameter estimation, and all other steps involved in the process for the analysis of the spectral distribution in the dye laser are presented through GUI based software.

Major instruments involved for the dye laser diagnostic are briefly described. Techniques for coherence measurement of narrow bandwidth source, particularly, dye laser and CVL are presented. Spatial coherence measurement using standard double slit experiment shows that dye laser have fringe visibility of 0.85 as compared to 0.23 for CVL. Though the technique is used for dye laser measurement, but in general, can be applied to any source too.

Publications based on this chapter

1. On the coherence measurement of a narrow bandwidth dye laser

Applied Physics ***B*** **110**, 483 (2013).

Nageshwar Singh and H. S. Vora

2. A composite (stacked) picture generation technique for spectral profile representation of dye laser

Optics Communication **282**, 4259 (2009)

H. S. Vora and **Nageshwar Singh**

3. The spectral measurement of a high repetition rate tunable dye laser output using Fabry-Perot fringe,

Optics and Laser Technology **39**, 733 (2007)

Nageshwar Singh and H. S. Vora

References

[2.1] R. J. Mckee, J. Lobin, W. A. Young, Appl. Opt. **21**, 725 (1982)

[2.2] K. Dasgupta, R. Khare, S. Daulatabad, and L. G. Nair, Appl. Opt. **29**, 1714 ((1990)

[2.3] T. T. Kajava, H. M. Lauranto, and R. R. Salomaa, Appl. Opt. **31**, 6987 (1992)

[2.4] A. A. Pease and W. M. Pearson, Appl. Opt. **16,** 57 (1977)

[2.5] H. S. Vora and and Nageshwar Singh, Opt. Commun. **282,** 4259 (2009)

[2.6] www.pco.de

[2.7] H. S. Vora et al, Proceedings of National Laser Symposium CAT, Indore, 1994

[2.8] D. Philips, *Image Processing in C*, R & D Publications Inc., Lawrence, Kansas, USA, 1994

[2.9] J. C. Russ, *The image processing handbook*, CRC Press, Fifth Edition, 2002

[2.10] P. Juncar, J. Pinard, Opt. Commun **14,** 438 (1975)

[2.11] J.J. Snyder, In: Hall J L, Carlsten J L, editors. Laser Spectroscopy 111, New work: Springer-Verlag Heidelberg; 1977, p. 419-420

[2.12] R. L. Byer, J. Paul, M. D. Duncan, In: Hall J. L, Carlsten J. L, editors. *Laser Spectroscopy 111*, New work: Springer-Verlag Heidelberg; 1977, p. 414-416

[2.13] A. Fischer, R. Kullmer, W. Demtroder, Opt. Commun. **39**, 277 (1981)

[2.14] N. Konishi, T. Suzuki, Y. Taira, H. Kato, T. Kasuya, Appl. Phys. **25**, 311 (1981)

[2.15] D. Rees, M. Wells, J. Phys. **E 19,** 301 (1986)

[2.16] J. L. Hall and S. A. Lee, Appl. Phys. Lett. **29**, 367 (1976)

[2.17] T. W. Hänsch. In: Hall J L, Carlsten J L, editors. Laser Spectroscopy 111, New work: Springer-Verlag Heidelberg; 1977, p. 423-424

[2.18] S. A. Lee, J. L. Hall, In: Hall J L, Carlsten J. L., editors. Laser Spectroscopy 111, New work: Springer –Verlag Heidelberg; 1977, p. 421-422

[2.19] F. V. Kowalski, W. Demtröder, A. L. Schawlow, J. Opt. Soc. Am. **66**, 965 (1976)

[3.20] D. A. Solomakha, A K. Toropov, Sov. J. Quantum Electron. **7**, 929 (1977)

[2.21] W. R. C. Rowley, K. C. Shotton, P. T. Woods, In: Hall J. L, Carlsten J L, editors. *Laser Spectroscopy 111*, New work: Springer-Verlag Heidelberg; 1977, p. 419-420

[2.22] M. J. Padgett, A. R. Harvey, A. J. Duncan, W. Sibbett, Appl. Opt. **25,** 6035 (1994)

[2.23] J. M. Vaughan, *The Fabry-Perot Interferometer*, Britol and Philadelphia: Adam Hilger; 1989

[2.24] M. Born, and E. Wolf, *Principles of Optics*, Oxford: Pergamon; 1975

[2.25] Nageshwar Singh and H. S. Vora, Opt. Laser Technol. **39,** 733 (2007)

[2.26] S. Lavi, E. Miron, I. Smilanski, Opt. Commun. **27,** 117 (1978)

[2.27] http://www.oceanoptics.com/technical/USB2000%20Operating%20Instructions.pdf

[2.28] W. Demtröder, *Laser Spectroscopy*, Springer, Kaiserslautern, 2002

[2.29] Kularatna, Nihal, *Digital and Analogue Instrumentation: Testing and Measurement*, pp. 165–208, ISBN 978-0-85296-999-1 (2003)

[2.30] Singh *et al*, Opt. Commun. **97**, 367 (1993)

[2.31] T. Omatsu, K. Kuroda, T. Shimura, K. Chihara, M. Itoh and I. Ogura, Optical and Quantum Electronics **23**, S477 (1991)

[2.32] D. W. Coutts, M. D. Ainsworth and J. A. Piper, Opt. Commun. **87**, 245 (1992)

[2.33] E. Hecht, *Optics*, 2nd ed., Addson-Wesley, New York, 1987

[2.34] M. Born and E. Wolf, *Principles of optics*, Pergamon, New York, 1980

[2.35] Robert D. Guenther, *Modern Optics*, John Wiley & Sons, New York, 1990

[2.36] Nageshwar Singh and H.S. Vora, Appl. Phys. ***B*** **110**, 483 (2013)

[2.37] J. M. Vaughan, *The Fabry-Perot Interferometer*, Britol and Philadelphia: Adam Higher; 1989

[2.38] Grant R. Fowles, *Introduction to Modern Optics*, Dover Publication, Inc., New York, 1968

[2.39] R. A. Lindley, R. M. Gilgenbach, and C. H. Ching, Appl. Phys. Lett. **63**, 888 (1993)

[2.40] http://www.k3pgp.org/Notebook/Lasersam/laserhen.htm

[2.41] http://cord.org/cm/leot/course01_mod08/mod01-08frame.htm

Chapter 3

Review and studies on Copper Vapour Laser

3.1 Pulsed Excitation Sources

Dye laser is optically excited either by flash lamp or another laser. The important parameters that decide the proper selection of excitation (pump) source are conversion efficiency (photon), spectral absorption range, peak power, pulse width and pulse repetition rate [3.1]. The broadband UV-VIS emission from flashlamp can excite the dye molecules; however, triplet effects become significant because of its long rise-time or duration of the optical pulse. Short-pulse lasers like second/third harmonics of Q-switched Nd:YAG, nitrogen and excimer lasers are attractive excitation sources, however, with a moderate repetition rate (~100 Hz). Copper vapor laser is one of the most efficient excitation sources at high pulse repetition frequency (4-6 kHz) for the Rhodamine dyes [3.1].

3.2 Copper Vapour Laser

3.2.1 Energy levels and laser transitions

Copper vapor laser (CVL) employs vaporized copper atoms as the lasing medium and produces green & yellow laser lights at 510.554 nm and 578.213 nm [3.2-3.3], respectively. This is one of the most useful lasers in the class of pulsed metal vapor lasers [3.3]. High repetition rate pulsed operation makes it ideal source for applications like material processing and laser isotope separation applications. In atomic vapor laser isotope separation (AVLIS) scheme, a CVL is used as excitation source for the tunable dye laser [3.4-3.8]. Therefore, knowledge of fundamentals of this laser is essential prior to its potential application, such as pumping the dye laser. The atomic number of the copper is 29; its electronic configurations are,

$$^{29}\mathrm{Cu}:1s^2\ 2s^2 2p^6\ 3s^2 3p^6 3d^{10}\ 4s^1,$$

$$^{29}\mathrm{Cu}:1s^2\ 2s^2 2p^6\ 3s^2 3p^6 3d^9\ 4s^2$$

The copper atom has ground state $^2S_{1/2}$, which is formed by the electronic configuration $3d^{10}\ 4s^1$. The configuration $3d^9\ 4s^2$ gives rise to $^2D_{5/2}$ and $^2D_{3/2}$ metastable states that constitute the lower laser level. By electron impact excitation the outer $4s$ electron, lifts to higher orbits and forms the configurations $3d^{10}\ 4p$, $3d^{10}\ 5p$ and so on. The $3d^{10}\ 4p$ configuration has the states $^2P_{3/2}$ and $^2P_{1/2}$, which form the upper laser levels of CVL. Fig.3.1 shows the typical energy level diagram of CVL. The upper laser levels $^2P_{3/2}$ and $^2P_{1/2}$, has energy of 3.82 eV and 3.79 eV, while the lower laser metastable levels are at 1.39 eV ($^2D_{5/2}$) and 1.64 eV ($^2D_{3/2}$) from the ground state [5.9-5.10], respectively. The upper levels form a series of resonance ^2P levels which are connected with the ground state via strong resonant transitions at wavelengths of 324.754 and 327.396 nm. The rapid relaxation (through radiative decay) of copper atoms from the resonance levels ^2P to the ground state $^2S_{1/2}$ brings about nonessential losses of copper atoms, because these are subjected to strong trapping of radiation. The other channel to decay of the resonance levels ^2P is via the metastable levels ^2D. The transition $^2P_{3/2} \to {}^2D_{5/2}$ and $^2P_{1/2} \to {}^2D_{3/2}$ are optically allowed transitions. The transition $^2P_{3/2} \to {}^2D_{5/2}$ leads to green line at wavelength $\lambda = 510.554\ nm$, while the transition $^2P_{1/2} \to {}^2D_{3/2}$ is yellow emission at wavelength $\lambda = 578.213\ nm$. As the ^2D states have same (even) parity as the ground state, the transitions from ^2D states to the ground state are forbidden.

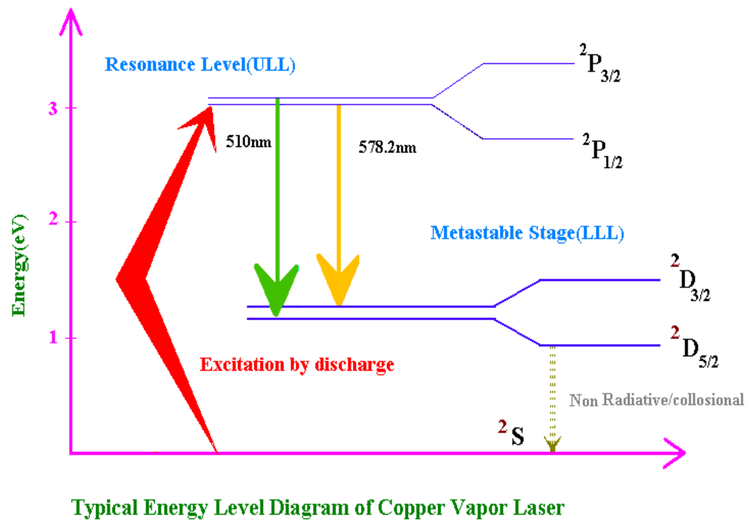

***Figure 3.1**: Typical energy level diagram of CVL*

Copper atoms are excited by electric field in the inert gaseous medium. Electrons in the electrical discharge collide with the vaporized copper atoms and excite them in a single step to the upper $^2P_{3/2}$ and $^2P_{1/2}$ laser levels, as illustrated in Fig.3.1. In an electrical discharge, the upper and the lower laser levels, both are excited by electron impact excitation but with different excitation cross-sections. The excitation to upper level is at a much faster rate than that for the lower laser level. The excitation cross-section of the upper levels are 9.7x10^{-16} cm^2 ($S_{1/2} \rightarrow P_{3/2}$) and 4.5x$10^{-16}$ cm^2 ($S_{1/2} \rightarrow P_{1/2}$), respectively. The radiative life times of $P_{1/2,3/2}$ are 10.5 ns and 9.8 ns, respectively, for an isolated atom. Although, the transition from ^2P to $^2S_{1/2}$ are resonance transitions i.e. highly optically allowed transitions, depopulation of the ^2P states does not take place through this route, due to radiations trapping [3.11]. The upper laser level lifetime is of the order of 500-600 ns while the lower laser level is of the order of 130 µs [3.12]. Hence, the population inversion reduces to zero and the laser action terminates after 30-60 ns. Because of this characteristic the laser is termed as *self-terminating*. The lower laser level is depopulated by diffusion of the excited atoms to the wall of the discharge tube and/or subsequent collisions with the buffer gas. Maximum pulse repetition frequency of the laser is governed by the time needed for the metastable level population to decay [3.13].

3.2.2 Kinetics of CVL

The CVL output characteristics depends mainly on excitation and decay of excited levels, copper density, electron density, etc. The peak electron temperature and the initial meta-stable density are the prime factors that decide the performance [3.14-3.15]. The ratio of excitation rates to ^2P, ^2D and higher energy levels depend on the electron temperature. The lower laser metastable level has lower excitation cross section than that of the upper laser level. At low electron temperature, the excitation rate for ($D_{3/2,\ 5/2}$) state exceeds the excitation rate to ($P_{3/2,1/2}$), as the metastable state is at low level (1.39 eV) as compared to the upper laser level (3.82 eV). At high electron temperatures, excitation to higher excited states and ionisation states dominate. The optimum electron temperature is in the range of 4.0 to 10.0 eV [3.14]. The electron temperature depends on various discharge parameters like buffer gas pressure, tube temperature, copper ground state density, pulse repetition rate, excitation voltage and current. At an optimum tube temperature (1400-1500 ^oC), the laser provides maximum output power. By increasing tube temperature, the copper density increases, which in turn decreases the peak electron temperature. This is due to the fact that momentum transfer cross-section for copper is large as compared to the buffer gas. Further increase in tube temperature increases the excitation rates to the copper atoms but the ratios of populations in upper laser level to lower laser decreases which reduces the output power. The electron temperature is low at low charging voltage, so that the rates of excitation to both lower and upper levels are comparable and competitive and hence the laser power decreases. High Cu ground state density, take over excitation to the lower laser level, hence laser oscillations cannot be continued. The optimum electron temperature ($T_{optimum}$), the charging voltage V_0 and the wall temperature (T_W) are approximately related as [3.16]

$$T_{optimum} = \frac{V_0}{\ln T_W} \tag{3.1}$$

The peak electron temperature increases with increasing the charging voltage. The laser power also depends on the buffer gas pressure. Decrease in laser power with increasing buffer gas pressure is due to decrease in the electron temperature [3.16]. As the pressure of the buffer gas is increased, peak current decreases but the current pulse duration increases, both result in decrease of electron densities. At buffer gas pressure below the optimum value, the excitation of copper to higher excited state and ionisation increases, hence the laser output power reduces.

The pulse repetition rate affects the metastable population. At lower repetition rate, sufficient time is available for the metastable state to decay to the ground state, which results in higher population inversion. As the pulse repetition rate is increased, energy per pulse decreases, the average power decreases if the rate of decrease in energy is slower than the rate of rise in pulse repetition rate. Maximum power is observed, in elemental CVL, depending on the discharge tube diameter for pulse repetition frequency in the range of 4.0 to 6.0 kHz.

3.2.3 Design, assembly and excitation source of CVL

An indigenously developed CVL [3.17-3.18], used in the present work consists of discharge tube (47 mm inner diameter, 1500 mm length) surrounded by thermal insulation, placed concentrically in a borosilicate glass tube envelope, which is placed in a water-cooled stainless steel jacket. Cooled water was circulated through external chiller unit to the stainless steel jacket assembly to remove thermal heat. The refractory re-crystallised alumina tube of high density was used for the discharge tube, because of its non-reactivity with copper at high temperature (1500^0C). This refractory tube is filled with pellets of high purity copper, distributed at regular intervals along the length. Generally, inert gas preferably neon is used as buffer gas to help in initiating the discharge under cold conditions and also minimise diffusion of copper vapour out of the hot zone. Though other inert gases like helium, nitrogen and argon were also used, but the best performance was reported with neon as buffer gas. Neon gas at a pressure of 25 mbar was used as the buffer gas to (a) provide a discharge medium before the tube has reached a temperature sufficient for the generation of Cu vapour, (b) inhibits loss of Cu atoms by diffusion into the cold window regions, (c) convey heat from the tube axis to the wall, and for many more advantages.

Hence neon gas of purity 99.999% was used as a buffer gas at 25 mbar tube pressures and the flow rate was maintained at around ~1 litre-atm/hr, inside the discharge tube. The annular space between the alumina tube and the glass tube was filled with insulating layers of bulk fibers at a suitable packing density. These thermal insulation confines the heat in the tube to maintain the operating temperature of CVL. The entire discharge tube and thermal insulator assembly was contained within an envelope of silica, and closed at both ends by silica windows set at Brewster's angle. Fig.3.2 shows the CVL discharge tube schematic [3.1]. The pulsed electrical discharge between electrodes at each end of the tube was used to raise the temperature of around 1500 ^{0}C. Since melting point of copper is 1028 ^{0}C, it requires sufficient electrical power to heat the discharge tube. The excitation source consists of high voltage variable DC power supply, charging capacitor, inductor and a hydrogen thyratron. This pulse forming network was used to initiate the fast excitation pulses at high voltage and at high repetition rate (~ kHz). In this self-discharge heated system, high repetition rate and high voltage discharge pulse itself heats and excites the copper vapour [3.19]. As the gain of the medium depends on the rate of excitation i.e. rate at which discharge current builds up, a high voltage pulse with rise time less than hundred nano-second (ns) is required for efficient excitation. Fig.3.3 shows typical power supply high voltage circuit [3.1]. Variety [3.20-3.21] of optical resonators has been commonly employed for CVL.

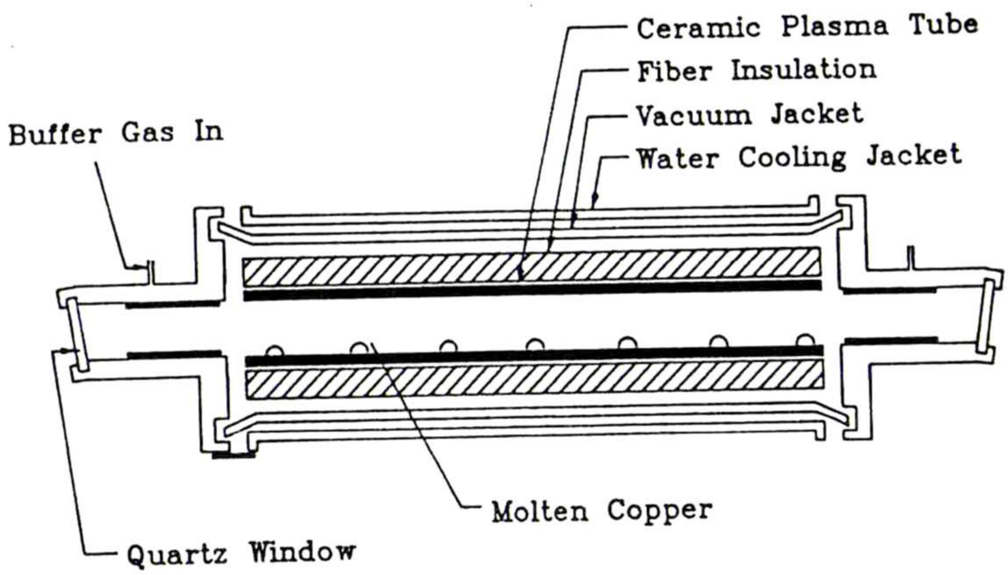

Figure 3.2*: Typical CVL discharge tube schematic [3.1]*

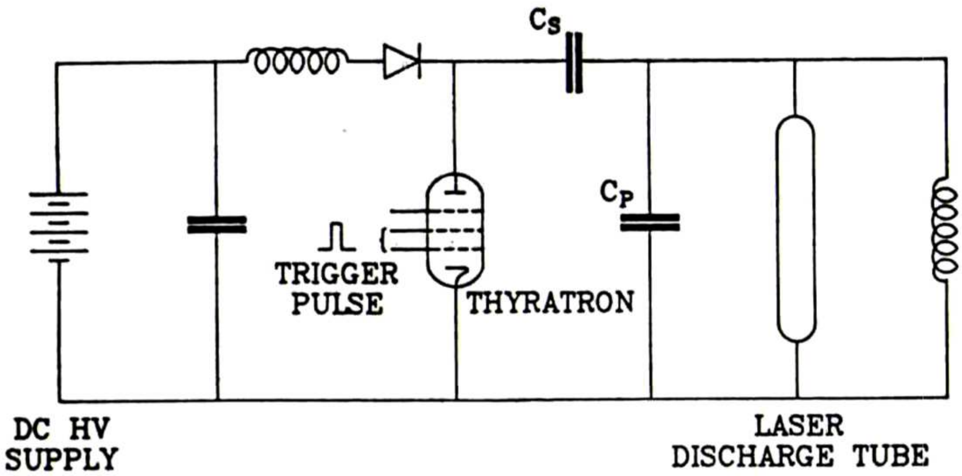

Figure 3.3*: Typical power supply high voltage circuit [3.1]*

3.2.4 Operating Characteristics of CVL

The typical operating characteristic of CVL is summarized in table 3.1.

Table 3.1: Typical operating characteristics of CVL

Pulse width	: 40-50 ns
Wavelengths	: 510.554 and 578.213 nm
Pulse repetition rate	: 5- 6 kHz
Operating temperature of the laser tube	: 1400-1500^{o}C.
Warm up time for lasing	: ~ 60 minutes
Average output power range	: ~ 20 W
Ratio between green and yellow	: 1.2, at 1500^{0}C
Beam diameter	: ~ 45 mm
Resonator	Plane-plane
Beam divergence	3-5 mrad

3.3 Spectral Characteristics of CVL

In the literatures, CVL characteristics namely peak power, average power, efficiencies, pulse duration, pulse repetition rate, etc. were extensively reported [3.14, 3.16, 3.22]. However, a very few reports are available on spectral characteristics of CVL. Also, these reports differ in experimental observations. Therefore, spectral characteristics of CVL are extensively investigated.

3.3.1 Review of spectral characteristics of CVL

A very few studies have been reported on the spectral characteristics of CVL [3.23-3.28]. Tenenbaum *et al* [3.29] have investigated the spectral structure of CVL and their dependence on temperature and buffer gas pressure. They observed that 510.6 nm lines have only one intense peak at threshold, two peaks slightly above the threshold, while third peak appears only after particular temperature. Moreover, the relative positions of the peaks and their relative intensities were temperature dependent, and the shape and width of these lines were almost insensitive to the neon buffer gas pressure (from 25 to 470 mbar). Similarly, the 578.2 nm line spectrum shows only one peak at threshold and two more at higher temperature. Yang *et al* [3.30-3.32] have studied the structure of the copper laser lines and observed three lines with different peak intensities at different time under same experimental conditions for the 578.2 nm. However, they did not observe multiple peaks for the 510.6 nm. Thus, varied observations were reported in the literatures regarding the spectral lines of CVL and influence of other physical parameters on them. Therefore, the needs for more detailed investigations were realized.

3.3.2 Relevant theory and analysis of hyperfine spectral lines of CVL

The copper has two isotopes ^{63}Cu and ^{65}Cu, which occur in the ratio 69:31 in the nature. Both isotopes have a nuclear spin $I = \frac{3}{2}$ and acquire nonzero magnetic dipole and electric quadrupole moments. This additional interactions of the electrons with the nuclear spin leads to splitting of the atomic levels having total electron angular momentum J into a number of hyperfine components, each of which corresponds to a definite value of the total angular momentum F of the atomic state such that

$$\vec{F} = \vec{I} + \vec{J} \tag{3.2}$$

where $\vec{I}$ is the nuclear spin and

$$\left|\vec{J} - \vec{I}\right| \le F \le \left|\vec{J} + \vec{I}\right| \tag{3.3}$$

In addition to this, isotopic shift is also combined with hyperfine structure. The state $^2P_{1/2}$, which is an upper state for 578.2 nm emission, splits into two hyperfine components, while the ${}^2P_{3/2}$, ${}^2D_{3/2}$ and ${}^2D_{5/2}$ states split into four components. The numbers of components are governed by equation (3.3). The allowed transitions between hyperfine components are restricted by the selection rule $\Delta F = 0, \ \pm 1$. A symbolic representation of the various allowed transitions between the hyperfine components of both green and yellow emission lines is shown in Fig. 3.4.

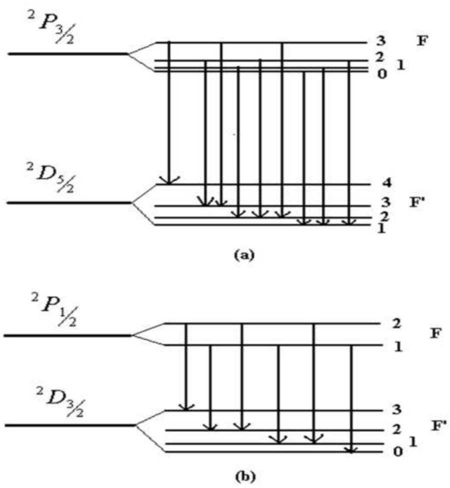

Figure 3.4: *Typical energy levels splitting of copper atom and its transitions (a) 510.6, (b) 578.2 nm*

The frequency shift $\Delta\nu$, of the hyperfine components can be calculated using formula [3.33]

$$\Delta\nu = \frac{AC}{2} + \frac{B}{4}\frac{\frac{3}{2}C(C+1) - 2I(I+1)J(J+1)}{I\,J(2I-1)(2J-1)} \tag{3.4}$$

where A is the magnetic dipole moment, B is the electric quadrupole moment of the nucleus and

$$C = F(F+1) - J(J+1) - I(I-1) \tag{3.5}$$

The transition probability between the hyperfine structure components of two different levels J and J' was determined by the expression [3.33],

$$W = \frac{4\,\omega^3}{3\,\hbar\, c^3}\frac{1}{2\,J+1}S(J,J') \qquad (3.6)$$

where

$$S(J,J') = g^2\left(\frac{e\hbar}{2mc}\right)^2 (2F+1)(2F'+1)\begin{Bmatrix} J & F & I \\ F' & J' & 1 \end{Bmatrix}^2 \times J(J+1)(2J'+1) \qquad (3.7)$$

Here, g is the Lande factor for this level. Therefore, the line strength or transition probability of the various transitions can be estimated numerically by solving the equation (3.6) and (3.7). The transition probability of different transitions (shown in Fig.3.4) has been calculated by solving $\begin{Bmatrix} J & F & I \\ F' & J' & 1 \end{Bmatrix}$ for different J, J', F and F'. The numerical value of $\begin{Bmatrix} J & F & I \\ F' & J' & 1 \end{Bmatrix}$ has been obtained using *Wigner j Symbol* [3.34-3.35]. Fig.3.5 shows the transition probabilities of the hyperfine components of 510.6 nm, (b) 578.2 nm. The frequencies are slightly shifted due to isotopic effects. Fig.3.6 shows transition probabilities versus frequency shifts of hyperfine transitions of (a) 510.6 nm, (b) 578.2 nm, for both the isotopes.

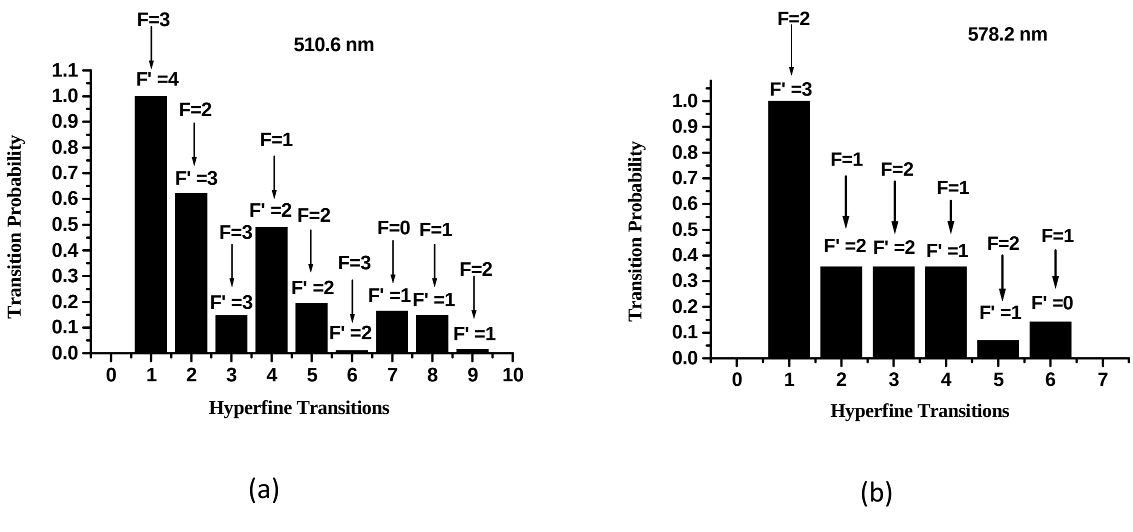

***Figure 3.5**: Transition probabilities of the hyperfine components of (a) 510.6 nm, (b) 578.2 nm emission*

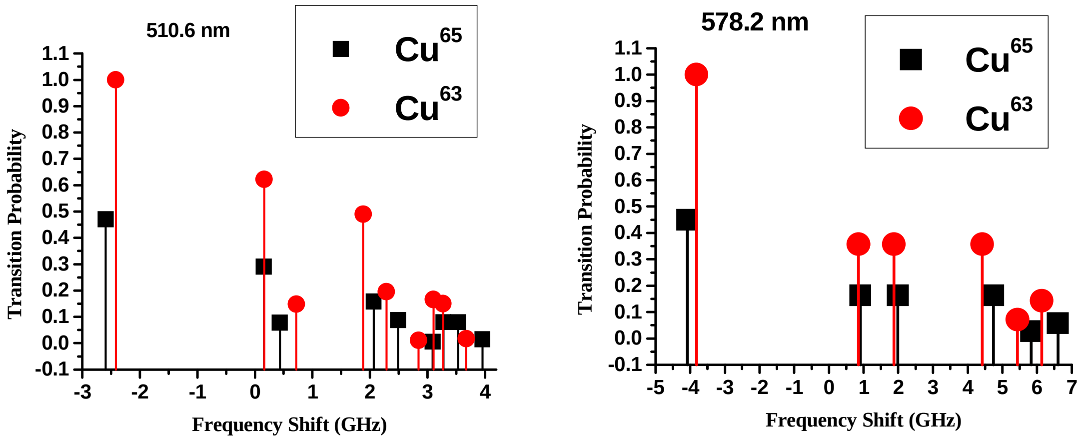

(a) (b)

***Figure 3.6**: Transition probabilities versus frequency shift of hyperfine transitions of (a) 510.6 nm, and (b) 578.2 nm, emissions for both the isotopes*

3.4 Results and discussion

The green and yellow components of CVL were separated through a dichroic mirror into two different beams. These separated laser beams were investigated through high resolution Fabry-Perot etalon (FSR 10 GHz and finesse ~100) and CCD camera based setup, as described in Chapter 2.

3.4.1 Hyperfine lines of CVL

Fig.3.7 shows typical (a) Fabry-Perot fringe, (b) intensity modulation along a line of the fringe, of 510.6 nm, just above threshold [3.36]. It has three distinct frequency components with difference in their relative intensities. The central peak, which is most intense, is accompanied by two side peaks of lower intensities. The three peaks are labeled as **A**, **B** and **C** in order of increasing frequency, as labeled in Fig.3.7 (b). The widths (FWHM) of the peaks **A**, **B**, and **C** are 0.87, 1.30 and 1.38 GHz, respectively. The peaks **A** and **B** are close as compared to **C**. The linewidth of **AB** is 3.50 GHz and **ABC** is 6.05 GHz. The separation between the peaks **B**, **C** is 2.50 GHz, and between **A**, **B** is 2.20 GHz.

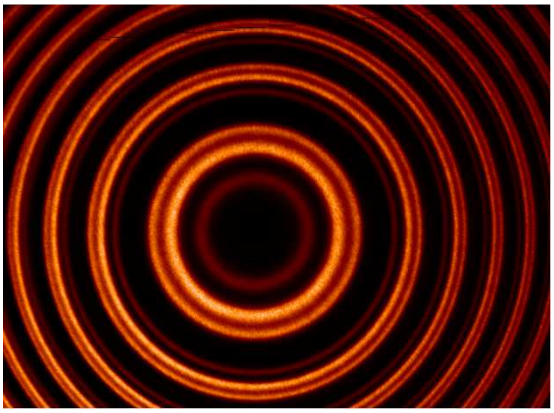

(a)

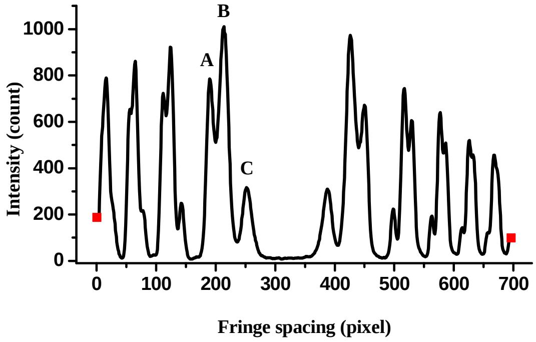

(b)

Figure 3.7: *Typical (a) Fabry-Perot fringe, (b) intensity modulation along a line of the fringe, for 510.6 nm just above threshold*

The transition probability and frequency shift analysis [3.36] suggests that the peak **B** is probably due to the transition $^2P_{3/2}(F=3)\rightarrow {}^2D_{5/2}(F'=4)$, **A** is $^2P_{3/2}(F=2)\rightarrow {}^2D_{5/2}(F'=3)$ and **C** is $^2P_{3/2}(F=1)\rightarrow {}^2D_{5/2}(F'=2)$. However, the other possible low intensity transitions were not detected.

Fig.3.8 (a) shows the typical Fabry-Perot fringe of 510.6 nm, far above the threshold. Composite image of the line scans across the diameter of the fringe has been generated over the time. Fig.3.8 (b) shows the composite image of a line scan across the diameter of the fringe of 510.6 nm lines. In Ref.3.31, fluctuations in the intensities of two higher frequency components of the 578.2 nm line of a CuBr laser were reported. It was proposed (Ref.3.31) that the two transitions starting from the same upper level compete in lasing action and this is responsible for intensity fluctuations. However, these intensity fluctuations may not be because of competition but may be due to instantaneous variation in other microscopic physical parameters such as electron density and electron temperature and other due to instability in electrical discharge of CuBr laser.

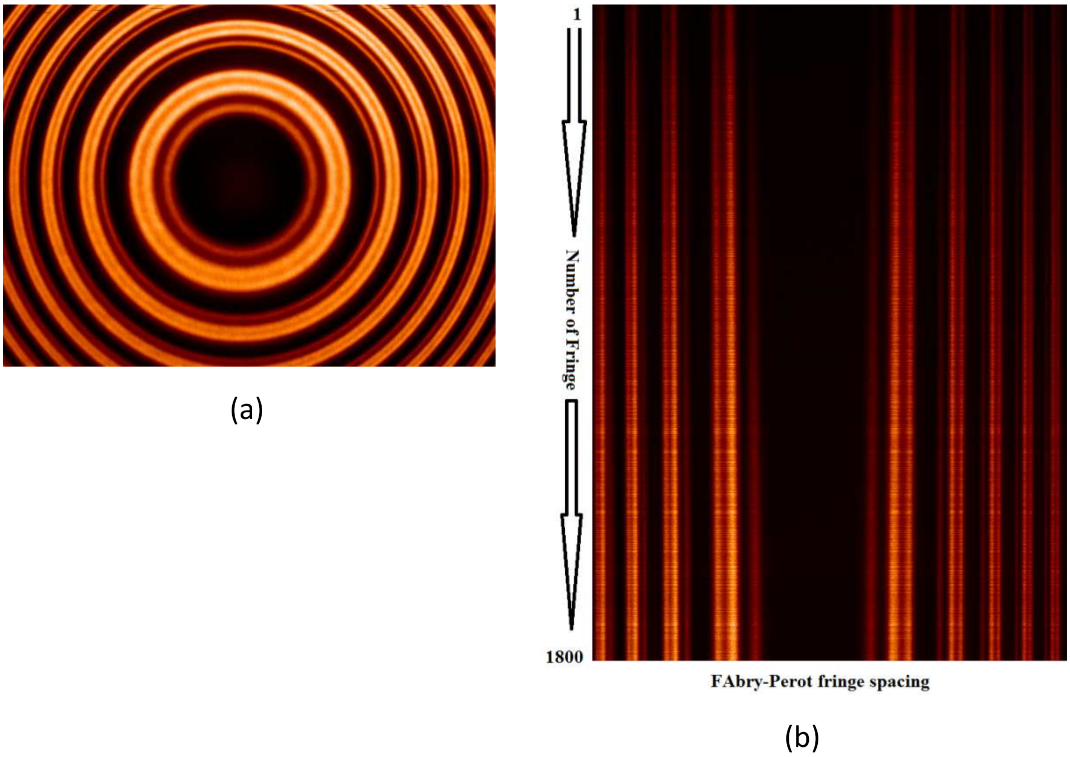

Figure 3.8*: Typical (a) Fabry-Perot fringe far above the threshold, (b) composite image of a line scan across the diameter of the fringe, of 510.6 nm lines*

Moreover, they had used a pressure-scanned Fabry-Perot etalon of FSR 30 GHz and finesse greater than 30, to analyze the fringe. This etalon (having low resolving power) was unable to resolve the hyperfine components and hence no explicit multiple line of 510.6 nm were observed.

Fig.3.9 (a) shows typical Fabry-Perot fringe of 578.2 nm line just above the lasing threshold. This has a single frequency component of 700 MHz linewidth. Fig.3.9 (b) shows the composite image of a line scans across the diameter of fringe 578.2 nm lines near threshold over the time. However, the observed behaviors for 578.2 nm at far above the threshold (i.e. at optimized parameters of operation) were different. Fig.3.10 shows the typical FP (a) fringe, (b) intensity modulation along a line scan across the fringe diameter, of 578.2 nm lines, far above the lasing threshold. It consists of three well-resolved frequency components. Two additional peaks of higher frequency and lower intensity accompany the most intense one.

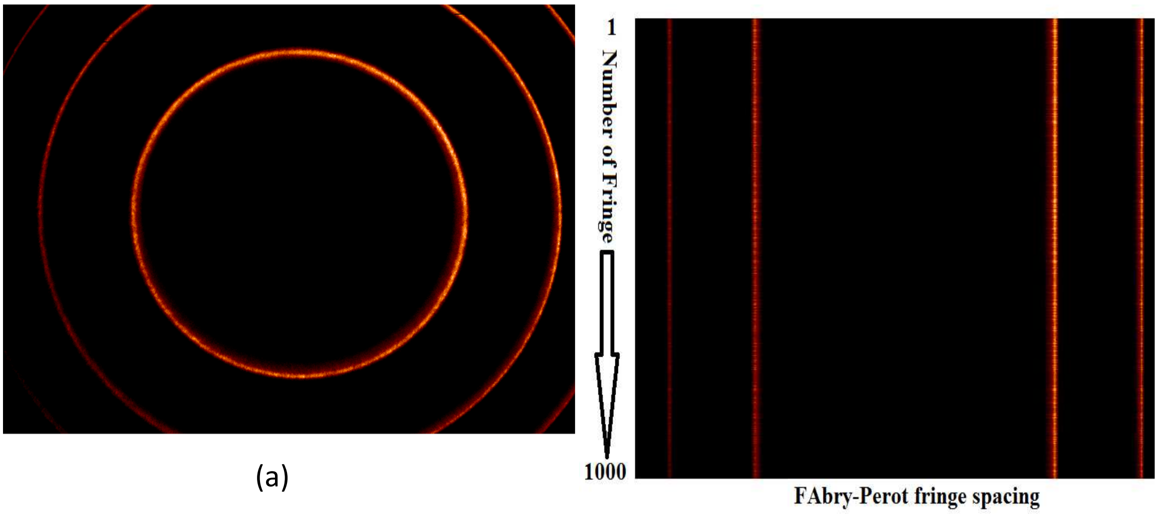

(a)

(b)

***Figure 3.9**: Typical Fabry-Perot (a) fringe, (b) composite image of a line scans across the diameter of the fringe, of 578.2 nm lines near the threshold*

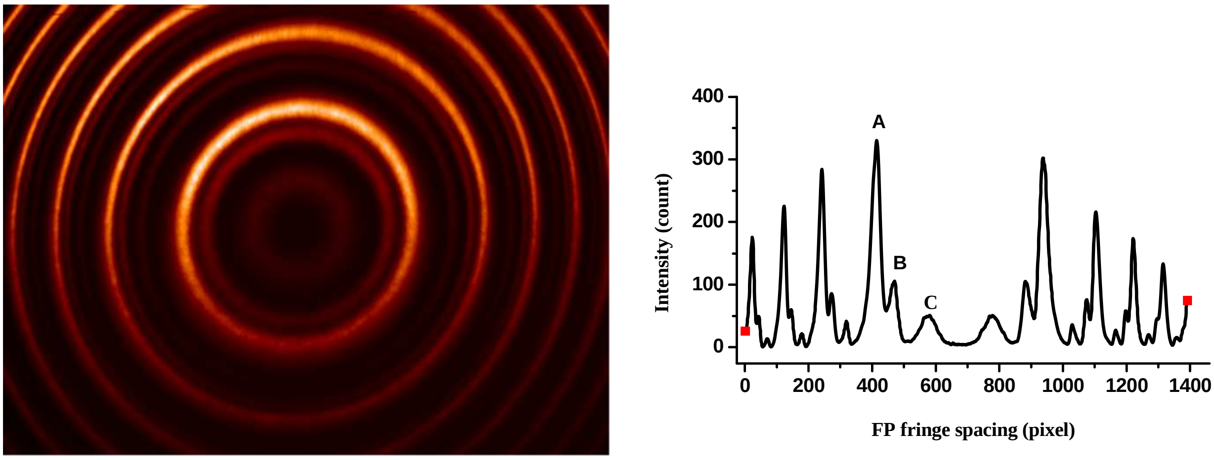

(a)

(b)

***Figure 3.10**: Typical Fabry-Perot (a) fringe, (b) intensity modulation along a line scan across the diameter of the fringe, of 578.2 nm, far above the lasing threshold*

The three peaks are labeled as **A**, **B** and **C** in the order of increasing frequency, as labeled in Fig.3.10. The linewidth of these peaks are 0.895, 0.960 and 1.380 GHz, respectively. The peak separations between (**A**, **B)** and (**B**, **C)** are 1.94 and 2.76 GHz, respectively. At the lasing threshold, only peak **A** is observed, while peaks **B** and **C** appeared at optimum operation.

3.4.2 Effect of electrical input power on spectral width of CVL

A CVL is a self heated electric discharge device, in which the discharge itself provides the energy needed to heat the lasing medium (inside the laser tube) and to vaporize the copper metal. The output characteristics of copper vapour laser depends on, (a) parameter of medium such as pressure of the vapour of an active substance, pressure and type of buffer gas, etc., and (b) gas discharge excitation parameters such as power supply voltage across the discharge tube, rate of rise of the discharge current density, characteristics impedance of the laser, etc. In addition to this, the other key parameters responsible for the output characteristics of CVL are gas temperature, electron temperature, electron density, copper atom density, upper level population and lower level population (metastable atom density), all interdependent as well as be a function of specific laser systems (e.g. thermal design, tube bore, electrical circuit, etc.).

Kushner [3.16] in his ‘self consisted model for high repetition rate CVL outlined the laser power, laser energy density, optimum tube temperature as a function of charging potential. The peak electron temperature, which is a function of the tube temperature, also depends on the charging voltage. Also an optimum tube temperature increases with increasing charging potential. Therefore, fields generated inside the discharge tube have major influence on the output characteristics of CVL. The spectral composition of the laser was investigated for different electric power sampled across the discharge tube. A very few study on the spectral width of CVL with electrical input power has been reported [3.29-3.31].

Study on spectral characteristics of 510.6 nm lines of CVL was carried out by varying the input power from 2.0 to 4.2 kW [3.37]. This has three distinct frequency components with difference in their relative intensities. **A**, **B**, and **C** identifies the peaks of the hyperfine lines, labelled in Fig.3.7 (b). Initially, when lasing starts, peak **B** dominant followed by peak **A** while peak **C** has the lowest intensity. The peak **B** has linewidth of 1.64 GHz. The linewidth of peak **ABC** lumped together was 4.82 GHz. The intensity and width of peaks increases with increasing an electric power, which finally makes it difficult to find FWHM of peak **A**, **B** and **C**, separately. Measurement of individual fringe provides linewidth transformation. The linewidth of peak **AB** lumped together increases from 3.12 GHz to 3.37 GHz with increasing power in 2.2 to 3.5 kW range. Further increasing power from 3.5 to 4.2 kW, the linewidth of peak **AB** lumped together varies from 3.35 to 3.92 GHz. The linewidth of peak **C** increase from 899 to 1132.8 MHz, from where it was difficult to find FWHM because of increased intensity of peaks. Fig.3.11 shows the typical Fabry-Perot interference (a) fringe pattern, (b) intensity modulation along a line scan across the diameter of the fringe, at 4.2 kW input power. This shows that resolution of the 510.6 nm spectral line decreased by increasing input power. Beyond 4.2 kW input power the laser tube was overheated leading to eventually decrease in output power slowly. Both, the intensity and the width of three peaks increase as the temperature inside the gain medium was increased by increasing the electrical input power. The change in temperature of the gain medium modifies the width of spectral transition. However, the peak separation between the components remains unchanged with increasing temperature through increasing electrical input power. As expected, the temperature of the gain medium does not alter the emission frequencies or increase the number of hyperfine components, but only increases the intensity and the width of the 510.6 emission lines. The lumped linewidth of peaks ABC was 6.51 GHz at 4.2 kW input power of CVL. The linewidth reduces with decreasing input power from 4.2 kW. However, the intensity and spectral width of peaks changes quickly and it become difficult to get linewidth of peaks together.

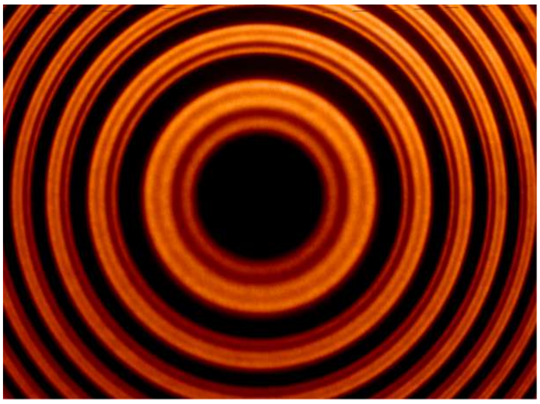

(a)

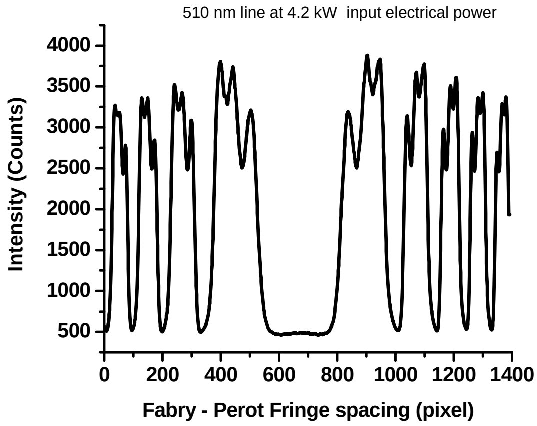

(b)

Figure 3.11*: Typical Fabry-Perot (a) fringe, (b) intensity modulation along a line scan across the diameter of the fringe, at 4.2 kW input power*

Therefore, voltage was reduced gradually (but not uniformly). The linewidth of peaks **AB** starts decreasing from 4.19 to 3.21 GHz. The peak **C** has initially linewidth of 1.39 GHz, which reduces to 899.8 MHz. The intensities of peak **A** and **C** decreases sharply, which make them difficult to get FWHM. However, the most intense central peak **B**, which left alone, shows linewidth variation from 1.69 to 1.31 GHz. Evident variations in the spectral widths are probably due to instantaneous pulse-to-pulse power levels variation because of the repetitive pulsing and instability in the gaseous discharge medium. This is probably due to instantaneous instability in environment of emitting atoms in the discharge tube.

Tenenbaum *et al* [3.29] have reported the spectrum of 510.6 nm lines at four temperatures. They observed one intense peak at threshold and two additional peaks above the threshold. Yubo *et al* [3.30] have shown that the resolution of the 510.6 nm spectral line decreases with increasing input power (0.99, 1.3, 1.51, and 1.74 kW). Yongjiang *et al* [3.31] observed in the spectra of the 510.6 nm of CuBr vapor laser line that the intensity experiencing the same process of increase first and then decrease last as the voltage increases (3.5, 4.0, 4.5, 5.0 kV). However, they observed that the linewidth is insensitive to the voltage applied. However, in this study, it was observed that spectral width of components was susceptible to the power [3.37]. An input electric power governs the tube/gas temperature and hence the linewidth of predominantly Doppler broadened CVL atomic transitions.

3.4.3 Buffer gas pressure

Buffer gas helps to (a) provide electrons for excitation of copper atoms, directly/indirectly to the upper laser level, (b) quickly cool electrons to allow superelastic collisions, electron-ion recombination, attachments, and in deactivation of the metastable lower level, (c) to provide a medium to run the discharge to heat up the copper atoms to the operating temperature and then prevents diffusion of the vapors from the hot zone to cold region of the discharge tube. The output power, average gain, saturation intensities strongly depends on the buffer gas pressure [3.1-3.2]. However, a very few study on the effect of buffer gas pressure on the spectral width of CVL has been reported [3.29-3.31]. Thus, influence of buffer gas pressure on the spectral width of 510.6 nm lines of CVL was investigated [3.38].

Tenenbaum *et al* [3.30] has reported that the shape and width of hyperfine lines of CVL were almost insensitive to the buffer gas pressure. Yongjiang *et al* [3.31] have found that the shape and width of CuBr vapour laser lines are sensitive to the neon buffer gas pressure (in the range 53.33-213.32 mbar). They have observed that the spectral width of 510.6 nm line decreases from 6.40 to 3.00 GHz by increasing the buffer gas pressure from 40 to 160 mbar. Yubo *et al* [3.29] have also analyzed the spectral profile of 510.6 nm line of copper at different buffer gas pressure and found that the increase of gas pressure from 14.4 to 77.1 mbar the intensity of the peaks of the

510.6 nm laser line shape decrease slightly while no appreciable change in spectral width was noticed.

In the present investigation, we have observed not only the intensity but also the spectral width of 510.6 nm laser line of an elemental CVL. Buffer gas pressure was varied from 5.0 to 470.0 mbar. The relative intensity and width of the frequency components were decreased at 5 mbar pressure [3.38]. Fig.3.12 shows the typical Fabry-Perot (a) fringe, (b) intensity modulation of a line scan across the diameter of the fringe, of 510.6 nm at 180 mbar pressure. The relative intensity and width of the frequency components decreased. Only peaks **A** and **B** dominating, while the peak **C** is barely seen at 180 mbar. The peak **AB** has 2.04 GHz linewidth. Fig.3.13 shows the typical Fabry-Perot (a) fringe, (b) intensity modulation of a line scan across the diameter of fringe, of 510.6 nm lines at 470 mbar. The relative intensity and width of the frequency components decreased drastically. Only two frequency components **A** and **B** are seen, in which peak B is dominating, which has 0.751 GHz linewidth. Fig.3.14 (a) shows variation of linewidth of peaks **AB** and **B** with buffer gas pressure. The peak **B** is sustained at all observed pressure range from 5-470 mbar range. However, intensity of peak **B** changes with buffer gas pressure. Fig.3.14 (b) shows the typical variation of relative intensity of peak **B** with buffer gas pressure. Initially, the intensity increases and then decreases with increasing buffer gas pressure. The spectral intensity and width decreases with increasing pressure. Therefore, one can see that with the increase of gas pressure from 25 mbar to 470 mbar the intensity of peaks of the 510.6 nm laser line shape decrease [3.38]. The energy is coupled to the discharge from the applied electric field principally via the electrons.

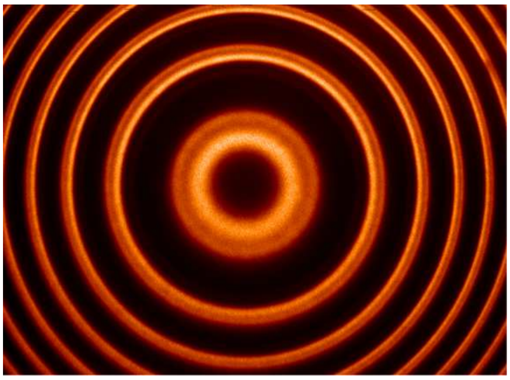

(a)

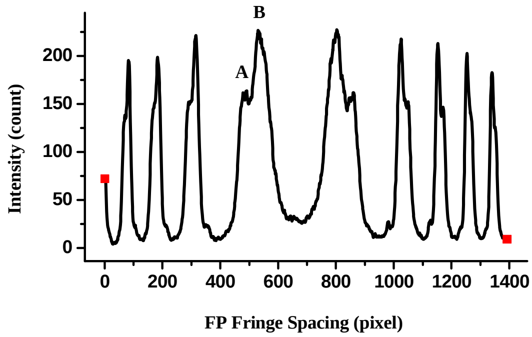

(b)

Figure 3.12: *Typical Fabry-Perot (a) fringe, (b) intensity modulation of a line scan across the diameter of the fringe, of 510.6 nm at 180 mbar pressure*

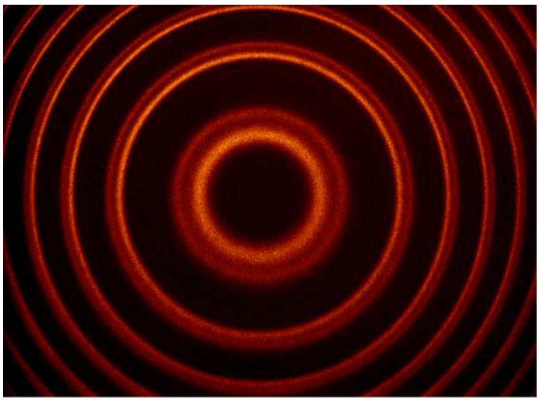

(a)

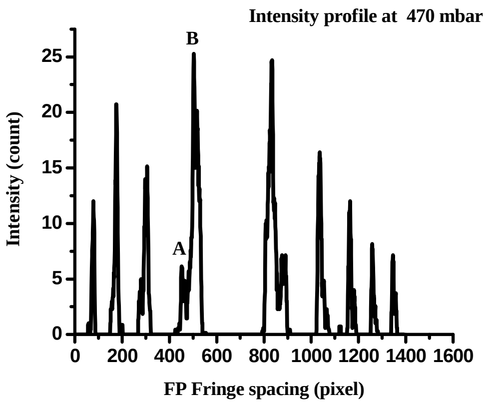

(b)

Figure 3.13: *Typical Fabry-Perot (a) fringe, (b) intensity modulation of a line scan across the diameter of the fringe, of 510.6 nm lines at 470 mbar*

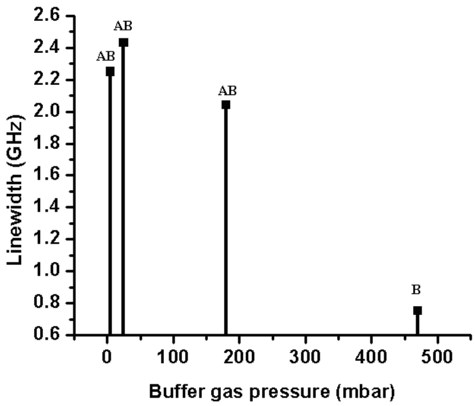

(a)

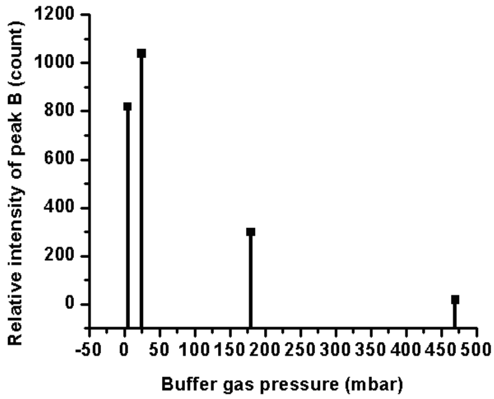

(b)

Figure 3.14: *Typical variation of (a) linewidth of peaks **AB** and **B**, (b) relative intensity of peak **B**, with buffer gas pressure*

The electric field influence the rate at which electrons pick up energy between collisions while the pressure controls the mean free path between these collisions i.e. electron temperature, $T_e = f\left(\frac{E}{p_0}\right)$, where E is the electric field and p_0 is the pressure that corresponds to the (hot) particle density in the tube reduced to standard temperature and pressure (STP).

The electron temperature depends on various discharge parameters like buffer gas density, copper atom density, and excitation discharge current pulse. With the increase of gas pressure the collision frequency increases among particles, which would decrease the electron temperature, the excitation rates and the lifetime of excited upper state particles. The decrease in laser intensity with increasing buffer gas pressure is due primarily to the decrease in electron temperature. Increasing of buffer gas pressure, decreases the electron density and hence electron temperature. At buffer pressure below optimum, excitation and ionization rates to states with thresholds greater than the ^2P copper levels become increasingly more probable and hence intensity decrease at low pressure.

In the present study, the pressure was varied from 5 mbar. At this low pressure the linewidth was less than the value at optimal operating pressure (20-25 mbar). The increased buffer gas pressures decrease the electron temperature and hence reduce the energy of the electrons. The excitation rates, which are proportional to electron temperature, decrease with increasing pressure. This results in decreasing the population in the upper state. Alternatively, gains of the components are proportional to the transition probabilities between these two laser states. Therefore, when the excitation rates decreases, the frequency components having comparative smaller gain will disappear. This causes the number of the hyperfine components, which reach the laser threshold decrease, and the width to reduce. Thus, in fact, the change of pressure may destabilize the optimum equilibrium of the gain medium.

3.5 Summary

In conclusion, succinct description of copper atom laser transition mechanisms, kinetics, design, construction and working principle of CVL are presented. The theoretical analyses of energy level splitting of copper atom, transition probabilities between these levels are also investigated. The emission of green lines starts somewhat earlier than that of the yellow lines. The 510.6 nm lines consist of three distinct frequency components, which are result from the transitions of the hyperfine components. For the 578.2 nm line, the observed behavior is quite different. At the lasing threshold, only one frequency component was observed. However, far above the threshold, two additional components of higher frequency (and lower intensity) accompanying the most intense line is observed. The frequency components are well resolved, stable and reproducible. Input electric power in the discharge tube also plays a significant role on the spectral width of CVL emission. An additional broadening of almost 1 GHz at the highest input power for optimum operation is observed. The input electrical power decides the tube/gas temperature and hence the linewidth of predominantly Doppler broadened CVL atomic transitions. The intensity and the spectral width of 510.6 nm laser line are sensitive to the buffer gas pressure. The hyperfine components having highest gain appear first in lasing and are also the last to disappear. Altering the buffer gas pressure reduces the number of components (and hence the overall linewidth). Typical CVL parameters such as repetition rate, power, pulse width, beam diameter etc. are also listed.

Therefore, very stable spectral characteristics in the visible region of electromagnetic radiation made CVL an ideal source for high repetition rate excitation of the dye laser as well as for other applications. The present high resolution spectral study also builds formidable experimental technique for such studies on dye laser, described in later chapters.

Publications based on this chapter

1. Study of the influence of the input electric power on the spectral width of the 510.6 nm line of an atomic copper vapor laser

   Optics and Laser Technology **42**, 866 (2010)

   Nageshwar Singh and H. S. Vora

2. On the hyperfine spectral lines of an atomic copper vapor laser

   Optics Communication **182**, 1393 (2009)

   Nageshwar Singh and H. S. Vora

3. Influence of buffer gas pressure on the spectral width of 510.6 nm line of an atomic copper vapor laser

   Optical Engineering **48**, 094201 (2009)

   Nageshwar Singh and H. S. Vora

References

[3.1] F. J. Duarte, *High Power Dye Lasers,* Springer-Verlag, Berlin 1991

[3.2] Chris E. Little and Nikola V. Sabotinov, *Pulsed Metal Vapour Lasers*, Kluwer Academic Publishers, London 1995

[3.3] Christopher E. Little, *Metal Vapour Lasers*, John Wiley & Sons, Chichester, London 1999

[3.4] R. Jensen, G. J. Marimuzzi, C. P. Robinson, and S. D. Rockwood, Laser Focus **12**, 5 (1976)

[3.5] J. A. Paisner, Appl. Phys. **B46**, 253 (1988)

[3.6] P. T. Greenland, Contemporary Phys. **31**, 405 (1990)

[3.7] Isaac L. Bass, Regina E. Bonanno, Richard P. Hackel and Peter R. Hammond, Appl. Opt. **31**, 6993 (1992)

[3.8] P. Ramakoteswara Rao, Current Science **85**, 615 (2003)

[3.9] W. T. Walter, N. Solimine, M. Piltch and G. Gould, IEEE J. Quantum Electron **QE-2**, 474 (1966)

[3.10] J. J. Kim, Optics and Quantum Electron. **23**, S469 (1991)

[3.11] William T. Silfvast, *Laser Fundamentals*, Cambridge University Press, 1998

[3.12] L. A. Weaver, C. S. Liu and E. W. Sukov, IEEE J. Quantum Electron **QE-10**, 140 (1974)

[3.13] P. A. Bokhan, V. A. Gerasimov, V. I. Solomonov and V. B. Scheglov, Sov. J. Quantum Electron. **8**, 1220 (1978)

[3.14] M. J. Kushner and B. E. Warner, J. Appl. Phys. **54**, 2970 (1983)

[3.15] R. J. Carman, D. J. W. Brown and J. A. Piper, IEEE j. Quantum Electron. **QE-30**, 1876 (1994)

[3.16] M. J. Kushner, IEEE J. Quantum Electron.**17**, 139 (1981)

[3.17] B. Singh, P. K. Badhani, J. K. Mittal, R. Bhatnagar, Rev. Sci. Instrum. **55**, 1542 (1984)

[3.18] J. K. Mittal, B. Singh, P. K. Badhani, R. Bhatnagar, J. Phys. E: Sci. Instrum. **21**, 435 (1988)

[3.19] A. A. Isaev, M. A. Kazaryan and G. G. Petrash, JETP Lett. **16**, 27 (1972)

[3.20] A.E. Siegman, Appl. Opt. **13**, 353 (1974)

[3.21] Bijendra Singh, Rev. Sci. Instrum. **83**, 123101 (2012)

[3.22] G G Petrash (ed), *Metal Vapor and Metal Halide Vapor Lasers*, Nova Science Publishers, Commack, 1989

[3.23] N. M. Nerheim, J. Appl. Phy. **48**, 3244 (1977)

[3.24] W.C. Kreye, L. Roesler, Appl. Opt. **22**, 927 (1980)

[3.25] J. Tenenbaum, I.Smilanski, S Gabay, G Erez and L. A. Levin, J. Appl. Phys. **49**, 2662 (1983)

[3.26] M. A. Kazaryan, G G Petrash and A N Trofimov, Sov. J. Quantum Electron. **10,** 328 (1980)

[3.27] A. A. Isaev, Sov. J. Quantum electron. **10**, 336 (1980)

[3.28] Wang Yubo, Mao Bangning, Chen Li, Wang Limin, Pan Bailiang, Opt. Commun. **278**, 138 (2007)

[3.29] J. Tenenbaum, I. Smilanski, S.Gabay, L. A. Levin, G. Erez, S. Lavi, Opt. Commun. **32**, 473 (1980)

[3.30] Y. J. Wang, Sheng Pen Shen, Tie Jun Xia, and Zhe Hua Wu, Appl. Phys. **B** 46, 191 (1988)

[3.31] Y. J. Wang, Sheng Pen Shen, Tie Jun Xia, Appl. Phys. **B 47**, 87 (1988)

[3.32] Y. J. Yang, B. L. Pan, X. D. Ding, Y. J. Qian, S. Y. Shi, SPIE **1412**, 60 (1991)

[3.33] I. I. Sobleman, *Introduction to the theory of atomic spectra*, Pergamon, Oxford, 1981

[3.34] A. R. Edmonds, *Angular Momentum in Quantum Mechanics*, Princeton University Press 1974

[3.35] E. Condon, and G. Shortley, *Theory of Atomic Spectra*, Cambridge 1935

[3.36] Nageshwar Singh and H. S. Vora, Opt. Commun. **182**, 1393 (2009)

[3.37] Nageshwar Singh and H. S. Vora, Opt. Laser Technol. **42**, 866 (2010)

[3.38] Nageshwar Singh and H.S. Vora, Opt. Eng. **48**, 094201 (2009)

Chapter 4

Studies on pulsed dye laser resonator

4.1 Introduction

A resonator plays a vital role in building up the laser beam characteristics. The spectral characteristics of a laser, such as spectral width and coherence length are primarily determined by the longitudinal modes; whereas beam divergence, beam diameter, and energy distribution are governed by the transverse mode structures that survive inside the resonator. The resonator has resonance frequencies of its own that interact with amplifying medium and controls energy, spatial, spectral and temporal properties i.e. output power, monochromaticity, divergence and spatial intensity distribution of the laser output.

Pulsed dye laser, like other lasers, typically consists of organic dye as gain medium, an excitation source, and an optical resonator. Optical resonator is the optical system that reflects radiation back to the gain medium and determines the mode properties and power/energy of the laser [4.1]. The most basic resonator, regardless of the method of excitation, is that composed of two mirrors aligned along a single optical axis. In general, optical resonator is made of two mirrors in which one of the mirrors is ~ 100 % reflective at the wavelength or wavelengths of interest while the other mirror is partially reflective. The amount of reflectivity depends on the characteristics of the gain medium. The optimum reflectivity for the output coupler is often determined empirically [4.1]. For a low-gain laser medium the reflectivity can approach 99%, whereas for a high-gain laser medium this reflectivity can be as low as a few % [4.1].

The dye laser is a high gain laser in which a ~ 100 % reflective optics is often replaced by a diffractive element(s) like prisms/grating in either Littrow or grazing incidence grating (GIG) configuration, as a part of the resonator [4.2]. The grating, which controls the wavelength of oscillation and reduces the laser emission spectral width, has been used as the principal element. In this type of laser resonator system, narrow wavelength operation is generally achieved by allowing the broadband emission emerging from the dye cell to pass over the surface of a diffraction grating and the grating exerts maximum angular dispersion on the spectral components of the incident light.

4.2 Theory of pulsed dye laser resonator

4.2.1 Theoretical analysis

The spectral width of the dye laser output depends mainly on the passive bandwidth of the resonator and the number of round trips taking place in the resonator [4.2]. Passive bandwidth of the resonator is determined by the angular dispersion of the wavelength selector and the divergence of the dye laser beam incident on it [4.1-4.3]. Narrow bandwidth laser output is obtained by making passive bandwidth small, using highly wavelength selective elements and/or by allowing a large number of round trips to take place within the resonator. For short pulse dye lasers where the number of round trips are only a few, the laser bandwidth is determined mainly by the passive bandwidth of the resonator.

For pulsed dye laser resonator incorporating dispersive elements, the single pass bandwidth is given to a first approximation [4.2] by

$$\Delta\lambda = \frac{\Delta\theta}{\left(\frac{\partial\Theta}{\partial\lambda}\right)_C} \tag{4.1}$$

where $\Delta\theta$ is the beam divergence and $\left(\frac{\partial\Theta}{\partial\lambda}\right)_C$ is the total dispersion provided by the optical components in the resonator. Thus, bandwidth is minimized by reducing $\Delta\theta$ and increasing the dispersion. For the grating-mirror cavity, the emission wavelength is governed by the grating equation

$$m\,\lambda = a(\sin\Theta \pm \sin\Theta') \tag{4.2}$$

where m is the order, a is groove spacing, Θ is the angle of incidence, and Θ' is the angle of diffraction.

For a grating utilized in Littrow configuration (i.e., $\Theta = \Theta'$), the grating dispersion becomes

$$\left(\frac{\partial\Theta}{\partial\lambda}\right)_G = {}^{2\tan\Theta}/_{\lambda} \tag{4.3}$$

And for grazing incidence grating configuration, the grating dispersion is

$$\left(\frac{\partial\Theta}{\partial\lambda}\right)_G = {}^{2\,(\sin\Theta \pm \sin\Theta')}/_{\lambda\cos\Theta} \tag{4.4}$$

Or equivalently,

$$\left(\frac{\partial\Theta}{\partial\lambda}\right)_G = {}^{2\,m}/_{a\cos\Theta} \tag{4.5}$$

Fig.4.1 and Fig.4.2 show the typical dye laser setup in Littrow and GIG configurations, respectively. While in GIG configuration, the resolution of the cavity is enhanced by illuminating the whole grating with the unexpanded beam (which is widened by natural beam divergence only) using the grating at a large angle of incidence. Thus, the way to reduce linewidth is to use a highly dispersive grating (a grating used at large angles of incidence) and simultaneously reduce the beam divergence $\Delta\theta$ by expanding the beam incident on the grating.

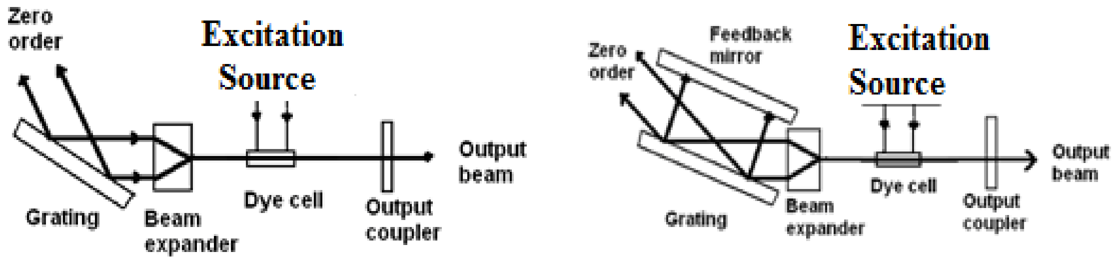

(a) (b)

***Figure 4.1**: Typical dye laser setup in (a) Littrow, (b) GIG configuration*

Beam expansion by a ratio M decreases the beam divergence $\Delta\theta$ by the same factor M, so that [4.2]

$$\Delta\lambda = \frac{\Delta\theta}{M}\frac{1}{\left(\frac{\partial\Theta}{\partial\lambda}\right)_C} \tag{4.6}$$

In other way, the angular dispersion of the beam expander-grating combination is M times the angular dispersion of the grating used alone, i.e.

$$\Delta\lambda = \frac{\Delta\theta}{M\left(\frac{\partial\Theta}{\partial\lambda}\right)_C} \tag{4.7}$$

The resolving power of grating depends on the order of diffraction. In a given order, it is proportional to the total number of lines illuminated. The illuminated width (G) of the grating is given by

$$G = \frac{W}{\cos\Theta} \tag{4.8}$$

where w is size of beam incidence on the grating. Therefore, to maximize the resolving power of grating either size of the incident beam is large enough or it should be kept at higher angle of incidence (i.e. at grazing incidence). The grating efficiency reduces drastically at grazing angle of incidence [4.4]. Therefore, effective way to increase the resolving power of the grating is to increase the beam size before its incidence on grating. Expansion of the beam inside the resonator is accomplished by using optical element, called beam expander. Several methods have been used to expand the beam inside the resonator and reduce the spectral width of pulsed dye laser [4.5-4.11]. Hänsch [4.5] used a telescope to expand the laser beam so that it illuminates maximum length of the diffraction grating, which was set in a Littrow configuration. Eesley *et al* [4.6] used mirror-telescope as an intra-cavity beam expander. Telescopic beam expander provides two dimensional beam expansion and made resonator length relatively long, although, in laser spectral narrowing mechanisms beam expansion along the length of grating is effectively useful. Keeping these facts in mind, Hanna *et* *al* [4.11] proposed prism as a one dimensional compact intra-cavity beam expander and demonstrated the narrow bandwidth operation of dye laser. After that a number of authors have implemented prism or multiple prisms to reduce the bandwidth and improve the efficiency of dye laser.

The main role of the beam expander is to expand the laser beam and fill maximum length of the grating. Magnification provided by the prism, which depends upon angle of incidence, apex angle and refractive index of material used for construction, plays an important role on the spectral narrowing of the dye laser. The magnification provided by the prism is given [4.12] by

$$\mathrm{M} = \frac{\cos\theta_2 \cos\theta_4}{\cos\theta_1 \cos\theta_3} \tag{4.9}$$

where θ_1, θ_2 and θ_3, θ_4 are the angles of incidence, refraction at the first surface and second surfaces, respectively. These involved angles in beam transmission through prism are shown in Fig.4.2 (a). The angles are related with prism parameters such as refractive index and apex angle through,

$$\theta_2 = \sin^{-1}[(\sin\theta_1)/n] \tag{4.10}$$

$$\theta_3 = A - \theta_2 \text{, and } \theta_4 = \sin^{-1}(n\sin\theta_3) \tag{4.11}$$

And angle between the entrance and the exit beams is by

$$\varepsilon = \theta_1 + \theta_4 - A \tag{4.12}$$

where n is the refractive index, A is the apex angle of prism.

To fully illuminate the grating and achieve maximum resolution, the frequency selectivity is improved using a prism as an intra-cavity beam expander. However, to reduce contraction on leaving the prism, the exit surface of the prism has been made approximately normal to the beam.

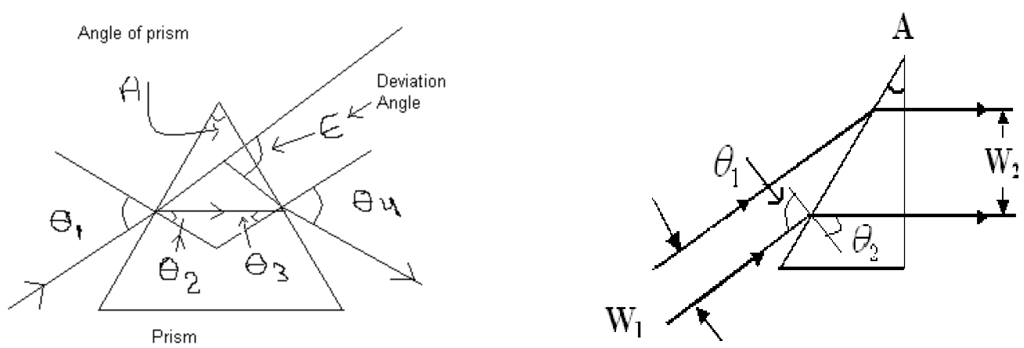

(a) (b)

***Figure 4.2**: Systematic of (a) angles involved in beam transmission through prism, and (b) beam expanding view through the right angle prism*

When a beam of size W_1 incident at an angle θ_1 on the first surface of the right angle prism and W_2 is the beam size after passing through it, then the magnification factor M of the beam is given by [4.2]

$$M = \frac{W_2}{W_1} = \left(\frac{n^2 - sin^2\,\theta_1}{n^2 - n^2\,sin^2\,\theta_1}\right)^{1/2} \tag{4.13}$$

The systematic of beam expanding view through the right angle prism is shown in Fig.4.2 (b). The reflection losses are also an important factor on the design of optical element because they affect significantly the efficiency of the system. According to electromagnetic wave theory, when a beam of light incident at an angle it is partly reflected and partly transmitted. The reflection coefficient R for p polarized light at first surface of the prism is given by [4.2],

$$R = \frac{tan^2\,(\theta_1 - \theta_2)}{tan^2\,(\theta_1 + \theta_2)} \tag{4.14}$$

The transmission coefficient T is related with reflection coefficient R by

$$T = 1 - R = \frac{\sin 2\,\theta_1 \sin 2\,\theta_2}{sin^2\,(\theta_1 + \theta_2) cos^2\,(\theta_1 - \theta_2)} \tag{4.15}$$

The multiple-return-pass linewidth for a multiple-prism grating oscillator is given by [4.2],

$$\Delta\lambda = \frac{\Delta\theta_R}{(R\,\nabla_\lambda\Phi_P + R\,M\,\nabla_\lambda\Theta_G)} \tag{4.16}$$

where $\nabla_\lambda\Theta_G$ is the total grating dispersion, $\nabla_\lambda\Phi_P$ is the total prism dispersion, M is the intra-cavity beam expansion ratio, here R is the total number of return passes. The multiple-return-pass beam divergence $\Delta\theta_R$ is given by [4.2]

$$\Delta\theta_R = \left(\frac{\lambda}{\pi W}\right)\left(1 + \left(\frac{L_R}{B_R}\right)^2 + \left(\frac{A_R L_R}{B_R}\right)^2\right)^{1/2} \tag{4.17}$$

Where L_R is the Rayleigh length, A_R and B_R are the multiple return pass transfer matrix coefficients, W is beam waist size, and λ is the wavelength.

4.2.2 Numerical analysis

In this section, the numerical analysis of beam magnification and dispersion provided by prism and grating is presented for the parameters used in the experiments of later chapter. Magnification provided by the prism, in fact, depends on the angle of incidence and refractive index of the prism material. Here, results of the calculations associated with dependent parameters are discussed. Fig.4.3 shows variation of magnification with (a) angle of incidence on the prism, (b) refractive index of the prism material. Magnification increases with increasing angle of incidence, for a given prism apex angle and refractive index. The increase in magnification is very small for angles less than 85^0, however, it changes drastically for angles in the ranges 86^0 to 89^0. Fig.4.4 shows variation of beam transmission and reflection coefficient with angle of incidence on the prism. The transmission below 55^0 is almost constant and reduces drastically in the range of 80-89 ^{0} angle of incidence, irrespective of the refractive index of material.

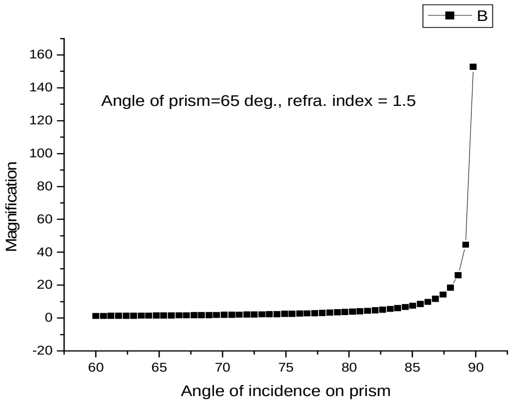

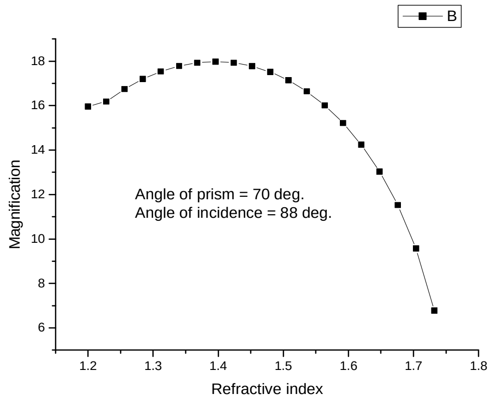

(a) (b)

Figure 4.3: *Variation of magnification with (a) angle of incidence, and (b) refractive index, of the prism*

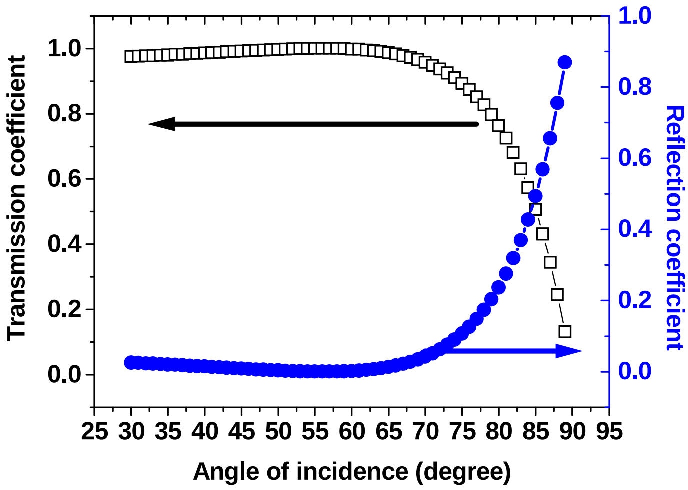

Figure 4.4: *Variation of beam transmission and reflection coefficient with the angle of incidence on the prism*

Therefore, in practice, to reduce the reflection losses and get higher magnification, multiple prisms are generally used at relatively lower angle of incidence.

The single pass dispersion of the prism [4.13] is

$$\nabla_\lambda \Phi_P = \frac{\sin A}{\cos\theta_2 \cos\theta_4}\frac{dn}{d\lambda} \tag{4.18}$$

where $\frac{dn}{d\lambda}$ is the dispersion of the prism material.

For prism apex angle 70^0, angle of incidence 88^0 to the first surface, hence 34^0 to the second surface, the typical calculation for the angles described above shows that the prism dispersion is

$$\left(\frac{\partial \Phi}{\partial \lambda}\right)_P = \frac{2\ \sin A}{\cos\theta_1 \cos\theta_3}\frac{dn}{d\lambda} = 0.3897\ \ {}^{mrad}/_{A} \tag{4.19}$$

where $\frac{dn}{d\lambda} = -6 * 10^{-6}\ /A$

For 88^0 angle of incidence to the grating (magnification 8.7, beam size 0.1 mm from dye cell), the illuminated width G, of the grating is 24.93 mm. For the grating with a = 4.17x 10^{-4} mm (grating 2400 lines /mm). Dispersion of the grating is

$$\left(\frac{\partial \Theta}{\partial \lambda}\right)_G = 9.7162\ \ mrad/A \tag{4.20}$$

Thus, the total dispersion $\left(\frac{\partial \Phi}{\partial \lambda}\right)_P + \left(\frac{\partial \Theta}{\partial \lambda}\right)_G = 10.1059\ \ mrad/A$

For a prism beam expander-grazing incidence grating-tuning mirror configuration, the typically passive bandwidth [4.13] is

$$\Delta\lambda = \frac{2\sqrt{2}\ \lambda}{\pi\ M\ W}\ \frac{1}{\left(\left(\frac{\partial \Phi}{\partial \lambda}\right)_P + \left(\frac{\partial \Theta}{\partial \lambda}\right)_G\right)} \tag{4.21}$$

These numerical analysis shows that the dispersion provided by the prism is very small as compared to the dispersion by the diffraction grating. For the dye laser emission peak wavelength λ = 576.00 nm, the typical estimated passive bandwidth is $\Delta\lambda = 4.28$ GHz. However, it is known that the passive bandwidth is always larger than that experimentally observed, due to the gain narrowing.

Numerical analysis of bandwidth is further estimated at different angle of incidence on prism and grating. Fig.4.5 shows variation of bandwidth with angle of incidence on the (a) prism, (b) grating. Fig.4.6 shows variation of (a) bandwidth with beam waist size, (b) the ratio of bandwidth and wavelength with beam waist size for different angle of incidence. The dispersion due to the prism is much smaller than that due to the grating, hence after neglecting the prism dispersion term, the ratio of bandwidth and wavelength were estimated for different angle of incidence on the grating with beam waist size.

$$\Delta\lambda = \frac{2\sqrt{2}\,\lambda}{\pi\, M\, W} \frac{1}{(\sin\Theta \pm \sin\Theta')} \tag{4.22}$$

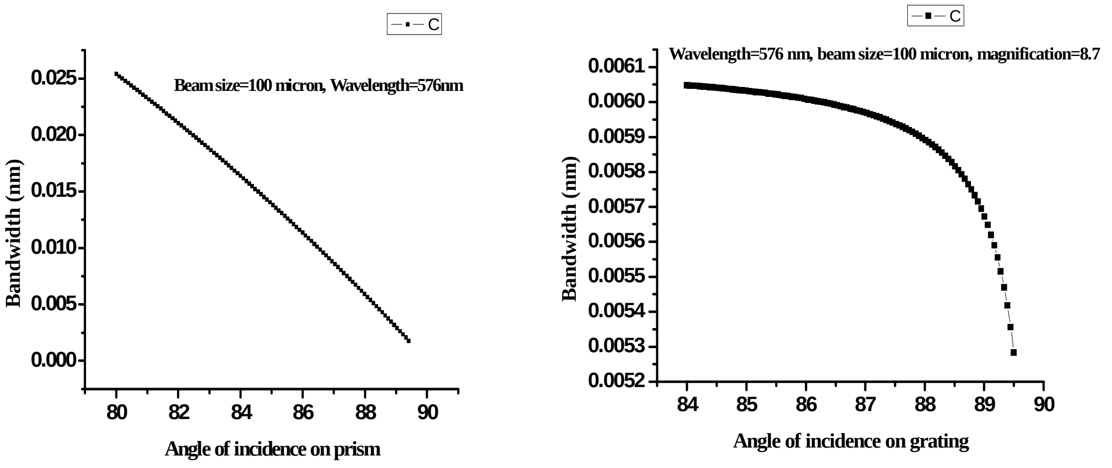

(a) (b)

Figure 4.5*: Variation of bandwidth with angle of incidence on the (a) prism, and (b) grating*

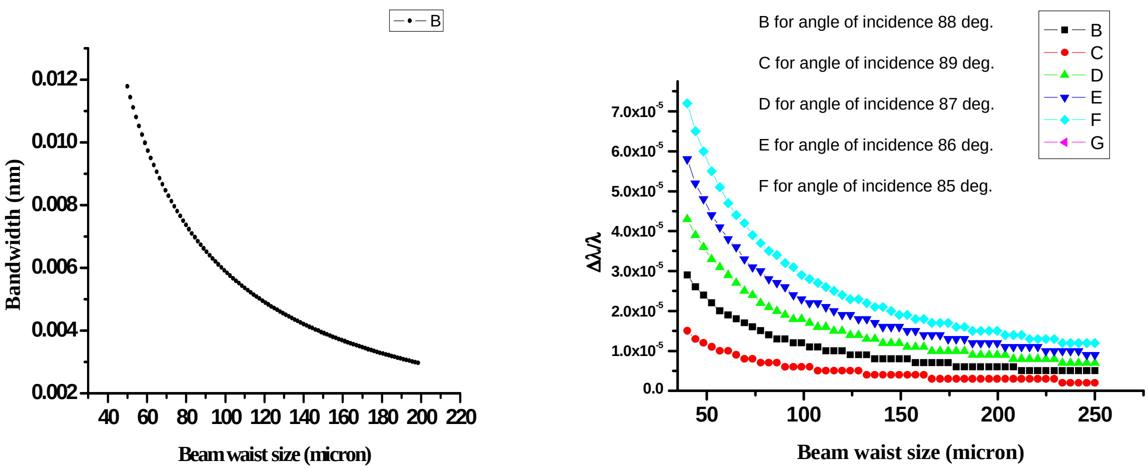

(a) (b)

Figure 4.6*: Variation of (a) bandwidth with beam waist size, (b) ratio of bandwidth and wavelength with beam waist size*

For constant angle of incidence Θ and diffraction angle Θ',

$$\Delta\lambda/\lambda = \frac{Z}{W} \tag{4.23}$$

where $Z = \frac{2\sqrt{2}}{\pi\, M}\ \frac{1}{(\sin\Theta \pm \sin\Theta\prime)}$. Therefore, variations of $\Delta\lambda/\lambda$ with beam waist size were estimated at different angle of incidence.

4.2.3 Optimization of dye laser output power

A typical tunable laser usually permits power output coupling from one side of the optical resonator with a partially transmitting mirror, whereas dispersive element is generally used as a reflective optics on the other side [4.2]. In the open cavity of Saikan [4.14] the laser output was taken directly from the grating in the form of the zero order beams. The closed cavity used by Littman and Metcalf [4.9], in which the output beam was taken from a partially transmitting mirror at the opposite end of the cavity. For power extraction the transmission coefficient of the output coupling mirror is a very important factor. If it is very large then loss exceed the gain and no lasing is possible and if it is small then laser may oscillate brightly inside the cavity but output coupling is very small. For an efficient laser operation and maximum power extraction, optimization of reflection coefficient of partially transmitting output coupling mirror is an important aspect.

Dasgupta and Nair [4.15] have optimized the gain length for maximum extraction efficiency. Zhang and Tokaryk [4.16] have proposed a new geometry for grating-tuned cavities that reduces optical losses from the gratings, lowers the lasing threshold, and enhances the laser output. Mashev et al [4.17] has treated the optimization of the grating efficiency in grazing incidence. Munz et al [4.18] have addressed the problem of output–coupling optimization dye laser in terms of a rate equation approach under steady state, spatial variation of the gain distribution, reabsorption, triplet effects and excited state absorption. In the present study, effect of output coupler mirror reflectivity on the optical power of dye laser in GIG configuration was investigated theoretically and experimentally. The two mirror cavity approach has been simplified and optimized for the dye laser output power. A schematic representation of the dye laser setup employed for this study is shown in Fig.4.7 (a). The prism beam expander, grating at grazing incidence, highly reflecting mirror M , and a partially transmitting mirror M_2 forms the resonator of dye laser. The tuning mirror M of reflectivity R and the grating with first order are positioned as shown in Fig.4.7 (a). The combination of the grating and the tuning mirror is lumped together and represented as a flat mirror of reflectivity $R_1 = R.(2R_d)$, where R_d is the grating diffraction efficiency. The simplified resonator, typically, consists of two mirrors of transmission coefficient T_1 (reflection coefficient,$1 - R_1$) and transmission coefficient T_2 (reflection coefficient,$1 - R_2$) separated by the active medium length l.

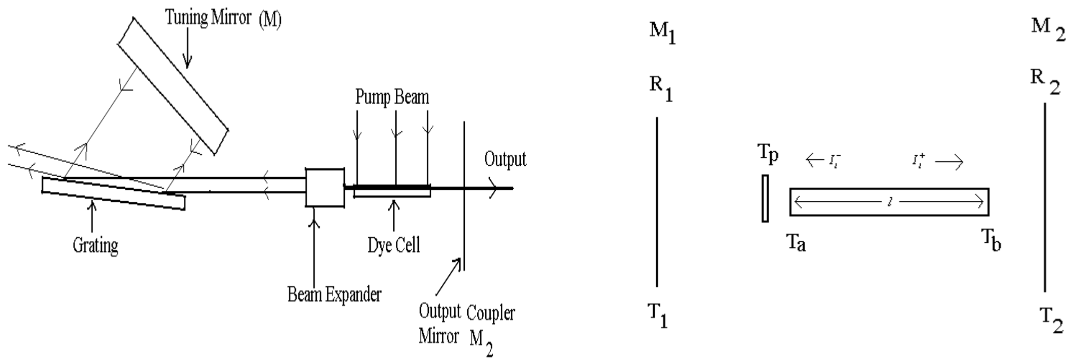

(a) (b)

Figure 4.7*: Schematic representation of the (a) dye laser setup, (b) simplified symbolic representation of the dye laser resonator*

The quantities I_l^+ and I_l^- are the internal photon intensities propagating in the positive and negative x-direction (as shown in Fig.4.7 (b)) with the total intensity I_l at any point given by

$$I_l = I_l^+ + I_l^- \tag{4.24}$$

In Fig.4.7 (b), T_a and T_b are the transmission coefficient of the dye cell windows, T_P is the transmission coefficient of the prism beam expander, respectively, R_1 is the lumped reflection coefficient of grating-mirror, R_2 is reflection coefficient of the output coupler mirror. It was assumed that the losses of the beam passing through both the windows are same i.e. $T_a = T_b$.

In the resonator, which support substantially plane electromagnetic waves, the loss due to output coupling is defined by

$$L_0 = \exp\left(-\frac{1}{2}\ln\left(1/_{R_1 R_2} \right)\right) \tag{4.25}$$

For an optical resonator containing an active medium as an amplifier, the self-oscillating condition for a resonator shown in Fig.4.7 can be written as,

$$R_2 \; R_1 T_p^2 T_a^2 \; T_b^2 \exp(2\alpha l) = 1, \tag{4.26}$$

where α is the gain coefficient.

The output intensity I_{out} of laser in a gain medium having small signal gain α_0 and saturation intensity I_s, in absence of expander, is given by [4.19]

$$\frac{I_{out}}{I_s} = \frac{T_b T_2 \left[\alpha_0 \, l - \frac{1}{2} In\left(\frac{1}{T_a^2 T_b^2 R_1 R_2}\right)\right]}{\left(1 - \sqrt{T_a^2 T_b^2 R_1 R_2}\right)\left(1 + \sqrt{T_b^2 R_2 / T_a^2 R_1}\right)} \tag{4.27}$$

With inclusion of another losses (prisms, windows etc.), above equation can be modified as,

$$I_{out} = T_b T_2 I_s \left[\alpha_0 \, l - \frac{1}{2}\ln\left(\frac{1}{T_b^2 \, T_a^2 T_p^2 \, R_1 \, R_2}\right)\right] \times$$

$$\left\{\left[1 - \left(T_a^2 \, T_b^2 \, T_p^2 \, R_1 \, R_2\right)^{\frac{1}{2}}\right]\left[1 + \left(R_2 \, T_b^2 \, / \, R_1 \, T_p^2 T_a^2\right)^{\frac{1}{2}}\right]\right\}^{-1} \tag{4.28}$$

For theoretical investigation, $R_1 = 0.2 - 0.3$, as feedback through grating-mirror in first order never exceeds 30% at grazing incidence [4.13], and $T_a = T_b = 0.96$ are used. For a specific and known values of T_a, T_b, T_p, R_1, and $\alpha_0 l$, the transmission coefficient, T_1 and T_2 varied in the range of 0.1 - 0.9. Fig.4.8 shows the variation of normalized output intensity with transmission coefficient of grating-mirror. Intensity decreases monotonically with increasing transmission coefficient. In dye laser resonator reflectivity R_1 of grating-mirror system mainly depends on the angle of incidence of light on the grating and diffraction efficiency, which governs the spectral properties of radiation [4.2, 4.13]. In dye laser, transmission coefficient of gratig-mirror system mainly depends on the angle of incidence of light on the grating and diffraction efficiency.

Fig.4.9 (a) shows variation of normalized output intensity with transmission coefficient of the coupler mirror. This showed maximum intensity coupled outside the cavity near transmission coefficient 0.7, i.e. 30 % reflectivity. Experiment has been carried out to optimize the output coupler mirror transmission coefficients for CVL pumped dye laser. Fig.4.9 (b) shows variation of dye laser output power at different transmission coefficients (0.1-0.9) of output coupler mirror. The maximum output power was observed in the range of 0.7-0.8 transmission coefficient.

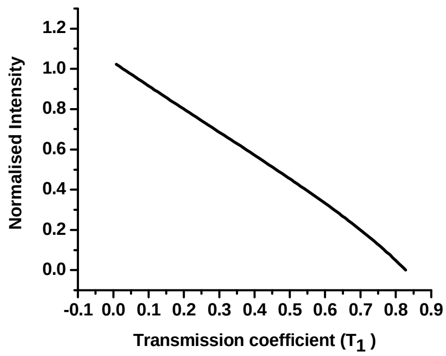

Figure 4.8: *Typical variation of normalized output intensity with transmission coefficient T_1 of the grating-mirror*

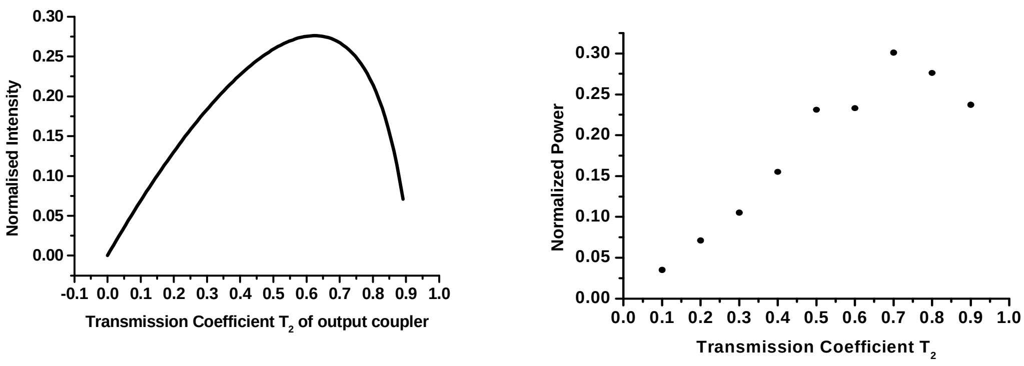

(a) (b)

Figure 4.9*: Typical variation of normalized output (a) intensity, (b) optical power with transmission coefficient (0.1- 0.9) of the coupler mirror*

Hence, the transmission coefficient of the coupler mirror has an effect on the output optical power of dye laser. Its selectivity is an important step for maximum average optical power extraction from the dye laser. Thus, a two-mirror simplified cavity approach has been used for optimization of output power through transmission coefficient of mirrors of the dye laser resonator, both theoretically and experimentally. The maximum output power was observed in the range of 20-30 % reflectivity of output coupler mirror. The experimental results well agree with the model developed. This study has helped us for selection of transmission coefficient of partially transmitting output coupler mirror in the design and development of the narrow bandwidth dye laser oscillator for further investigations of other issues of dye laser undertaken in the subsequent chapters.

4.3 Spectral width of a dye laser

Dye lasers have their very wide gain bandwidth (~ 50 nm). In a laser with cavity length of few tens of centimeters, numbers of modes oscillating are large and the laser is said to be multimode or broadband laser. For many spectroscopic applications, a narrow bandwidth dye laser is essential. Narrow-bandwidth dye laser is defined as a source of highly coherent emission having a bandwidth [4.1] narrower than $\Delta\nu \approx 3GHz$, which is approximately $\Delta\lambda \approx 0.0017\, nm$ at 510 nm. Therefore, a rigorous attempt was on the development of tunable optics for narrow linewidth operation of dye laser. The dye laser is a homogeneously broadened system; hence the gain available can be efficiently channeled into a narrow bandwidth output. Therefore, spectral narrowing occurs, without appreciable change in energy, when a wavelength selector is introduced in the resonator. A large variety of wavelength selective optics has been used for spectral narrowing of the dye laser. The reported typical bandwidth of dye laser using broadband dielectric mirrors resonator was ~ 6.0 nm [4.20]. Replacing one of the broadband mirrors by a grating in Littrow configuration reduced the linewidth to ~ 0.06 nm [4.20]. Bradley et al [4.21] reported a refinement of the grating-mirror cavity that incorporate an intra-cavity etalon to achieve bandwidth of about 0.05 nm. Myers [4.7] incorporated a prism positioned at a very large angle of incidence approaching 90^o in the optical cavity of dye laser. He found that the bandwidth was narrowed from 10 nm to 0.2 nm when the prism was placed in a broadband cavity consisting of two high reflecting mirrors. When the same setup was put in a grating cavity-mirror, the reduction in bandwidth was from 1.1 nm to 0.09 nm.

Hänsch [4.5] demonstrated bandwidth of about 0.003 nm at $\lambda{\sim}600\, nm$, using intracavity telescopic beam expansion in Littrow-grating configuration and a further refinement (reduced to less than 0.0004 nm) in the telescopic device was achieved by employing an intracavity etalon. As telescopic beam expander is long, expensive and cumbersome to align, an alternative beam expander, which is much simpler to use, compact and also less expensive, is a prism at a grazing angle of incidence to expand the beam in one dimension (in the plane of incidence). Hanna *et al* [4.11] have incorporated prism as an intracavity beam expander and etalon in Littrow and achieved bandwidths in the 0.003-0.007 nm range.

A significant development in the area of resonator compactness and narrow bandwidth operation was the GIG resonator, developed independently by Shoshan [4.8] and Littman and Metcalf [4.9]. It provided a alternative design for compact narrow-bandwidth dye laser in which grating was illuminated at a grazing angle of incidence, in conjunction with a tuning mirror and reported linewidth of 0.003 nm at 600 nm. Littman [4.10] used a grating-grating combination and reported single mode linewidth of 300 MHz.

Shoshan *et al* [4.8] have used a 100% reflecting mirror at one end of the cavity, grating in grazing incidence, and tuning mirror at the other end. The laser output was taken directly from the grating in the form of the zero-order beam and they have achieved narrow linewidth of 2.4 GHz. Since the output was taken from the grating zero-order, it contains a large fraction of amplified spontaneous emission (ASE). The ASE has several undesirable effects on the performance of a narrow band pulsed dye laser [4.22] such as reduction of the laser efficiency, restriction of the tuning range, and formation of a broad band spectral background superimposed on the narrow band laser output. Littman *et al* [4.9] have used partially reflecting output mirror, grating in grazing incidence with tuning mirror and have achieved bandwidth of 1.25 GHz. Littman [4.10] have used another grating in Littrow configuration in place of tuning mirror and achieved a single mode linewidth of 750 MHz. Duarte et al [4.13] have used additional prism beam expander in configuration used by Littman *et al* [4.9] to obtain the bandwidth of ~ 1 GHz with improved efficiency. Maruyama *et al* [4.23] have used double prism beam expander in Littrow configuration with intra cavity etalon of FSR 30 GHz and a finesse of around 20 and achieved a bandwidth of 62 MHz. Bernhardt *et* *al* [4.24] have used intra cavity etalon (FSR 20 GHz, finesse ~ 13) in addition to a multiple prism beam expander (magnification ~ 40) in Littrow configuration to force the oscillations into a single mode and have achieved 60 MHz linewidth. In all these cases, narrow bandwidth of dye laser has been achieved by effectively increasing the dispersion in the cavity and single mode operate by increasing the losses for all except one mode.

4.4 Single mode dye laser

Single mode pulsed dye laser is widely used in resonance ionization spectroscopy, high-resolution optical spectroscopy as well as in the efficient optical pumping of the excited species, where the spectral lines are very close to each other. Narrow bandwidth dye lasers have been realized in Littrow, multiple prisms Littrow (MPL), grazing–incidence grating (GIG), multiple prisms grazing incidence grating (MPGIG), or hybrid multiple prism grazing incidence grating (HMPGIG) dispersive cavities [4.2]. These usually operated with a number of axial modes. In a laser with cavity length L, the longitudinal modes spacing in frequency domain is given by $\delta v = \frac{c}{2L}$ and the number of longitudinal modes N_{LM} is given by $N_{LM} = {}^{\Delta v}/_{\delta v}$, where Δv is the gain bandwidth. Thus, number of longitudinal modes, within the gain profile, can be reduced to single mode by reducing the cavity lengths appropriately. The reduced/compact cavity length realization is limited by physical dimensions of the components of the resonator.

It is common practice to use long cavity and introduce additional optics (to suppress all modes except one below the loss line) to get single mode. Laser oscillation on a single mode can be achieved if the losses for all, except the desired mode, are increased to such an extent that they do not reach oscillation threshold. Another approach to ensure single longitudinal mode operation is to increase the effective gain of the desired mode by injecting radiation seed at that mode so that it builds up faster and dominates. However, the power needed to lase at a particular mode will increase rapidly as the desired mode moves farther from the line center. Further, the injected radiation must be an allowed mode of the resonator, which requires a careful control of the resonator length. All these approaches have their own technological challenges.

A number of techniques [4.8-4.9, 4.14, 4.23, 4.25-4.31] have been reported for the single mode operation of pulsed dye lasers, including pulse amplification of cw single mode [4.32], external filtering of a multimode laser oscillator [4.33], and a very short cavity oscillator incorporating frequency selective elements [4.26] such as intra-cavity etalons [4.23-4.24]. Single mode operation by using intra cavity etalon can be achieved by varying the optical path length of the etalon (by adjusting its tilt or temperature) such that one of its transmission maxima coincides with the desired mode and no other transmission maximum falls in the gain bandwidth. The later condition requires that the free spectral range (FSR) of the etalon should be greater than half the gain bandwidth if the desired mode coincides with the center frequency, or in general, greater than the gain bandwidth. This requires precise selection of the FSR and finesse of the etalon to force the lasing in single mode. The Free spectral range (FSR) of an etalon is given by $\frac{\lambda^2}{2nd_e}$, where d_e is thickness of the etalon, n is the refractive index of the medium of the etalon. The estimate of minimum resolvable linewidth or resulting laser linewidth obtainable from the etalon is given by ratio $\frac{FSR}{\mathcal{F}}$, $\mathcal{F}$ is the effective finesse of the etalon. The finesse of the etalon is a function of the flatness of the surface (often in the range of ${}^{\lambda}/_{100} - {}^{\lambda}/_{50}$), the dimension of the aperture, and the reflectivity of the surfaces. The effective finesse is given [4.1] by

$$\frac{1}{\mathcal{F}^2} = \frac{1}{\mathcal{F}_R^2} + \frac{1}{\mathcal{F}_F^2} + \frac{1}{\mathcal{F}_A^2} \tag{4.29}$$

where F_R, F_F and F_A are the reflective, flatness, and aperture finesse, respectively.

Hung *et al* [4.25] have reported a novel simple cavity for grazing incidence pulsed dye laser in which the tuning mirror was rotated from Littman's working position so that the beam diffracted at an angle was reflected back to the grating at the Littrow incidence angle. This modification is equivalent to the use of the second grating in Littman's double grating design. Thus, single mode operation with a spectral bandwidth of 385 MHz was achieved using only one dispersive element (grating) in the linear cavity. However, in this technique the tuning mirror was rotated about the same axis for single mode operation and tuning of the dye laser. Hence adjustment of angle of tuning mirror for single mode operation may also result in tuning of wavelength of the dye laser. A new technique for single mode operation of dye laser was anticipated and successfully demonstrated, in this thesis, in a grazing incidence grating long cavity without using any additional optics or modifications in prism GIG long cavity, by introducing losses in the resonator through beam walk-off [4..34]. Fig.4.10 shows schematic diagram of CVL pumped dye laser. In this setup, resonator typically consists of output coupler mirror (20% reflectivity), dye cell, single prism beam expander (magnification ~ 8) and grating (2400 lines / mm) in grazing incidence with tuning mirror. The overall cavity length was 16 cm, in which dye laser oscillates in three axial modes successfully.

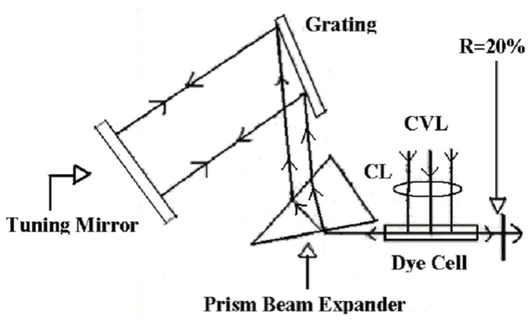

***Figure 4.10**: Schematic diagram of dye laser*

Fig.4.11 shows dye laser FP fringe of (a) three axial modes, (b) double axial modes, and (c) single mode. In normal operation of the dye laser, without any additional loss in the resonator, the observed separation of the axial modes was ~ 990 MHz, close to the value of ~ 937 MHz estimated from the resonator length. The number of axial modes was reduced by introducing losses in the cavity through rotating the tuning mirror about an axis parallel to the plane of incidence of diffracted beam from the grating. When the tuning mirror was aligned in such a way that the first order diffracted beam from grating is incident normally on the tuning mirror, three axial modes lasing. It was observed that the rotation of the tuning mirror about an axis parallel to the plane of incidence, rather than perpendicular, discriminates the number of axial modes. Fig.4.12 shows the schematic of the rotated positions and direction of the tuning mirror.

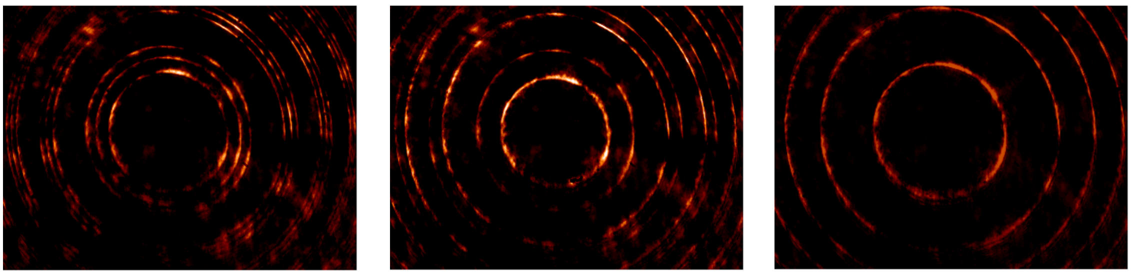

(a) (b) (c)

***Figure 4.11**: Dye laser fringe of (a) three axial modes, (b) double modes, and (c) single mode*

The maximum angle of rotation of tuning mirror in one direction depends on the beam size perpendicular to the plane of incidence and distance of tuning mirror from the grating. If d is the distance between grating and tuning mirror and w is the beam size (along minor axis), then the maximum angle of rotation θ in either direction is $\theta \approx \frac{w}{2d}$. The angles of rotation θ are very small and require precise control on the rotation to discriminate the number of modes.

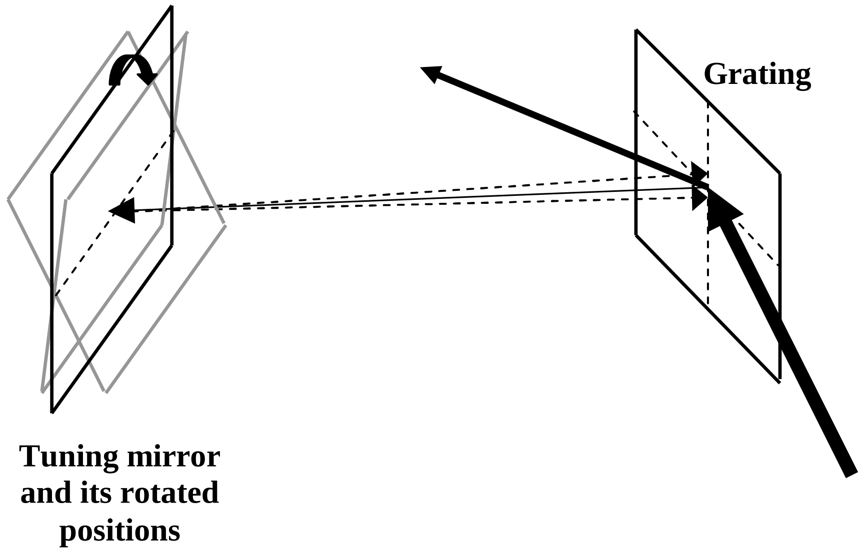

***Figure 4.12**: Schematic of rotated positions and direction of tuning mirror*

Precise rotations in either direction resulted in single mode, as shown in Fig.4.11 (c). Thus the position of tuning mirror plays significant role on the performance of the dye laser. As a result, the same cavity, without using any additional optics, can be made to operate in single axial mode just by controlling the rotation of tuning mirror along an axis parallel to the plane of incidence of the diffracted beam from the grating. This novel technique gives single mode of 360 MHz [2.34] bandwidth from a dye laser which normally (i.e. in symmetrically aligned condition) operating in three axial modes. The beam diffracted from the grating suffers beam walk–off through tuning mirror, which introduces losses in the resonator. As our configuration employs minimum number of optical components, hence misalignment and instability are greatly reduced.

4.5 Summary

In conclusion, pulsed dye laser resonator characteristics are extensively investigated. The dispersion theory for narrow bandwidth pulsed dye laser is analyzed theoretically and numerically. The pulsed dye laser dispersive resonator is analyzed. The simplified two-mirror cavity is used for optimization of the output coupler mirror transmission/reflection coefficients for maximum optical power extraction from the resonator. The optical power of the dye laser is influenced by the reflectivity of an output coupler mirror. Maximum output power is observed at 20-30 % reflectivity of the partially transmitting output coupler mirror. The experimental results agree well with the model developed, which should help in development of the tunable dye laser oscillator.

The bandwidth issues associated with pulsed dye laser resonators are reviewed. A cavity with single prism beam expander and grating in grazing incidence with tuning mirror, which operates in three axial modes is used for single mode operation, without using any additional optics. This technique is very simple for reducing the number of modes in a multi-mode long cavity.

Publications based on this chapter

1. Single mode operation of a narrow bandwidth dye laser in single prism grazing incidence grating cavity

   Optics and Laser Technology **39**, 1140 (2006)

   Nageshwar Singh

References

[4.1] F. J. Duarte, *Tunable Laser Optics*, Elsevier Academic, New York 2003

[4.2] F. J. Duarte and L. W. Hillman, *Dye Laser Principle*, Academic Press, New York 1990

[4.3] L. G. Nair, Dye laser, Prog. Quant. Electron. **7**, 153 (1982)

[4.4] I. J. Wilson, B. Brown and E. G. Loewen, Appl. Opt. **18**, 426 (1979)

[4.5] T W Hänsch, Appl. Opt. **11**, 895 (1972)

[4.6] G. L. Eesley and M. D. Levenson, IEEE J. Quant. Electron. **QE-12**, 440 (1976)

[4.7] S. A. Myers, Opt. Commun. **4**, 187 (1971)

[4.8] I Shoshan, N. N. Danon and U. P. Oppenheim, J. Appl. Phys. **48**, 4495 (1977)

[4.9] M. G. Littman and H. J. Metcalf, Appl. Opt. **17**, 2224 (1978)

[4.10] Michael G. Littman, Opt. Lett. **3**, 138 (1978)

[4.11] D. Hanna, P. Karkainen and R. Wyatt, Opt. Quantum Electron **7**, 115 (1975)

[4.12] R. Kingslake, *Applied Optics and Optical Engineering*, Vol.5, Academic Press, New York 1965

[4.13] F. J. Duarte, and J. A. Piper, Appl. Opt. **20**, 2113 (1981)

[4.14] S. Saikan, Appl. Phys. **17**, 41 (1978)

[4.15] K. Dasgupta, S. Kundu and L. G. Nair, Appl. Opt. **34**, 982 (1995)

[4.16] Guanghi Z. Zhang and Dennis W. Tokaryk, Appl. Opt. **36**, 5855 (1997)

[4.17] Lyuben B. Mashev, E K. Popov, and Erwin G. Loewen, Appl. Opt. **22**, 4738 (1987)

[4.18] M. Munz, G. Haag and G. Marowsky, Appl. Phys. **22**, 175 (1980)

[4.19] W. J. Rigrod, J. Appl. Phys. **36**, 2487 (1965)

[4.20] B. H. Soffer and B. B. McFarland, Appl. Phys. Lett. **10**, 266 (1967)

[4.21] D. J. Bradley, G. M. Gale, M. Moore, P. D. Smith, Phys. Lett. **26A**, 378 (1968)

[4.22] L. G. Nair and K. Dasgupta, IEEE J. Quantum Electronics **21,** 1782 (1985)

[4.23] Y. Maruyama, M. Kato, A. Sugiyama, T. Arisawa, Opt. Commun. **81**, 67 (1991)

[4.24] A. F. Bernhardt and P. Rasmussen, Appl. Phys. **B26,** 141 (1981)

[4.25] Nguyen Dai HUNG and Ph. BRECHIGNAC, Opt. Commun. **54**, 151 (1985)

[4.26] I. G. Koprinkov, K. V. Stamenov and K. A. Stankov, Opt. Commun. **42,** 264 (1982)

[4.27] S. G. Dinev, I. G. Koprinkov, K. V. Stamenov and K. A. Stankov, Appl. Phys. **22,** 287 (1980)

[4.28] I. Shoshan and U. P. Oppenheim, Opt. Commun. **25**, 375 (1978)

[4.29] I. T. McKinnie, H. B. Ahmad, A. J. Berry and T. A. King, J. Phys. D: Appl. Phys. **25**, 1687 (1992)

[4.30] H. W. Schröder, H. Welling and B. Wellegehausen, Appl. Phys. **1**, 343 (1973)

[4.31] Yoichiro Maruyama, Masaaki Kato and Takashi Arisawa, Japanese J. Appl. Phys. **30** (4B), L748 (1991)

[4.32] F. Trehin, F. Biraben and B. Cagnac and G. Grynberg, Opt. Commun. **31,** 76 (1979)

[4.33] U. Rebhan and J. Hildebrandt, Opt. Commun. **31,** 69 (1979)

[4.34] Nageshwar Singh, Opt. Laser Technol. **39**, 1140 (2006)

Chapter 5

Studies on high repetition rate dye laser subsystem

High repetition rate dye laser typically consists of dye cell for containing the gain medium, excitation (pump) source, resonator for obtaining narrow bandwidth, dye solution circulation (DSC) and cooling system for minimization of thermal effects. In the previous chapters, the excitation source and the narrow bandwidth resonators for the dye laser have been extensively investigated. In this chapter, significance of associated sub systems like DSC system, dye cell flow channel geometry and flow characteristics of a high repetition rate dye laser has been studied.

5.1 Studies on dye laser flow subsystem

For efficient and long-life stable operation of dye laser at high repetition rate, the active dye volume exposed by the excitation source needs to be rapidly removed between successive pulses. Thus, it becomes imperative to flow the dye solution through the dye cell at a sufficiently high speed. High clearing ratios of dye volume results in minimum thermal effects and extended dye lifetime. Therefore, dye-flow handling system considerations become a major concern for dye lasers operating at high repetition rates. The mechanical pump motor system associated with the DSC system is the largest source of heat generation and mechanical vibrations. Thus, a design detail of DSC system, which is major subsystem of the dye laser, is presented in this chapter. Design of flowing type dye cells of different flow channel and numerical analysis of velocity vectors inside the dye cells is briefly presented. Theoretical analysis of the microstructure of the liquid flow is also presented in the subsequent sections.

5.1.1 Design detail of the dye circulation system

Passive stability of dye lasers is affected by the DSC system [5.1]. Therefore, first of all DSC system was especially designed and fabricated for the flowing the dye solution through the laser gain medium. The DSC system typically consisted of a closed loop dye solution reservoir, mechanical pump motor, compact brazed plate heat exchanger, SS sintered filter, temperature sensor (PT-100), pressure gauge, self-tuned PID temperature controller and digital flow meter. The SS 316 material, which is non-corrosive and compatible with the organic dye, was used for all mechanical components which are in direct contact to the dye solution. To adjust the flow rate, a part of the dye solution returns through an adjustable by-pass valve while remaining part of the solution flows through a filter system to the dye cell and finally return to the dye reservoir. In this way, mass flow rate through the dye cell can be adjusted by means of by-pass valves at constant pressure. Fig.5.1 shows dye circulation and cooling unit schematic.

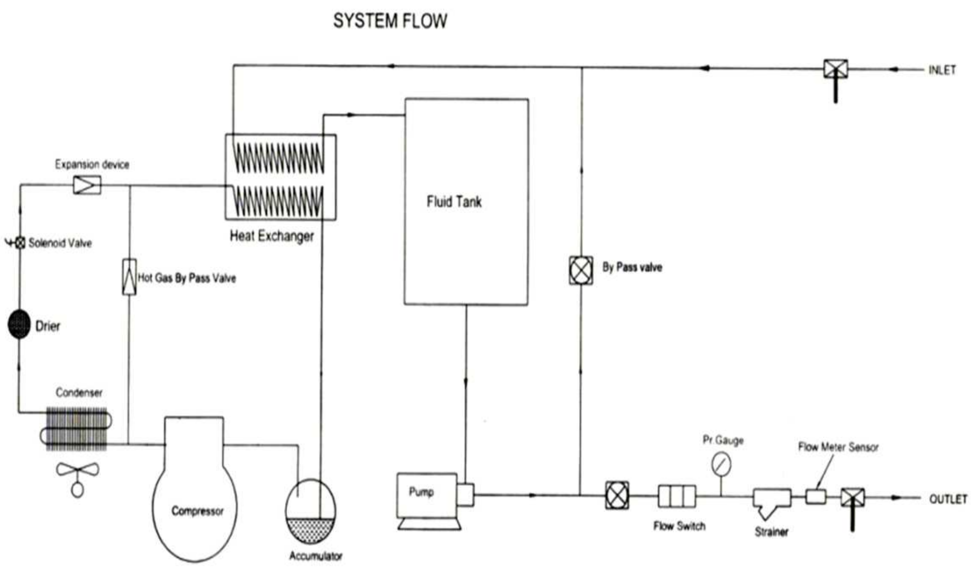

***Figure 5.1**: Dye circulation and cooling unit schematic*

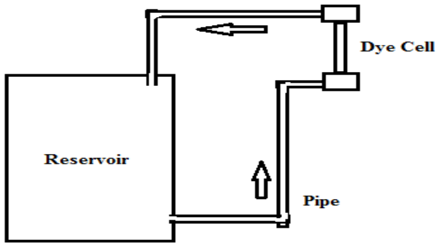

***Figure 5.2**: Simplified schematic of dye cell and flow loop*

The liquid volume capacity (∽ liters) of the dye solution reservoir was chosen in such a way that flow can be adjusted up to 20 liters per minute (LPM) while dye solution temperature controlled within ± 0.1 ^{0}C by PID controller. Fig.5.2 shows simplified schematics of dye cell and flow loop.

5.1.2 Studies on mechanical vibrations

Liquid dye laser, operating at high repetition rate (~ kHz), is coupled with the DSC system. One of the key components in the DSC system is mechanical pump motor, which inherently generates vibrations. These vibrations are transmitted through the flow loop system to the dye cell. In this way, it can cause the mechanical vibration of the dye cell, which is intra-cavity part of the dye laser. Therefore, identification of these vibrations is essential for stable operation of the dye laser. There is a possibility that mass flow may also generate vibrations. Reynolds numbers, which characterize the liquid flow, was estimated for the mass flow rates of the dye solution (dye dissolved in ethylene glycol and ethanol mixture). Thus, vibrations transmitted through mechanical pump motor and Reynolds number of the flow were measured using commercially available portable vibration meter (Cardvibro VM-2004 Neo model). Vibrational frequencies were measured at different location on the flexible pipe used for connecting the dye cell to the outlet of dye circulation system. Fig.5.3 (a) shows frequencies present at different locations away from the dye cell. The distance towards pump motor from dye cell was taken as positive while in other direction as negative.

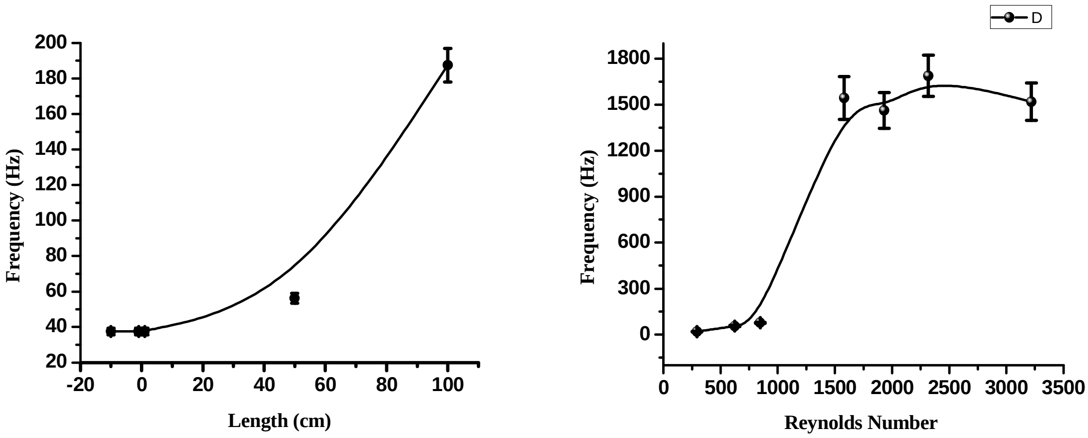

(a) (b)

***Figure 5.3**: Variation of vibrational frequency (a) on pipe from the dye cell at Reynolds number 1000 (b) with Reynolds number of the flow*

Vibration of 38 Hz frequency was detected near the dye cell while maximum frequency present on the pipe was less than 200 Hz, at Reynolds number of 1000. Frequency of vibrations was also measured at the dye cell as a function of Reynolds number. Fig.5.3 (b) shows variation of vibrational frequency with Reynolds number of the liquid flow. As the Reynolds number of flow increases the frequency of vibrations also increase and approach saturation. The vibration frequency of the optical table was 487.5 Hz during DSC flow system off while it was 1143.75 Hz during on condition. The lower frequencies are always present while higher frequencies in kHz range were due to the DSC system. This exercise of measurement helped in design and development of experimental work station for the characteristic investigation of dye laser. Based on these observations, rubber stud pads were used to isolate these kHz range frequencies. It was observed that the pads offer the most effective and easily applicable vibration/shock isolating resilient material for passive stabilization of the dye laser system. The pads reduce ground borne vibration. Further it also isolate the vibration produced by flow & noise from heavy machinery and even passing traffic for giving protection from external disturbances.

5.2 Development and studies on dye cells

Dye cell, used to enclose the gain medium, is one of the critical components of a high repetition rate dye laser. A number of dye cell geometries have been reported in the literatures for a high repetition rate pulsed dye lasers. Many of these have specific experimental objectives in mind or offer specific advantages. The planar cell is the most commonly used dye cell. In the planar duct dye cell, the flow channel is profiled on the inner surfaces such that the cross sectional area reduces to increase flow speed in the pump beam region.

For a high repetition rate dye laser, several types of dye cell conduits were reported in the literatures [5.2-5.12]. Zemskov *et al* [5.2] used planar nozzle of 0.5 x 6.0 mm^2 dimensions for studying the energy and time characteristics of jet dye laser pumped by CVL (10 kHz). Pease and Pearson [5.3] investigated pulse to pulse mode structure fluctuations in narrow linewidth dye laser pumped by CVL (6 kHz) using 8 mm dye cell. Zherikin *et al* [5.4] used slit-like gap of 15.0 x 0.5 mm^2 rectangular quartz cell and studied the efficiencies, narrow bandwidth operation, and tunable second harmonic generation of a dye laser operating at 10 kHz. Bernhardt and Rasmussen [5.5] have used quartz dye cell having internal dimensions approximately 8 x 8 x 22 mm^3 and inserted a curved metal piece into the dye cell to constrict the flow through an area of 8.0 x 0.3 mm^2 across the pumping region. Broyer *et al* [5.6] have used a dye cell, assembled from four optically contacted fused silica plates, in which the dye solution flow channel was restricted by an inserted ventury, which left a total clearance of 13.5 x 0.4 mm^2. Duarte and Piper [5.7] characterized the high pulse repetition frequency (8-13 kHz) dye laser resonator using flowing dye cell of trapezoidal cross-section of dimensions 11 mm wide x 1 mm thick. Lavi *et al* [5.8] had designed the dye cell (10.0 mm x 0.1 mm) and studied the pulse to pulse mode structure fluctuations of a CVL (at 4 kHz) pumped dye laser. Amit *et al* [5.9] had investigated the temperature gradients, generated by a high pulse frequency (4 kHz) CVL, in a planar dye cell (gap, 0.5 mm). Maruyama *et al* [5.10] characterized the output of high repetition rate dye laser, using 8 mm gain length of the dye medium in a rectangular cross-section dye cell. Sugiyama *et al* [5.11] reported temperature and pressure controlled frequency tuning of a dye laser using a dye cell active region dimensions 8 x 0.2 x 1 mm^3.

All of these dye cells, used for the high repetition rate dye lasers, were of diverse liquid flow characteristics and hence differed in flow induced inhomogeneity in the gain medium. Therefore, high repetition rate dye laser still needs a good optical quality lasing medium for better passive stabilization. In this road, we made an effort to develop dye cells with enhanced spectral stability for a high repetition rate dye laser. In this thesis work, new dye cells for a high repetition rate dye laser were designed. Numerical simulations of the dye solution flow in some of the dye cell were also carried out for better understanding. The brief description of the dye cells design is presented as follows.

5.2.1 Planar duct dye cell

A planar duct dye cell is generally used for CVL pumped dye laser. Fig.5.4 shows side view of schematic of the planar dye cell. The dye cell is typically consisted of glass windows which were assembled in such a way that straight long channel function for the liquid flow. These windows were sealed with the help of ‘O’ rings. The dimension of these glass windows typically provides the characteristic flow area cross-section. The gap between the optical windows can be adjusted manually during the assembly. Hence the flow speed of the dye solution can be varied also by changing the gap between the windows to have optimum flow velocity. During the operation of dye laser using planar dye cell, it was noticed that the output of dye laser suffer from fluctuations, in spite of the best efforts towards mechanical stabilizations.

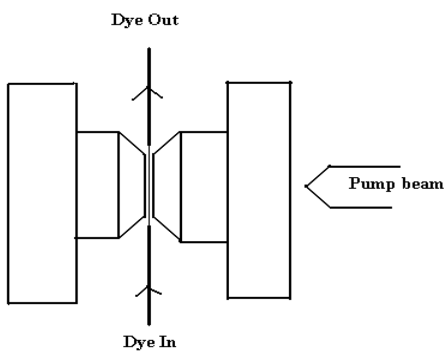

***Figure 5.4**: Side view of schematic of the planar duct dye cell*

Then it was anticipated that sudden change of flow cross-section in the planar dye cell, to some extent, is responsible for these fluctuations. Therefore, a need was felt for other dye cell geometries which intend to minimize the sudden change in flow cross-sectional area near to the pumping region.

5.2.2 Concave-convex duct dye cell

For a gradual change in flow cross-sectional area near the pumping region, a curved profiled flow channel dye cell was used. In this dye cell, the flow profile was nearly 360^0 curved with aspect ratio continuously decreasing/increasing from 22 mm to 0.5 mm and height 25 mm. Schematic of flow channel of curved duct dye cell is shown in Fig.5.5. The duct was formed by two cylinders of radii of curvatures of 46 mm (outer radii) and 35.5 mm (inner radii) with a height of 25 mm [5.12]. The axis of the inner cylinder was shifted such that a gap of 0.5 mm was maintained at the pump region. The cross sectional area at the pump region was thus 25 x 0.5 mm^2. The inlet and the outlet were located close to 0/360^0 with a suitable separator. Thus, this curved geometry has concave-convex flow channel for the liquid flow.

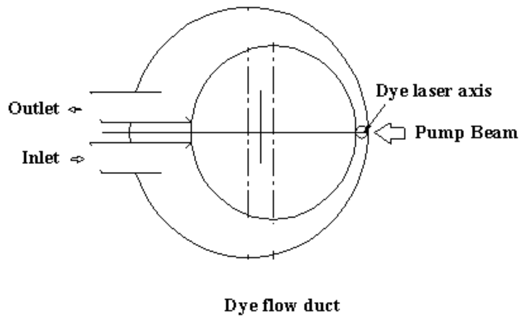

Figure 5.5*: Schematic of flow channel of concave-convex duct dye cell*

5.2.3 Pinched dye cell

For smooth flow of liquid in the pumping region, another dye cell was designed. The dye cell was made by pinching a glass tube from two sides. The borosilicate glass tube was heated and then quickly transferred for pinching the heated region between two spatially profiled graphite jaws in such a way that it is flat in the pinched region of height 5 mm and length 10 mm, inside the dye cell [5.13]. Special technique was applied to obtain uniform gap inside the pinched region of the dye cell. The flow channel gap can be adjusted from 0.02 to 0.5 mm during the pressing operation. The ends of the tube were maintained at positive pressure to keep the walls from collapsing, during the pressing operation. The uniformities of the gap were inspected physically. The outer sides of the glass tube, in the pinched region were polished with tapering of 6^0 on both sides to avoid the reflection from it. Ends of the glass tube were fitted in a stainless steel (SS 304) blocks and sealed with help of EDPM ‘O’ ring. It offers narrow region for dye solution to flow at high velocities in the pump region. Fig.5.6 shows photograph of dye cell fitted in SS assembly and flowing dye solution with (a) optical pumping region, (b) dye laser emission region, faces.

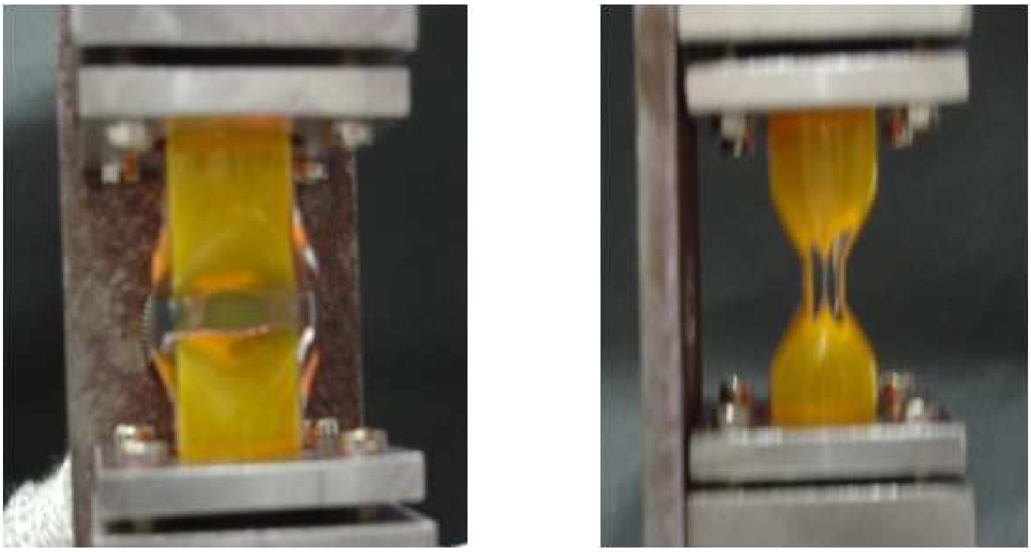

(a) (b)

Figure 5.6: *Photograph of dye cell fitted in SS assembly and flowing dye solution with (a) optical pumping region, (b) dye laser emission region, face*

Further, an investigation of the liquid flow through this dye cell has been carried out via computational fluid dynamics (CFD) analysis. The cell was modeled with NX software. A finite volume analysis technique was preferred to calculate the flow velocity distribution in and around the pinched region of dye cell. Ansys fluent software (NX7) was adapted for meshing and analysis. A fine mesh was taken in the pinched region to take care of the boundary effects. A simple algorithm has been used to solve the flow equations.

Fig.5.7 shows velocity profile of the liquid flow through the dye cell as analyzed by CFD (a) along the width, (b) along the length. Fig.5.8 shows liquid flow (a) velocity contour, (b) velocity vector, through the dye cell. There is no signature of any kind of flow disorder noticeable in the velocity vector and contour of the liquid flow, before and near the pinched region inside the dye cell.

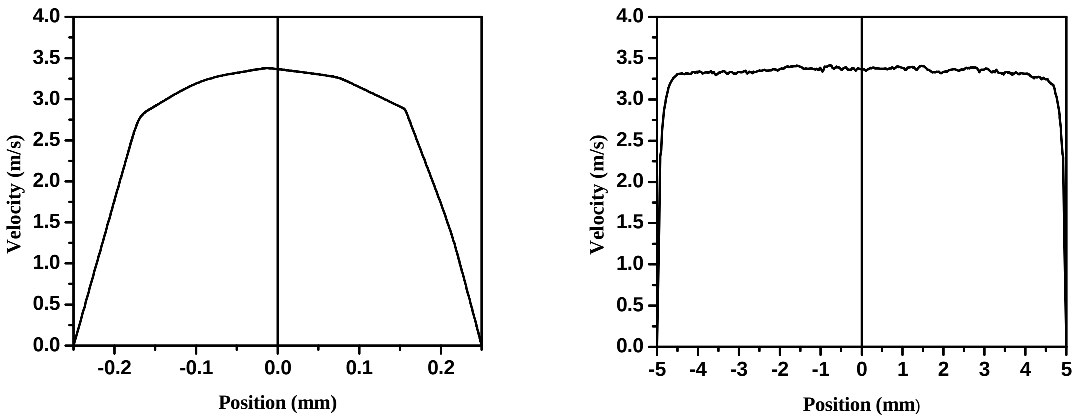

(a) (b)

Figure 5.7*: Typical velocity profile of the liquid flow through the dye cell as analyzed by CFD along (a) width, (b) length*

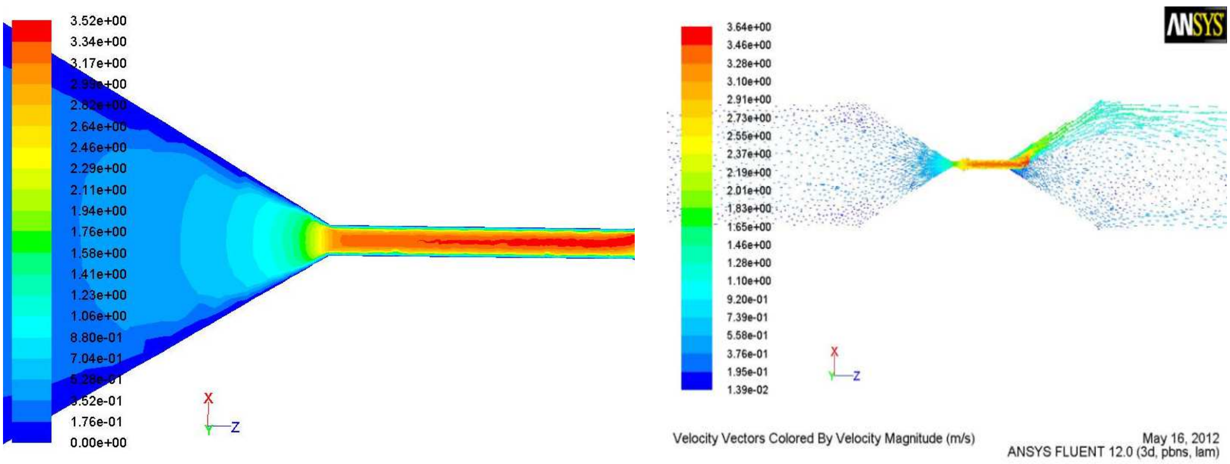

(a) (b)

Figure 5.8*: Liquid flow (a) velocity contour, (b) velocity vector, through the dye cell*

5.2.4 Convex-plano duct dye cell

Another dye cell with specially profiled flow channel was designed. The cell was made from solid 30 x 30 x 30 mm^3 single piece borosilicate glass cube. Two perpendiculars through holes of diameter 20 mm were made in the cubical solid glass. The inside and outside surfaces were optically polished. Fig.5.9 (a) shows the photograph of exposed outlook of glass piece of the dye cell. A stainless steel (SS) cylinder of length 24 mm with specially profiled curved surface was designed. The cylinder has been designed to seal the flow from one side and allow 1 mm gap from other side. The cylindrical rod was made of two half cylinders of radius 19 mm and 18 mm. The cylinder was inserted in the glass piece in such way that it provides nearly 24 mm length and 1 mm gap between metal and glass in one side [5.14]. The opposite side was sealed with help of EDPM ‘O’ ring, inserted in cut made in the cylinder. In this way liquid flow through the one side only. Fig.5.9 (b) shows 3D model of the dye cell flow channel. In this model, white, gray and yellow color represents glass, steel and dye liquid flow zone, respectively. The flow channel gap can be adjusted by varying the diameter of the cylinder. Ends of the cylinder were sealed with help of EDPM ‘O’ ring and optical windows. Also, an investigation of the liquid flow through this dye cell has been carried out as described in section 5.2.4.

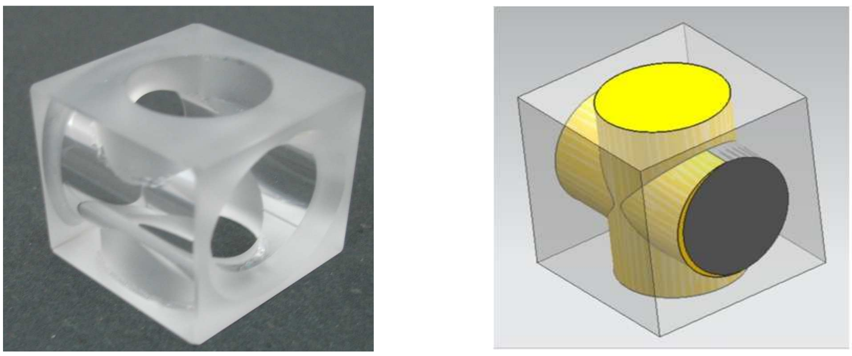

(a) (b)

Figure 5.9*: (a) Typical photograph of glass piece, (b) 3D model, of the dye cell flow channel*

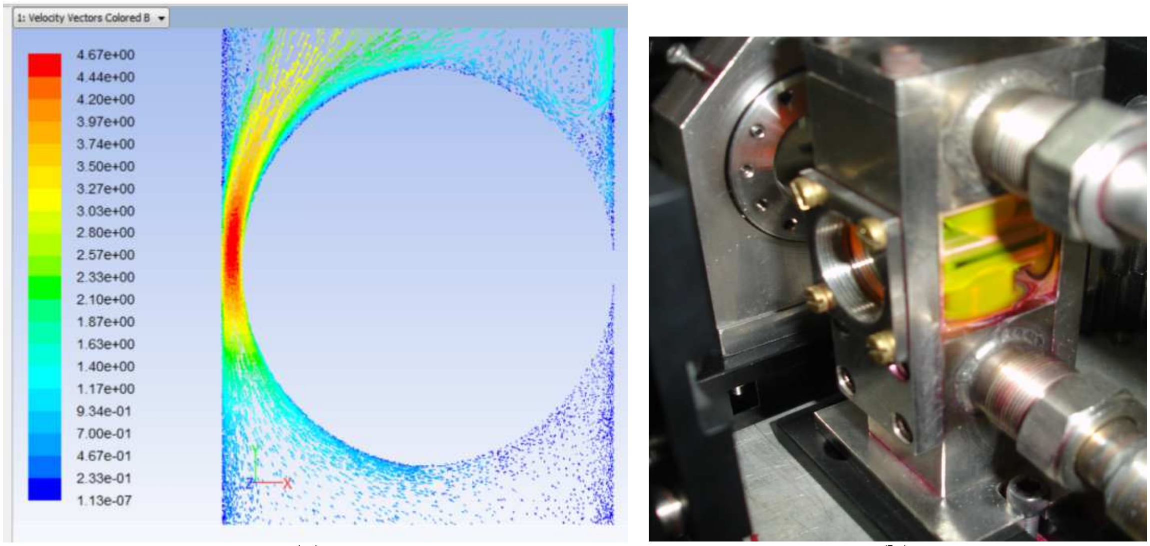

(a) (b)

Figure 5.10: *Typical (a) velocity vector of the liquid flow through the dye cell, (b) photograph of dye cell assembly along with dye solution*

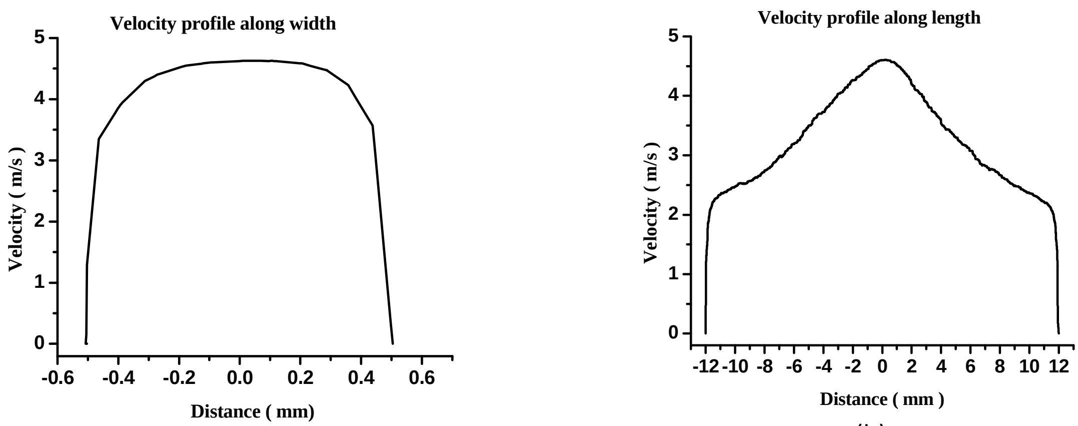

(a) (b)

Figure 5.11: *Velocity profile of the liquid flow through the dye cell as analyzed by CFD along (a) length, (b) width*

Fig.5.10 shows (a) velocity vector of the liquid flow through the dye cell, (b) photograph of dye cell assembly along with dye solution. Fig.5.11 (a) shows liquid flow velocity profile along the width of the dye cell. Fig.5.11 (b) shows liquid flow velocity profile along the length of the dye cell. It appears that the velocity vectors of the liquid flow, near the pumping region in the dye cell, are free from any kind of vortices.

5.3 Microstructure of the flowing gain medium

In the dye laser operating at low repetition rate, the gain medium remains stationary or flowed at a relatively low speed transverse to the dye laser axis. However, for the high repetition rate dye laser, the dye solution is necessarily flown at high speed and cooled to minimize thermal problems. The flow speed of the dye solution depends on the pulse-repetition-frequency and power of the pump laser. Generally, flow rate is chosen to replace the optically pumped dye molecules after each pump laser pulse. For this, the mass flow rate must be sufficient to remove the slow moving boundary layer, existing at the window surface. Thus, the volume flow rate must exceed the average volume flow rate i.e. $V_a < \frac{V_P}{T}$ where V_a is the average volume flow rate, V_P is the cell volume being optically pumped , and T is the pulse repetition period. Typically, the number of dye volume replaced per pulse is at least two or more and also a high clearing ratio is necessary to have extended window and dye lifetimes [5.15].

The liquid flow is characterized by Reynolds number. In fact, the value of the kinematic viscosity ν, the characteristics velocity u, and the characteristics dimension D characterize the viscous liquid flow. The quantity D characterizes the dimension of the flow as a whole, and arises from the boundary conditions of the fluid dynamics problem. The Reynolds number, which is the ratio of inertial and viscous forces, is defined as,

$$R = \frac{u\,D}{\nu} \tag{5.1}$$

The characteristics dimension of the flow is defined as

$$D = \frac{4\,A}{P} \tag{5.2}$$

where A is the cross sectional area of the flow, and P is the wetted perimeter. The values of Reynolds number describe the flow features (i.e. laminar or turbulent) in the dye cell. The average flow velocity can be estimated from the mass flow rate measurements. These equations estimate the corresponding Reynolds numbers for the solvent and dye cell parameters used in the experiments. In the laminar flow, liquid layers move parallel to each other in an orderly manner. As the Reynolds number increases by increasing the flow velocity, it encounters large disorder in the liquid, and the liquid flow becomes turbulent. In the turbulent flow, irregular and chaotic movement of liquid chunks involved [5.16-5.17]. As a consequence, a multitude of small eddies are created by the viscous shear between adjacent particles. These eddies grow in size and then disappear, as their particles merge into adjacent eddies. Thus, turbulent flow degrades the optical quality of the medium.

The velocity fluctuations give rise to a turbulent shear stress (τ), defined [5.18] as

$$\tau = \eta \frac{du}{dy} \tag{5.3}$$

where $\frac{du}{dy}$ is velocity gradient, and η is the eddy viscosity, which is a function of the liquid motion. In general, the total shear stress in turbulent flow is the sum of the laminar shear stress plus the turbulent shear stress, i.e.,

$$\tau = \mu \frac{du}{dy} + \eta \frac{du}{dy} = \rho(\nu + \varepsilon_M)\frac{du}{dy} \tag{5.4}$$

Where μ, ν are the dynamic and kinematic viscosity, respectively, ρ is the density, $\varepsilon_M = \frac{\eta}{\rho}$ is the kinematic eddy viscosity. The flow is laminar near the smooth dye cell window wall and the shear is $\tau = \mu \frac{du}{dy}$. The flow remains laminar for a small distance, however, at some distance from the window, the value of $\frac{du}{dy}$ becomes small in turbulent flow, and hence the viscous shear becomes negligible in comparison with the turbulent shear. The latter can be large, even though $\frac{du}{dy}$ is small, because of the possibility of η being very large. Between the two, there must be a transition zone where both types of shear are significant. This transition zone is called buffer region. The flow is fully turbulent after the buffer region. Thus, turbulent flow is generally categorized in three regions; a) *a laminar sub-layer,* which is a very thin region immediately adjacent to the window wall, where the shear is due to viscosity alone, b) *buffer region,* away from wall where some turbulence action is experienced, but the molecular viscous action and heat conduction are still important, and c) *fully turbulent region,* in which the main momentum and heat exchange mechanism is one involving macroscopic lumps of liquid moving about in the flow.

The viscous sublayer is extremely thin but its effect is large because of the very steep velocity gradient within it. At a distance from the pump window surface the viscous effect becomes negligible, but the turbulent shear is then large. The thickness of viscous sublayer d_l, is approximated [5.18] as

$$d_l = C_{sl} \frac{\nu}{U\sqrt{C_f}} = \frac{C_{sl}}{\sqrt{C_f}} \frac{D}{R} \tag{5.5}$$

where C_{sl} is sublayer constant, whose magnitude depends on the region of flow, C_f is wall friction coefficient. Higher the velocity or lower the kinematic viscosity, thinner the viscous sublayer. Thus, for a given constant and flow channel geometry, the thickness of the viscous sublayer decreases as the Reynolds number increases.

A number of models like mixing length, Van Driest, $k-\varepsilon$ model, second-order model, stress-flux, and many more were generally used for turbulent flow [5.18, 5.19] analysis. The time averaged turbulence kinetic energy, which is produced and decays in the boundary layer and also diffuses across the boundary layer in much same manner as heat, equation for boundary layer is given by [5.18],

$$\bar{u}\frac{\partial \bar{k}}{\partial x} + \bar{v}\frac{\partial \bar{k}}{\partial y} - \frac{\partial}{\partial y}\left[\left(\nu + \varepsilon_k\right)\frac{\partial \bar{k}}{\partial y}\right] = \varepsilon_M \left(\frac{\partial \bar{u}}{\partial y}\right)^2 - \varepsilon \tag{5.6}$$

where $\varepsilon_M \left(\frac{\partial \bar{u}}{\partial y}\right)^2$ accounts for the production of turbulent kinetic energy, and ε the dissipation of that energy into thermal energy through the action of viscosity. Similarly a differential equation for dissipation rate ε, can be written as

$$\bar{u}\frac{\partial \varepsilon}{\partial x} + \bar{v}\frac{\partial \varepsilon}{\partial y} - \frac{\partial}{\partial y}\left[\left(\nu + \varepsilon_\varepsilon\right)\frac{\partial \varepsilon}{\partial y}\right] = C_1 \frac{\varepsilon}{\bar{k}}\left[\varepsilon_M \left(\frac{\partial u}{\partial y}\right)^2\right] - C_2 \frac{\varepsilon^2}{\bar{k}} \tag{5.7}$$

The solution of equation (5.6) for $\bar{k}$ and (5.7) for ε, gives the eddy diffusivity for momentum

$$\varepsilon_M = C_\mu \frac{\bar{k}^2}{\varepsilon} \tag{5.8}$$

where constants having values, $C_\mu = 0.09$, $C_1 = 1.44$, and $C_2 = 1.92$. The numerical value of these constants depends on the streamline curvature function. The curvature of the flow channel surface, which is either convex or concave, substantially changes the structure of the boundary layer. Convex curvature causes the friction coefficient to decrease, while concave curvature has the opposite effect. Convex curvature has a stabilizing effect on the boundary layer, while concave curvature is destabilizing [5.18]. Depending on the applications and advantage specific curvature of the flow channel can be used.

The velocity profile is not uniform through flow passage. As a boundary layer of very slow moving dye exists at the pump window surface, the flow rates must be sufficient to remove this slow moving layer, which are exposed to the highest pumping fluence. The thermal field moves 1-2 mm upstream in the flow field [5.9]. The Reynolds number requirement for the complete replacement of this thermal field, before the arrival of next pulse, can be approximated as

$$R \geq \frac{f\ h_t\ D}{\nu} \quad , \tag{5.9}$$

where h_t is the distance covering thermal field in upstream from the exposed position, and f is the repetition frequency of pump pulse.

5.4 Summary

In summary, a special dye circulation & cooling system is conceptualized, fabricated and incorporated into high repetition rate dye laser system. Furthermore, mechanical pump motor and mass flow induced vibrational frequencies are studied. The circulation system is capable of flowing liquid at high velocity with dye solution bulk temperature stability within ±0.1 ^{0}C. Additionally, it has high precision calibrated digital liquid flow meter and pressure gauges connected at the inlet/outlet. Mechanical by-pass valves are incorporated to adjust the flow rates at constant pressure.

During our initial experiments using planar dye cell, it is noticed that the dye laser has spectral instability, in spite of the stabilization of all the mechanical components involved in the cavity. It is anticipated that sudden change of flow cross-section in the planar dye affected the stability. To validate the significant role of dye cell profile channel, various geometries are tried. Out of many such geometries studied, three new dye cells namely, nearly 360^0 curved, pinched dye cell and convex-plano dye cell are proposed for high repetition rate applications. The flow stability is the main motive behind the variety of the dye cells. The velocity vector through the pinched and convex-plano geometries are also numerically analyzed using computational fluid dynamics. The characteristic of laminar and turbulent flow is described. The role of shear stress and eddy viscosity of the flow in the dye cell is discussed.

Publications based on this chapter

1. Study of a new dye cell for a high repetition rate dye laser

Optics and Laser Technology **45**, 256 (2013)

Nageshwar Singh, H. K. Patel, and H. S. Vora

2. Design, modeling and performance evaluation of a novel dye cell for a high repetition rate dye laser

Review of Scientific Instruments **83,** 105114 (2012)

Nageshwar Singh, H. K. Patel, S. K. Dixit, and H. S. Vora

3. On the microstructure of thermal and fluid flow field in a lasing medium of a high repetition rate dye laser

Optik: International Journal for Light and Electron Optics **121**, 1642 (2010)

Nageshwar Singh

4. Comparison of the performance of a near 360^{0} curved and a straight channel dye cell for high repetition rate copper vapor laser pumped dye laser

Journal of Physics D: Applied Physics ***39,*** 2084 (2006)

Nageshwar Singh

5. Design of a transversely pumped, high repetition rate, narrow bandwidth dye laser with high wavelength stability

Review of Scientific Instruments **75**, 5126 (2004)

R. Bhatnagar, **Nageshwar Singh**, R. Chaube and H. S. Vora

References

[5.1] H. Elkashef and G. E. Hassan, Acta Phys. Slov.**42** 305 (1992)

[5.2] Zemskov *et al*, Sov. J. Quantum Electron **6**, 727 (1976)

[5.3] A. A. Pease and W. M. Pearson, Appl. Opt. **16**, 57 (1977)

[5.4] Zherikin *et al*, Sov. J. Quantum Electron **11**, 806 (1981)

[5.5] A. F. Bernhardt and P. Rasmussen, Appl. Phys. **B 26,** 141 (1981)

[5.6] M. Broyer, J. Chevaleyre, G. Delacretaz and L. Wöste, Appl. Phys. B **35**, 31 (1984)

[5.7] F. J. Duarte and James A. Piper, Appl. Opt. **23**, 1391 (1984)

[5.8] S. Lavi, M. Amit, G. Bialolanker, E. Miron, and L. A. Levin, Appl. Opt. **24**, 1905 (1985)

[5.9] M. Amit, G. Bialolenker, D. Levron and Z. Burshtein, J. Appl. Phys. **63**, 1293 (1988)

[5.10] Y. Maruyama, M. Kato, A. Sugiyama, T. Arisawa, Opt. Commun. **81**, 67 (1991)

[5.11] A. Sugiyama, T. Nakayama, M. Kato, Y. Maruyama, T. Arisawa, Optical Eng. **35**, 1093 (1996)

[5.12] R. Bhatnagar, Nageshwar Singh, R. Chaube, H. S Vora, Rev. Sci. Instrum. **75**, 5126 (2004)

[5.13] Nageshwar Singh, H. K. Patel, H. S. Vora, Opt. Laser Technol. **45**, 256 (2013)

[5.14] Nageshwar Singh, H. K. Patel, S. K. Dixit, H. S. Vora, Rev. Sci. Instrum. **83,** 105114 (2012)

[5.15] F. J. Duarte, *High Power Dye Lasers,* Springer-Verlag, Berlin 1991

[5.16] J. P. Holman, *Heat Transfer*, p. 150, McGraw-Hill Book Company, London 1989

[5.17] V. I. Tatarski, *Wave propagation in a turbulent medium,* McGraw-Hill Book Company, Inc., USA 1961

[5.18] W. M. Kays and M. E. Crawford, *Convective heat and mass transfer*, 3rd ed., McGraw-Hill 1993

[5.19] Louis C Burmeister, *Convective heat transfer*, John Wiley & Sons, New York 1982

Chapter 6

Studies on spectral stability of a high repetition rate dye laser

The issues of dye cell flow channel geometry and Reynolds number of liquid flow, affecting the spectral stability of high repetition rate dye laser, were largely ignored so far by the researchers working in the field [6.1-6.12]. The planar flow channel in the pump region has been conventionally used for the high repetition rate dye laser with an objective to replace the dye solution between successive pump laser pulses. Schröder *et al* [6.1] have investigated several planar dye cells to reduce the flow-induced fluctuations. They observed that after an abrupt narrowing of the cross-section, it takes some time before the final turbulent flow with velocity fluctuations builds up. Hence, it was suggested that the active zone of the dye laser should be as close as possible to the entrance of the narrow-flow channel to avoid the fluid flow induced fluctuations. They also observed that maximum velocity fluctuations occurred at the boundary layers rather than at the center of the dye cell. Broyer *et al* [6.2] have used a dye cell in which the dye solution passage was restricted by an inserted ventury, which left a total clearance of 13.5 x 0.4 mm^2. For a narrow bandwidth stable dye laser, it is therefore necessary to find a dye cell with small velocity fluctuations and with a small boundary zone of decreasing velocities. No reliable theory for the microscopic flow fluctuations in the gain medium is available at present. Therefore, dye cells of various profiles have been tried for fluid flow stability. During our initial course of studies, it was observed that dye solution flow channel profile and mass flow rates both significantly affect the dye laser spectral stability. Therefore, the spectral stability of dye laser was experimentally investigated using planar, curved, pinched and convex-plano dye cells. In addition, spectral stability with curved duct dye cells as a function of Reynolds number was also studied experimentally.

6.1 Experimental details

Dye cells have been employed in GIG narrow bandwidth dispersive resonator. Fig.6.1 shows schematic layout of the dye laser setup. The dye laser setup used in the experiments typically consists of an output coupler mirror (20% reflectivity), a dye cell, intra-cavity etalon (FSR 20 GHz, finesse 13) and a grazing incidence grating (2400 lines/mm) in conjunction with a tuning mirror. The dye laser is based on the grazing incidence diffraction grating with intra-cavity etalon to provide narrow spectral width emission. This is a very convenient configuration to obtain narrow spectral width with minimum number of optical components. The Rhodamine 6G dye in ethanol solvent was used as the gain medium. A copper vapor laser (λ = 510.6 nm, average power 4 W, 60 ns pulse duration, 5.6 kHz pulse repetition frequency) was used as the optical excitation source.

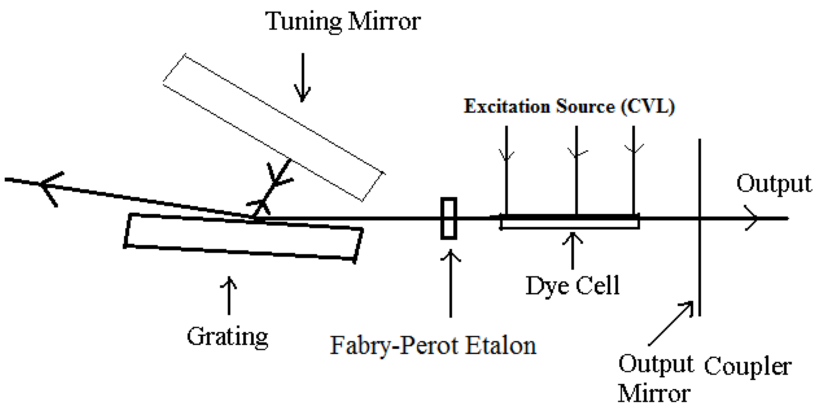

Figure 6.1: *Schematic layout of the dye laser setup*

The pump beam was transversely line focused onto the dye cell through a combination of spherical (focal length 40 cm) and cylindrical lens (focal length 6 cm). The performance of the dye laser was investigated using high resolution spectroscopy based technique and a composite image generation software [6.13-6.14]. In composite image generation technique, an image of fringe generated by Fabry-Perot etalon was acquired through an imaging lens and a CCD camera based setup. The FP etalons of different FSR (4, 5, 10 GHz, etc.) and finesse (100, 60, 25 etc.) are used, depending upon situation. The detail about spectral diagnostic technique was described in Chapter 3. Experiments have been performed for spectral stability using the dye cells of flow channel profiles whose design details has been described in chapter 5. Only the dye cells have been changed in the setup and other experimental conditions were kept same. Therefore, in this chapter, only experimental results and discussions related with the spectral stability of the dye laser with different dye cells [6.15-6.18] are presented. For the comparative studies, Fabry-Perot fringes were acquired through a setup, as shown in Fig.2.1 of Chapter 2, and composite images were generated with each dye cell for a long-term spectral stability.

6.2 Results and discussion

6.2.1 Planar dye cell

Fig.6.2 (a) shows typical Fabry-Perot fringe of dye laser generated through planar dye cell. The composite image of a line scan across the diameter of the fringe, over an observation period of about 90 minutes was generated for the spectral investigation through planar dye cell, as shown in Fig.6.2 (b). Spectral measurement from the composite image data was carried out. Fig.6.3 shows the variation of bandwidth and wavelength with time, using planar dye cell. The bandwidth and wavelength fluctuates within 1.214 GHz and 0.035 nm, respectively, over the observation period.

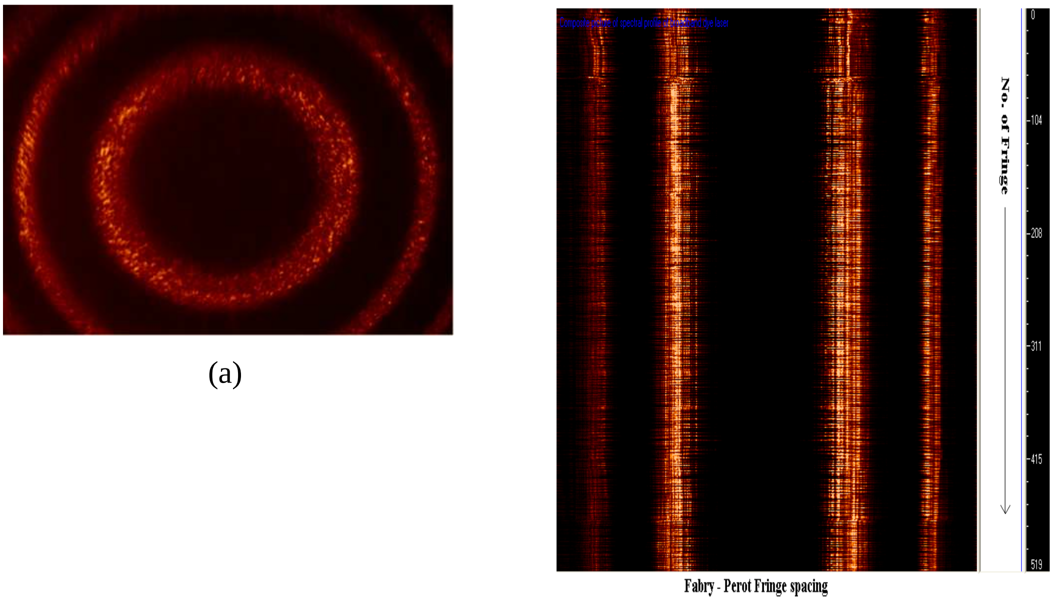

(a)

(b)

***Figure 6.2**: Typical Fabry-Perot (a) fringe, (b) composite image generated from a line scan across the diameter of the fringes, using the planar dye cell*

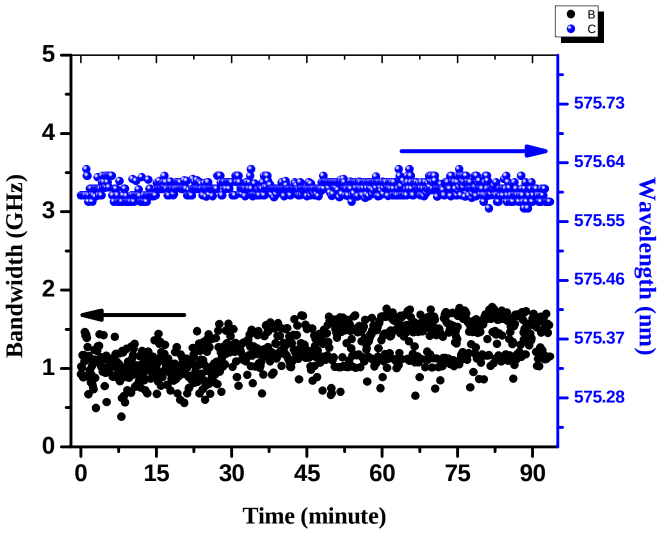

***Figure 6.3**: Variation of bandwidth and wavelength with time, using planar dye cell*

6.2.2 Concave-convex duct dye cell

Fig.6.4 shows typical Fabry-Perot (a) fringe, (b) composite image, generated using curved duct dye cell. Spectral measurement from the composite image data was carried out. Fig.6.5 shows variation of bandwidth and wavelength with time, using curved duct dye cell. The bandwidth fluctuates within 900 MHz and wavelength varies within 0.0196 nm over the observation period of 90 minutes.

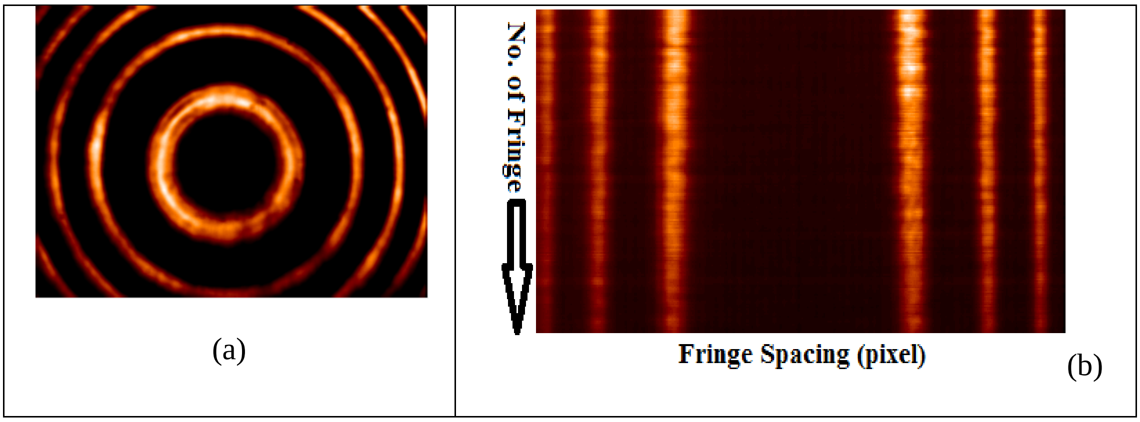

Figure 6.4: *Typical Fabry-Perot (a) fringe, (b) composite image generated from a line scan across the diameter of the fringes, using the concave-convex duct dye cell*

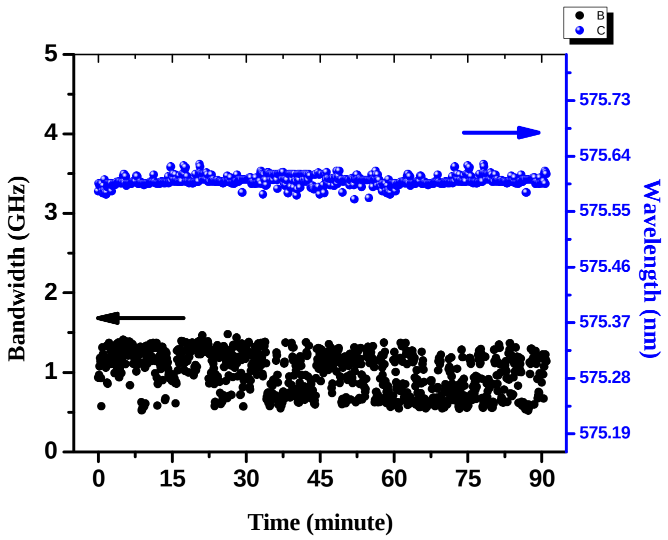

Figure 6.5: *Variation of bandwidth and wavelength with time, using concave-convex duct dye cell*

6.2.3 Pinched dye cell

The pinched glass tube dye cell was employed for a high repetition rate pumping. Fig.6.6 shows the typical Fabry-Perot (a) fringe, (b) composite image generated using pinched dye cell. Spectral measurement from the composite image data was carried out. Fig.6.7 shows variation of bandwidth and wavelength with time, using pinched dye cell. The variation of the bandwidth was within 400 MHz and wavelength varies within 0.0128 nm over the observation period of 75 minutes.

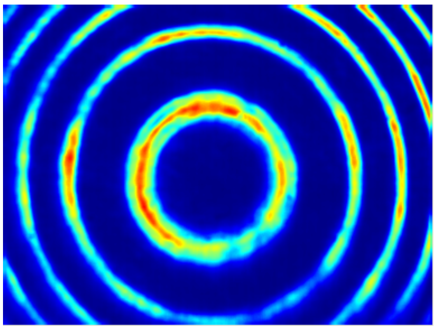

(a)

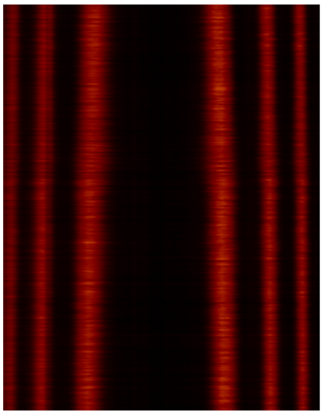

(b)

***Figure 6.6**: Typical Fabry-Perot (a) fringe, (b) composite image generated from a line scan across the diameter of the fringes, using pinched dye cell*

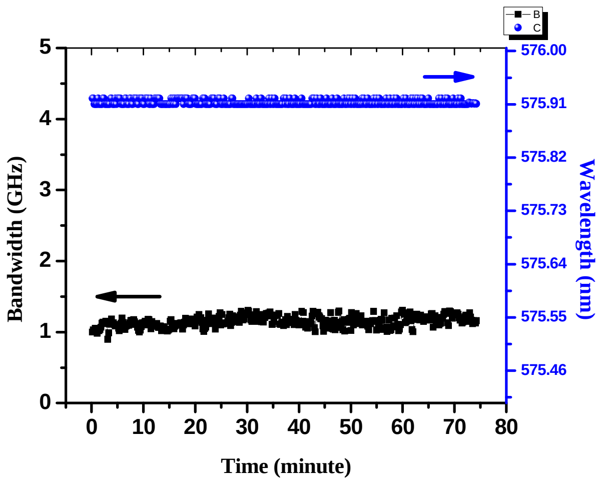

***Figure 6.7**: Variation of bandwidth and wavelength with time, using pinched dye cell*

6.2.4 Convex-plano dye cell

Fig.6.8 shows typical Fabry-Perot (a) fringe, (b) composite image generated using convex-plano dye cell. The spectral measurement from the composite data generated over the period of time has been carried out using convex-plano duct dye cell. Fig.6.9 shows typical variation of bandwidth and wavelength with time, using convex-plano dye cell. The dye laser bandwidths fluctuate within the range 170 MHz, while wavelengths fluctuate within the range 0.0098 nm over the period of an hour.

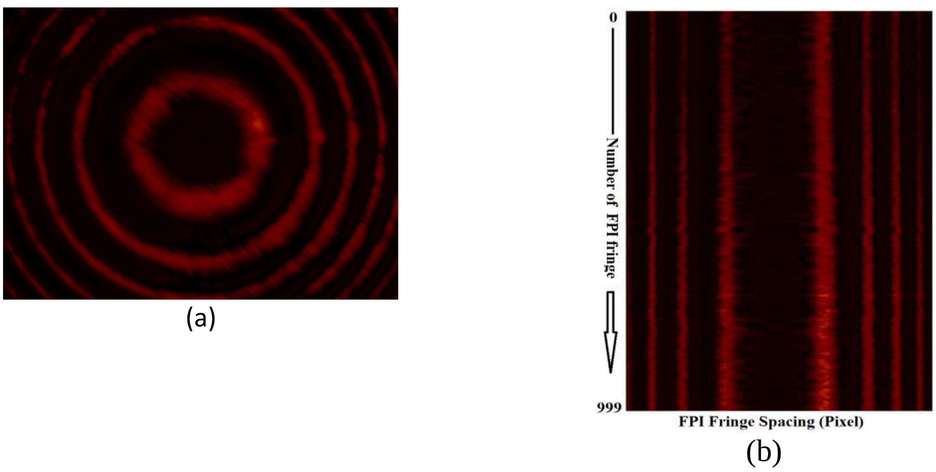

Figure 6.8: *Typical Fabry-Perot (a) fringe, (b) composite image generated from a line scan across the diameter of the fringes, using convex-plano dye cell*

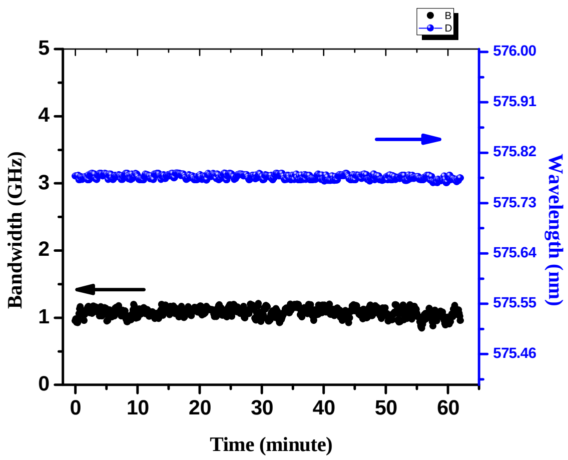

Figure 6.9: *Typical variation of bandwidth and wavelength with time, using convex-plano duct dye cell*

These relative investigations, give the spectral stability of high repetition rate dye laser with the dye cell flow channel geometries. The spectral fluctuations are summarized in Fig.6.10. It was demonstrated that the convex-plano flow profile dye cell provides better stability amongst the dye cells investigated.

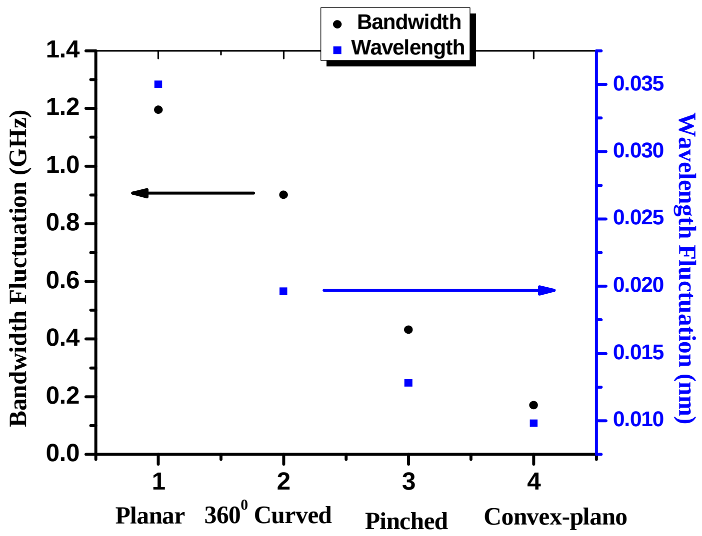

Figure 6.10*: Fluctuations of bandwidth and wavelength with dye cells*

It is experimentally demonstrated that the curved duct dye cells show minimum spectral fluctuations. Therefore, these studies established that the dye cell flow channel geometry, which determines the fluid flow, has significantly role on the spectral stability of the high repetition rate dye laser. The microscopic velocity fluctuations of the flow through the laser active zone can be minimized by a proper design of the dye cell. For this purpose, a curved (convex-plano) dye cell [6.18] was found to be much superior to the conventional planar flow channel dye cell, due to the stabilizing effect on the flow by the convex surface.

6.3 Spectral fluctuations with Reynolds number of the gain medium flow

During the experimental investigations of spectral characteristics of dye laser, it was anticipated that the Reynolds number of the dye gain medium flow would affect the spectral stability. Thus, comprehensive experimental investigation has been carried out to demonstrate this apprehension. First of all, curved (convex-concave) dye cell was used to study the flow induced effects on spectral stability [6.19], seeing that it demonstrated better stability than the planar dye cell. Fig.6.11 shows typical Fabry-Perot fringe of the dye laser at 1012 Reynolds number. The dye laser oscillates in three distinct longitudinal modes. For the spectral investigations at other Reynolds numbers, composite image from the Fabry-Perot fringes has been generated at different Reynolds number to enumerate the spectral fluctuations over the long period of time. For the investigations, flow of the dye solution was adjusted at the Reynolds numbers 221, 681 and 1012. Fig.6.12 shows composite images at typical Reynolds numbers (a) 221, (b) 681, and (c) 1012 over the period of more than an hour. The dye laser output essentially consists of three axial modes, in which two side modes within the gain profile compete for gain.

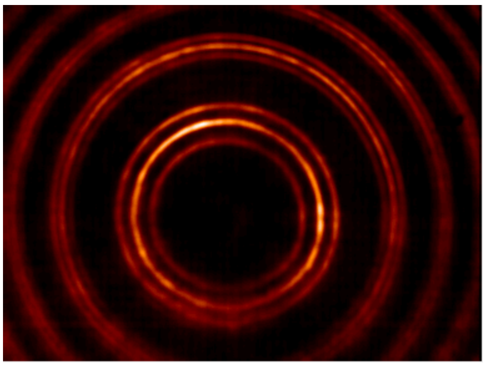

Figure 6.11*: Typical Fabry-Perot fringe of dye laser at 1012 Reynolds number*

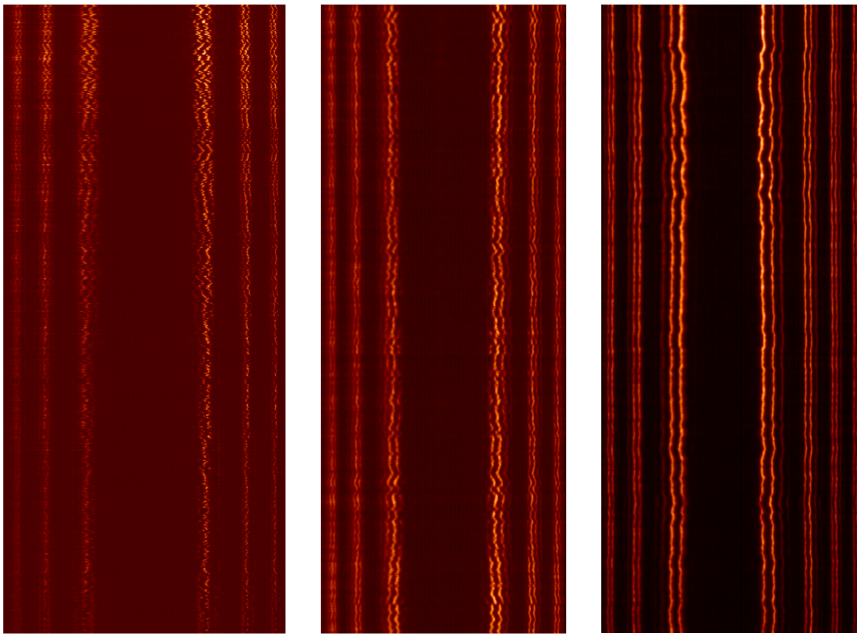

(a) R = 221 (b) R = 681 (c) R = 1012

Figure 6.12*: Composite images at typical Reynolds number (R) (a) 221, (b) 681, and (c) 1012*

It is evident from these composite images that there is a large variation in spectral structure at low Reynolds number, which makes it difficult to distinguish, whereas the individual modes are clearly distinguishable at higher Reynolds number. The number of modes and mode separation varies from pulse to pulse, depending on the strength of instantaneous fluctuations present in the medium. Optical stability of dye laser degrades at lower Reynolds numbers. Measurements from the composite data show that the bandwidth, wavelength and its fluctuation were large at the Reynolds number 221 while slightly reduces at 681. Further increase in Reynolds number of dye solution flow decreases the bandwidth and its fluctuations. The central mode wavelength varies from 576.2281 to 576.2289 nm, 575.9966 to 576.003 nm and 575.9861 to 575.9928 nm while bandwidths from 235 to 324 MHz, 282 to 545 MHz, and 330 to 1.75 GHz at the Reynolds number 1012, 681 and 221, respectively. Fig.6.13 shows typical variation of wavelength of modes with time at Reynolds number 1012 [6.20].

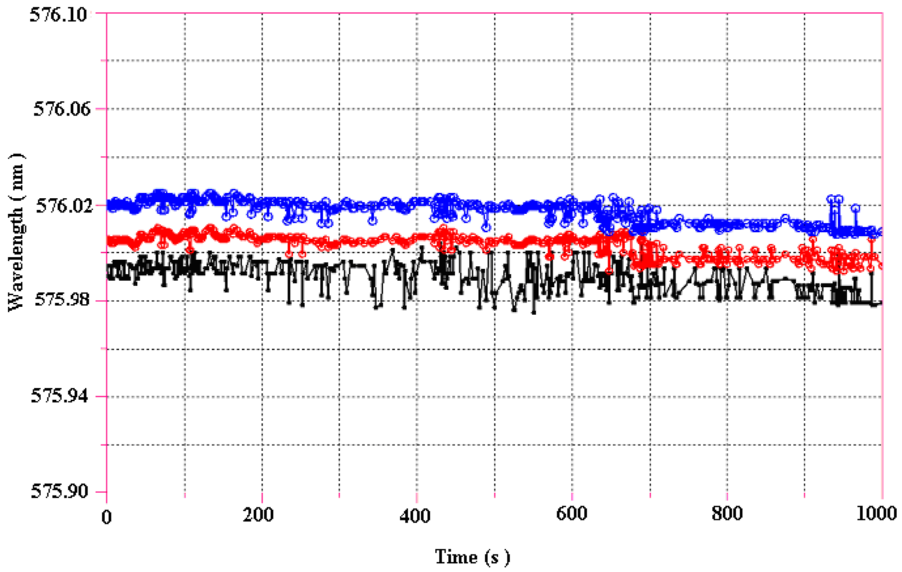

***Figure 6.13**: Typical variation of wavelength of modes with time*

The bandwidth and the wavelength fluctuations of the most stable central mode with Reynolds number is shown in Fig.6.14 (a). Fig.6.14 (b) shows $\Delta\lambda/\lambda$ variation of the central mode with Reynolds number [6.21].

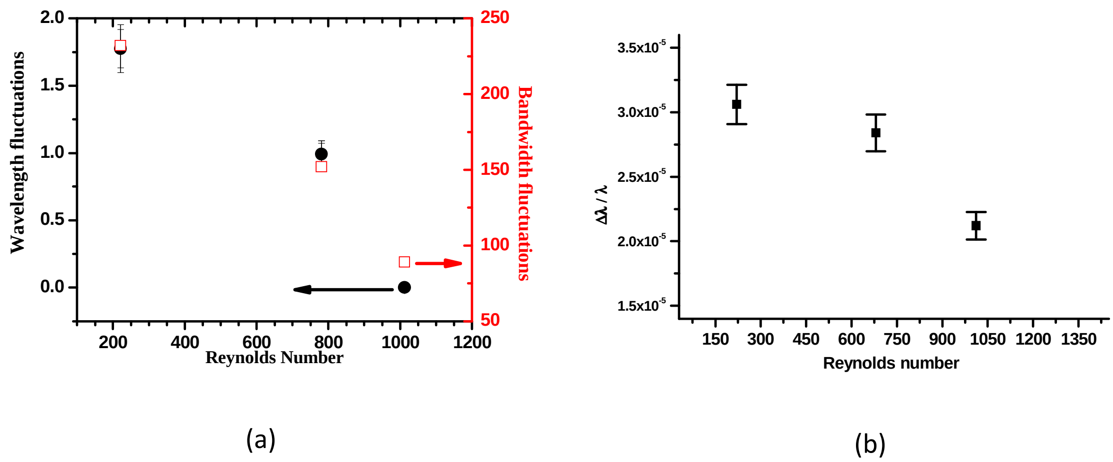

***Figure 6.14**: (a) Bandwidth and wavelength fluctuations of the central mode, (b) fluctuations in $\Delta\lambda/\lambda$ with Reynolds number*

In another experiment, composite image was generated during slowly decreasing the flow speed of the dye solution. Fig.6.15 shows composite image of the line scans of fringe generated during continuing Reynolds number variation in the range 1012-221. Measurement was carried out from this composite image data. Fig.6.16 shows variation of bandwidth and wavelength with number of spectrum taken during the gradually Reynolds number variation from 1012-221 range. These observations obviously demonstrate that the bandwidth and wavelength fluctuations increase drastically with reducing the flow of the dye gain medium.

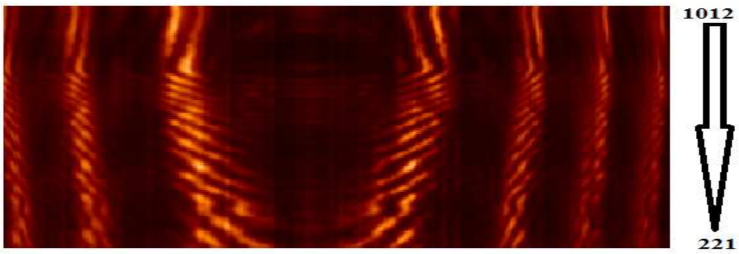

Figure 6.15*: Typical composite image of line scans of fringe generated during continuing Reynolds number variation in the range 1012-221*

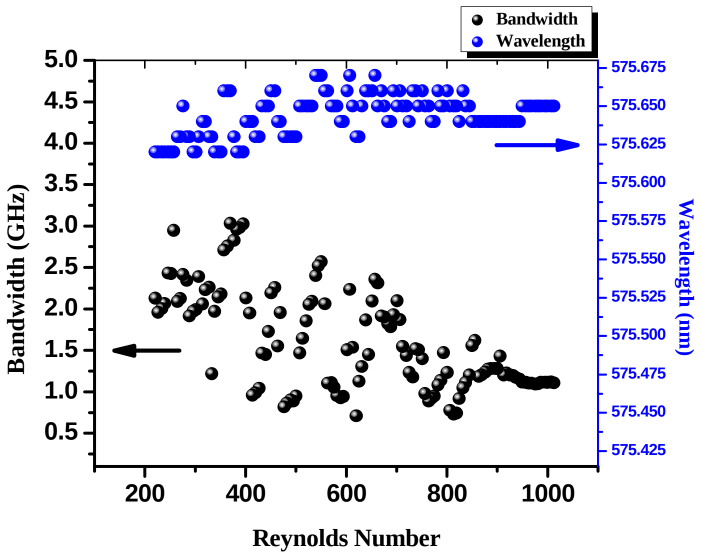

Figure 6.16*: Typical variation of bandwidth and wavelength with flow rates the continuing Reynolds number variation in the range 1012-221*

The spectral property of dye laser was further investigated at discrete flow rates in a convex-plano dye cell. To further visualize and analyse spectral fluctuations by gain medium inhomogeneity, a large number of dye laser Fabry-Perot fringes were generated at Reynolds numbers 1129, 2258, 3387, 4516, 5645 and 6774, respectively. The liquid flow adjustments were carried out with a suitable time gap. After each acquisition of data for spectral profile, there was a waiting period of about 10 minutes for stabilization of the medium. Fig.6.17 show the composite image of line scan of fringe generated at Reynolds numbers 1129, 2258, 3387, 4516, 5645 and 6774, respectively. Estimation of bandwidths and wavelengths were carried out from this composite data. Fig.6.18 shows variation of bandwidth and wavelength fluctuations as a function of Reynolds number. The fluctuations decrease as the Reynolds number of the gain medium flow increases from laminar to the turbulent regimes. However, it again begins to increase at high Reynolds number (> 6000).

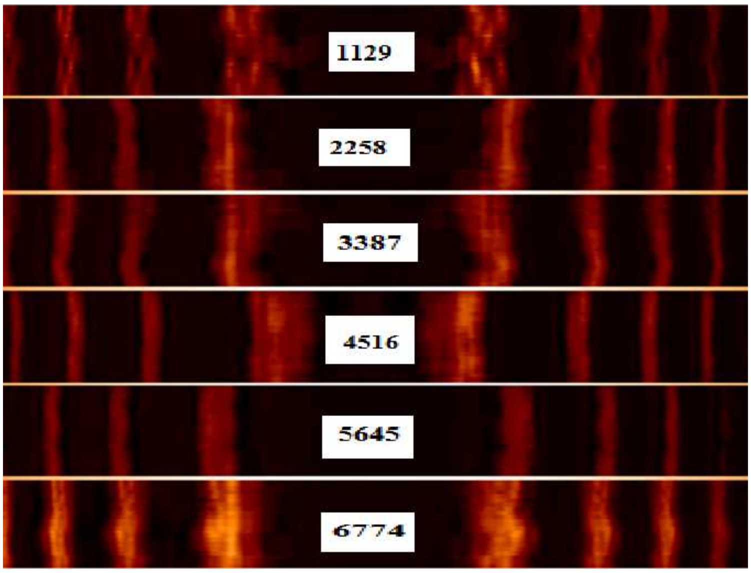

***Figure 6.17**: Composite image of line scan of fringe generated at Reynolds numbers 1129, 2258, 3387, 4516, 5645 and 6774*

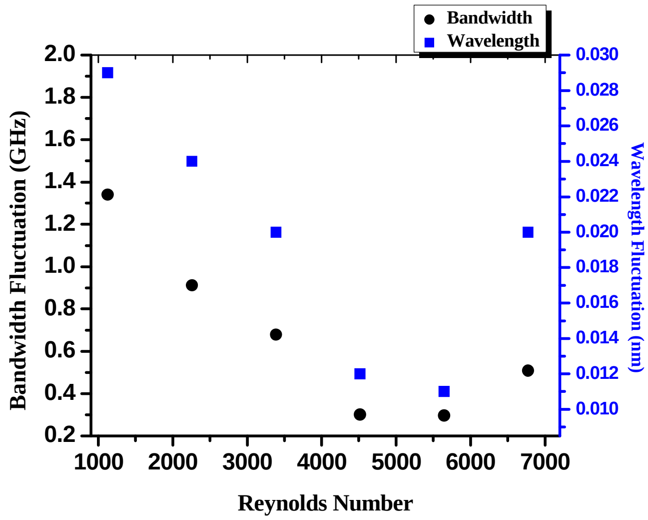

Figure 6.18: *Variation of bandwidth and wavelength fluctuation as a function of Reynolds number*

To further investigate the effect of flow induced inhomogeneity [6.21] in the medium, a He-Ne laser beam, which is not absorbed by the Rh6G dye, was passed through dye cell along the dye laser axis containing the dye solution after removing the optical components of the resonator and putting the pump laser beam off. The intensity and beam spot size (or beam spread) of the He-Ne laser beam were monitored on the other side of the dye cell through a CCD camera. Fig.6.19 shows variation of the beam size and the intensity of the He-Ne laser with the Reynolds number. When the dye solution was stationary, the beam size of He-Ne laser was small and intensity was high. This is due to the maximum transmission and minimum scattering losses. When the dye solution was flown, initially the size of beam increased and intensity decreased and after that it becomes constant, irrespective of flow rate in the observed range of Reynolds number. Increasing of the He-Ne laser beam size after passing through the solution is a clear evidence of scattering in the medium reflecting in increased geometrical divergence.

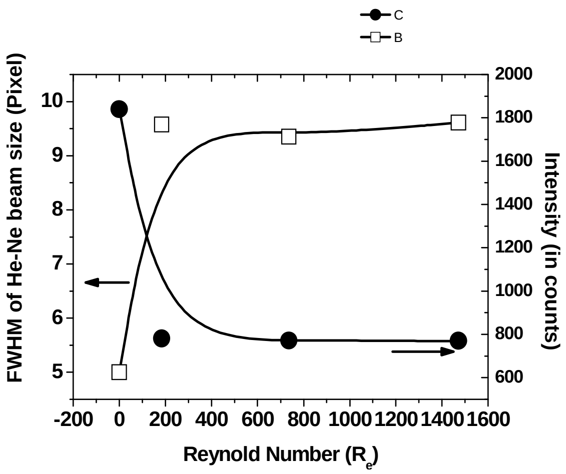

Figure 6.19*: Variation of beam size and intensity of He-Ne laser with Reynolds number*

The gain medium optical quality plays a vital role in the performance of the dye laser. It has been established that the characteristics of the gain medium flow affect the spectral (wavelength and bandwidth) properties of the dye laser [6.22-6.23]. To elucidate the mechanism responsible for relative spectral fluctuations, computational study of the flow and the corresponding heat transfer processes through a volumetric heat deposition was done. For this purpose, computational fluid dynamics (CFD) analysis by the finite volume method [6.24] using ANSYS^{TM} CFX version 14.0 has been carried out. The average flow velocity at 0.5, 1.0 and 1.5 m/s in the laminar regime and 2-8 m/s in the turbulent regimes was used for the study. Also a very low flow velocity 0.019 m/s was used in order to elucidate the deterioration of the medium properties by processes such as boiling and decomposition of the dye gain medium.

The environment of the gain medium, near the dye cell window wall, dictates the optical quality of the medium and hence spectral stability of the dye laser. Therefore, in order to get temperature distribution inside the effective gain medium, 'near the wall model' is highly appropriate. Thus, a hybrid model called '*k-ω shear stress transport (SST)* *turbulence model'* [6.25] was used to evaluate the flow and thermal field near the wall, without losing the accuracy of the flow behavior away from the wall. This hybrid model [6.25] combines the Wilcox k-ω model [6.26] near the wall and the k-ε models [6.27] away from the wall. The finite volume mesh near the surface has been kept fine to capture the flow conditions and temperature in the near wall region [6.28]. Fig.6.20 shows typical temperature variation as a function of distance from the wall, at average flow velocity 0.019 m/s. The temperature gradient is very large in the gain medium region below 200 μm at mean flow velocity of 0.019 m/s.

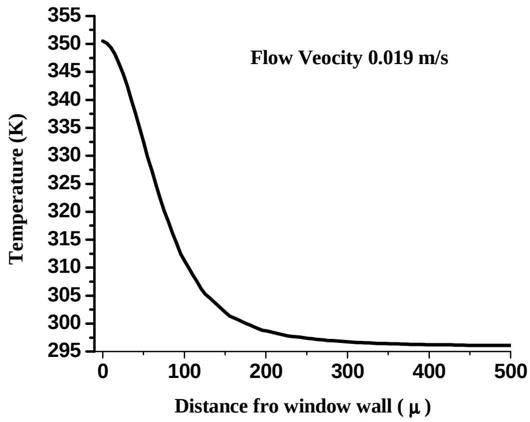

***Figure 6.20**: Typical temperature variation as a function of distance from the wall, at average flow velocity 0.019 m/s*

It is obvious that the temperature near the dye cell-wall has almost reached the boiling point of the dye gain medium. Therefore, mean flow velocity below 0.019 m/s would lead to nucleation of boiling near the cell-wall. This would cause drastic changes in the density/refractive-index of the dye gain medium, which leads to a quick degradation of optical homogeneity as well as severe change in the thermo-optical properties of the gain medium. This is the reason why lasing action cannot be sustained without flow of the dye gain medium. In fact, it was observed that the pump beam entrance window start appearing blackish after a few minutes of operation in the stationary gain medium. Fig.6.21 (a) shows typical temperature variation as a function of distance from the wall at mean flow velocity 0.5, 1.0 and 1.5 m/s. There is a temperature difference of ~ 3 to 6 K in the effective gain medium, which enforces sufficient thermal inhomogeneity in the effective gain medium. Fig.6.21 (b) shows typical temperature variation as a function of distance from the wall, in the mean flow velocity range 2-8 m/s. Now the thermal zone with a very small gradient is available in $< 50\ \mu m$ distance from the wall. Hence thermal inhomogeneity is reduced, due to high heat transfer rates.

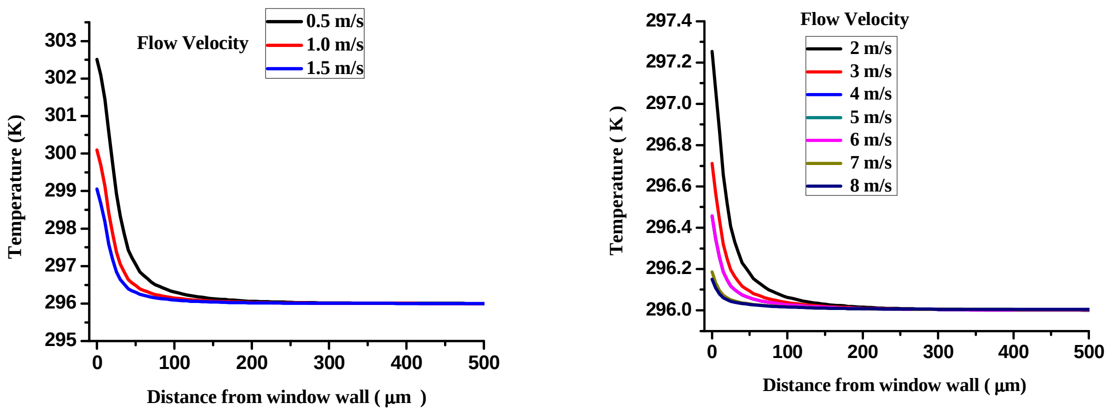

Figure 6.21: *Typical temperature variation as a function of distance from the wall at mean flow velocity (a) 0.5, 1.0 and 1.5 m/s, and (b) 2-8 m/s*

It has been exclusively illustrated, in Refs. 6.29, 6.30 and other references there in, that the turbulent fluctuations of the flow affect the refractive index fluctuations of the medium. Therefore, the presence of turbulent fluctuations in the region of 100 μm from the wall would generate appreciable fluctuations in the refractive index. Two important parameters is generally used to quantify the level of turbulence; turbulence kinetic energy (k) and turbulence intensity (I_v). The turbulence kinetic energy measures the intensity of turbulence fluctuations and is defined as a sum of specific kinetic energies associated with fluctuating components of velocities in three orthogonal directions [6.31-6.32].

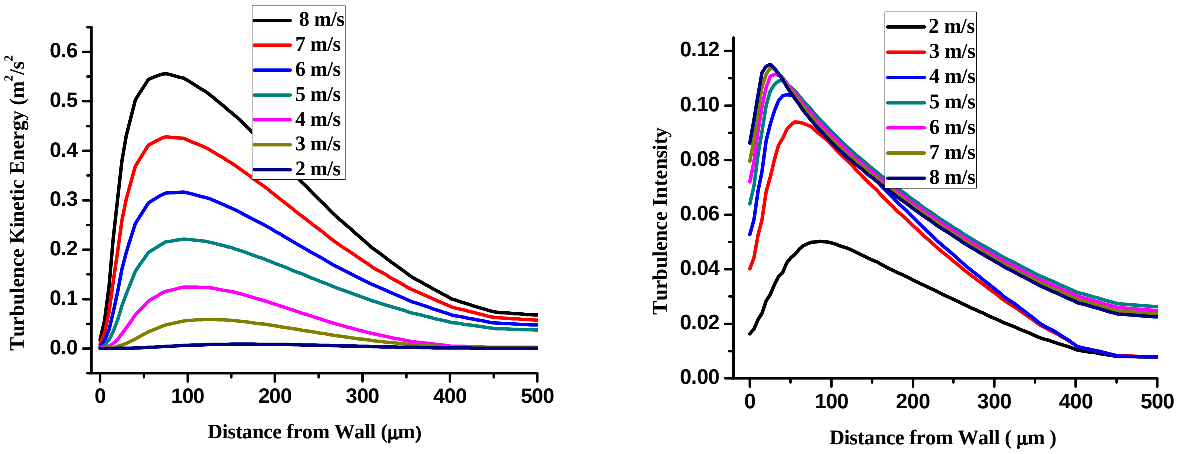

Figure 6.22: *Typical variation of (a) turbulence kinetic energy, and (b) turbulence intensity as a function of distance from window wall*

Fig.6.22 (a) shows typical variation of turbulence kinetic energy as a function of distance from window wall. The order of turbulence over the average flow characteristics was evaluated in terms of turbulence intensity (I_v), which is a ratio of r.m.s. of fluctuating velocity orthogonal components divided by the mean velocity. Fig.6.22 (b) shows typical variation of turbulence intensity as a function of distance from the window wall. The maximum turbulence kinetic energy and its distance from the wall were estimated at various flow velocities. Fig.6.23 shows variation of maximum kinetic energy and its distance from the wall as a function of Reynolds number. The maximum kinetic energy increases while its location intruded more towards the wall (i.e. in the region of effective gain medium) by increasing the flow Reynolds number. This is also accompanied by existence of high extent of turbulent intensity in the effective gain medium region at higher Reynolds number.

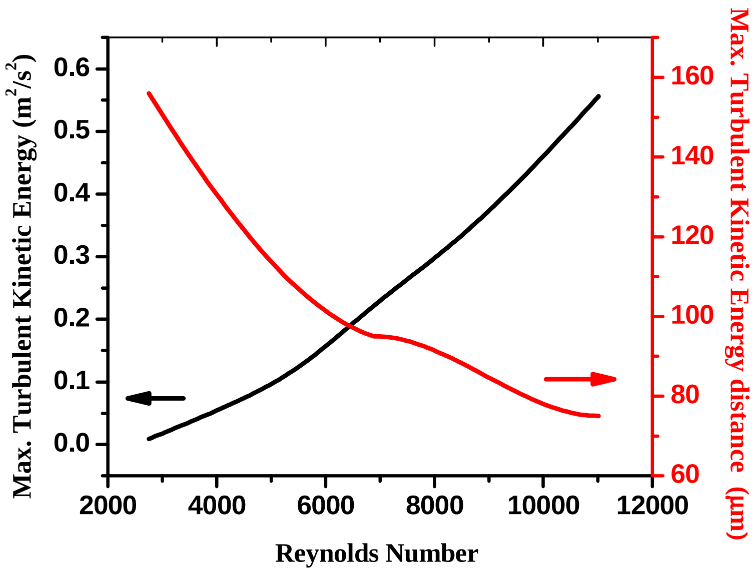

Figure 6.23*: Variation of maximum kinetic energy and its distance from the wall as a function of Reynolds number*

The effective gain medium region from the dye cell window wall is of the utmost importance for the performance of the dye laser. At low Reynolds number, the temperature gradients are present in the effective gain medium region. Therefore, in high repetition rate dye laser, the temperature variation is not only local to the wall but is also very fast [6.32-6.33]. Pulse to pulse and intra pulse variation of the pump beam fluxes, due to evolving intensity and divergence can also cause non-uniformity and fluctuations in temperature, leading to fluctuations in density/refractive-index. In this way, at low Reynolds number, the thermal inhomogeneity is dominant mechanism for degradation of optical quality of the gain medium, which in turn causes instability in the emission passing through it. This resulted in large spectral fluctuations of the dye laser. As the Reynolds number of the flow increases; the scale length of thermal gradients decreases due to added heat transfer, consequently, the optical homogeneity of the gain medium then tends to improve. The dye laser spectral fluctuation was the least for the Reynolds number in the range of 4000 to 6000. This corresponds to the mean flow velocity in the range of 3 to 4 m/s. When the flow velocity was increased to 5 m/s (Reynolds number, ~ 6800), the temperature difference reduces to 0.26 K while the peak values of turbulence kinetic energy penetrate within effective gain medium, where most of the heat is being deposited. Simultaneously, the I_v increased to more than 10% (a high turbulence) and k is significantly high as compared to the value at flow velocity $\leq$4 m/s. The high value of k together with higher I_v signifies the higher level of turbulent fluctuations.

In real turbulent flows, the mean density may vary but the instantaneous density always exhibit turbulent fluctuations [6.24]. The local density fluctuations, which may or may not contribute to the average flow characteristics [6.24]; however, randomly contribute to the instantaneous refractive index of the medium [6.33]. Yokomotti *et al* [6.31] showed, through optical technique, that large density fluctuations were clustered in an isotropic, homogeneous and subsonic air jet flow (Reynolds number ~ 10000, Mack number ~ 0.02, at 0.5 bar). They also observed that clusters resemble an oscillatory dynamics and the segments of oscillations were separated by more irregular behavior. A higher compressibility of ethanol would also promote turbulent density fluctuations. For the Reynolds number exceeding 6000, these turbulent flows stimulate significant density fluctuations prevailed in the effective gain medium region. As a result of this, dye laser spectral fluctuations increase all over again.

At low Reynolds number, the heat transfer from the gain medium is low, consequently, the thermal inhomogeneity is large. At the same time, the effective gain medium region is in either fully laminar or laminar sub-layer region of the flow i.e. away from turbulent fluctuations. Thus, flow related inhomogeneity was not appreciable in the gain medium, although the flow was in the turbulent regime (Reynolds number < 5000). However, for Reynolds number > 6000, turbulent fluctuations penetrate into the effective gain medium region so that the flow related inhomogeneity dominated in the gain medium [6.34]. It is entirely responsible for the degradation of the optical quality of the medium and hence further increase of spectral fluctuations of the dye laser. Thus, thermal inhomogeneity is the dominant mechanism responsible for the large spectral fluctuations at low Reynolds number, however, fast flow related inhomogeneity increase the spectral fluctuations again at higher Reynolds numbers.

6.4 Summary

It has been comprehensively established through experimental investigations that the dye cell flow geometry, which determines the fluid flow characteristics, significantly affects the spectral stability of the dye laser. The spectral fluctuations of the dye laser can be minimized by a proper design of the dye cell as well as the gain medium flow at optimum rates. To validate this, the performances of the dye laser are evaluated in terms of spectral stability using various dye cell geometries and Reynolds number of the flow. The curved profiles of the flow channel geometry provided improved performance as compared to the planar dye cell. Out of the curved profiles studied, nearly convex-plano profile provides the best spectral stability. This is probably because of the fact that the curvature of the flow channel surface minimizes the flow instability considerably. Convex curvature has a stabilizing effect on the boundary layer, while concave curvature is destabilizing. Thus, the flow stabilizing nature and enhanced heat removal capability of the convex geometry is responsible for the better optical quality of the medium, which in turn improves the spectral stability of the dye laser emission.

The temperature distributions in the dye laser gain medium, in laminar and turbulent flow regimes, are computed using finite volume method of computational fluid dynamics. An appreciable temperature gradient ($> 60\ K$) at 0.019 m/s reduces to 0.67 K for mean flow velocity at 4 m/s and it reduces further to 0.26 K at the mean flow velocity 7 m/s. At low Reynolds number, the flow velocity is not sufficient to transfer the heat from the gain medium and promotes the large thermal inhomogeneity, which remains present in the effective gain medium. These substantial thermal inhomogeneity leads to large spectral fluctuation of the dye laser. The minimum dye laser spectral fluctuations are observed for the Reynolds number in the range 4000-6000. In this range of flow, the thermal causes are almost insignificant due to high heat transfer while the gain medium is in the regime of laminar sub-layers i.e. flow related inhomogeneity is yet not appreciable. At high Reynolds numbers, turbulent fluctuations begin to penetrate the regions of the dye gain medium, as a result, the optical quality of the medium degraded. Substantial effects of local density fluctuations, associated with k and I_v, at higher Reynolds number are evidenced. Therefore, characteristics of thermal and hydrodynamic boundary region in the gain medium appreciably influence the optical homogeneity and hence spectral fluctuations of the dye laser emission as experimentally observed.

Publications based on this chapter

1. Study of flow characteristics of a high repetition rate dye laser gain medium,

   Laser Physics, In Press (2013)

   Nageshwar Singh, Abhay Kumar and H. S. Vora

2. Studies on gain medium inhomogeneity and spectral fluctuations coupled with high repetition rate dye laser

   Laser Physics **23,** (2013), doi:10.1088/1054-660X/23/12/125003

   Nageshwar Singh, Abhay Kumar and H. S. Vora

3. Spectral fluctuations of a high repetition rate dye laser through a flowing gain medium

   Laser Physics **23,** *(2013),* doi:10.1088/1054-660X/23/8/085008

   Nageshwar Singh and H. S. Vora

4. High repetition rate dye laser spectral fluctuations through dye cells

   Optik: International Journal for Light and Electron Optics **124**, 7027 (2013)

   Nageshwar Singh and H. S. Vora

5. Effect of liquid flow on spectral properties of a dye laser pumped a copper vapor laser

   Optics Journal **2,** 2 (2008)

   Nageshwar Singh

6. On the stability of the output characteristics of a grazing incidence grating dye laser transversely pumped by a copper vapor laser

   Applied Physics **B 82**, 71 (2006)

   Nageshwar Singh and H. S. Vora

7. Influence of optical in-homogeneity in the gain medium on the bandwidth of a high repetition rate dye laser pumped by copper vapor laser

   Optical Engineering **45**, 104204 (2006)

   Nageshwar Singh

References

[6.1] H. W. Schröder, H Welling and B Wellegehausen, Appl. Phys. **1**, 343 (1973)

[6.2] M. Broyer, J. Chevaleyre, G. Delacretaz and L. Wöste, Appl. Phys. **B 35**, 31 (1984)

[6.3] Zemskov *et al*, Sov. J. Quantum Electron 6, 727 (1976)

[6.4] A. A. Pease and W. M. Pearson, Appl. Opt. **16**, 57 (1977)

[6.5] Zherikin *et al*, Sov. J. Quantum Electron **11**, 806 (1981)

[6.6] A. F. Bernhardt and P. Rasmussen, Appl. Phys. **B 26,** 141 (1981)

[6.7] F. J. Duarte and James A. Piper, Appl. Opt. **23**, 1391 (1984)

[6.8] S. Lavi, M. Amit, G. Bialolanker, E. Miron, and L. A. Levin, Appl. Opt. **24**, 1905 (1985)

[6.9] M. Amit, G. Bialolenker, D. Levron and Z. Burshtein, J. Appl. Phys. **63**, 1293 (1988)

[5.10] Y. Maruyama, M. Kato, A. Sugiyama and T. Arisawa, Opt. Commun. **81**, 67 (1991)

[6.11] Sugiyama *et al*, Optical Eng. **35**, 1093 (1996)

[6.12] F. J. Duarte, *High Power Dye Lasers,* Springer-Verlag, Berlin, 1991

[6.13] H. S. Vora and and Nageshwar Singh, Opt. Commun. **282,** 4259 (2009)

[6.14] Nageshwar Singh and H. S. Vora, Opt. Laser Technol. **39,** 733 (2007)

[6.15] R. Bhatnagar, Nageshwar Singh, R. Chaube, H. S. Vora, Rev. Sci. Instrum. **75**, 5126 (2004)

[6.16] Nageshwar Singh, J. Phys. D: Appl. Phys. ***39,*** *2084* (2006)

[6.17] Nageshwar Singh, H. K. Patel, H.S. Vora, Opt. Laser Technol.**45**, 256 (2013)

[6.18] Nageshwar Singh**,** H. K. Patel, S.K. Dixit, H.S. Vora, Rev. Sci. Instrum. **83,** 105114 (2012)

[6.19] Nageshwar Singh and H. S. Vora, Appl. Phys. **B 82**, 71 (2006)

[6.20] Nageshwar Singh, Optical Engineering **45**, 104204 (2006)

[6.21] Nageshwar Singh, Optics Journal **2,** 2 (2008)

[6.22] Nageshwar Singh and H. S. Vora, Laser Physics **23** *(2013)*, doi:10.1088/1054-660X/23/8/085008

[6.23] Nageshwar Singh, Abhay Kumar and H. S. Vora, Laser Phys. **23** (2013), doi:10.1088/1054-660X/23/12/125003

[6.24] Versteeg and Malalasekra, *An introduction to Computational Fluid Dynamics*: The Finite Volume Method, 2nd Ed. 2007, Pearson Education Limited

[6.25] F. R. Menter, AIAA-Journal **32**, 1598 (1994)

[6.26] D. C. Wilcox, Multiscale model for turbulent flows, AIAA 24th Aerospace Sciences, Meting, American Institute of Aeronautics and Astronautics, 1986

[6.27] B. E. Launder, and, D. B. Spalding, The numerical computation of turbulent flows, Comp Meth Appl. Mech. Eng **3**, 269 (1974)

[6.28] ANSYS CFX Modeling Guide, ANSYS, Inc., Canonsburg, PA, USA, Release 14.0, Nov. 2011, http://www.ansys.com

[6.29] ANSYS CFX Theory Guide, ANSYS, Inc., Canonsburg, PA, USA, Release 14.0, Nov. 2011, http://www.ansys.com

[6.30] Alejandro M. Yacomotti, Pascale Hennequin, Cyrille Honor´e, Jean-Luc Raimbault, Dominique Gr´esillon, Physica **D 200,** 165 (2005)

[6.31] John L. Lumley, Hendrik Tennekes, Henk Tennekes, A First Course in Turbulence, MIT Press, 1972, pp 63

[6.32] M. E. Lusty and M. H. Dunn, Appl. Phys. **B 44**, 193 (1987)

[6.33] T. H. Chyba, E. C. Gage, R. Ghosh, P. Lett and L. Mandel, Opt. Lett. **12**, 422 (1987)

[6.34] Nageshwar Singh, Abhay Kumar and H. S. Vora, Laser Phys., In Press (2013)

Chapter 7

Studies on fluorescence of Rhodamine 6G dye under high repetition rate excitation

The fluorescence from dye molecules is forced by the resonator to develop as coherent laser radiation. Therefore, photo-physics of dye laser is principally governed by the dye fluorescence emission. The exploration of fluorescence characteristics is essential prior to choosing an amplifying medium for the dye laser. In this chapter, fluorescence a characteristic of Rh6G dye is briefly reviewed and a significant investigation coupled with high pulse frequency excitation is presented.

7.1 Review of Rhodamine 6G fluorescence characteristics

Fluorescence spectrum of Rh6G closely resembles the mirror image of the long-wavelength absorption band [7.1]. However, its intrinsic fluorescence spectrum is affected by environmental factors [7.1-7.4] such as the solvent (solute-solvent interaction, polarity and pH of the solution), temperature, concentration of the dye, etc. Apart from these, excited-state and self-absorption of fluorescence [7.5-7.6] also affect the emission characteristics of Rh6G dye. The characteristic of the solvent [7.7-7.8] appreciably affects the fluorescence quantum efficiency, spectral width and the spectra of dye molecules. The concentrations of dye also alter the efficiency of dye laser [7.1, 7.4]. The kinetics of intersystem crossing rate and the triplet state life time of Rh6G, also influence the fluorescence spectrum [7.9, 7.10]. The fluorescence and lasing characteristics are influenced by the thermo-optical properties of the solvent [7.1, 7.3, 7.11-7.12].

Ahmed *et al* [7.13] have reported fluorescence of Rh6G dye dissolved in liquid solvent with added TiO_2 particles (in a thin 0.016 cm x 1.0 cm and a thick 1.0 cm x 1.0 cm cell) to provide random scattering under lamp excitation (514.0 nm) and found that fluorescence in thick (1 cm) cell was red shifted with respect to the intrinsic fluorescence from thin (0.016 cm) cell. They observed that the presence of random scattering in the luminescent bodies affects the spectrum of the fluorescent radiation observed at the surface of these bodies. The primary effect observed was red shift in the emission spectra with respect to the intrinsic fluorescence emission. Hunga *et al* [7.14] reported the shift in fluorescence of Rhodamine 6G in ethanol solutions under a wide range of pumping field fluence. Blue shift of the fluorescence spectra and fluorescence quenching of the dye molecule in solution was observed at high excitation fluence field. These effects were interpreted as the results of population redistribution in the solute-solvent molecular system induced by the high fluence field and the fluence dependence of the radiationless decay mechanism. Fischer and Georges [7.15] had measured the fluorescence quantum yield of Rh6G in ethanol. Hammond [7.5] had reported the self absorption of fluorescence, amplified fluorescence, spectral properties such as emission maximum (553 nm), Stokes shift (21 nm), quantum yield (0.93), decay times of Rh6G in ethanol under nitrogen laser (5 Hz pulse repetition frequency, 8 ns pulse width). Zhang *et al* [7.16] had reported that the fluorescence peak wavelength shift to the longer wavelengths by increasing the hydrostatic pressure of Rh6G dye in ethanol, on excitation with argon-ion laser (514.5 nm). Sinha *et al* [7.17] have evaluated the fluorescence of Rh6G in ethanolic, normal water based aqueous solution, and heavy water based solution and found that the fluorescence shifted by ~5 nm towards the longer wavelengths in water and heavy water based aqueous medium as compared to ethanolic solution, under copper vapor laser (6.5 kHz pulse repetition frequency, 30 ns pulse duration, at 510.6 nm) excitation.

7.2 Studies on fluorescence characteristics under high repetition rate excitation

The physical properties of the medium surrounding the dye molecules significantly affect the fluorescence features of an organic dye. However, to the best of our knowledge, literature rarely reported any study on the fluorescence characteristics of Rh6G dye in stationary as well as in the flowing dye media. Modern advancement of high repetition rate dye laser technology need studies on dye emission characteristics, both in the stationary and the flowing media. Therefore, study on fluorescence properties of Rh6G was carried out in the diverse cases. In the first case, fluorescence spectral width, peak wavelength and its intensity were investigated in the stationary dye solution [7.18]. In the second case, fluorescence spectral width, peak wavelength & intensity were investigated in the flowing medium as a function of the Reynolds numbers of the fluid flow [7.19]. Finally, fluorescence characteristics [7.20] were investigated, in stationary and dynamic media, sequentially.

7.2.1 Fluorescence characteristics in the stationary medium

The experimental setup consists of a dye cell, CVL (510.6 nm) as a high repetition rate excitation source and the compact USB-2000 spectrometer as fluorescence detector. Schematic diagram of the setup used in the experiment is shown in Fig.7.1. A cylindrical lens of suitable focal length was used to line focus the excitation radiation in the dye medium. The dye cell used in the experiment was connected with the dye solution circulation system in closed loop. The details about spectrometer, diagnostic techniques were described in Chapter 2 while dye circulation system was explained in Chapter 5**.** Fig.7.2 shows typical fluorescence spectrum of Rh6G in the stationary dye solution. The small peak, to the left of the main spectrum, is the excitation wavelength (510.6 nm) of the CVL. The peak emission wavelength was at 587.45 nm which has spectral width (FWHM) of 35.73 nm. The high repetition rate excitations in stationary solution heat up the medium and hence affect the fluorescence spectrum [7.18]. A number of spectrums over a time (~ few minutes) have been recorded through composite image generation technique to visualize the effects of high repetition rate excitation on peak emission wavelength and spectral width, during this period.

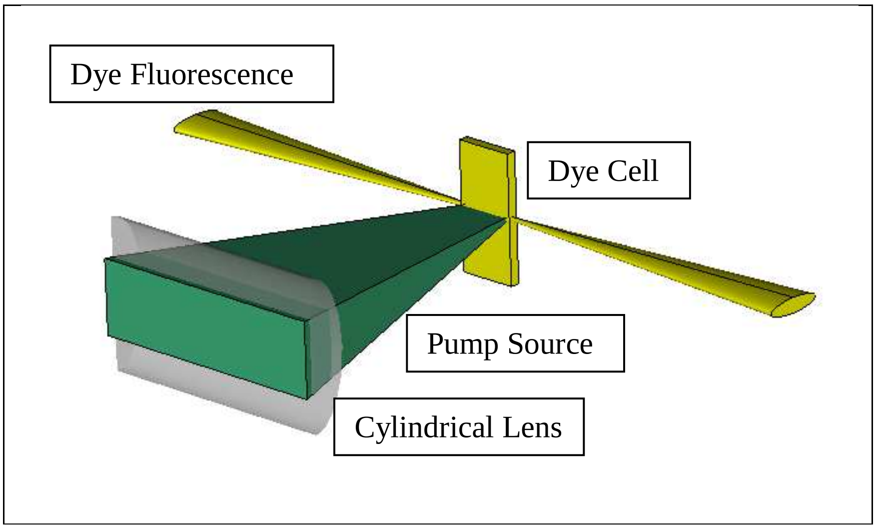

Figure 7.1: *Systematic of experimental layout for dye excitation and fluorescence measurement*

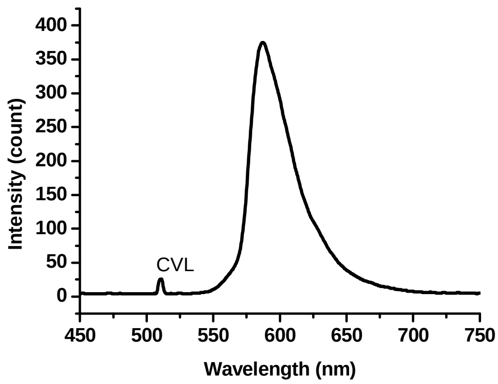

Figure 7.2*: Typical fluorescence spectrum of Rh6G in the stationary dye solution*

To investigate fluorescence fluctuations, online composite image was generated from the individual spectrums. About 1000 spectra were recorded during the observation period of approximately 5 minutes. It was observed that the black particles start depositing near the pump window solid-liquid interface very quickly and hence fluorescence was not recorded for longer time. In fact, the surface infection reduces the pump laser beam intensity in the gain medium. This is the reason for observation of fluorescence spectrum only for few minutes in the stationary solution. Fig.7.3 shows variation of fluorescence spectral width and peak wavelength with number of spectrum taken during the observation period. The fluorescence width and peak wavelength both show appreciable fluctuation during the excitation in stationary solution. Fig.7.4 shows variation of fluorescence peak wavelength intensity and total counts under the lines with number of spectrum taken during the observation period. The peak wavelength intensity decreases with time over the observation period. The peak wavelength intensity decreased by approximately 21%. Relative estimate of photon flux emission was also analyzed through total counts under the spectrum. Total counts under the line decreased also by approximately 21% during the observation period.

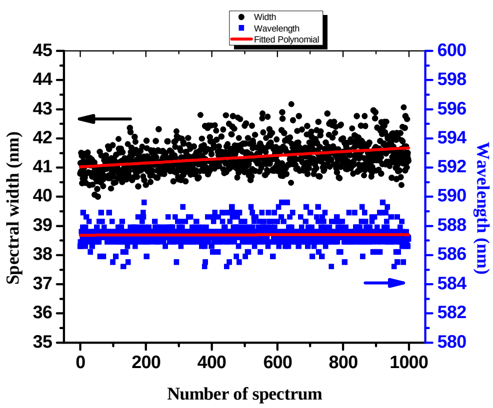

***Figure 7.3**: Variation of the fluorescence spectral width and peak wavelength with number of spectrum taken during the observation period*

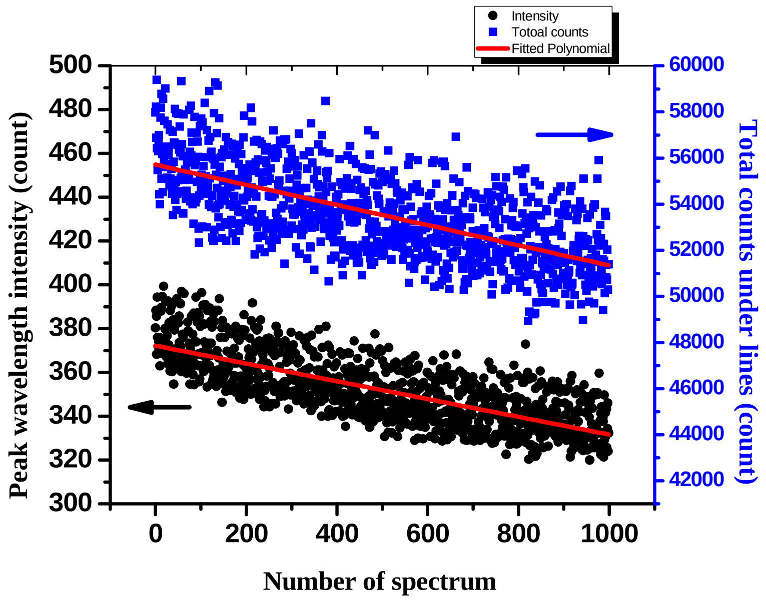

Figure 7.4: *Variation of peak wavelength intensity and total counts under the lines with number of spectrum taken during the observation period*

7.2.2 Fluorescence characteristic in the flowing medium

Investigation of fluorescence in the flowing media (Rh6G dye dissolved in ethylene glycol and ethanol mixture) and has been carried out. The estimated Reynolds numbers variations were in the ranges 90.6-1630.8, which correspond to the mass flow rates in the ranges 1.0-18.0 LPM, respectively. The fluorescence spectrum has been observed as a function of the Reynolds number. Fig.7.5 shows typical fluorescence spectra at Reynolds number 0, 88, 264, 703 and 1630. These were respectively leveled as a, b, c, d and e. Fluorescence spectral width and peak wavelength varies with the Reynolds number of the flow [7.19]. Again number of spectra had been recorded at Reynolds number 0.0-1630 ranges and subsequently analysis has been carried out. Fig.7.6 shows variation of fluorescence width and peak wavelength with Reynolds number. The width of the fluorescence spectra initially shows sharp decrease with increasing Reynolds number.

However, after Reynolds number 996.6 the change is small. It has been observed that the fluorescence width is always less than that in the stationary case.

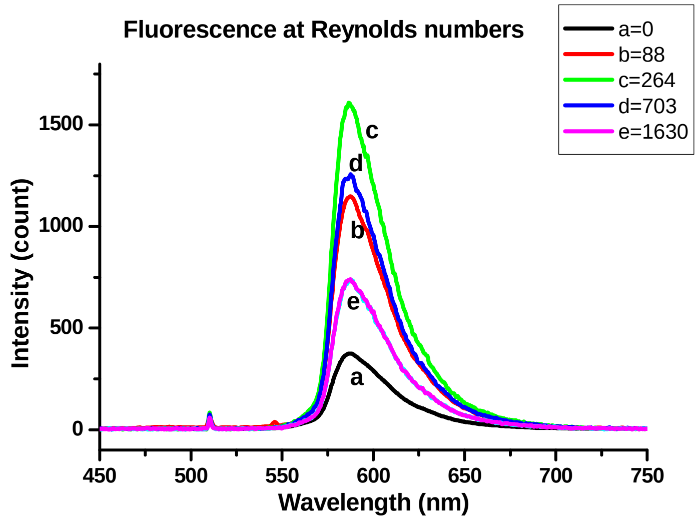

Figure 7.5: *Typical fluorescence spectrum at different Reynolds number*

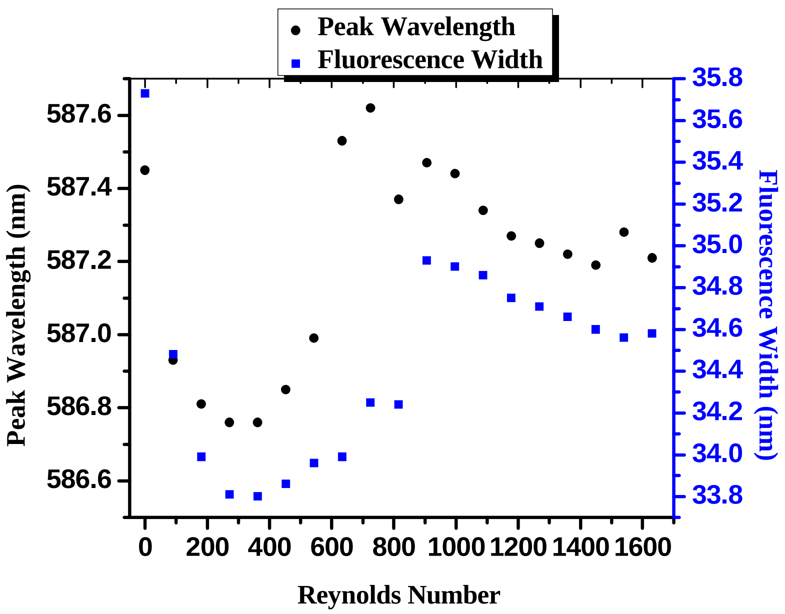

Figure 7.6: *Variation of fluorescence peak wavelength and width with Reynolds number*

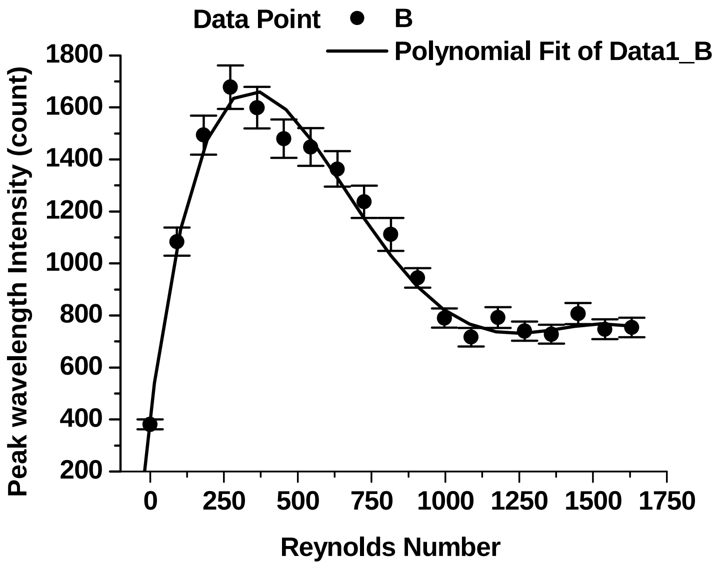

Figure 7.7*: Variation of peak wavelength intensity with Reynolds Number*

The fluorescence peak wavelength changes significantly with increasing Reynolds number. It shows sharp decrease from stationary solution to the Reynolds number of 150, after that increase up to 700 from where it starts decreasing again. The Reynolds number of the flow significantly affects the fluorescence widths and peak wavelength. The peak wavelength intensity also changes with the Reynolds number of the fluid flow. Fig.7.7 shows variation of peak wavelength intensity with Reynolds number. In stationary solution, the peak wavelength intensity was less. As the flow velocity increases, the intensity increased to a maximum value and after that trends reverse to the certain flow rate, however, after Reynolds number ∽1100 the intensity was almost constant.

7.2.3 Fluorescence characteristics in alternatively stationary and flowing medium

In a mixed set of experiment, fluorescence fluctuations of Rh6G dye, dissolved in ethanol, in stationary dye solution and their minimization by the flow of the dye solution was carried out. The experimental setup used for this study is same as shown in Fig.7.1. In this experiment, investigation on fluorescence peak wavelength, spectral width and intensity fluctuations on switching the stationary dye solution into flow and vice versa has been carried out.

The fluorescence characteristic of Rh6G was recorded and investigated, through composite image generation technique, in stationary and dye flowing medium. The composite image of the spectral profile of successive fluorescence spectrum with time in stationary and flow on condition is shown in Fig.7.8. Many spectrums were recorded in stationary dye medium and then in flowing medium. Switching of stationary medium into flow was repeated, as shown in Fig.7.8. Range of spectrum in stationary and flowing medium is indicated in Fig.7.8. It is clearly evident from the composite image that the spectra were more randomly distributed and broadened in stationary medium as compared to dye flowing medium [7.20].

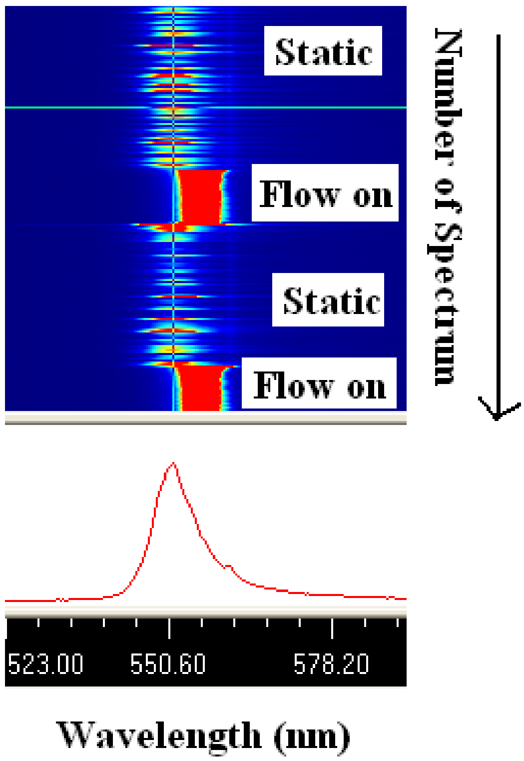

***Figure 7.8**: Composite image of number of successive fluorescence spectrum with time in stationary and flowing medium*

The shift in fluorescence peak wavelength was also evident in these two different physical environments. An estimation of the peak wavelength, spectral width and total counts under the widths of an individual spectrum were carried out from the composite image of the recorded spectra, shown in Fig.7.8. Fig7.9 (a) shows variation of the fluorescence width (FWHM) in stationary and flow on condition. Fluorescence width varies from 7.0 to 12.0 nm in stationary solution. A fluctuation in emission width was reduced by replacing the irradiated dye molecules through flow of the dye solution and was shifted towards minimum width [7.20]. Fig.7.9 (b) shows variation of fluorescence peak wavelengths in stationary and in the flowing medium. The peak wavelength fluctuates by 1.0 nm in stationary where as it is red-shifted by 2.0 nm in the flow on condition.

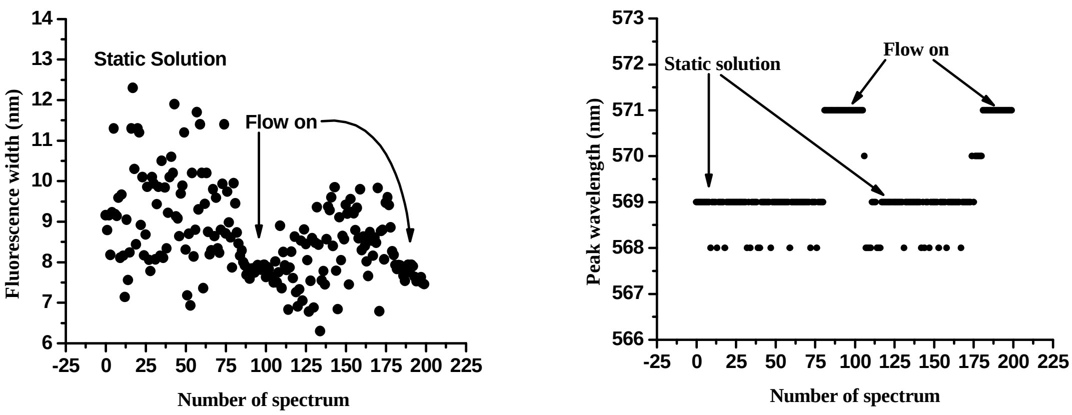

(a) (b)

Figure 7.9: *Variation of the fluorescence (a) width, (b) peak wavelengths, with number of spectrum in stationary and flowing medium*

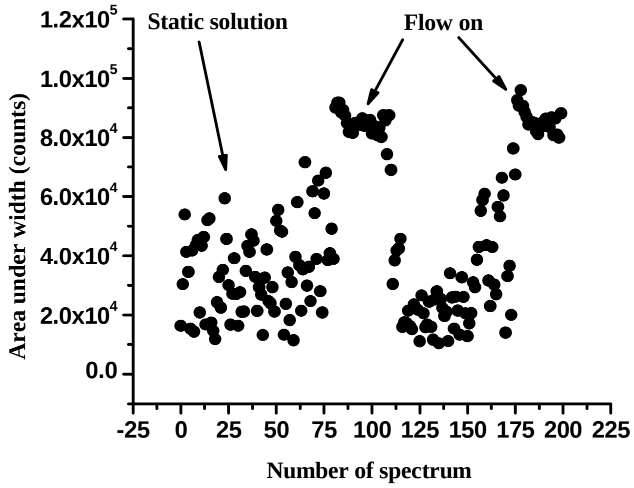

Figure 7.10*: Variation of fluorescence accumulated counts under the width with number of spectrum in the stationary and in the flowing medium*

Fig.7.10 shows the variation of total counts under the width of the fluorescence. It varies from 10,000 to 70,000 counts in stationary medium. The value is large, above 80,000 counts, and less scattered in the flowing medium.

The excitation source (pump laser) operating at 6.0 kHz was focused ($l = 10\,mm,\ \ h \backsim 0.2\,mm,\ d \backsim 0.1\,mm$) in the dye medium, which necessitate no less than 1.2 m/s flow velocity for inclusive replacement of the liquid from the pump beam region before arrival of the next pulse. However, in the present setup, the mass flow rate was adjusted to ensure liquid flow velocity nearly at 4.0 m/s in the dye cell. Heat absorption profile in the dye plays the dominant role in generating the temperature gradients. This temperature distribution produces a spatial variation of the refractive index, which may act as a thermal lens, leading to a phase distortion of the emissions. Both the density and the refractive index of the dye solution are functions of temperature. In stationary solution, refractive index fluctuations of the dye solution are exaggerated by pulse to pulse statistical flux fluctuations of the high pulse frequency excitation source (CVL). These sequentially enlarge the fluctuations of the spectral width of dye emission. Large fluctuations in refractive index of the medium set the peak emission wavelength towards lower side. The absorption depth of pump beam in the dye solution is less than 200 microns, while the cell thickness is 500 microns. The beam deflections are large near the illuminated window-liquid interface. In stationary solution, second derivative of the refractive index $\frac{d^2n}{dz^2}$ is also non-vanishing along with $\frac{dn}{dz}$, away from the pump beam window-liquid interface surface. These gradients effectively contribute to the beam refraction/deflection passing through it, and hence large scattering and losses of spectral intensity, which in turn decrease the fluorescent counts at the detector. The random spectral fluctuations are connected with random temperature fluctuations, as spectral variation is directly affected by temperature. Therefore, spectral intensity variation and emission wavelength spread are induced by instantaneous temperature fluctuations in the stationary dye solution. In flowing dye medium, forced heat transfer phenomenon is taking place and hence temperature and refractive index fluctuations are reduced further, which leads to decrease in fluorescence width and its fluctuations, increase in peak emission wavelength and emission counts.

Apart from the refractive index gradient formation, effect of temperature has many effects on its molecular levels too. The temperatures have an effect on the emission characteristics of dyes in many ways [7.1, 7.21-7.22]. The fluorescence spectrum of organic dye in solution often shows a time-dependent peak shift, when it is excited by a short light pulse even at low temperature. It is energy relaxation process due to rearrangement of the molecule-solvent system after the photo-absorption. Kinoshita et al [7.23] studied the spectral and temporal behavior of fluorescence from Rh6G in ethanol at various low temperatures between 120 and 220 K. The characteristics of shift in peak wavelength and broadening of the spectral width was assumed due to relaxation and fluctuation in the electronic excited state of the dye molecule. The dyes used for laser gain medium at room temperature experiences enhanced thermal heating, particularly excited by high repetition rate laser. The induced thermal field perturbs the solvation energy, excited state reactions, caging surroundings and increasing the rate of non-radiative processes, which in turn increases the fluctuation, broadened the profile and diminishes the fluorescence quantum yield. Replacing the irradiated dye molecules before the arrival of next excitation pulse decrease the variation in spectral widths, increase the stability of the peak emission and quantum yield by curtailing the nearby thermal field to the dye-solvent caging environment. Temperature distribution analysis inside the dye cell validates the influence of heat generation in stationary medium and heat reduction in the flowing medium.

7.3 Summary

The fluorescence spectral width, peak wavelength and intensity of Rh6G dye changes with time during high repetition rate excitation in stationary dye solution. Spectral width increases slightly, accompanied by a slight shift in the emission peak wavelength, while spectral intensity decline with high repetition rate excitation over the period of time. Additions of flow field through Reynolds number try to nullify the surroundings thermal field. The temperature dependent non-uniform refractive index of the medium, due to absorption of the pump beam, have an effect on the fluorescence at low Reynolds number, while the flow field induced turbulences due to the high velocity gradients created within the boundary layers at higher Reynolds number affects the spectrum of the fluorescent organic dyes.

Experimental investigation of fluorescence fluctuation shows large fluctuations in spectral width and intensity in stationary dye solution. Replacement of the irradiated dye molecules from the region of excitation by flow of the dye solution amplify the spectral intensity and minimize the spectral fluctuation. Therefore, these studies of fluorescence feature of dyes under high repetition rate excitation is of fundamental importance to understand the processes responsible, and help in the development of a stable and good optical quality amplifying medium.

Publications based on this chapter

1. Fluorescence fluctuation of Rhodamine 6G dye for high repetition rate laser excitation

   Journal of Luminescence **134**, 607 (2013)

   Nageshwar Singh, H. K. Patel, S. K. Dixit, and H. S. Vora

2. Influence of the medium on the fluorescence of copper vapor laser pumped rhodamine 6 G dye: introduction, experimental details and stationary case

   Optics Journal **1**, 13 (2007)

   N. Sharma, **Nageshwar Singh**, H. S. Vora and S. Goyal

3. Influence of the medium on the fluorescence of copper vapor laser pumped rhodamine 6 G dye: dynamic case

   Optics Journal **1**, 18-22 (2007)

   N. Sharma, **Nageshwar Singh**, H. S. Vora and S. Goyal

References

[7.1] F. P. Shäfer, *Dye Laser*, Springer-Verlag, Berlin, 1990

[7.2] C. V. Shank, Rev. Mod. Phys. **47**, 649 (1975)

[7.3] F. J. Duarte and L. W. Hillman, *Dye Laser Principle*, Academic Press, New York, 1990

[7.4] F. Lopez Arbeloa, T. Lopez Arbeloa, and I. Lopez Arbeloa, *Handbook of Advanced Electronic and Photonic Materials and Devices,* ed. H.S. Nalwa, Vol. **7**, 2001

[7.5] P. R. Hammond, IEEE J. of Quantum Electronics **QE-15**, 624 (1979)

[7.6] P. R. Hammond, J. Chem. Phys. **70**, 3884 (1979)

[7.7] V. V. Maslow, M. I. Dzyubenko, and V. M. Nikitchenko, Sov. J. Quantum Electron **19**, 463 (1989)

[7.8] L. V. Levshin, A. M. Saletskii, and V. I. Yuzhakov, Sov. J. Quantum Electron **13**, 917 (1983)

[7.9] I. L Gandel'man, M. V. Melishchuk, and E. A. Tikhonov, Sov. J. Quantum Electron **13**, 817 (1983)

[7.10] J. P. Webb, W. C. McColgin, O. G. Peterson, D. L. Stockman, and J. H. Eberly, J. Chem. Phys. **53**, 4227 (1970)

[7.11] M. E. Lusty and M. H. Dunn, Appl. Phys. **B 44**, 193 (1987)

[7.12] El-Kashef Hassan, Rev. Sci. Instrum. **69,** 1243 (1998)

[7.13] S. A. Ahmed, Zhi -Wei Zang, K. M. Yoo, M. A. Ali, and R. R. Alfano, Appl. Opt. **33**, 2746 (1994)

[7.14] J. Hung, J. Castillo and A. Marcano O., J. Luminescence, **101**, 263 (2003)

[7.15] M. Fischer and J. Georges, Chem. Phys. Lett. **260**, 115 (1996)

[7.16] B. Zhang, M. Chandrasekhar and H. R. Chandrasekhar, Appl. Opt. **24**, 2779 (1985)

[7.17] Sinha *et al*, Appl. Phys. **B 75**, 85 (2002)

[7.18] N. Sharma, Nageshwar Singh, H. S. Vora and S. L. Goyal, *Opt. J.* **1**, 13 (2007)

[7.19] N. Sharma, Nageshwar Singh, H. S. Vora and S. L. Goyal, *Opt. J.* **1**, 18 (2007)

[7.20] Nageshwar Singh**,** H. K. Patel, S. K. Dixit, H. S. Vora, J. Luminescence. **134**, 607 (2013)

[7.21] Joseph R. Lakowicz, *Principles of fluorescence spectroscopy*, 3rd ed., Plenum Press, New York, 1968

[7.22] M. U. Belyi and A. B. Leontev, Opt. Spektrosc. **34**, 715 (1972)

[7.23] S. Kinoshita, N. Nishi and T. Kushida, J. Luminescence **40&41,** 561 (1988)

Chapter 8

Studies on thermo-optic characteristics of high repetition rate dye laser

8.1 Introduction

It is well known that a fraction of the absorbed pump radiation by the dye gain medium is converted into heat [8.1], within a confined area, through nonradiative deactivation of molecules and Stokes shift. Thus, a major limitation on achieving stable, spectrally narrow and spatially coherent radiation from high repetition rate dye laser lies in the formation of refractive index gradients due to non-uniform heating [8.2] by the pump radiation in the region of optical gain. These thermal problems accumulate during high repetition rate pumping, and have severe consequences on the yield of the dye laser. Therefore, studies on thermo-optic properties of dye laser are essential, particularly under high repetition rate pumping. In this chapter, theoretical investigation of dye solution temperature distribution in the dye cell and spectral deviation in the presence of thermal field is presented. Dye laser characteristics in the presence of thermal field under high repetition rate excitation are experimentally investigated. Studies on optical characteristic of a high repetition rate dye laser have been carried out by dye solution bulk temperature alteration as well as its stabilization. Mathematical treatment for spectral intensity fluctuations by inhomogeneous medium is outlined.

8.2 Theoretical analysis of thermo-optics of a high repetition rate dye laser

8.2.1 Theoretical analysis

The optical pump beam is absorbed in the dye medium following the exponential absorption. Hence the maximum absorption predominantly lies close to the pump beam entrance window of the dye cell. This results in the change of density and hence changes in the refractive index of the gain medium. Also, a statistical fluctuation of the pump beam flux induces spatially random fluctuations in temperature of the gain medium. The temperature T at any point in the dye medium is

$$T = \overline{T} + T', \tag{8.1}$$

where $\overline{T}$ is mean temperature and T' is fluctuating component, about the mean value. Therefore, the refractive index of medium also fluctuates accordingly i.e.

$$n = \overline{n} + n' \tag{8.2}$$

where $\overline{n}$ is the mean refractive index, and n' is the fluctuations in n around $\overline{n}$. The variation in n' is much smaller than $\overline{n}$. Therefore, instantaneous refractive index in the presence of thermal field can be approximated as,

$$n = \overline{n} + \frac{dn}{dT}\Delta T \tag{8.3}$$

where $\frac{dn}{dT}$ is the temperature gradient of the refractive index and ΔT is the temperature fluctuation.

The dye laser characteristics are affected by the refractive index of the materials and physical change in the length of the mechanical mounts, housing the optics. If n is the refractive index of the cavity and l is the geometrical length of the cavity, then optical length L is given by,

$$L = n_a l_a + n_d l_d + n_g l_g \tag{8.4}$$

where a, d and g stands for air, dye and glass medium, respectively.

The change in wavelength due to change in refractive index and geometrical length is approximated as

$$\Delta\lambda = \frac{2}{k}\ (l\,\Delta n + n\,\Delta l) \tag{8.5}$$

$$\Rightarrow \Delta\lambda = \frac{2nl}{k}\left(\frac{\Delta n}{n} + \frac{\Delta l}{l}\right) = \lambda\left(\frac{\Delta n}{n} + \frac{\Delta l}{l}\right) \tag{8.6}$$

The wavelength variation due to change in the refractive index alone is

$$\frac{\Delta\lambda}{\lambda} \approx \left(\frac{\Delta n}{n}\right) , \tag{8.7}$$

$$\Rightarrow \quad \frac{1}{\lambda}\frac{d\lambda}{dT} = \frac{1}{n}\frac{dn}{dT} , \tag{8.8}$$

As

$$\Delta n = \frac{1}{l}\Delta L = \frac{1}{l}\left(l_a \Delta n_a + l_d \Delta n_d + l_g \Delta n_g\right) \tag{8.9}$$

$$\Rightarrow \frac{1}{\lambda}\frac{d\lambda}{dT} = \frac{1}{L}\left(l_a \frac{dn_a}{dT} + l_d \frac{dn_d}{dT} + l_g \frac{dn_g}{dT}\right) \tag{8.10}$$

where $\frac{dn_a}{dT}$, $\frac{dn_d}{dT}$, and $\frac{dn_g}{dT}$ are the index gradient of air, dye and glass medium, respectively. The variation of refractive index of the dye medium, n_d with temperature is identical to that of solvent.

The wavelength variation of the dye laser, due to variation of geometrical length of the cavity is

$$\frac{\Delta\lambda}{\lambda} \approx \frac{\Delta l}{l} \tag{8.11}$$

$$\Rightarrow \frac{1}{\lambda}\frac{d\lambda}{dT} = \frac{1}{l}\frac{dl}{dT} = \alpha_m \tag{8.12}$$

where α_m is the thermal expansion coefficient of the materials involved. Therefore, change in dye laser wavelength can be approximated as

$$\frac{1}{\lambda}\frac{d\lambda}{dT} = \frac{1}{L}\left(l_a\frac{dn_a}{dT} + l_d\frac{dn_d}{dT} + l_g\frac{dn_g}{dT}\right) + \alpha_m \tag{8.13}$$

$$\Rightarrow \Delta\lambda = \lambda\left[\frac{1}{L}\left(l_a\frac{dn_a}{dT} + l_d\frac{dn_d}{dT} + l_g\frac{dn_g}{dT}\right) + \alpha_m\right] \Delta T \tag{8.14}$$

The most sensitive part of the dye laser affected by temperature is the gain medium refractive index [8.1]. Under this approximation, the dye laser wavelength is

$$\lambda \approx \lambda_0 + \frac{\lambda_0}{n_d}\frac{dn_d}{dT}\,\Delta T \tag{8.15}$$

where λ_0 is the wavelength in the homogeneous medium (i.e. at $\Delta T = 0$). In this way, dye laser output wavelength is affected significantly by the fluctuations in refractive index and temperature gradient of refractive index of the medium.

8.2.2 Numerical analysis

The numerical analysis of typical parameters of the dye laser is presented below for spectral variation with temperature. Table 8.1 summarizes the typical parameter of the materials used for the analysis.

Table 8.1: Typical parameter of the materials [8.3]

Materials parameters		
	Ethanol	
1	n_d	1.360
2	$\frac{dn_d}{dT}$	-4.38 *10^{-4} /^{0}C
3	C_p	2.438 J/g-C
4	ρ	0.789 g/cm^3
	BK-7 glass	
5	n_g	1.5
6	$\frac{dn_g}{dT}$	$\approx 1.8*10^{-6}/C$
	Air	
7	n_a	1.000
8	$\frac{dn_a}{dT}$	$\approx 1*10^{-6}/C$
9	α_m (SS)	$0.5*10^{-6}/\ ^0C$

The change in temperature of the medium can cause the variation in refractive index and consequently changes the dye laser wavelength. The changes in wavelength per unit wavelength per degree Celsius change in the temperature, for the typically estimated cavity optical path length of 16.0 cm, is

$$\frac{1}{\lambda}\frac{d\lambda}{dT}=\frac{1}{L}\left(l_d\,\frac{dn_d}{dT}\right)=-\frac{1}{16}2*4.38*10^{-4}\,/\,C=-0.547*10^{-4}\,/\,C \qquad (8.16)$$

Thus, the change of the dye laser wavelength, at λ =576.00 nm, per degree rise in temperature becomes,

$$\frac{d\lambda}{dT}=0.0315\; nm/\;{}^{0}C \qquad (8.17)$$

And the corresponding frequency change, i.e.

$$\left[\frac{d\nu}{dT}\right]\;\approx -28\; GHz/\;{}^{0}C \qquad (8.18)$$

The variation of the geometrical length of the cavity due to temperature rise can cause the wavelength shift i.e.

$$\frac{1}{\lambda}\frac{d\lambda}{dT}=\frac{1}{l}\frac{dl}{dT}=\alpha_s\;=0.5*10^{-6}\,/\;{}^{0}C \qquad (8.19)$$

$$\frac{d\lambda}{dT}=\alpha_s\lambda=0.0029nm/\;{}^{0}C \qquad (8.20)$$

And the corresponding frequency change, i.e.

$$\frac{d\nu}{dT}=-2.62\,\mathrm{GHz}\,/\,{}^{0}\mathrm{C} \qquad (8.21)$$

The variation of refractive index of air of the cavity can cause variation of the wavelength of dye laser, i.e.

$$\frac{1}{\lambda}\frac{d\lambda}{dT}=\frac{1}{L}l_a\,\frac{dn_a}{dT}=\frac{11}{16}1*10^{-6}\,/\,C=0.69x10^{-6}\,/\;{}^{0}C \qquad (8.22)$$

$$\frac{d\lambda}{dT}=576.0*0.69*10^{-6}\,nm/C=0.000397*nm/\;{}^{0}C \qquad (8.23)$$

Corresponding frequency change becomes

$$\frac{d\nu}{dT} = -0.36 \text{ GHz} / {}^0\text{C} \tag{8.24}$$

Thus, frequency change of the gain medium by the temperature is much larger than the other components of the cavity.

8.3 Dye laser characteristics during gain medium bulk temperature variation

8.3.1 Introduction

The output of dye laser is influenced by the thermal, mechanical and environmental properties [8.1, 8.4]. Duarte and Piper [8.5] noticed that the variation in laboratory temperature by 2-3 ^{0}C due to fluctuations in the external weather conditions shifted the dye laser frequency. Consequently, Duarte [8.6] investigated the behavior of output characteristics of dye laser, particularly output power, beam divergence, bandwidth, and frequency stability, by placing the dye laser cavity in an electrically heated oven and varied the cavity temperature in the 20-35 ^{0}C range. Bernhardt and Rasmussen [8.7] demonstrated the operating characteristics of CVL pumped dye laser and summarized the laser properties in terms of materials (like stainless, invar, methanol-ethanol, water, fused silica, air) thermal properties along with their corresponding frequency changes. The temperature of the dye gain medium is a sensitive parameter that influences the optical properties of the dye laser [8.8-8.9]. Number of solvents such as organic solvents, normal water, and heavy water were used to improve the thermo-optical characteristics of a high repetition rate dye laser [8.1, 8.10-8.12]. In these studies [8.10-8.11], thermo-optic properties such as quantum yield of fluorescence and photo degradation of the dye molecules under high repetition rate excitation by CVL were evaluated. El-Kashef [8.13-8.14] had theoretically and experimentally investigated the dye solution refractive index and its thermo-optic constants extensively, through high precision interferometric technique. Widely differing results on macroscopic and microscopic parameter of the dye solvents were reported for thermal analysis of dye laser solutions media [8.13]. Amit *et al* [8.2] have studied the thermal properties of dye laser medium, pumped by CVL (4 kHz pulse repetition frequency). They investigated the temperature gradients generated in the dye cell by CVL, through the transient angular deflection and blooming of a probing He-Ne laser beam after passing throughout the dye medium. They found that the steady temperature gradients extended from 1 to 2 mm in the upstream direction relative to the pump laser impact position to the entire cell length in the downstream direction. The probing He-Ne laser beam experiences about 10-20 mrad angular deflection, depending on the pump laser energy and the dye solution flow velocity.

To the best of our knowledge, literature are deficient in studies on thermo-optic properties of narrow spectral width high repetition rate dye laser for the gain medium temperature above the room/cavity temperature. Therefore, a comprehensive investigation was carried out on the output characteristics such as spectral width, wavelength, average output power, beam divergence and pulse width of a narrow spectral width high repetition rate dye laser, during the dye gain medium bulk temperature alteration from nearly 23-35 ^{0}C ranges. The gain medium bulk temperature was altered by supplying additional heat through the dye solution. A PC based data acquisition system for the temperature measurement was developed to record the bulk temperature of the solution at the dye cell. Dye laser Characteristics was investigated by high resolution spectroscopy based Fabry-Perot (FP) etalon and a composite image generation technique. The thermal inhomogeneity in the gain medium was visualized through composite images.

8.3.2 Experimental details

The dye laser used in the experiment consists of an output coupler mirror (20% reflectivity), a dye cell, intra-cavity etalon (FSR 20 GHz, finesse 13) and a grating

(2400 lines/mm) in conjunction with a tuning mirror. The grating at nearly grazing incidence with intra-cavity etalon was used to provide narrow spectral width emission. This is a very convenient design to provide narrow spectral width with minimum number of optical components. The Rh6G dye in ethanol solvent was used as the gain medium. A CVL (λ = 510.6 nm, average power 4 W, 60 ns pulse duration, 5.6 kHz pulse repetition frequency) was used as the optical excitation source. The schematic layout of the dye laser setup is shown in Fig.8.1 (a), while photograph of arrangement of components of the dye laser is shown in Fig.8.1 (b). The pump beam was transversely line focused onto the flowing type dye cell [8.15] through a combination of spherical (focal length, 40 cm) and cylindrical lens (focal length, 6 cm). An image of fringe generated by Fabry-Perot etalon was acquired through an imaging lens and a CCD camera based setup. The output power was measured using USB based power meter (Ophir). The dye laser beam divergences were estimated from width of the far-field intensity distributions.

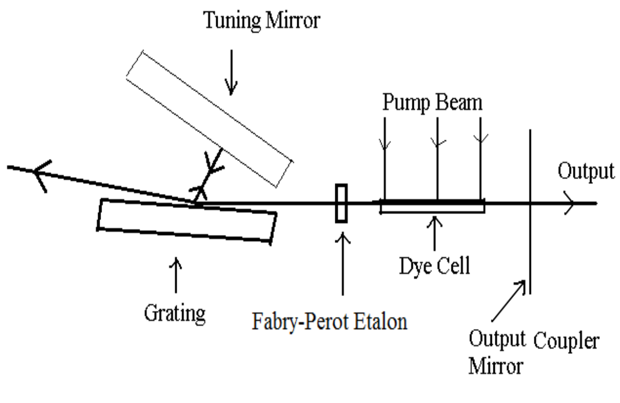

(a)

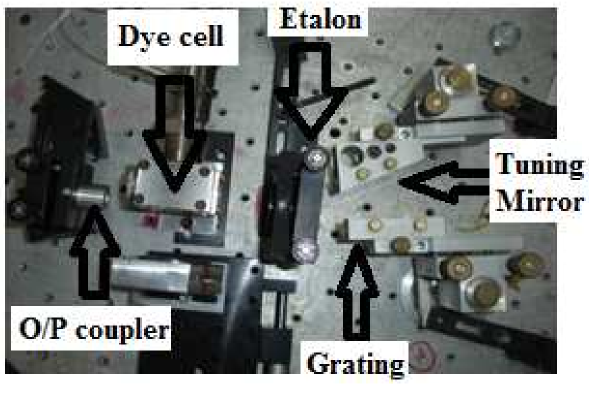

(b)

Figure 8.1: *Schematic of the (a) dye laser layout, (b) photograph of setup*

8.3.3 Results and discussion

The dye solution bulk temperature was monitored at the dye cell for the investigation of characteristics of dye laser under high repetition rate excitation in the presence of thermal field. The temperature of the dye solution, just at exit of the liquid through the dye cell, was observed for more than an hour. The gain medium bulk temperature was raised by putting dye solution cooling mechanism off. The heat generated by the mechanical pump motor, associated with the dye circulation system, slowly increase the temperature of the circulating dye solution. It was observed that temperature of the dye solution was raised ~ 0.5 ^{0}C per minute and dye solution bulk temperature of 35 ^{0}C was attained in nearly 23 minutes. The dye solution bulk temperature was again observed in the presence of gain medium optical excitation by CVL till the temperature attained 35 ^{0}C. When the cooling set temperature was switched from 35 to 20 ^{0}C, the temperature of the dye solution goes down rapidly. Fig.8.2 shows variation of the dye solution bulk temperature with time during (a) cooling off, (b) cooling on. In the presence of optical excitation of the gain medium, there is no change in the slope of the temperature rise of the dye solution.

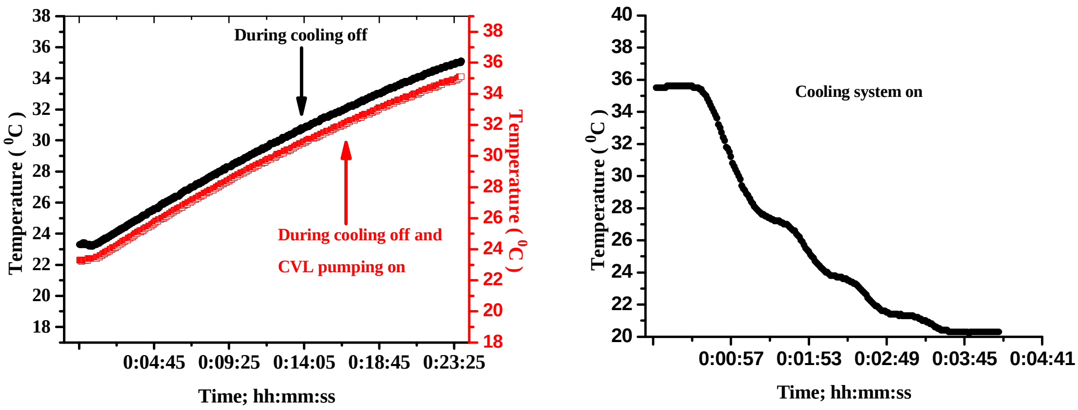

(a) (b)

Figure 8.2*: Variation of the dye solution temperature with time during (a) cooling off, and (b) cooling on*

This is because of the fact that the thermal load added by optical excitation is negligible as compared to the external heat. The dye laser output parameter such as average optical power, divergence, pulse shape, spectral width and wavelength were investigated during the dye solution temperature rise from 23.0 to 35.0 ^{0}C and then cooling back to 20.0 ^{0}C.

The average power of the dye laser declines monotonically with temperature rise of the dye solution. Fig.8.3 shows variation of dye laser average power with temperature. The decrease in dye laser average power was approximately 3% per degree rise in the dye solution temperature. The observed deterioration in the output average power was about 36% for a 12 ^{0}C rise in the dye gain medium bulk temperature [8.16]. Fig.8.4 (a) shows typical dye laser FP fringe at 23.3 ^{0}C temperature. The separation and fringe width measurement showed narrow spectral width (1.13 GHz) of the dye laser. A composite image of the fringes were generated during the temperature rise in the 23-35 ^{0}C range and cooling from 35.0-20.0 ^{0}C. Fig.8.4 (b) shows composite image of the line scan across the diameter of the fringe during temperature alteration. The region **A** is labeled for the number of fringes taken during the temperature rise while region B for during the cooling down, in the Fig.8.4 (b). The region **C**, in the Fig.8.4 (b), is the spectral patterns taken at nearly 20 ^{0}C, after recovering the medium from large thermal inhomogeneities.

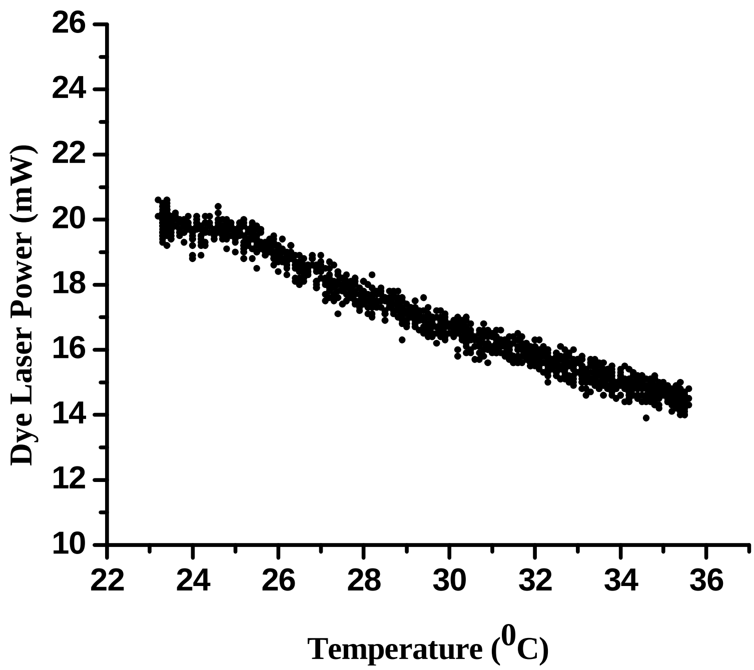

Figure 8.3: *Variation of dye laser average power with temperature*

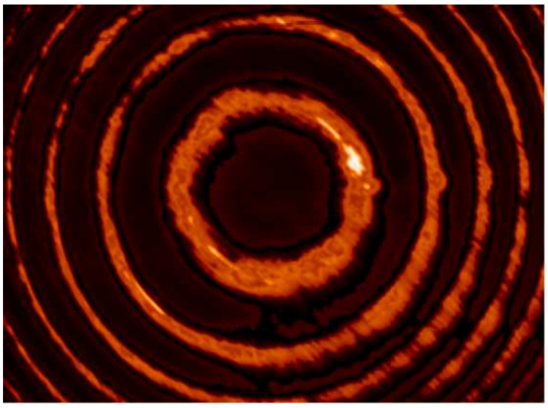

(a)

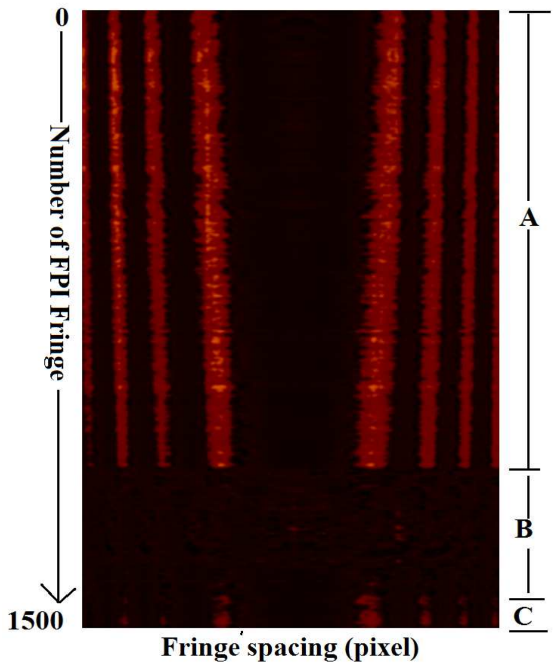

(b)

Figure 8.4: *Typical dye laser (a) FP fringe at 23.3 ^{0}C, (b) composite image of the line scan across the diameter of the fringe during temperature alteration*

The composite image generated from successive FP fringes, clearly indicates the variation in diameter of the fringes while raising the gain medium bulk temperature. While cooling from 35.0-20.0 ^{0}C, the homogeneity of the medium was significantly perturbed, as a result only random noises patterns were visible, denoted as region **B** in the Fig.8.4 (b). The analysis of the spectral width and wavelength, during the temperature rise of the gain medium, has been carried out. Fig.8.5 (a) shows variation of dye laser spectral width with time, in the temperature 23-35 ^{0}C range. The dye laser spectral width fluctuations increase slightly with the enhancement of the medium volume temperature. Fig.8.5 (b) shows variation of dye laser wavelength with number of fringes taken in the temperature 23-35 ^{0}C range. The dye laser wavelength changes from 575.6967 to 575.7534 nm, in this temperature range. Apart from the shift, fluctuation of the wavelength was also observed. Fig.8.6 shows the variation of horizontal and vertical dye laser beam divergence with time, in the temperature ranges

23-35 ^{0}C and 35-23 ^{0}C. It changes from 6.0 to 8.3 mrad in the horizontal direction, while 1.2 to 1.5 mrad in the vertical direction, with pulse to pulse fluctuations.

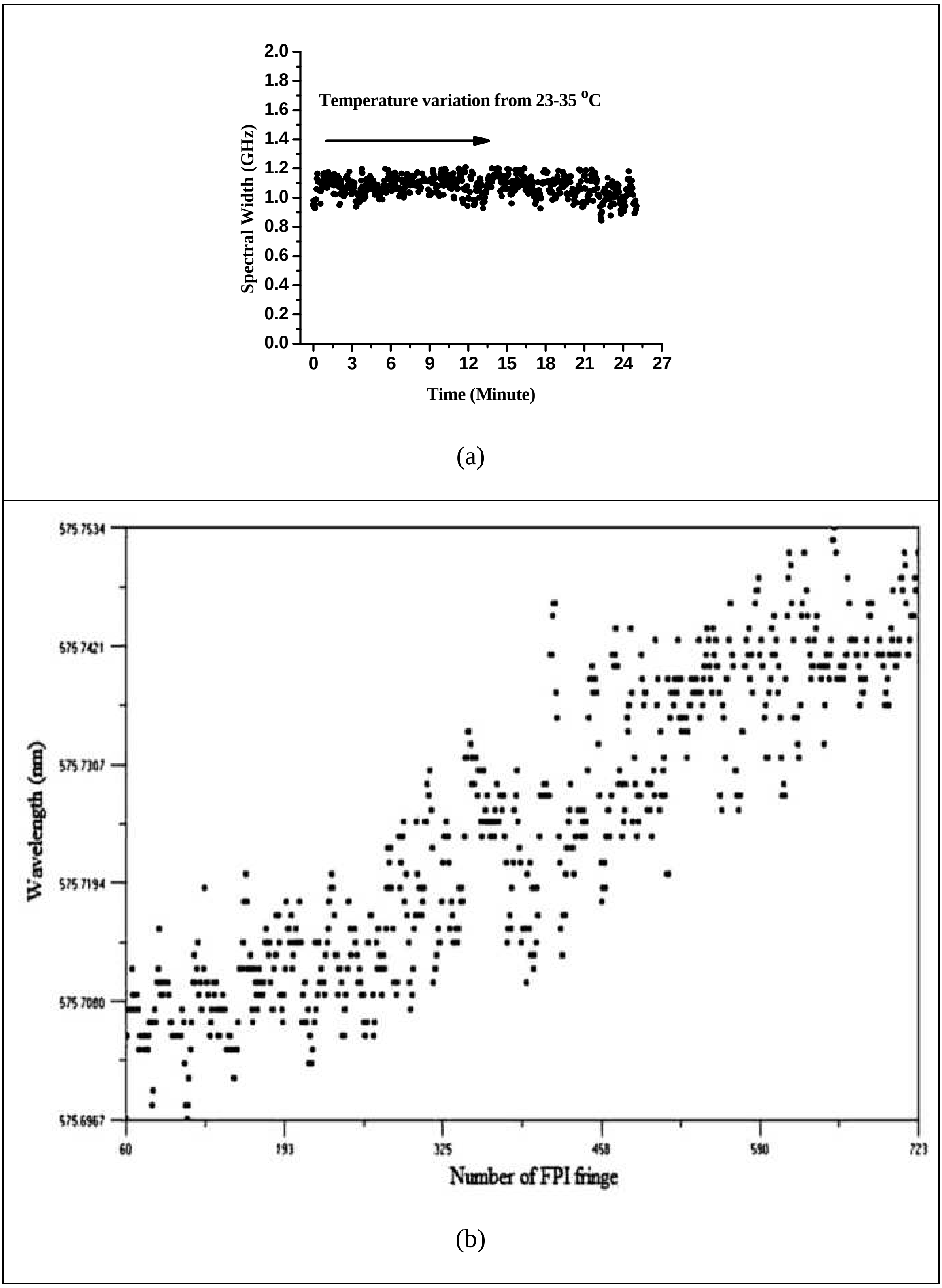

Figure 8.5: *Typical variation of dye laser (a) spectral width with time, and (b) wavelength with number of fringes taken, in the temperature 23-35 ^{0}C range*

Fig.8.7 shows the variation of the pulse width and total counts under the widths with number of pulses taken during the temperature range 23.0 - 35.0 ^{0}C. The dye laser pulse width increases from 34.6 to 36.9 ns. The total counts under the pulse width nearly changes from 8850 to 7650 counts in this temperature range.

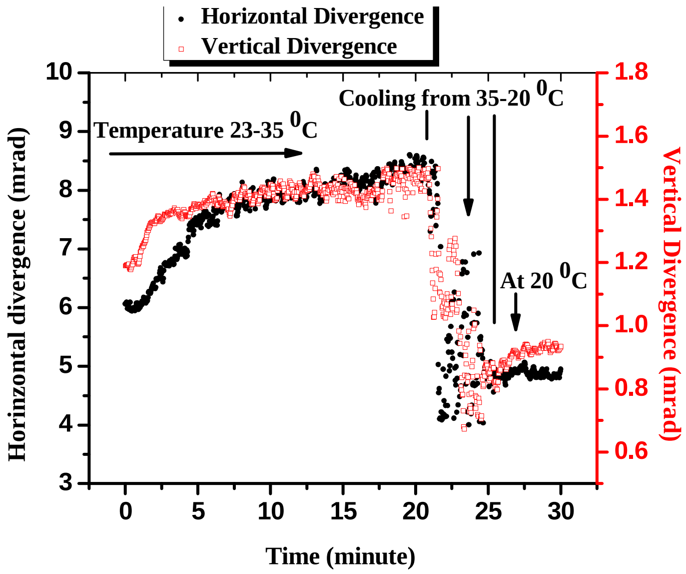

Figure 8.6: *Variation of the dye laser horizontal and vertical divergence with time during the gain medium temperature change*

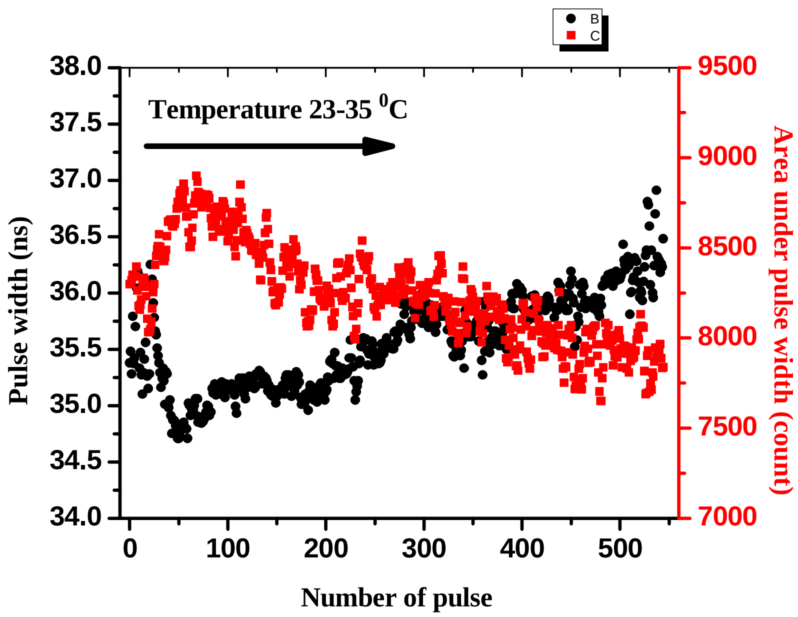

Figure 8.7: *Typical variation of pulse width and total counts under the pulse width with number of pulses taken during the temperature rise in 23.0-35.0 ^{0}C range*

A very few studies [8.6, 8.17] reported on effect of temperature variation on dye laser characteristics. Duarte [8.6] had studied the variation of dye laser, pumped by low repetition rate nitrogen laser, outputs such as output peak power, beam divergence, linewidth and frequency stability by varying the cavity temperature in 20.0 - 35.0 ^{0}C. Peters and Mathews [8.17] have investigated the low repetition rate nitrogen laser pumped dye laser peak power and divergence angle by cooling the dye solution temperature from 28.0 to 13.0 ^{0}C. They found that the dye laser peak power increased while beam divergence decreased during cooling process. Though the effect of temperature on pulsed dye laser is acknowledged, high repetition rate dye laser still needs attention on consequence of gain medium thermal inhomogeneities on the output characteristics. During the present course of investigation, studies on the deterioration in the performance by temperature alteration from 23.0 to 35.0 ^{0}C range, while the cavity temperature was kept constant at normal room temperature was carried out. In this way, optical characteristics of a high repetition rate dye laser have been investigated by varying the temperature of a highly sensitive laser element, dye gain medium. Indeed, wavelength of dye laser in presence of temperature-dominated inhomogeneous medium depends on the refractive index and temperature gradient of the refractive index. Shift in the observed dye laser wavelength with bulk temperature rise is a consequence of variation of the spatial refractive index gradient of the gain medium. The increase of the dye medium bulk temperature changes the effective refractive index gradient of the medium, which in turn red shifts the wavelength of the dye laser. The fluctuations in the wavelengths are due to the transient fluctuations in the refractive index gradients. The dye laser spectral width, effectively, replicated the band-pass of the dispersive components of the cavity. This is indeed the reason why there is no appreciable change in the spectral width, as the dispersive elements, grating and etalon, are distant from the heating zone. Spectral widths were influenced by the pump beam penetration depth fluctuations and by the inhomogeneity of the gain medium. These subsequently cause the variation of geometrical divergence of emission passing through it and hence angle of incidence on grating.

The thermal energy deposited in the dye gain medium by the optical pump beam causes maximum change in density and hence perturbations in refractive index within the thin boundary layers of the medium, next to the pump beam entrance window. As the temperature in the thermo and hydrodynamic boundary layers/sub-layers is much larger than the dye solution bulk temperature, while in this region, the velocity is much smaller whereas the pump intensity is largest. This leads to maximum spatial and temperature gradient of the refractive index in the thin boundary layers of the dye solution. The refractive index gradient in this narrow boundary region is significantly affected by pump power and velocity fluctuations, rather than the dye solution bulk temperature. However, temperature of the solution, around the thermal and hydrodynamic boundary region, tries to adjust the gradients. The divergence characteristics of dye laser emission differ in longitudinal and transverse to the pump beam penetration direction in the gain medium [8.8-8.9]. This is also evident from our experimental measurements, which shows that the dye laser has different beam divergence characteristics in horizontal and vertical directions. The temperature induced inhomogeneities of the medium changes the divergence angles [8.2]. Investigation of the dye laser spectral and divergence characteristics during the bulk temperature rise (23.0-35.0 ^{0}C) and sudden cooling of the bulk medium (from 35.0-20.0 ^{0}C) clearly showed inhomogeneity generated in the pumping region of the medium. During the cooling, the degree of inhomogeneity was too high and hence unable to measure the spectral variations. These inhomogeneities were also replicated in the dye laser beam divergence measurements during this range of temperatures variations. The maximum deflection of the laser beam occurs during the cooling, which was also clearly visible by naked eye at the time of experimentation. The decline in average power along the dye laser axis with temperature rise is a consequence of collective effect of increased deflection angles of the beam as well as channelization of energy through nonradiative routes. The dye laser pulse profile depends on the number of round trips, within the available gain time. Inhomogeneities of the gain medium affect the optical path length of the emission propagating through it. The fluctuations in the optical path length by thermal inhomogeneity have an effect on transit time, and hence pulse profile, of the light passing through it. The increased effective path length by refraction/deflection in the dye medium slightly influence the pulse duration during the increased inhomogeneity by the temperature. The counts under the pulse width are a measure of photon flux. The decrease in optical average power with temperature rise is a sign of decreasing photons flux at the detector. Thus, decrease in average power, counts under the pulse width with temperature rise of the bulk medium is an assessment of decrease in quantum yield due to the increase in non-radiative rates as well as fractional photons lost from the cavity. The present observation [8.16] of average power declination and almost no change in bandwidth is well in conformity with the earlier measurements [8.6, 8.17].

8.3.4 Summary

In summary, an effect of dye gain medium bulk temperature on the optical properties of a CVL pumped narrow bandwidth dye laser is investigated. A data acquisition system is developed to record the temperature of the dye solution at the dye cell. The dye gain medium bulk temperature of about 12.0 ^{0}C was raised in nearly 23 minutes and cooled down from 35.0-20.0 ^{0}C within 3 minutes. The dye laser spectral width is almost unaffected while wavelength changes from 575.6967 to 575.7434 nm by the temperature variation in 23.0-35.0 ^{0}C range. The pulse width slightly increased, whereas counts under the pulse width decreased by approximately 1200 counts in the 23.0-35.0 ^{0}C range of temperature. The dye laser horizontal beam divergence increased almost by 2.5 mrad, while the vertical beam divergence by 0.3 mrad, for an increase of the dye solution bulk temperature by 12.0 ^{0}C. For these ranges of temperature variations, the dye laser average power declined by approximately 36%.

8.4 Dye laser characteristics during gain medium bulk temperature stabilization

It is well known that the temperature of the dye gain medium brings about considerable changes not only in the dye photo physics but also on the lasing characteristics. In this section, optical characteristics of high repetition rate dye laser over the period of time, by stabilizing dye solution bulk temperature within ±0.1^{o}C, was investigated. For the completeness, a review of the work reported in literature on the spectral stability of dye lasers by means of temperature stabilization is briefly presented.

In past, studies [8.18-8.19] on the performance of CVL pumped narrow linewidth dye laser, by keeping the dye solution temperature fluctuation within 0.01 ^{0}C at the dye solution reservoir, were reported. The recent studies [8.20] also reports on the beam divergence, pointing stability, linewidth and wavelength stability of CVL pumped narrow linewidth dye laser with [8.22, 8.23], over a few minutes. All these studies [8.18-8.21] have been performed in different perspectives, in terms of dye laser system mechanical structure and the dye solution temperature stability. In another laser system, studies of spectral stability had been reported for a few minutes with the temperature of dye laser solution controlled within ±0.1 ^{0}C [8.22]. In similar narrow linewidth laser system [8.7] where all optical mounts were attached to thick invar base and the dye solution temperature was kept stable to within ±0.1 ^{0}C. In all these studies, the temperature was controlled from ±0.01 ^{0}C to ±0.1 ^{0}C in the dye solution reservoir. Additionally, the dye laser spectral stability was reported [8.21] for few minutes both for coarse control of temperature 23±2 ^{0}C and fine control of temperature 23±0.1 ^{0}C of the dye solution. It was reported that the linewidth varied between 100 and 770 MHz for a observation period of 30 seconds, with dye solution temperature controlled within 23 ± 2 ^{0}C, while linewidth variation was less than equal to 100 MHz for few minutes, with dye solution temperature controlled to 23.0 ± 0.1 ^{0}C. In another study [8.22], it was reported that the linewidth variation was from 200 to 300 MHz over a period of 10 minutes, by controlling the dye solution temperature ± 0.1 ^{0}C. In this fashion, attention was drawn to the importance of dye solution temperature controlled either ± 0.1 ^{0}C or ± 0.01 ^{0}C, and significance of thermal stability for better spectral stability of the dye laser. In the present course of investigation, not only the dye laser spectral stability but also average optical power and beam divergence characteristics were investigated, over the long period of time more than hours, by controlling the dye solution bulk temperature ± 0.1 ^{0}C. Experimental details and diagnostic techniques were same as described in section 8.3.2. In this investigation, the temperature of the dye solution was controlled within 23.3 ± 0.1 ^{0}C by PID controller. The room and cavity temperatures were also stabilized to near 23.3^{0}C. Fig.8.8 shows variation of cavity and gain medium bulk temperature with time. The temperature of the dye laser cavity changes slightly from 23.4 to 22.8 ^{0}C and hence was fairly stable over the period of more than an hour. The gain medium bulk temperature was also steady over the same period.

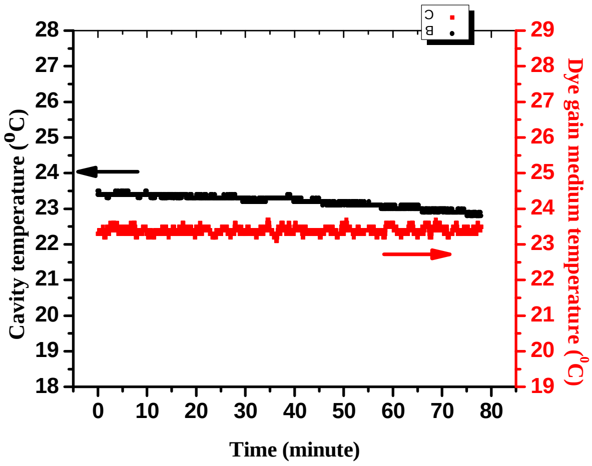

Figure 8.8: *Variation of cavity temperature and gain medium temperature with time*

The dye laser spectral variations were investigated through fringe capturing and composite image generation techniques. For a long-term spectral stability investigation, a composite image of a line scan across the diameter of the FP fringe pattern was generated. Fig.8.9 shows typical Fabry-Perot (a) fringe, (b) composite image of fringes taken during the observation period. The measured spectral width of the dye laser emission was 0.824 GHz. Fig.8.9 (b) shows typical composite image of 1000 successive FP fringes during the observation period of more than an hour. Measurement of dye laser spectral width and wavelength was carried out from this composite image data. Fig.8.10 shows the variation of dye laser spectral width and wavelength with time. The short-term (in 1 minute) fluctuations in the spectral width were within ±75 MHz, while its central value drifted from 0.824 MHz to 1.124 GHz over the observation period of 75 minutes. Fig.8.10 shows variation of dye laser wavelength with time.

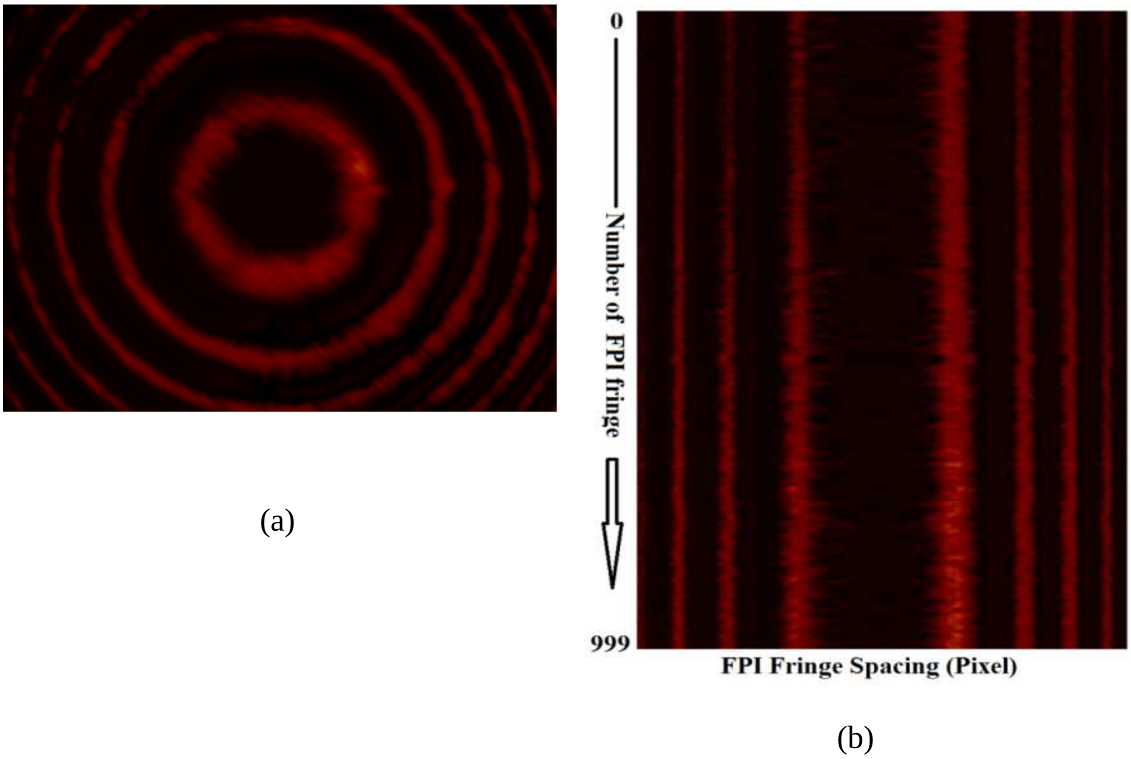

Figure 8.9: *Typical Fabry-Perot (a) fringe, (b) composite image of the successive fringe*

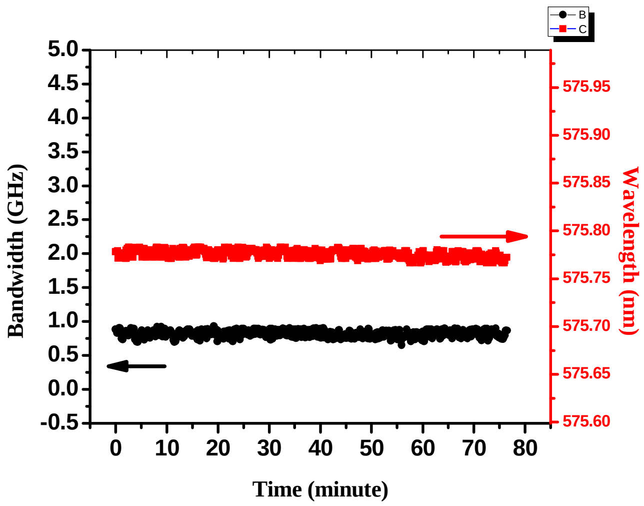

Figure 8.10: *Typical variation of bandwidth and wavelength with time*

It was analyzed that the short-term fluctuations in wavelength were from 575.7713 to 575.7791 nm. The dye laser wavelength drift were from 575.7791 to 575.7662 nm over the observation period of more than an hour. Further, fluctuation of spectral width at a particular wavelength was analyzed. Fig.8.11 (a) shows variation of dye laser spectral width with wavelength over the observation period.

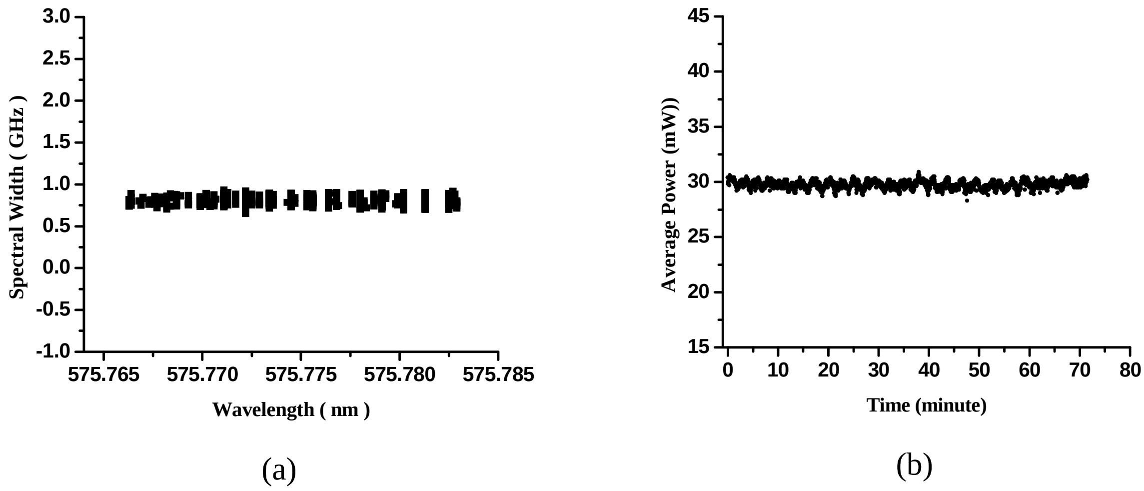

Figure 8.11: *Variation of (a) spectral width with wavelength, (b) average power with time*

Fig. 8.11 (b) shows variation of dye laser average power with time. The measured dye laser output average optical power was 30 mW. The fluctuations of average power about the mean were within 3 %.

In conclusion, optical stability of CVL pumped narrow bandwidth dye laser was experimentally investigated over the period for more than an hour. It was observed that the short-term spectral width varies within ± 75 MHz, while in a long-term, more than an hour, it was drifted by about 180 MHz. The short-term wavelength fluctuations were within 0.0065 nm, while in a long-term, more than an hour, it was drifted by about 0.0105 nm. Dye laser average power was fairly stable.

8.5 Theoretical studies for dye laser intensity fluctuations

It was observed that dye laser has output fluctuations were present even with very precise temperature control of the dye solution. In this section, attempts were made to correlate microscopic parameter of the medium, responsible for intensity fluctuations.

The propagation of waves through random media is a subject matter that had been of considerable theoretical and practical interest for a long time, as is evident from the number of books and papers written on the subject [8.23-8.32]. However, most of the works were on the problem of wave propagation and scattering in the atmosphere, the ocean, and in biological media, which are, in general, randomly varying in time and space so that the amplitude and phase of the waves may also fluctuate randomly in time and space.

Jannson *et al* [8.33] derived the expression for the spectral intensity of the field, produced by scattering of radiation, in the far zone. They showed that the spectral intensity depends on the spatial correlation function of the field and degree of spatial coherence of the incident field. The field generated by scattering of light from a quasi-homogeneous source on a quasi-homogeneous random medium was investigated by Visser *et al* [8.34]. The far field generated by scattering of a plane monochromatic wave incident on a quasi-homogeneous, random medium, was explained with the help of correlation function of the scattering potential of the random scatterer [8.34]. A theory was developed [8.35] for the fluctuations in the phase and amplitude of a laser beam probing a locally homogeneous and anisotropic medium with the help of correlation functions, which are related to the corresponding stochastic properties of the scattering medium.

Most of the theoretical and experimental works were related to the coherent/incoherent or partially coherent beam propagation through homogeneous, quasi-homogeneous, random and/or turbulent media. All of these models considered propagation and scattering of light through macroscopic gaseous media. To the best of our knowledge, no report is available on the spectral intensity variation by the correlation function of the refractive index fluctuation of the microscopic liquid media, particularly dye emission through inhomogeneous liquid gain medium. In this section, analytical expression for the spectral intensity variation of the radiation scattered by the correlation function of the refractive index fluctuations of the inhomogeneous liquid medium is derived.

The physical properties of the medium is generally characterized by the dielectric constant ε . Thus , from the Maxwell's equation

$$div\,\varepsilon\,\vec{E} = \varepsilon\; div\,\vec{E} + \vec{E}\cdot grad\;\varepsilon = 0 \tag{8.25}$$

We have

$$div\;\vec{E} = -\frac{\vec{E}\cdot grad\;\varepsilon}{\varepsilon} = -\vec{E}\cdot grad\,(\log\varepsilon) \tag{8.24}$$

Using $\varepsilon = n^2$, simplification of Maxwell's equations gives

$$\nabla^2\,\vec{E} + k^2\,n^2\,\vec{E} + 2\;grad\left(\vec{E}\,.\,grad\log n\right) = 0 \tag{8.27}$$

where n is refractive index, $k = \omega/c$ the wave number associated with the frequency ω, c is the speed of light in vacuum. The refractive index is expressed as sum of mean and a fluctuating part i.e. the instantaneous refractive index is given by

$$n = \bar{n} + n_1 \tag{8.28}$$

where n_1 is the deviation of n from its mean value, $\bar{n}$. Therefore,

$$\nabla^2\,\vec{E} + k^2\left(\bar{n} + n_1\right)^2\,\vec{E} + 2\;grad\left(\vec{E}\,.\,grad\,\log\left(\bar{n} + n_1\right)\right) = 0 \tag{8.29}$$

$$\nabla^2\,\vec{E} + k^2\,\bar{n}^2\,\vec{E} = -2\;grad\left(\vec{E}\,.\,grad\log\left(\bar{n} + n_1\right)\right) - k^2\left(n_1^2 + 2\,n_1\,\bar{n}\,\right)\vec{E} \tag{8.30}$$

As $|n_1| \langle\langle 1$, it can be approximated that $\left(n_1^2 + 2\,n_1\,\bar{n}\right) \approx 2\,n_1\,\bar{n}$

$$grad\left(\log\left(\bar{n} + n_1\right)\right) = grad\left(\log\bar{n}\right) + grad\left(\log\left(1 + \frac{n_1}{\bar{n}}\right)\right) \tag{8.31}$$

$$grad\left(\log\bar{n}\right) + grad\left(\log\left(1 + \frac{n_1}{\bar{n}}\right)\right) \approx 0 + grad\left(\frac{n_1}{\bar{n}} - \frac{1}{2}\left(\frac{n_1}{\bar{n}}\right)^2\right) \tag{8.32}$$

This give on approximation

$$grad\left(\log \bar{n}\right)+grad\left(\log\left(1+\frac{n_1}{\bar{\bar{n}}}\right)\right)\approx\frac{1}{\bar{\bar{n}}}grad\ \left(n_1\right) \tag{8.33}$$

$$\nabla^2\vec{E}+k^2\,\bar{n}^2\,\vec{E}=-\frac{2}{\bar{\bar{n}}}grad\left(\vec{E}.grad\,n_1\right)-2\bar{n}\,n_1\,k^2\,\vec{E} \tag{8.34}$$

This gives the reduced scalar field equation,

$$\nabla^2 u+k^2\,u=f\left(\vec{r}\right) \tag{8.35}$$

where u can denote any of the field components, and $f\left(\vec{r}\right)$ the scattering potential, which is given by expression

$$f\left(r\right)=-\frac{2}{\bar{\bar{n}}}grad\left(\vec{E}.grad\,n_1\right)-2\bar{n}\,n_1\,k^2\,\vec{E} \tag{8.36}$$

It well known that the solution of eq. (8.35) corresponding to outgoing is given by

$$u(r)=-\frac{1}{4\pi}\int_V\frac{f\left(r'\right)e^{ik\left(r-r'\right)}}{\left|r-r'\right|}dV' \tag{8.37}$$

where $\vec{r'}$ is a variable vector ranging over the scattering volume V. It is shown in Appendix A that under approximation eq. (8.37) can be transformed to

$$u(r)\approx\frac{1}{4\pi}\frac{e^{ikr}}{r}\int_V f\left(\vec{r'}\right)\quad e^{-ik\,\vec{m}\cdot\vec{r'}}\ dV' \tag{8.38}$$

Therefore, from eq. (8.36) and eq. (8.37), we get

$$u(r)\approx\frac{2k^2}{4\pi}\frac{e^{ikr}}{r}\int_V\left(\bar{n}n_1\,\vec{E}\quad+\frac{1}{\bar{\bar{n}}}\ grad\left(\vec{E}\cdot grad\,n_1\right)\right)\quad e^{-ik\,\vec{m}\cdot\vec{r'}}\ dV' \tag{8.39}$$

$$u(r)\approx\frac{\bar{n}k^2}{2\pi}\frac{e^{ikr}}{r}\int_V n_1\,\vec{E}\quad e^{-ik\,\vec{m}\cdot\vec{r'}}\ dV'+\frac{k^2}{2\pi\bar{\bar{n}}}\frac{e^{ikr}}{r}\int_V grad\left(\vec{E}\cdot grad\,n_1\right)e^{-ik\,\vec{m}\cdot\vec{r'}}\ dV' \tag{8.40}$$

Using Gauss' theorem, under vanishing surface integral

$$grad\left(\vec{E}\cdot grad\,n_1\right)e^{-ik\vec{m}\cdot\vec{r'}}=\left(\vec{E}\cdot grad\,n_1\right)grad\,e^{-ik\vec{m}\cdot\vec{r'}}=\left(-ik\,\vec{m}\right)e^{-ik\vec{m}\cdot\vec{r'}} \tag{8.41}$$

Therefore,

$$u(r) \approx \frac{\bar{n} k^2}{2\pi} \frac{e^{ikr}}{r} \int_V n_1\left(\vec{r}'\right) \vec{E} \quad e^{-ik\,\vec{m}\cdot\vec{r}'}\, dV' + \frac{ik\vec{m}k^2}{2\pi\bar{n}} \frac{e^{ikr}}{r} \int_V \left(\vec{E} \cdot grad\, n_1\right) e^{-ik\,\vec{m}\cdot\vec{r}'}\, dV' \qquad (8.42)$$

$$= \frac{\bar{n}\, k^2\, e^{ikr}}{2\pi r} C_1 + \frac{ik^3\, \vec{m}\, e^{ikr}}{2\pi r \bar{n}} C_2 \qquad (8.43)$$

where

$$C_1 = \int_V n_1\left(\vec{r}'\right) \vec{E}\; e^{-ik\vec{m}\cdot\vec{r}'} dV', \qquad (8.44)$$

and

$$C_2 = \int_V \vec{E} \cdot grad\, n_1\left(\vec{r}'\right) e^{-ik\vec{m}\cdot\vec{r}'} dV' \qquad (8.45)$$

Both terms of Eq. (8.43) represent spherical waves whose amplitudes and phases depend on the refractive index fluctuations inside the volume V (through the random variables C_1 and C_2). Indeed, second term can simply, be ignored in calculating the flow of scattered energy.

$$u(r) \cong \frac{\bar{n}\, k^2\, e^{ikr}}{2\pi r} C_1 \qquad (8.46)$$

The (spectral) intensity of the scattered field at any point $\vec{r}$, at frequency ω, is just the diagonal element of the cross –spectral density of the scattered field and hence is given by

$$I(r, \omega) = \left(\frac{\bar{n}\, k^2}{2\pi r}\right)^2 \iint \left(n_1\left(\vec{r}'_1\right) n_1^*\left(\vec{r}'_2\right)\right)\left(\vec{E}_1\, \vec{E}_2^{\,*}\right) e^{-ik\vec{m}.\left(\vec{r}_1 - \vec{r}_2\right)} dV_1\, dV_2^* \qquad (8.47)$$

If the refractive index $n\left(\vec{r}, \omega\right)$ of the medium is a random function of position, then scattering potential $F\left(\vec{r}, \omega\right)$ will also be a random function of position, and the corresponding expression for the cross-spectral density and for the spectral intensity of the scattered field are obtained at once by averaging over the ensemble of the scattering potential (denoted by angular bracket with subscript n).

Let $C_n(\overrightarrow{r_1}, \ \overrightarrow{r_2}) = C_n(\overrightarrow{r_1} - \ \overrightarrow{r_2})$ denote the two-point spatial correlation function of the refractive index fluctuations, viz.,

$$C_n(r_1, r_2, \omega) = \langle n_1(\overrightarrow{r_1})\, n_1^*(\overrightarrow{r_2})\rangle \tag{8.48}$$

where the angle bracket represent the statistical average, taken over the ensemble $n_1(r, \omega)$ of the refractive index.

$$C_n(\overrightarrow{r_1}, \overrightarrow{r_2}) = C_n(\overrightarrow{r_1} - \overrightarrow{r_2}), \tag{8.49}$$

Thus, by introducing the change of variables $\overrightarrow{r_1} - \overrightarrow{r_2} = \vec{\rho}$, and $\overrightarrow{r_1} + \overrightarrow{r_2} = 2\,\vec{r}$

$$I(r, \omega) = \left\{\frac{\bar{n}\, k^2}{2\,\pi\, r}\right\}^2 \int C_n(\vec{\rho})\ \left|\vec{E}\right|^2 e^{-ik\overline{m}.\,\vec{\rho}}\, dV_\rho \tag{8.50}$$

This formula shows explicitly how the spectral intensity of the scattered radiation depends on the correlation function of the refractive index fluctuations and on the field passing through it.

For $\vec{E} = \overrightarrow{A_0} \exp\left(i\,\vec{k}\,.\vec{r}\right)$

$$I(r, \omega) = \left\{\frac{\bar{n}\, A_0 k^2}{2\,\pi\, r}\right\}^2 \int C_n(\vec{\rho})\ e^{i\,[\vec{k} - k\,\overline{m}].\,\vec{\rho}}\, dV_\rho \tag{8.51}$$

The spectral intensity is in fact Fourier transform of correlation function of the refractive index fluctuations. Thus, by knowing the information about correlation function of the refractive index, intensity fluctuations can be approximated. The exact form of refractive index correlation function depends on the characteristics of inhomogeneities. For example the spatial correlation function of the refractive index of the liquid medium, at higher Reynolds numbers, can be approximated in the form

$$C_n(\vec{\rho}) = C_n(0)\, exp\left[-\beta\, \left(\frac{\rho}{\rho_0}\right)^2\right] \tag{8.52}$$

where β and ρ_0 are positive constants, which depends upon the scale length and nature of the medium inhomogeneity.

Though, this analysis applies to a single frequency component of the field, however, it can be extended to multiple or broad bandwidth too.

A spectral intensity fluctuation from a liquid gain medium of a pulsed dye laser is known from long time. The non-uniform changes in the refractive index gradient of the dye solution lead to the refractive index fluctuations. Variation of the spectral intensity of laser emission in liquid media is directly coupled with spatial correlation function of the refractive index fluctuations and can be used to explain the experimental observations of spectral fluctuations in the high repetition rate dye laser.

In summary, a macroscopic theory of propagation and scattering of light through random media can be used under approximation for the microscopic dye liquid media. The spatial correlation function known for a long time is correlated with the refractive index fluctuations of the dye medium. Analytical expression for the spectral intensity of the scattered radiation and the correlation function of the refractive index of the medium is formulated. It shows how the spectral intensity of the field scattered by random medium depends on the correlation function of the refractive index fluctuations. Experimentally observed spectral intensity variation of the fluorescence emission of the dye and the dye laser emission in liquid media in the presence of thermal and flow field is found to be a corollary of scale length of spatial refractive index unsteadiness. Scattering, which is considered to be detrimental to the propagation of the light, of the spectral intensity of laser emission in liquid media is found to be directly coupled to the spatial correlation function of the refractive index fluctuations.

Appendix A: Derivation of an approximation relating to expression (8.37).

We derive here the approximation that is applied in expression (8.38), viz.

We choose the origin of coordinates inside the scattering volume. If the observation point $\vec{r}$ is at a great distance from the scattering volume V as compared to the dimensions of V, then for all $\vec{r}'$ the quantity $\left|\vec{r}-\vec{r}'\right|$ is almost constant and close to $r=\left|\vec{r}\right|$. In this case, the quantity $\left|\vec{r}-\vec{r}'\right|$ can be expanded in a series of powers i.e.

$$\left|\vec{r}-\vec{r}'\right| = r-\vec{m}\cdot\vec{r}' + \frac{1}{2r}\left[r'^2-\left(\vec{m}\cdot\vec{r}'\right)^2\right]+\cdots, \tag{A1}$$

where $\vec{m}=\vec{r}/r$ is a unit vector directed from the origin of coordinates (chosen within the scattering volume) to the observation point. If the inequality

$$\frac{k}{2r}\left[r'^2-\left(\vec{m}\cdot\vec{r}'\right)^2\right] \langle\langle 1. \tag{A2}$$

holds for all values of r', i.e. if the dimensions L of the scattering volume satisfy the condition

$\lambda r \rangle\rangle L^2$, then

$$\exp\left(ik\left|\vec{r}-\vec{r}'\right|\right)\approx \exp\left[ik\left(r-\vec{m}\cdot\vec{r}'\right)\right] \tag{A3}$$

Moreover, in the denominator can be replace $\left|\vec{r}-\vec{r}'\right|$ by r. Thus, we have in far filed zone

$$u(r)\approx\frac{1}{4\pi}\frac{e^{ikr}}{r}\int_V f\left(\vec{r}'\right)\; e^{-ik\,\vec{m}\cdot\vec{r}'}\,dV' \tag{A4}$$

Publications based on this chapter

1. Studies on thermo-optic characteristics of a high repetition rate dye laser

 Optics & Laser Technology **48**, 309 (2013)

 Nageshwar Singh, R. Jain, S. K. Dixit, and H. S. Vora

2. Spectral intensity variation by the correlation function of refractive index fluctuations of the liquid medium

 International Journal of Optics **2013**, (2013), doi:10.1155/2013/525142

 Nageshwar Singh

References

[8.1] Zhou Chi Sheng, Appl. Opt. **23,** 2879 (1984)

[8.2] M. Amit, G. Bialolenker, D. Levron and Z. Burshtein, J. Appl. Phys. **63**, 1293 (1988)

[8.3 CRC Handbook of Chemistry and Physics 57th ed. (1976)

[8.4] A. F. Bernhardt and P. Rasmussen, Appl. Phys. **B 26,** 141 (1981)

[8.5] F. J. Duarte and J. A. Piper, Opt. Commun. **35**, 100 (1980)

[8.6] F. J. Duarte, IEEE J. Quantum Electronics **QE-19**, 1345 (1983)

[8.7] A. F. Bernhardt and P. Rasmussen, Appl. Phys. **B 26,** 141 (1981)

[8.8] F. J. Duarte and L. W. Hillman, *Dye Laser Principle,* Academic Press, New York 1990

[8.9] F. J. Duarte, *High Power Dye Lasers,* Springer-Verlag, Berlin 1991

[8.10] Ray *et al*, App. Opt. **41,** 1704 (2002)

[8.11] Sinha *et al*, Appl. Phys. **B75,** 85 (2002)

[8.12] M. E. Lusty, M. H. Dunn, Appl. Phys. **B 44,** 193 (1987)

[8.13] El-Kashef Hassan, Opt. Laser Technol. **30,** 367 (1998)

[8.14] El-Kashef Hassan, Rev. Sci. Instrum. **69,** 1243 (1998)

[8.15] Nageshwar Singh, H. K. Patel, S. K. Dixit, H. S. Vora, Rev. Sci. Instrum. **83,** 105114 (2012)

[8.16] Nageshwar Singh**,** R. Jain, S. K. Dixit, H. S. Vora, Opt. Laser Technol. **48**, 309 (2013)

[8.17] D. W. Peters, and C. W. Mathews, Appl. Opt. **19,** 4131 (1980)

[8.18] Maruyama *et al*, Opt. Commun. **81**, 67 (1991)

[8.19] Sugiyama *et al*, Optical Eng. **35**, 1093 (1996)

[8.20] R. Mahakud, J. Kumar, O. Prakash, H. S. Vora, S. V. Nakhe, S. K. Dixit, Opt. Laser Technol. **44**, 412 (2012)

[8.21] O. Prakash, R. Mahakud, P. Saxena, V. K. Dubey, S. K. Dixit, J. K. Mittal, Opt. Commun. **283**, 5099 (2010)

[8.22] O. Prakash, J. Kumar, R. Mahakud, P. Saxena, V. K. Dubey, S. K. Dixit, J. K. Mittal, Opt. Laser Technol. **43**, 1475 (2011)

[8.23] L. A. Chernov, *Wave Propagation in a Random Medium*, McGraw-Hill, New York 1960

[8.24] V. I. Tatarskii, *Wave Propagation in a Turbulent Medium*, McGraw-Hill, New York 1961

[8.25] M. J. Beran, J. Opt. Soc. Am. **56**, 1475 (1966)

[7.26] Z. I. Feizulin and Yu. A. Kravtsov, Radio Quantum Electron. **10**, 33 (1967)

[8.27] A. Ishimaru, Radio Sci. **4**, 295 (1969)

[8.28] R. L. Fante, *Progress in Optics*, E. Wolf, ed., Elsevier, Amsterdam, 1985

[8.29] J. Wu, J. Mod. Opt. **37**, 671 (1990)

[8.30] J. Wu and A. D. Boardman, J. Mod. Opt. **38**, 1355 (1991)

[8.31] L. C. Andrews and R. L. Phillips, *Laser Beam Propagation through Random Media* (SPIE Press, Bellingham, Washington, 1998)

[8.32] M. Santarsiero, F. Gori, R. Borghi, G. Cincotti, and P. Vahimaa, J. Opt. Soc. Am. **A 16**, 106 (1999)

[8.33] Joanna Jannson, Tomasz Jannson, Emil Wolf, Opt. Lett. **13**, 1060 (1988)

[8.34] Taco D. Visser, David G. Fischer, Emil Wolf, J. Opt. Soc. Am. A **23**, 1631(2006)

[8.35] Greg Gbur and Emil Wolf, J. Opt. Soc. Am. A **19**, 1592 (2002)

Chapter 9

Summary, conclusion and scope for the future work

9.1 Summary and conclusion

This thesis presents investigations on a narrow bandwidth Rhodamine 6G (Rh6G) based dye laser, pumped by copper vapour laser. More specifically, it looks at the effects of high repetition rate excitation on the stability of the output laser parameters. The high repetition rate and narrow bandwidth operation of the tunable dye laser has been extensively investigated for potential applications such as atomic vapor laser isotope separation for enrichment experiments and other spectroscopic schemes. This scheme requires that the dye laser spectral parameters such as wavelength and bandwidth should be highly stable over sufficiently long period of time. Therefore, the stability of a high repetition rate narrow bandwidth dye laser remains a major area of research in order to enhance its applicability in these potential applications. With this aim in view, to improve the stability of the dye laser, the important factors which influences the output of the high repetition rate dye laser, were investigated. The studies have brought to light the high repetition rate dye laser related issues, which were hitherto largely unexplored.

The first issue is the geometry of the dye cell, which is being used as a container for the gain medium (dye). Conventionally, planar dye cell flow channel geometry has been used for transversely pumped high repetition rate dye laser. We felt that the geometry of the dye cell flow channel may significantly affect the optical stability of the high repetition rate dye lasers. To experimentally demonstrate this, new dye cells of different geometries were designed, modeled, fabricated, and their performances were evaluated.

Secondly, there was a necessity to have diagnostic tools for visualization and examination of the fluctuations in the output of a high repetition rate dye laser over a considerable period of time. Precise pinpointing of the dye laser spectral characteristics requires a scheme to evaluate the outcome over a period of time. There were no diagnostic tools available (either commercially or in the literature) to examine the spectral fluctuations over short/long periods of time. A novel diagnostic technique for large scale data acquisition, its presentation, and its precise measurements were formulated and effectively executed to explore the dye fluorescence and lasing features, over a period of time.

The third factor is the optimum gain medium mass flow rate which is required to minimize the thermal effects imposed by high repetition rate excitations. A thumb rule which is commonly adopted for the flow of the dye solution is that the number of dye volumes replaced between shots should be at least two or more. The liquid mass flow rate is more rationally characterized through the Reynolds number. The spectral diagnostic of neither fluorescence nor lasing characteristics with the Reynolds number of flow, during high repetition rate excitation, has been being considered so far in the literature. In the present work, the spectral characteristics of both the dye laser as well as the dye fluorescence, as a function of the Reynolds number, have been experimentally investigated. In addition, the numerical analysis of the temperature profile/ contour, as well as the gain medium flow velocity inside the dye cell has been carried out through computational fluid dynamics.

Fourthly, the thermo-optic characteristics of the dye gain medium under high repetition rate excitations have been investigated. A dye laser operating at a high pulse repetition rate needs dye gain medium circulation and cooling mechanism devices to keep the gain medium temperature gradient and its fluctuations as low as possible.

However, there is no qualitative or quantitative information available in the literature on the thermo-optic properties of a narrow spectral width dye laser, particularly operating at a high repetition rate. A comprehensive study has been carried out on the output characteristics such as spectral width, wavelength, average optical power, beam divergence, pulse width, total counts under the pulse width, of a narrow spectral width CVL pumped dye laser, by having the dye gain medium bulk temperature alteration of nearly 12 ^{o}C from normal room/cavity temperature.

The other subject area of the thesis related to the gain medium characteristics, narrow bandwidth pulsed dye laser resonator and high repetition rate excitation source (CVL) spectral characteristics were also theoretically and experimentally investigated. Effect of solvent, its concentration and temperature on the absorption characteristics of Rh6G dye was experimentally investigated. These studies on gain medium have immensely helped in the understanding of photo physics of dye laser. The dispersion theory for narrow bandwidth pulsed dye laser resonator was applied analytically as well as numerically. Optimization of the output coupler mirror transmission and the reflection coefficient for maximum optical power extraction from the resonator was carried out numerically and experimentally. The operation of a single mode dye laser through long cavity was experimentally demonstrated using a novel technique.

The main results of our studies during the course of the above stated investigations are summarized as follows.

The characteristics of a dye laser gain medium have been reviewed comprehensively. Measurements on the absorbance of Rh6G dye in commonly used organic solvents such as methanol, ethanol, ethylene glycol, and glycerol were carried out. It was observed that the Rh6G dye has maximum absorbance in ethanol at 529.9

nm wavelength. The absorbance of Rh6G dye decrease as temperature is increasing from 25 to 35 ^{o}C.

For tunability and narrow bandwidth operation, dye lasers utilize dispersive resonator. A pulsed dye laser resonator has been theoretically and numerically investigated. The analysis of the beam magnification provided by the prism in the resonator, which depends on the angles of incidence, refractive index, and apex angles of the prism, has been carried out numerically. Magnification factor drastically increases for the angle of incidence greater than 85^0 and the reflection losses also increase within 85^0–90^0 angles of incidence to the prism. The typical dispersion provided by the prism (apex angle 70^0, incidence angle 88^0) was estimated to be 0.3897×10^{-3} rad/Å, while the typical grating dispersion in grazing incidence (88^0) for 2400 lines/mm ruling was estimated to be $9.7162 * 10^{-3}$ rad/Å. This numerical analysis showed that the dispersion provided by the grating is much larger than that by the prism.

The dependence of the passive bandwidth of the resonator as a function of the beam waist size and the angle of incidence on the grating was also analysed numerically. It was observed that the bandwidth decreases sharply for the angle of incidence on the grating in the 87.0-89.5^0 range. The passive bandwidth of the resonator also decreases appreciably when the beam waist size in the gain medium was increased from 40 to 140 μm.

The influence of the reflectivity of the output coupler mirror on the optical average power of CVL pumped Rh6G dye laser with a grazing incidence grating-mirror resonator has also been theoretically and experimentally investigated. The dye laser dispersive resonator was also modeled into two-mirror cavity, equivalent to Rigrod scheme, for optimization of the optical output power-coupling coefficient for the dye laser. The maximum output power was observed in the range of 20-30 % coefficient of reflectivity of output coupler mirror. The experimental results are in good agreement with the model calculations.

A long cavity with a single prism beam expander and a grating in grazing incidence with a tuning mirror, which operates in multi axial modes, was used to obtain single mode operation by rotating the tuning mirror about an axis parallel to the plane of incidence. As a result, the same cavity, without using any additional optics, was used to obtain single axial mode operation just by controlling the rotation of the tuning mirror. The beam diffracted from the grating suffers beam walk-off through the tuning mirror, which introduces additional losses to the other side modes in the gain profile, thereby forcing the lasing in a single mode. This novel technique gave single mode of 360 MHz bandwidth from a dye laser which normally (i.e. in symmetrically aligned condition) operates in three axial modes with a bandwidth greater than 2 GHz.

As mentioned earlier, the temporal diagnostics of the spectral characteristic is of fundamental importance for its potential applications. Therefore, software for acquisition of a large number of sequential data, over a period of time, and its qualitative analysis, is essential. Novel software for data acquisition, presentation and diagnostics of the dye laser output has been developed in-house and very effectively utilized for precise measurements. A large number of sequential line scans across the diameter of FP rings, have been presented as a stacked (composite) image. By generating a composite image, the variation (drift/ fluctuation in short term and long term) in the output characteristics of the dye laser, over the observation period of more than an hour, has been successfully represented. Details of this technique for spectral structure investigation, as well as those of the other major instruments and techniques involved for the dye laser diagnostics, have been presented.

Details of subsystems needed for the high repetition rate dye laser such as dye circulation and cooling system, dye cells and liquid flow characteristics are presented. Novel dye cells of geometries such as a) near 360^0 curved (convex-concave) flow channel with continuously decreases/increasing widths, b) pinched tube dye cell, and c) a especially profiled convex-plano flow contour in the optical pumping region for the high repetition rate pumping were designed and their performance was experimentally investigated, and compared with a conventional planar duct dye cell. Spectral stability such as wavelength and bandwidth fluctuations with these dye cells was experimentally examined through the composite image. It was observed that the curved (i.e. convex-concave) flow channel dye cell offered least spectral fluctuations as compared to the routinely used planar duct dye cell.

In the output of the dye laser with curved channel dye cell, three axial modes were clearly distinguishable, while the axial modes were indistinguishable in the planar duct dye cell. The experimental results showed that curved profiling of the flow channel provides comparatively improved performances over a planar dye cell. Using a pinched dye cell, it was demonstrated that in this case, the variation of the bandwidth was within 220 MHz over the observation period of 75 minutes. Our experimental findings with planar, curved, and pinched dye cells motivated us to try out other geometries to further improve the performance (i.e. better passive stabilization) of a narrow spectral width high repetition rate dye laser. A new scheme, which essentially involves the profiling of the cubical glass and stainless steel cylindrical rod such that plano-convex contour be present near the optical pumping region. In this way, the design was an amalgamation of straight and curved periphery to enhance the dye solution flow stabilities near the dye laser axis. The design details and results of numerical analysis of flow and temperature distribution inside the dye cell have been presented.

The dye laser output characteristics such as spectral width, wavelength, average power, and pulse shape were evaluated using the convex-plano flow channel dye cell. Over a short-term, the dye laser spectral width was within ±75 MHz, while, the wavelength was within ± 0.0065 nm. In a long-term, over more than an hour, the spectral width drifted by about 180 MHz, whereas, the wavelength drifted by about 0.0105 nm. The average power was steady for a long time, more than an hour. In this way, the dye laser has demonstrated fairly good long-term stability over the observation period, without the use of either low expansion material or close loop control on the output. From our experimental findings, it was established that convex-plano dye cell channel geometry offered the best optical stability among the dye cells investigated for high repetition rate excitations. This is probably because of the fact that the curvature of the flow channel surface, which is either convex or concave, substantially changes the structure of the boundary layers. Convex curvature causes the friction coefficient to decrease, while concave curvature has the opposite effect. In this way, convex curvature has a stabilizing effect on the boundary layers, while concave curvature is destabilizing.

The spectral stability of dye laser is influenced by the mass flow rate, which was not explored earlier. This was extensively demonstrated experimentally and detailed results are presented. It was observed that the fluctuations in both the bandwidth and the wavelength decrease with increasing Reynolds number of the flow. The fluctuations in both the bandwidth and the wavelength drastically vary as the Reynolds number of the gain medium flow is changed laminar to turbulent regimes. Different set of experiments were carried out to establish the influence of gain medium flow characteristics on the spectral stability of the dye laser. Computational fluid dynamics of the gain medium convincingly validated the experimental outcomes.

The fluorescence from dyes is forced by resonator to develop functional coherent laser radiation. The photo-physics of dye laser is principally governed through the dye fluorescence. The fluorescence characteristics of Rh6G dye were briefly reviewed and significant investigations coupled with high repetition rate excitation have been carried out. Fluorescence properties such as fluorescence peak wavelength, its intensity, and spectral width were investigated, separately, in a stationary dye solution as well as in a flowing medium. The peak wavelength intensity was found to decrease by approximately 21% over the observation period in stationary solution. The total counts of the spectrum were found to fluctuate approximately within ±10% during the observation period in the stationary solution. Investigation of Rh6G dye fluorescence in flowing dye media at different Reynolds numbers has been carried out. Experimental results have shown that fluorescence spectra were broadened and had large fluctuations in the stationary dye medium as compared to flowing dye medium. The fluorescence peak wavelength is also observed to get slightly shifted in different physical environments. High pulse frequency excitations amend the material background of fluorescent molecules through thermal fields. Additions of the flow field through the Reynolds number try to nullify the surroundings thermal field gradients. The temperature dependent non-uniform refractive index of the medium has an effect on fluorescence at low Reynolds number. The flow field induced turbulences due to the high velocity gradients created within the boundary layers affect the spectrum of the fluorescent organic dyes at much higher Reynolds number. Therefore, these studies of fluorescence feature of dyes under high repetition rate excitation help in developing a stable and a good optical quality amplifying medium.

The thermo-optic properties of a narrow spectral width CVL pumped dye laser were experimentally investigated by changing the dye gain medium bulk temperature in the 23.0-35.0 ^{o}C range. It was observed that the average power of the dye laser declines monotonically with the dye solution temperature rise. The decrease in the dye laser average power was approximately 3% per degree rise in the dye solution temperature. In this span i.e. 12 ^{o}C rise in the dye bulk temperature, 36% reduction of output average power was observed. The dye laser spectral width fluctuations slightly increase with the enhancement of the dye medium temperature. The dye laser wavelength changed by 0.02% in this temperature range. The dye laser beam divergence changed in horizontal direction by 38%, while, by 25% in the vertical direction. The fluctuations in the pulse shape were also noticeable during dye medium bulk temperature variation. The dye laser pulse width increased 6%, while the total counts area under the pulse width nearly decreased by 13 % in these temperature ranges.

In a nutshell, studies on a complete dye laser system starting from gain medium, resonator, excitation source, diagnostics tools, dye cell, flow characteristics and other issues from microscopic to macroscopic levels associated with the high repetition rate have been extensively investigated in this thesis. Passive stability of the high repetition rate narrow bandwidth dye laser in terms of dye cell and gain medium flow was investigated. These studies have brought out technologically advanced and highly stable high repetition rate and narrow bandwidth tunable dye laser suitable for its potential applications

9.2 Scope for further research work

The detailed investigations performed in the present work opens up some new avenues for future, as no work, however detailed, is ever complete. The dye cell geometry and the optimum mass flow rates minimize the fluctuations associated with high repetition rate excitations. The experiments performed were at low average power (∽ 5 W) excitations. Studies on spectral fluctuations at high average power (tens of watts) through good optical quality gain medium (i.e. best dye cell and mass flow rates) have not been studied so far. Therefore, further investigations on the influence of high excitation intensity with the best dye cell geometry at optimum mass flow rate could be helpful to further investigate high average power dye laser with minimum fluctuations. Moreover, experimental visualization of the thermal and hydrodynamic boundary layers through interferometric techniques, as well as flow velocity mapping using particle image velocitometry technique inside the dye cell, are the major areas in which further research could be taken up. Essentially, the thermal and hydrodynamic boundary layer thicknesses govern the gain medium homogeneity and hence the characterization and minimization of these thicknesses is a very important research area. Also the effect of spectral characteristic of pump laser on the dye laser would also be very interesting. These are some of the technologically challenging research areas that could be taken up as a continuation of the present work.